Micro and Macro Level Damage Mechanics of the Cement-Bone Interface in Total Hip Arthroplasty

Daan Waanders

Micro and Macro Level

Damage Mechanics of the Cement-Bone Interface in Total Hip Arthroplasty

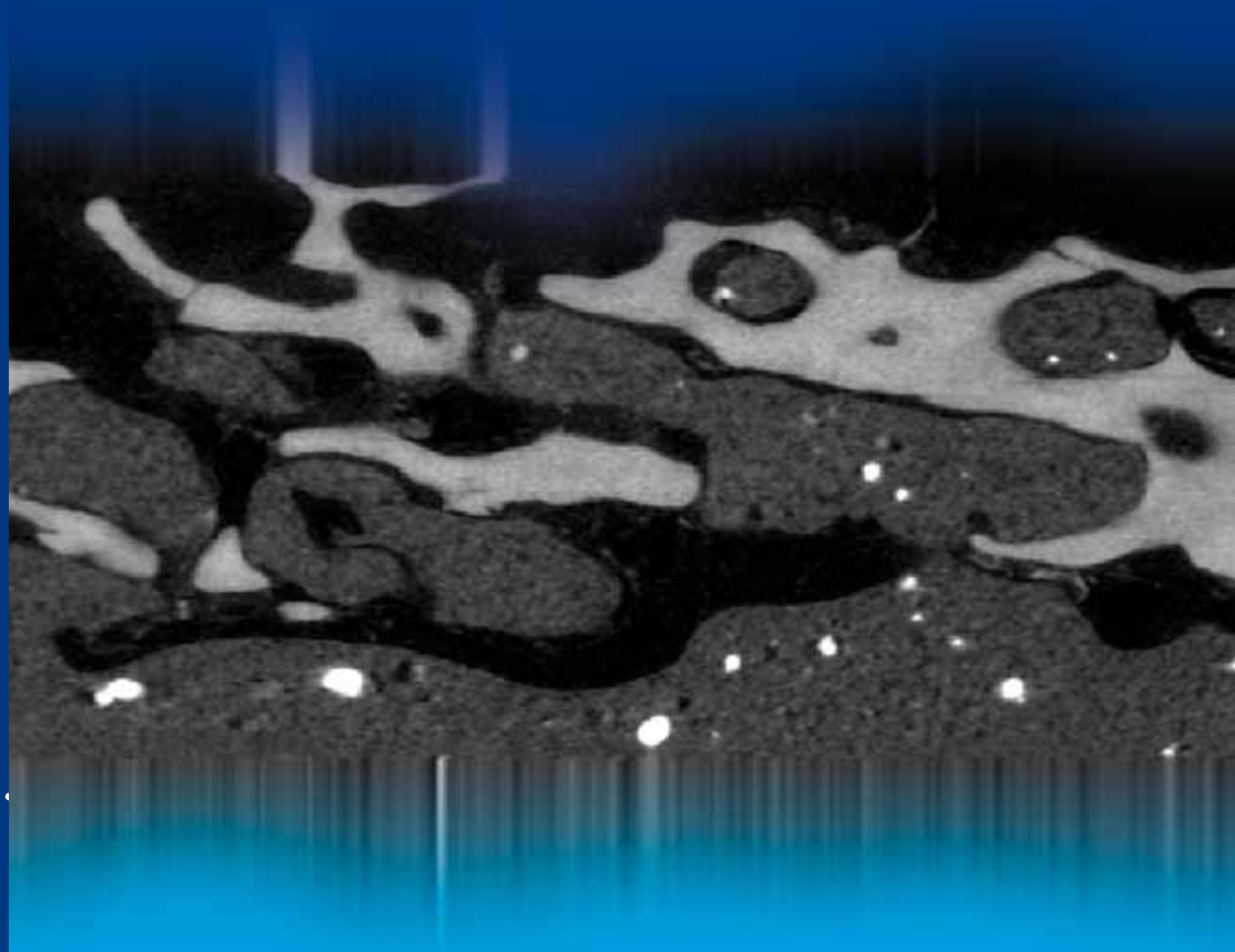

Daan Waanders

Micro and Macro Level Damage Mechanics of the Cement-Bone Interface in Total Hip Arthroplasty

daan waanders

Copyright
© 2012, Daan Waanders
All rights reserved.
No part of this book may be reproduced in any form
without written permission from the author.

ISBN
978-90-9026613-8

Lay-out and design
Monique Wassink, www.studio4graphics.nl

Printing
Enk Druck, Bocholt, Germany

The research described in this thesis was performed at the Orthopaedic Research Laboratory (Radboud University Nijmegen Medical Centre, Nijmegen, The Netherlands) and is part of the Nijmegen Centre for Evidence Based Practice (NCEBP)

Micro and Macro Level Damage Mechanics of the Cement-Bone Interface in Total Hip Arthroplasty

Een wetenschappelijke proeve op het gebied van de
Medische Wetenschappen

proefschrift

ter verkrijging van de graad van doctor
aan de Radboud Universiteit Nijmegen
op gezag van de rector magnificus prof. mr. S.C.J.J. Kortmann,
volgens besluit van het college van decanen
in het openbaar te verdedigen op

dinsdag 3 april 2012 om 15.30 uur precies

door

Daan Waanders

geboren op 8 september 1983
te Lichtenvoorde

Promotor
Prof. dr. ir. N. Verdonschot (Universiteit Twente)

Copromotoren
Dr. ir. D. Janssen
Prof. K.A. Mann (Syracuse University of New York)

Manuscriptcommissie
Prof. dr. N. Karssemeijer
Prof. dr. N.H.J. Creugers
Prof. dr. ir. J. Huétink (Universiteit Twente)

Contents

Chapter 1	Introduction	**008**
Chapter 2	Fatigue creep damage at the cement-bone interface: an experimental and a micro-mechanical finite element study	**026**
Chapter 3	The effect of cement creep and cement fatigue damage on the micromechanics of the cement-bone interface	**044**
Chapter 4	The mechanical effects of different levels of cement penetration at the cement-bone interface	**060**
Chapter 5	Mixed-mode loading of the cement-bone interface: a finite element study	**078**
Chapter 6	Multi-axial loading micromechanics of the cement-bone interface in post-mortem retrievals and lab-prepared specimens	**098**
Chapter 7	Morphology based cohesive zone modeling of the cement-bone interface from postmortem retrievals	**116**
Chapter 8	The behavior of the micro-mechanical cement-bone interface affects the cement failure in total hip replacement	**140**
Chapter 9	Interface micromechanics of transverse sections from retrieved cemented hip reconstructions: an experimental and finite element comparison	**158**
Chapter 10	Discussion	**182**
Chapter 11	Summery	**198**
Chapter 12	Samenvatting	**206**
	Dankwoord	**216**
	Curriculum Vitea	**220**

Introduction

Chapter

1

Background

Total hip artrhoplasty (THA) is one of the most successful and reliable surgical procedures in orthopaedics. Patients who suffer hip disorders, such as degenerative hip joint diseases or a femoral neck fracture, can effectively be treated by an artificial hip reconstruction. The direct postoperative findings, such as immediate pain relief and a restored hip function, make this operation very valuable and grateful for patients. In addition, over the long term, THA has proven to be very successful with survival rates between 90 and 95% after of 10 years in vivo service[24, 55, 56]. As a result of this clinical success, THA has become a very popular procedure. Annually, an estimated 21,000 THA operations are performed in the Netherlands alone and about 280,000 in the United States and the current trend shows that these numbers will increase over the upcoming years[18, 75].

During a THA operation, the diseased hip joint is replaced by an artificial reconstruction, which consists typically of a femoral stem and an acetabular cup (Figure 1.1). The stem, which is provided with a spherical head, is implanted in the femur, and the cup in the acetabulum. The two parts together act as a ball-and-socket joint and restore the range of motion in the hip joint. Prior to stem insertion, the diseased or fractured femoral head is removed and the intramedullary canal is reamed or broached. A spherical rotary reamer is used to remove the cartilage in the acetabulum prior to cup placement. Hip implants can be fixed to bone in two ways: cemented or uncemented. In the case of uncemented THA, the primary stability relies on a press-fit fixation between the bone and the implant. The long-term stability of uncemented implants is achieved by bone growing on- and into the implant surface. For cemented THA, the cavity between the implant and the bone is filled up with acrylic bone cement, which provides the fixation over both the short and long term. There is a significant geographical difference in the method of implant fixation between North America and Europe, with a predisposition for uncemented THA in the USA[21]. This thesis is concentrated on cemented THA only.

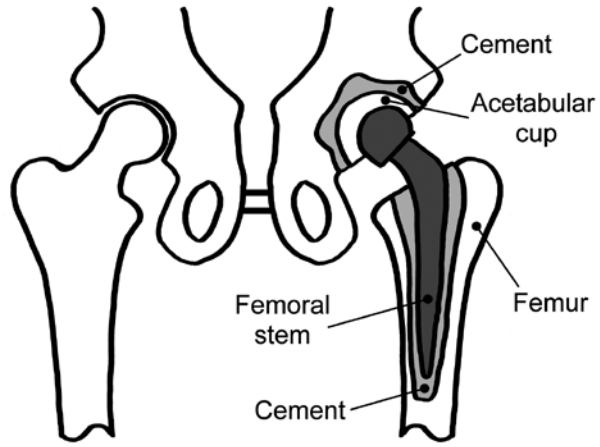

Figure 1.1 *Schematic representation of a healthy human hip joint (left) and a cemented THA reconstruction (right).*

Cemented THA

During the 1960's, Sir John Charnley developed the technique of cemented THA in clinical orthopaedics[14]. Currently, cemented THA is the gold standard for almost all patients with femoral neck fractures and for older patients (> 65 years)[29], although it is also a reasonable option for younger patients[13]. The utilized acrylic bone cement is a two component material consisting of the powder polymethylmethacrylate (PMMA) and the liquid monomethylmethacrylate (MMA). When these two components are mixed, the mixture remains viscous initially, while further polymerization makes it solid in a matter of minutes. In the viscous phase, the cement mixture is injected into the reamed intramedullary canal and acetabular cavity. Subsequently, the implant is inserted and held in place by the surgeon until the bone cement has fully polymerized, which finalizes the artificial hip reconstruction.

Since the introduction of acrylic bone cement in cemented THA 50 years ago, cementing techniques have evolved enormously in order to enhance the clinical survival. In general, three different generations of cementing techniques can be distinguished: The first generation was developed by Charnley and involved cement mixing in a bowl at room temperature and atmospheric pressure. Manual finger packing was used to insert the doughy cement into the femoral cavity[14,15,16]. The second generation technique included the use of an intramedullary plug, water lavage of the intramedullary canal, retrograde filling using a cement gun and pressurization of the cement to enhance cement penetration into the bone[71,73]. Centralizers and cement spacers characterized the third generation in order to achieve an optimal alignment of the implant within the cavity. Furthermore, vacuum mixing and cement centrifugation were introduced in order to reduce air inclusions in the bone cement, which improves its mechanical characteristics[12,19,22,48,70].

As a result of the evolution of cementing techniques, the durability of cemented THA reconstructions has improved[31,69]. Despite the success of cemented THA, failure eventually may occur. Hence, particularly in young patients, a reasonable number of patients still need a revision surgery. The most common complication causing failure of the cemented THA reconstruction is aseptic loosening[34,81,88]. Clinically, the symptoms of aseptic loosening are pain associated with radiographic evidence of bone which has been resorbed and replaced by fibrous tissue[26]. Over the years, several studies have been performed in order to ascertain the cause of the bone resorption. Analyzed retrieved cemented reconstructions relate the periprostetic bone resorption to the presence of PMMA and PE particles. These particles were found in the periprosthetic fibrous tissue, at or in the vicinity of the cement-bone interface, and it was suggested that these particles led to an inflammatory reaction, subsequently resulting in osteolysis[6,39,80]. Hence, it can be assumed that aseptic loosening seems to be caused by biological processes, but initiated by mechanical failure of the bone cement in terms of wear debris particles. These wear debris particles are a result of cement abrasion at the implant-cement interface, and are able to migrate to the periprosthetic bone due to the pumping mechanism of the dynamically loaded reconstruction[3,39].

Another cause that leads to loosening on the long term is fatigue (micro) cracking of the cement mantle[40,42,65,89]. The cracking is governed by local stresses in the cement and can result in severe cement mantle fractures (Figure 1.2). Several factors affect these local stresses, such as pores in the cement[23,47,70], the cement mantle thickness[40,42,60] and the geometrical and material properties of the implant[32,35]. Moreover, it has been shown that early cement damage is concentrated at the cement-bone interface rather than at the implant-cement interface or cement pores, which increases the compliance of the cement-bone interface in a relative early stage of in vivo service[78,85]. This results in an increase in interfacial motions, that subsequently can result in fibrous tissue formation at the cement-bone interface[38,84] (Figure 1.2).

The aforementioned findings emphasize that the cement-bone interface plays a vital role in the survival of cemented THA. Therefore, this thesis focuses on this particular region.

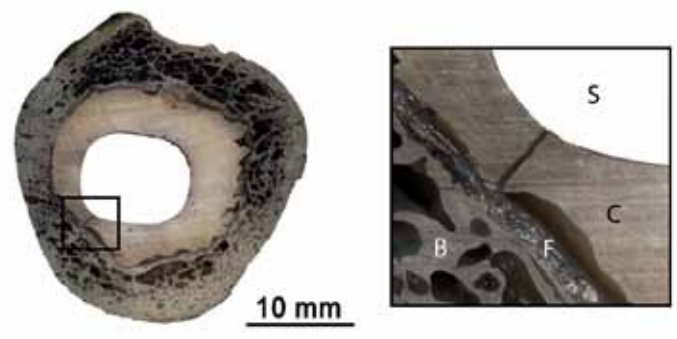

Figure 1.2 *A transverse section of a retrieved cemented hip reconstruction with a severe fracture in the cement mantle. In the right image, the stem (S), cement (C), bone (B) and fibrous tissue are indicated (taken from Mann et al (2010)[63]).*

The cement-bone interface

In cemented THA, the cement-bone interface is formed during the cement injection into the intramedullary canal and subsequent pressurization to enhance cement penetration into the bone. As a result of this, the cement fills up the trabecular and lacunar spaces, ensuing an interlaced structure with great morphological complexity (Figure 1.3). Neither osteoconduction, nor physicochemical bonding between the bone and cement can be expected[74,83]. Therefore, the fixation at the cement-bone interface relies on the interlock between the two constituents, which is achieved by cement penetrating the bone[25,37,51,61,91]. The amount of cement penetration is dependent on several factors, including cement viscosity[79,87] and bone preparation technique[10,54]. Also the degree of cement pressurization affects cement penetration[27,72]. However, over pressurizing of the cement can lead to a fat and bone-marrow embolism syndrome, which can cause complications and can sometimes even be fatal for the patient[77,82]. It is therefore essential to know how much cement penetration is needed in order to achieve a mechanically stable cement-bone interface.

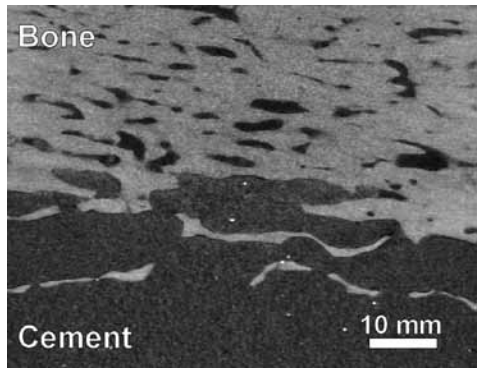

Figure 1.3 *µCT image of the cement-bone interface.*

However, in vivo, the cement-bone interface is subjected to harmful conditions, which can considerably degenerate the quality of the interface. Direct post-operatively, for instance, the cement-bone interface is subjected to heating due to the exothermal polymerization of the cement[9,20] and to cement monomer toxicity[49,50]. But also over the long term, the cement-bone interface is affected by fatigue cracking of the cement[62,78] and bone resorption[38,84] (Figure 1.4). It is obvious that these processes have a negative effect on the mechanical properties of the cement-bone interface.

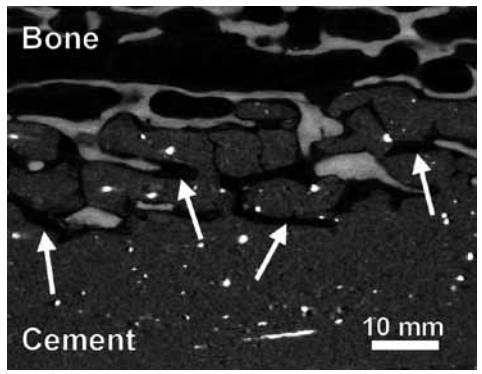

Figure 1.4 *µCT image of a post-mortem retrieved cement-bone interface. Cavities that appeared to have previously contained bone are indicated by white arrows.*

From a mechanical point of view, the mechanics of the cement-bone interface have been previously investigated by focusing on the strength[7,11,57]. In most studies, relative large cement-bone interface specimens were generated, which were subsequently used for static tensile or push-out tests from which the tensile and shear strength could be determined, respectively. In several studies, the strength of the cement-bone interface was related to the

morphology in terms of cement penetration. While several studies found a positive relationship between penetration depth and interfacial strength[5,28,30,45,52,58], others did not find such a relationship[53,67]. What remains unclear, however, is how the penetration depth of the cement affects the mechanical properties of the cement-bone interface, since this is confounded in experiments by the specimen-to-specimen variability. Moreover, it is unlikely that cement penetration is the only morphological feature that dictates the mechanical response. Based on Figures 1.3 and 1.4, it is obvious that despite the same approximate amount of cement penetration the interface of Figure 1.3 is much stronger than in Figure 1.4. Previous studies have also shown that the mechanical properties of the cement-bone interface are also dependent on the contact area between the bone and cement[61,66].

Most of the previously performed experiments considered only unidirectional loading in either the tension or shear direction. During in vivo service, however, the cement-bone interface is not only loaded in the two aforementioned principal directions, but in multi-axial directions[8]. Experimentally, the issue of mixed-mode loading of cement-bone interface specimens remains challenging, since destructive mechanical testing is only possible in one direction. The failure response in other directions can obviously not be determined with the same specimen. However, the mixed-mode response has previously been investigated by loading many cement-bone interface specimens to failure in multiple directions[64,91]. The results of these studies showed a wide range in mechanical responses as a result of the specimen variety.

The cement-bone interface has previously not only been subjected to static loads, but also to repetitive loads in order to capture the fatigue response. Research on the fatigue response of the cement-bone interface has focused mostly on documenting the overall apparent structural response, such as permanent creep damage[4,43,44,85,92]. Another experiment, which studied the fatigue response of the cement-bone interface on a more detailed scale, showed that fatigue loading resulted in micro cracks, which were mainly found in the cement rather than in the bone[62]. Furthermore, this study showed that the measured creep damage was not presumed to be manifested as traditional creep, but as gapping and sliding between the cement and the bone at the contact interface. The aforementioned experiments provide insight into the mechanism of failure, but it remains unclear which particular mechanical features of the material constituents can be attributed to the mechanism of failure. It is for instance experimentally impossible to delineate how fatigue cracking and creep of the cement interact at the cement-bone interface.

From all the above it is apparent that physical experiments can provide lots of insight into the mechanical behavior of the cement-bone interface, but they also have their limitations. A solution to overcome these limitations is the utilization of Finite Element Analysis (FEA).

FEA and the cement-bone interface

FEA has proven to be a useful tool to study the micromechanical behavior of the cement-bone interface[36,37]. From interfacial µCT-data, three-dimensional FEA models can be generated, which can for instance subsequently been used to study stress transfers between the cement

and the bone (Figure 1.5). These micromechanical FEA models are, however, not suitable for implementation in FEA models of complete cemented hip reconstructions, due to their huge computational costs. Therefore, in previous models of complete cemented hip reconstructions, the complex behavior of the cement-bone interface has often been neglected[33,41,86], or modeled as a frictional contact layer[1,46], or a soft tissue layer[17,90]. However, the validity of these three approaches to represent the interface mechanics is debatable, since experiments showed a huge variation in stiffness and strength, which was not consistent with the three aforementioned assumptions.

A more appropriate approach to model the actual mechanical response of the cement-bone interface is through the use of cohesive zone models[59,68,76]. In these cohesive zone models a constitutive relationship has to be defined, which describes the interaction between the interface tractions and displacements in normal and shear direction. However, a consistent cohesive model, which is able to realistically reproduce the mixed-mode behavior of the cement-bone interface, does not yet exist. The previously developed cohesive models for the cement-bone interface were based on theoretical models[2] and fitted to experimental mixed-mode experiments, which had a huge spread in mechanical responses due to morphological variations[v].

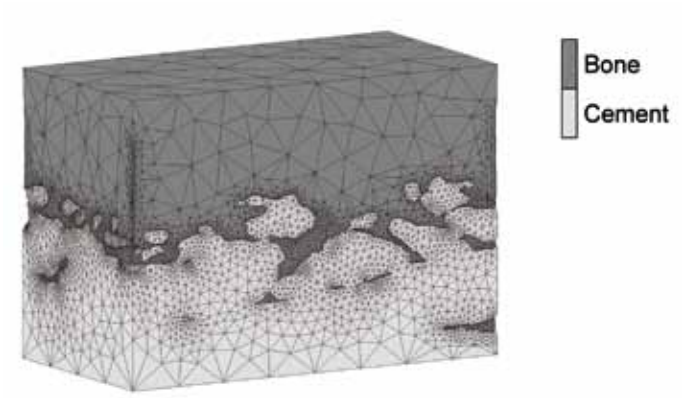

Figure 1.5 *µCT-based FEA model of the cement-bone interface.*

Thesis outline

The main issue addressed in the current thesis is to investigate how the cement-bone interface behaves on a micro scale and how this micro behavior affects the macro mechanics of the cemented reconstruction.

Chapter 2 concerns the fatigue response of the cement-bone interface. It is investigated whether the experimental fatigue response can be reproduced using FEA in terms of plastic displacements and micro-crack formation.

In Chapter 3 it is discussed which deformation modes are responsible for the fatigue response of the cement-bone interface. Is this due to fatigue damage in terms of micro-cracking, creep of the cement, or both?

Chapter 4 concentrates on the mechanical effects of different levels of cement penetration at the cement-bone interface. Are there different mechanical responses in tension and shear due to the diverse cement infiltrations, and which constituent is the weakest link: bone or cement?

In the Chapters 5 to 7 the response of the cement-bone interface under multi-axial loading is investigated. Chapter 5 describes the mixed-mode response of lab-prepared cement-bone interfaces utilizing micromechanical FEA models. Additionally, it was investigated whether the response could be related to the amount of cement penetration. In Chapter 6, the multi-axial stiffness of lab-prepared and postmortem retrieved cement-bone interface specimens is studied in vitro. Besides the penetration depth, it was investigated whether the mechanics could be related to more micromechanical morphological characteristics. Chapter 7 describes how a cohesive zone model was developed based on the mixed-mode response of postmortem retrieved cement-bone interfaces and their micro morphological parameters.

In Chapter 8 it was investigated how the micromechanical behavior of the cement-bone interface affects the failure of the cement mantle. Conversely, the effect of cement mantle failure on the load distribution of the cement-bone interface was analyzed.

Chapter 9 focuses on the mechanics of transverse sections of retrieved cemented hip reconstructions. The response of FEA models, in which the cement-bone interface is modeled through a morphological based cohesive zone model, is compared with the response of in vitro experiments.

Chapter 10 discusses the results as described in this thesis and puts them in a clinically relevant perspective. Furthermore, suggestions for future research are formulated in order to further enhance the mechanical survival of cemented THA.

Finally, the summary of this thesis is presented in English (Chapter 11) and Dutch (Chapter 12).

References

1. **Afsharpoya, B., Barton, D. C., Fisher, J., Purbach, B., Wroblewski, M., Stewart, T. D., (2009).**
   Cement mantle stress under retroversion torque at heel-strike.
   Med.Eng Phys. 31, 1323-1330.
2. **Alfano, G., Crisfield, M. A., (2001).**
   Finite element interface models for the delamination analysis of laminated composites: Mechanical and computational issues. International Journal for Numerical Methods in Engineering 50, 1701-1736.
3. **Anthony, P. P., Gie, G. A., Howie, C. R., Ling, R. S., (1990).**
   Localised endosteal bone lysis in relation to the femoral components of cemented total hip arthroplasties. J Bone Joint Surg.Br. 72, 971-979.
4. **Arola, D., Stoffel, K. A., Yang, D. T., (2006).**
   Fatigue of the cement/bone interface: the surface texture of bone and loosening.
   J.Biomed. Mater.Res.B Appl.Biomater. 76, 287-297.
5. **Askew, M. J., Steege, J. W., Lewis, J. L., Ranieri, J. R., Wixson, R. L., (1984).**
   Effect of cement pressure and bone strength on polymethylmethacrylate fixation.
   J.Orthop.Res. 1, 412-420.
6. **Bauer, T. W., Schils, J., (1999).**
   The pathology of total joint arthroplasty.II. Mechanisms of implant failure.
   Skeletal Radiol. 28, 483-497.
7. **Bean, D. J., Convery, F. R., Woo, S. L., Lieber, R. L., (1987).**
   Regional variation in shear strength of the bone-polymethylmethacrylate interface.
   J.Arthroplasty 2, 293-298.
8. **Bergmann, G., Graichen, F., Rohlmann, A., (1995).**
   Is staircase walking a risk for the fixation of hip implants? J Biomech. 28, 535-553.
9. **Berman, A. T., Reid, J. S., Yanicko, D. R., Jr., Sih, G. C., Zimmerman, M. R., (1984).**
   Thermally induced bone necrosis in rabbits. Relation to implant failure in humans.
   Clin. Orthop Relat Res 284-292.
10. **Berry, D. J., (2004).**
    Cemented femoral stems: what matters most. J.Arthroplasty 19, 83-84.
11. **Bugbee, W. D., Barrera, D. L., Lee, A. C., Convery, F. R., (1992).**
    Variations in shear strength of the bone-cement interface in the proximal femur.
    Trans Orthop Res Soc 17:22.
12. **Burke, D. W., Gates, E. I., Harris, W. H., (1984).**
    Centrifugation as a method of improving tensile and fatigue properties of acrylic bone cement.
    J Bone Joint Surg.Am. 66, 1265-1273.
13. **Busch, V., Klarenbeek, R., Slooff, T., Schreurs, B. W., Gardeniers, J., (2010).**
    Cemented hip designs are a reasonable option in young patients.
    Clin.Orthop Relat Res 468, 3214-3220.
14. **Charnley, J., (1960).**
    Anchorage of the femoral head prosthesis to the shaft of the femur.
    J Bone Joint Surg.Br. 42-B, 28-30.

15. **Charnley, J., (1961).**
    Arthroplasty of the hip. A new operation. Lancet 1, 1129-1132.
16. **Charnley, J., (1964).**
    The bonding of prostheses to bone by cement. J Bone Joint Surg.Br. 46, 518-529.
17. **Colombi, P., (2002).**
    Fatigue analysis of cemented hip prosthesis: model definition and damage evolution algorithms. International Journal of Fatigue 24, 895-901.
18. **Cram, P., Lu, X., Kaboli, P. J., Vaughan-Sarrazin, M. S., Cai, X., Wolf, B. R., Li, Y., (2011).**
    Clinical characteristics and outcomes of Medicare patients undergoing total hip arthroplasty, 1991-2008. JAMA 305, 1560-1567.
19. **Davies, J. P., Burke, D. W., O'Connor, D. O., Harris, W. H., (1987).**
    Comparison of the fatigue characteristics of centrifuged and uncentrifuged Simplex P bone cement. J Orthop Res 5, 366-371.
20. **DiPisa, J. A., Sih, G. S., Berman, A. T., (1976).**
    The temperature problem at the bone-acrylic cement interface of the total hip replacement. Clin.Orthop Relat Res 95-98.
21. **Dunbar, M. J., (2009).**
    Cemented femoral fixation: the North Atlantic divide. Orthopedics 32.
22. **Dunne, N. J., Orr, J. F., (2001).**
    Influence of mixing techniques on the physical properties of acrylic bone cement.
    Biomaterials 22, 1819-1826.
23. **Dunne, N. J., Orr, J. F., Mushipe, M. T., Eveleigh, R. J., (2003).**
    The relationship between porosity and fatigue characteristics of bone cements.
    Biomaterials 24, 239-245.
24. **Espehaug, B., Furnes, O., Engesaeter, L. B., Havelin, L. I., (2009).**
    18 years of results with cemented primary hip prostheses in the Norwegian Arthroplasty Register: concerns about some newer implants. Acta Orthop 80, 402-412.
25. **Freeman, M. A., Bradley, G. W., Revell, P. A., (1982).**
    Observations upon the interface between bone and polymethylmethacrylate cement.
    J.Bone Joint Surg.Br. 64, 489-493.
26. **Goldring, S. R., Jasty, M., Roelke, M. S., Rourke, C. M., Bringhurst, F. R., Harris, W. H., (1986).**
    Formation of a synovial-like membrane at the bone-cement interface. Its role in bone resorption and implant loosening after total hip replacement. Arthritis Rheum. 29, 836-842.
27. **Gozzard, C., Gheduzzi, S., Miles, A. W., Learmonth, I. D., (2005).**
    An in-vitro investigation into the cement pressurization achieved during insertion of four different femoral stems. Proc.Inst.Mech.Eng [H.] 219, 407-413.
28. **Graham, J., Ries, M., Pruitt, L., (2003).**
    Effect of bone porosity on the mechanical integrity of the bone-cement interface.
    J.Bone Joint Surg.Am. 85-A, 1901-1908.
29. **Hailer, N. P., Garellick, G., Karrholm, J., (2010).**
    Uncemented and cemented primary total hip arthroplasty in the Swedish Hip Arthroplasty Register. Acta Orthop 81, 34-41.
30. **Halawa, M., Lee, A. J., Ling, R. S., Vangala, S. S., (1978).**
    The shear strength of trabecular bone from the femur, and some factors affecting

the shear strength of the cement-bone interface. Arch.Orthop Trauma Surg. 92, 19-30.

31. **Herberts, P., Malchau, H., (2000).**
Long-term registration has improved the quality of hip replacement: a review of the Swedish THR Register comparing 160,000 cases. Acta Orthop Scand. 71, 111-121.
32. **Huiskes, R., (1990).**
The various stress patterns of press-fit, ingrown, and cemented femoral stems. Clin.Orthop.Relat Res. 27-38.
33. **Hung, J. P., Chen, J. H., Chiang, H. L., Wu, J. S., (2004).**
Computer simulation on fatigue behavior of cemented hip prostheses: a physiological model. Comput.Methods Programs Biomed. 76, 103-113.
34. **Jacobs, J. J., Roebuck, K. A., Archibeck, M., Hallab, N. J., Glant, T. T., (2001).**
Osteolysis: basic science. Clin.Orthop Relat Res 71-77.
35. **Janssen, D., Aquarius, R., Stolk, J., Verdonschot, N., (2005).**
Finite-element analysis of failure of the Capital Hip designs. J Bone Joint Surg.Br. 87, 1561-1567.
36. **Janssen, D., Mann, K. A., Verdonschot, N., (2008).**
Micro-mechanical modeling of the cement-bone interface: The effect of friction, morphology and material properties on the micromechanical response. J.Biomech. 41, 3158-3163.
37. **Janssen, D., Mann, K. A., Verdonschot, N., (2009).**
Finite element simulation of cement-bone interface micromechanics: a comparison to experimental results. J.Orthop.Res. 27, 1312-1318.
38. **Jasty, M., Bragdon, C., Burke, D., O'Connor, D., Lowenstein, J., Harris, W. H., (1997).**
In vivo skeletal responses to porous-surfaced implants subjected to small induced motions. J Bone Joint Surg.Am. 79, 707-714.
39. **Jasty, M., Jiranek, W., Harris, W. H., (1992).**
Acrylic fragmentation in total hip replacements and its biological consequences. Clin.Orthop Relat Res 116-128.
40. **Jasty, M., Maloney, W. J., Bragdon, C. R., O'Connor, D. O., Haire, T., Harris, W. H., (1991).**
The initiation of failure in cemented femoral components of hip arthroplasties. J.Bone Joint Surg.Br. 73, 551-558.
41. **Katoozian, H., Davy, D. T., (2000).**
Effects of loading conditions and objective function on three-dimensional shape optimization of femoral components of hip endoprostheses. Med.Eng Phys. 22, 243-251.
42. **Kawate, K., Maloney, W. J., Bragdon, C. R., Biggs, S. A., Jasty, M., Harris, W. H., (1998).**
Importance of a thin cement mantle. Autopsy studies of eight hips. Clin.Orthop. Relat Res. 70-76.
43. **Kim, D. G., Miller, M. A., Mann, K. A., (2004).**
A fatigue damage model for the cement-bone interface. J.Biomech. 37, 1505-1512.
44. **Kim, D. G., Miller, M. A., Mann, K. A., (2004).**
Creep dominates tensile fatigue damage of the cement-bone interface. J.Orthop. Res. 22, 633-640.
45. **Krause, W. R., Krug, W., Miller, J., (1982).**
Strength of the cement-bone interface. Clin.Orthop.Relat Res. 163, 290-299.
46. **Lewis, G., Duggineni, R., (2006).**
Finite element analysis of a three-dimensional model of a proximal femur-cemented femoral THJR component construct: Influence of assigned interface conditions on strain energy density. Bio-Medical Materials and Engineering 16, 319-327.
47. **Lewis, G., Nyman, J. S., Trieu, H. H., (1997).**
Effect of mixing method on selected properties of acrylic bone cement. J Biomed Mater Res 38, 221-228.
48. **Lidgren, L., Drar, H., Moller, J., (1984).**
Strength of polymethylmethacrylate increased by vacuum mixing. Acta Orthop Scand. 55, 536-541.
49. **Linder, L., (1977).**
Reaction of bone to the acute chemical trauma of bone cement. J Bone Joint Surg. Am. 59, 82-87.
50. **Lu, J. X., Huang, Z. W., Tropiano, P., Clouet, D. B., Remusat, M., Dejou, J., Proust, J. P., Poitout, D., (2002).**
Human biological reactions at the interface between bone tissue and polymethylmethacrylate cement. J Mater Sci Mater Med. 13, 803-809.
51. **Lucksanasombool, P., Higgs, W. A., Ignat, M., Higgs, R. J., Swain, M. V., (2003).**
Comparison of failure characteristics of a range of cancellous bone-bone cement composites. J.Biomed.Mater.Res.A 64, 93-104.
52. **MacDonald, W., Swarts, E., Beaver, R., (1993).**
Penetration and shear strength of cement-bone interfaces in vivo. Clin.Orthop. Relat Res. 286, 283-288.
53. **Majkowski, R. S., Bannister, G. C., Miles, A. W., (1994).**
The effect of bleeding on the cement-bone interface. An experimental study. Clin.Orthop.Relat Res. 299, 293-297.
54. **Majkowski, R. S., Miles, A. W., Bannister, G. C., Perkins, J., Taylor, G. J., (1993).**
Bone surface preparation in cemented joint replacement. J.Bone Joint Surg.Br. 75, 459-463.
55. **Makela, K., Eskelinen, A., Pulkkinen, P., Paavolainen, P., Remes, V., (2008).**
Cemented total hip replacement for primary osteoarthritis in patients aged 55 years or older: results of the 12 most common cemented implants followed for 25 years in the Finnish Arthroplasty Register. J Bone Joint Surg.Br. 90, 1562-1569.
56. **Malchau, H., Herberts, P., Eisler, T., Garellick, G., Soderman, P., (2002).**
The Swedish Total Hip Replacement Register. J Bone Joint Surg.Am. 84-A Suppl 2, 2-20.
57. **Mann, K. A., Allen, M. J., Ayers, D. C., (1998).**
Pre-yield and post-yield shear behavior of the cement-bone interface. J.Orthop. Res. 16, 370-378.
58. **Mann, K. A., Ayers, D. C., Werner, F. W., Nicoletta, R. J., Fortino, M. D., (1997).**
Tensile strength of the cement-bone interface depends on the amount of bone interdigitated with PMMA cement. J.Biomech. 30, 339-346.
59. **Mann, K. A., Damron, L. A., (2002).**
Predicting the failure response of cement-bone constructs using a non-linear fracture mechanics approach. J.Biomech.Eng 124, 462-470.
60. **Mann, K. A., Gupta, S., Race, A., Miller, M. A., Cleary, R. J., Ayers, D. C., (2004).**
Cement microcracks in thin-mantle regions after in vitro fatigue loading.

J Arthroplasty 19, 605-612.
61. **Mann, K. A., Miller, M. A., Cleary, R. J., Janssen, D., Verdonschot, N., (2008).** Experimental micromechanics of the cement-bone interface. J.Orthop.Res. 26, 872-879.
62. **Mann, K. A., Miller, M. A., Race, A., Verdonschot, N., (2009).** Shear fatigue micromechanics of the cement-bone interface: An in vitro study using digital image correlation techniques. J.Orthop.Res. 27, 340-346.
63. **Mann, K. A., Miller, M. A., Verdonschot, N., Izant, T. H., Race, A., (2010).** Functional interface micromechanics of 11 en-bloc retrieved cemented femoral hip replacements. Acta Orthop 81, 308-317.
64. **Mann, K. A., Mocarski, R., Damron, L. A., Allen, M. J., Ayers, D. C., (2001).** Mixed-mode failure response of the cement-bone interface. J.Orthop.Res. 19, 1153-1161.
65. **McCormack, B. A., Prendergast, P. J., (1999).** Microdamage accumulation in the cement layer of hip replacements under flexural loading. J Biomech. 32, 467-475.
66. **Miller, M. A., Eberhardt, A. W., Cleary, R. J., Verdonschot, N., Mann, K. A., (2010).** Micromechanics of postmortem-retrieved cement-bone interfaces. J.Orthop.Res. 28, 170-177.
67. **Miller, M. A., Race, A., Gupta, S., Higham, P., Clarke, M. T., Mann, K. A., (2007).** The role of cement viscosity on cement-bone apposition and strength: an in vitro model with medullary bleeding. J.Arthroplasty 22, 109-116.
68. **Moreo, P., Perez, M. A., Garcia-Amar, J. M., Doblare, M., (2006).** Modelling the mixed-mode failure of cement-bone interfaces. Engineering Fracture Mechanics 73, 1379-1395.
69. **Mulroy, R. D., Jr., Harris, W. H., (1990).** The effect of improved cementing techniques on component loosening in total hip replacement. An 11-year radiographic review. J Bone Joint Surg.Br. 72, 757-760.
70. **Murphy, B. P., Prendergast, P. J., (2002).** The relationship between stress, porosity, and nonlinear damage accumulation in acrylic bone cement. J Biomed Mater Res 59, 646-654.
71. **Noble, P. C., Collier, M. B., Maltry, J. A., Kamaric, E., Tullos, H. S., (1998).** Pressurization and centralization enhance the quality and reproducibility of cement mantles. Clin.Orthop Relat Res 77-89.
72. **Oates, K. M., Barrera, D. L., Tucker, W. N., Chau, C. C., Bugbee, W. D., Convery, F. R., (1995).** In vivo effect of pressurization of polymethyl methacrylate bone-cement. Biomechanical and histologic analysis. J.Arthroplasty 10, 373-381.
73. **Oh, I., Carlson, C. E., Tomford, W. W., Harris, W. H., (1978).** Improved fixation of the femoral component after total hip replacement using a methacrylate intramedullary plug. J Bone Joint Surg.Am. 60, 608-613.
74. **Oonishi, H., Ohashi, H., Oonishi, H., Jr., Kim, S. C., (2008).** THA with hydroxyapatite granules at cement-bone interface: 15- to 20-year results. Clin.Orthop Relat Res 466, 373-379.
75. **Otten, R., Van Roermund, P., Susan, H., Picavet, J., (2010).** Trends in aantallen knie- en heuparthroplastieken.

Nederlands Tijdschrift voor Geneeskunde 154:A1534.
76. **Perez, M. A., Garcia-Aznar, J. M., Doblare, M., (2009).** Does increased bone-cement interface strength have negative consequences for bulk cement integrity? A finite element study. Ann.Biomed.Eng 37, 454-466.
77. **Pitto, R. P., Koessler, M., Kuehle, J. W., (1999).** Comparison of fixation of the femoral component without cement and fixation with use of a bone-vacuum cementing technique for the prevention of fat embolism during total hip arthroplasty. A prospective, randomized clinical trial. J.Bone Joint Surg.Am. 81, 831-843.
78. **Race, A., Miller, M. A., Ayers, D. C., Mann, K. A., (2003).** Early cement damage around a femoral stem is concentrated at the cement/bone interface. J.Biomech. 36, 489-496.
79. **Race, A., Miller, M. A., Clarke, M. T., Mann, K. A., Higham, P. A., (2006).** The effect of low-viscosity cement on mantle morphology and femoral stem micromotion: a cadaver model with simulated blood flow. Acta Orthop. 77, 607-616.
80. **Schmalzried, T. P., Kwong, L. M., Jasty, M., Sedlacek, R. C., Haire, T. C., O'Connor, D. O., Bragdon, C. R., Kabo, J. M., Malcolm, A. J., Harris, W. H., (1992).** The mechanism of loosening of cemented acetabular components in total hip arthroplasty. Analysis of specimens retrieved at autopsy. Clin.Orthop Relat Res 60-78.
81. **Schwarz, E. M., Looney, R. J., O'Keefe, R. J., (2000).** Anti-TNF-alpha therapy as a clinical intervention for periprosthetic osteolysis. Arthritis Res 2, 165-168.
82. **Sierra, R. J., Timperley, J. A., Gie, G. A., (2009).** Contemporary cementing technique and mortality during and after exeter total hip arthroplasty. J.Arthroplasty 24, 325-332.
83. **Skripitz, R., Aspenberg, P., (1999).** Attachment of PMMA cement to bone: force measurements in rats. Biomaterials 20, 351-356.
84. **Soballe, K., Hansen, E. S., Rasmussen, H., Jorgensen, P. H., Bunger, C., (1992).** Tissue ingrowth into titanium and hydroxyapatite-coated implants during stable and unstable mechanical conditions. J Orthop Res 10, 285-299.
85. **Stoffel, K. A., Yang, D. T., Arola, D., (2008).** The influence of surface topography on wear debris generation at the cement/bone interface under cyclic loading. J.Mater.Sci.Mater.Med. 19, 1935-1943.
86. **Stolk, J., Janssen, D., Huiskes, R., Verdonschot, N., (2007).** Finite element-based preclinical testing of cemented total hip implants. Clin.Orthop.Relat Res. 456, 138-147.
87. **Stone, J. J., Rand, J. A., Chiu, E. K., Grabowski, J. J., An, K. N., (1996).** Cement viscosity affects the bone-cement interface in total hip arthroplasty. J.Orthop.Res. 14, 834-837.
88. **Sundfeldt, M., Carlsson, L. V., Johansson, C. B., Thomsen, P., Gretzer, C., (2006).** Aseptic loosening, not only a question of wear: a review of different theories. Acta Orthop 77, 177-197.
89. **Topoleski, L. D., Ducheyne, P., Cuckler, J. M., (1990).** A fractographic analysis of in vivo poly(methyl methacrylate) bone cement failure mechanisms.

J Biomed Mater Res 24, 135-154.

90. **Verdonschot, N., Huiskes, R., (1997).**
The effects of cement-stem debonding in THA on the long-term failure probability of cement.
J.Biomech. 30, 795-802.

91. **Wang, J. Y., Tozzi, G., Chen, J., Contal, F., Lupton, C., Tong, J., (2010).**
Bone-cement interfacial behaviour under mixed mode loading conditions.
J Mech Behav Biomed Mater 3, 392-398.

92. **Yang, D. T., Zhang, D., Arola, D., (2010).**
Fatigue of the bone/cement interface and loosening of tatal joint replacements.
International Journal of Fatigue 32, 1639-1649.

Chapter 2

Fatigue creep damage at the cement-bone interface: an experimental and a micro-mechanical finite element study

Journal of Biomechanics
(2009); 42(15): 2513-9

Abstract

The goal of this study was to quantify the micromechanics of the cement-bone interface under tensile fatigue loading using finite element analysis (FEA) and to understand the underlying mechanisms that play a role in the fatigue behavior of this interface. Laboratory cement-bone specimens were subjected to a tensile fatigue load, while local displacements and crack growth on the specimen's surface were monitored. FEA models were created from these specimens based upon micro-computed tomography data. To accurately model interfacial gaps at the interface between the bone and cement, a custom-written erosion algorithm was applied to the bone model. A fatigue load was simulated in the FEA models while monitoring the local displacements and crack propagation. The results showed the FEA models were able to capture the general experimental creep damage behavior and creep stages of the interface. Consistent with the experiments, the majority of the deformation took place at the contact interface. Additionally, the FEA models predicted fatigue crack patterns similar to experimental findings. Experimental surface cracks correlated moderately with FEA surface cracks (r^2=0.43), but did not correlate with the simulated crack volume fraction (r^2=0.06). Although there was no relationship between experimental surface cracks and experimental creep damage displacement (r^2=0.07), there was a strong relationship between the FEA crack volume fraction and the FEA creep damage displacement (r^2=0.76). This study shows the additional value of FEA of the cement-bone interface relative to experimental studies and can therefore be used to optimize its mechanical properties.

Introduction

The most common cause of failure in cemented total hip arthroplasty (THA) is aseptic loosening of the hip reconstruction[5]. Aseptic loosening is initiated by failure of the implant-cement interface[25], the bulk cement mantle[8] or the cement-bone interface[4,8], although early loosening of a femoral implant may be concentrated in the interdigitated area of the cement-bone interface[18].

The cement-bone interface is an interlaced structure with great morphological complexity and a highly variable interlock between the cement bulk and the bone. Laboratory studies of the mechanical behavior of the cement-bone interface have focused on static parameters such as interface strength[2,13]. Research on the fatigue response of the cement-bone interface has focused mostly on documenting the overall structural response such as permanent creep damage[1,9,10,19], although recently the shear fatigue response has been studied on a more detailed scale[14]. The results of the latter study showed that fatigue failure of the interface arose at the contact interface between cement and bone. Fatigue cracks were mainly found in the cement, emanating from the contact interface. Creep damage was not presumed to be manifested as traditional creep, but as gapping and sliding between the cement and the bone at the contact interface.

A limitation of these laboratory experiments is that the mechanism of failure is observational, but cannot be attributed to a particular feature of the material constituents. In addition, only deformation on the outer surface of the test specimen can be examined. Whether this reflects failure inside the specimen is questionable. On the other hand, finite element analysis (FEA) has proven to be a convenient tool to gain more insight into the (micro) mechanics of cemented THA[11,20,26]. Combining experimental studies of the fatigue damage response of the cement-bone interface with micro-mechanical finite element analysis (μFEA) models is an approach that could be used to understand the mechanisms of failure of the cement-bone interface. Recently, the static behavior of the cement-bone interface[14] has been simulated by means of μFEA models[6,7]. In such μFEA models, additional micro-phenomena could potentially be investigated, such as crack formation in the cement mantle[21]. Currently, the fatigue failure response of the cement-bone interface has only been simulated on a macro scale[17].

The goal of this study was to quantify the micromechanics of the cement-bone interface under tensile fatigue loading and to determine if the fatigue damage response could be explained using μFEA models that incorporated detailed geometry of the structure and provision for failure of the cement. We put forward three research questions: (1) Can the μFEA models reproduce the creep damage behavior as observed in the experiments in terms of crack patterns and creep displacements?; (2) Does the majority of peak motion of the experimental specimens and of the μFEA models take place at the contact interface?; and (3) Is there a relationship between the length of cracks found on the experimental specimen surfaces and the crack volume fraction in the μFEA models?

Methods

Experimental protocol

Ten rectangular-prism shaped specimens (~8x8x4mm) containing the cement-bone interface were fabricated from laboratory-prepared, cemented femoral hip replacements, using a previously described method[14]. Specimens were scanned in a microCT scanner (Scanco Medical AG, Basserdorf, Switzerland) at an isotropic resolution of 12µm. Specimens were placed in a 37° saline bath apparatus of a mechanical test frame (MTS Systems, Eden Prairie, MN). The initial stiffness of the specimens was determined by applying a small tensile load. Next, the static strength of each specimen was estimated based on an established stiffness-strength relationship[14]. The magnitude of the applied fatigue tensile load was set to 50% of the estimated static tensile strength for each specimen.

Specimens were sinusoidally loaded in tension using an R-ratio of 0.1 at 3Hz for 50,000 load cycles. Local deformations were measured by tracking sampling points on the interface using digital image correlation (DIC) techniques[14,15] at 10, 100, 1k, 3k, 5k, 33k, and 50k cycles (Figure 2.1). Stress-displacement plots were determined at each of the seven sampling times and were used to calculate the *creep damage displacement* (δ_{cd}) which served as the primary outcome variable. Here, the creep damage displacement was defined as the permanent deformation at zero applied load. If a specimen reached a global displacement of 72µm before 50k cycles, the test was terminated to prevent complete fracture of the specimen.

The initial (pre-test) and final micro-crack damage present on the four exposed surfaces of the cement and bone was determined using a previously described approach[14]. Briefly, high resolution (5.8µm) reflected white light and epifluoresence images were obtained after calcein staining of the bone and use of a fluorescing dye penetrant for the cement. Cracks were divided into pre-existing cracks (before loading), growth from pre-existing cracks, new cracks and total crack growth (growth from pre-existing and new cracks).

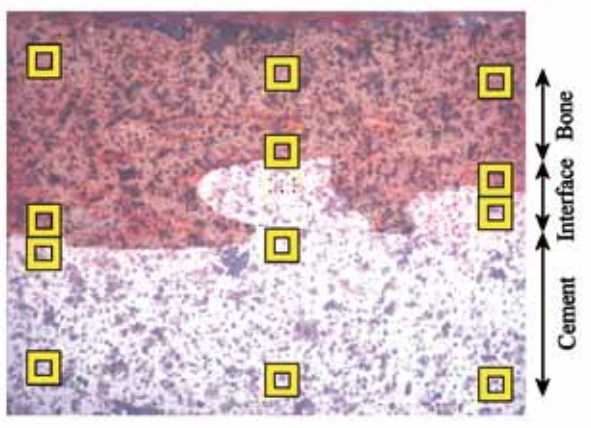

Figure 2.1 *The locations of the DIC measurements consisted of three columns of four sampling points. For each column, two sampling were located in the bone and two in the cement. The local displacements were subsequently averaged to obtain a 'global' deformation of the bone, cement and contact interface.*

FEA Modeling

The FEA models of the specimens comprised two parts: bone and cement. The bone FEA meshes were created from µCT-data using MIMICS 11.0 (Materialise, Leuven, Belgium; Figure 2.2a). First, the µCT-data was segmented based on the image grayscale, ranging from -1,024 to 3,071 (Figure 2.2b). Next, the 3D voxel meshes were transformed to triangular surface meshes, using a 6x6x6 voxel interpolation with smoothing, and remeshed to reduce the number of triangles and to remove low quality triangles. The surface meshes were meshed as a tetrahedral 3D solid (Patran 2005r2, MSC Software Corporation, Santa Ana, CA, USA) and mapped back to the µCT-data set (Figure 2.2c), after which the weighted average of the grayscale was calculated for each solid element using MIMICS.

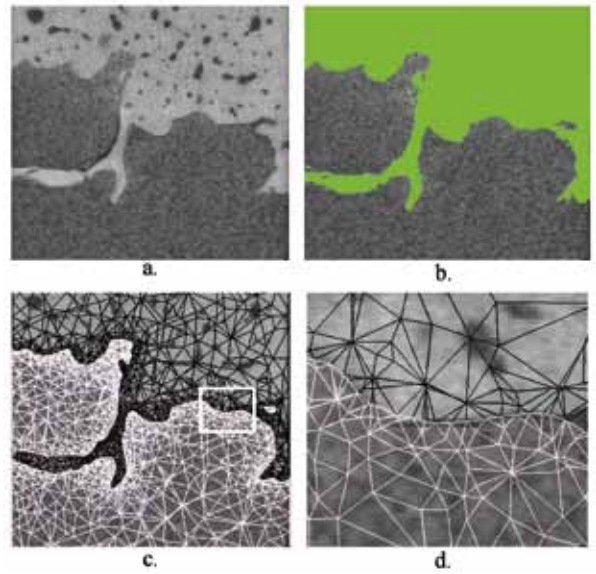

Figure 2.2
a. µCT-data of the cement-bone interface.
b. Segmentation of the µCT-data into bone (1,000 to 3,071) and cavities (-1,024 to 100). Remaining gaps in the bone were filled manually.
c. Solid mesh of the bone and cement plotted on top of the µCT-data.
d. Zoomed node-to-node interface from figure c.

FEA meshes of the cement were based on the triangular surface mesh of the bone and not on the segmentation of the µCT-data. First, a surface mesh of the cement was created using node-to-node contact between the bone and cement (Figure 2.2d). Next, to create appropriate gaps at the cement-bone contact interface, an 'erosion' algorithm was applied to the bone mesh. Nodes on the bone surface were displaced away from the interface with a magnitude dependent on the nodal equivalent Hounsfield Unit (eqHU). The parameter eqHU was determined as:

$$\mathbf{eqHU} = \frac{1}{\sum_{i=1}^{N} \mathbf{area}_i} \left(\sum_{i=1}^{N} \mathbf{area}_i \cdot \mathbf{HU}_i \right)$$

(Figure 2.3a).

The magnitude of the nodal erosion was determined by a piece-wise linear relation between the eqHU and the applied erosion (Figure 2.3b). The direction of the nodal erosion (d_{ero}) was determined as: $$\mathbf{d}_{ero} = \sum_{i=1}^{N} \frac{1}{2} \cdot \left| \mathbf{v}_{1_i} \times \mathbf{v}_{2_i} \right| \cdot \mathbf{u}_i$$ (Figure 2.3c).

The final erosion vector (v_{ero}) was defined by the magnitude and direction of erosion:

$$\mathbf{v}_{ero} = -\frac{\text{magnitude}}{|\mathbf{d}_{ero}|} \cdot \mathbf{d}_{ero}$$

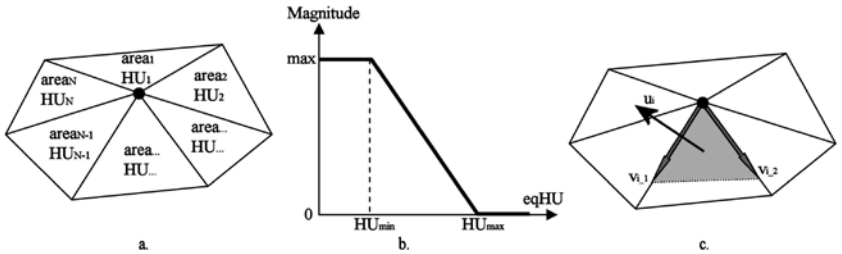

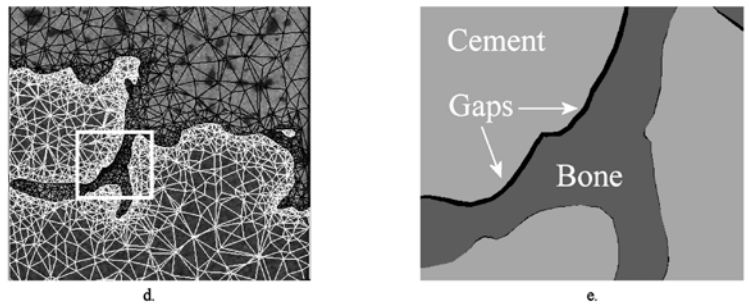

Figure 2.3
a. The parameter of 'eqHU' is dependent on the Hounsfield Units of the surrounding elements.
b. Piece-wise linear relation between eqHU and the applied erosion. The maximum erosion was set to 20µm and HUmin and HUmax to 100 and 1500, respectively.
c. Direction of nodal erosion. The unit edge lengths, v_{1_i} and v_{2_i}, were the unit element edges. The unit normal vector of the element face, u_i, was always pointing outwards.
d. The eroded solid mesh of the bone and the solid mesh of the cement plotted on top of the µCT-data.
e. Zoomed interface of figure d. with bone (dark grey), cement (light grey) and gaps (black).

The erosion procedure resulted in a new surface mesh with physical gaps at the interface. Subsequently, the eroded surface mesh was meshed in PATRAN to create a solid tetrahedron-based mesh and the average grayvalues were calculated again for each solid element in MIMICS (Figure 2.3d-e). To simulate the experimental boundary conditions and distribute the applied load gradually over the bone, a layer of homogeneous bone and a stiff top layer were manually added to the top of the bone (Figure 2.4). The resulting models of the complete bone and cement contained, on average, approximately 480,000 tetrahedral ele-

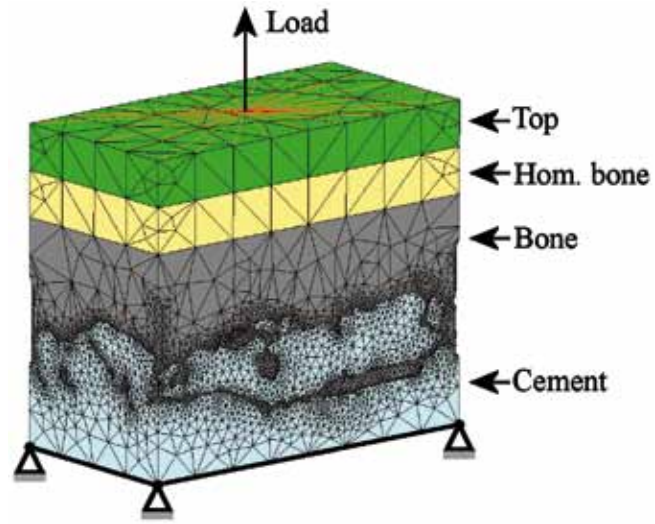

Figure 2.4 *The cement model was fixed in all three directions at the bottom plane. A tensile load, representing the applied stress in the experiment, was applied to a single node at the top plane. All other nodes in the same plane were connected to the loaded node with rigid links to prevent the top plane from tilting, while displacements in the transverse and axial direction were allowed. The top and homogeneous bone layers both had a thickness of 1mm.*

The bone and cement were considered as isotropic linear elastic materials. The bone material properties were based on the local average element gray value, which was converted to an equivalent HA-density using a calibration phantom. The elastic modulus was assumed to be linearly dependent on the equivalent HA-density[12] and resulted in bone modulus values ranging from 0.1 to 20,000MPa (ν=0.3). The cement, homogeneous bone and top layer were assumed to have constant material properties with an elastic modulus of 3,000, 20,000 and 210,000MPa, respectively (ν=0.3).

A double-sided node-to-surface contact algorithm was used to simulate contact between bone and cement. Contact was assumed to be debonded; no tensile loads could be transferred at the contact interface. Interfacial friction was modeled using a bilinear Coulomb friction model with a friction coefficient of 0.3[6,7].

Tensile fatigue loading was simulated for a total of 50,000 cycles in each model. Fatigue failure was calculated by means of a custom-written FEA algorithm that simulated separately creep and damage accumulation in the cement using a previously described method[22]. In this method, the element's deformation, {ε}, was calculated as $\{\varepsilon\}=[S]\{\sigma\}+\{\varepsilon^c\}$, in which [S] was the compliance matrix which also included the damage by locally reducing the element stiffness to zero. The creep strain tensor, $\{\varepsilon^c\}$, was determined as: $\varepsilon^c = 7.985 \cdot 10^{-7} \cdot n^{0.4113-0.116\log(\sigma)} \cdot \sigma^{1.9063}$ [24]. Both cement damage and creep was predicted based on

the local stress level, stress orientation, and number of loading cycles.
During the first increment of loading, the static displacement was calculated by mimicking the DIC-measurements from the experiments. Subsequently, the creep damage displacement (δ_{cd}) was calculated, defined here as the difference between the actual displacement and the static displacement. To account for the experimental pre-conditioning and running-in phenomena, the FE-creep damage displacement that arose in the first load cycle was ignored. The peak motion (second research question) was defined as the displacement of the bone, interface and cement at 50,000 cycles, when the specimen was maximally loaded. The crack volume fraction (V_{cr}) of the cement was also monitored during the simulation:

$$V_{cr} = \frac{1}{3 \cdot V_{tot}} \cdot \sum_{i=1}^{N_{ele}} n_i \cdot V_i$$

In this formula, V_{tot} was the total volume of the bulk cement and n_i and V_i were the number of cracks in the element and the element volume, respectively.

Linear regression analysis was used to determine relationships between the experimental and FEA creep damage displacements, experimental cement crack growth and FEA crack volume fraction, experimental cement crack growth and FEA surface cracks and experimental cement and bone cracks.

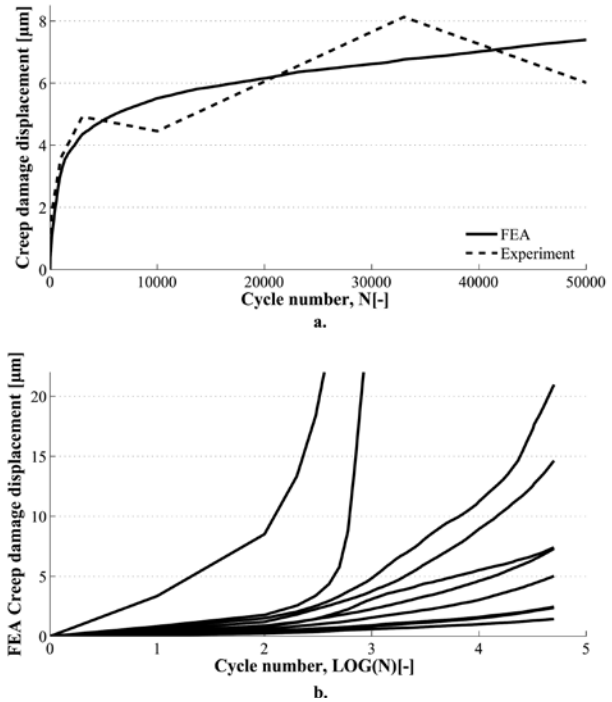

Figure 2.5 *a. FEA and Experimental creep damage displacement of specimen 5.*
b. All the ten predicted FEA creep damage responses. The FEA simulations of specimen 7 and 8 failed within 2,000 cycles. Note that the simulations predict a considerable variety in creep responses, despite variation in the applied fatigue tensile load (50% of the estimated stiffness as measured in the experiments).

Results

The interfacial creep damage displacements found in the experiments and FEA models both displayed the typical phase I and II of a creep curve (Figure 2.5a). However, there were distinct differences between the progression of interfacial creep damage displacements in the various models (Figure 2.5b). In the FEA simulations and experiments, two specimens failed (displacement>72µm); in one case this concerned the same specimen (specimen 8, Table 2.1). This specimen failed experimentally after 10,000 cycles, whereas the FEA simulation failed within 2,000 cycles . For the seven non-broken specimens, six displayed a higher final FEA interfacial creep damage displacement, while one model had a lower creep damage displacement (Table 2.1). Incorporating all the data collection points, this resulted in a moderate correlation (r^2=0.49) between FEA and experiment (Figure 2.6). However, if the results of specimen 9 would not be incorporated in this analysis, the correlation would increase to r^2=0.89.

	Creep damage displacement [µm]		Cracks in the cement	
Specimen	*Experiment*	*FEA*	*Total crack growth, Experiment [mm]*	*Crack volume fraction, FEA [%]*
1	3.1	7.3	10.68	0.31
2	4.2	5.0	1.64	0.17
3	0.7	2.5	3.03	0.09
4	2.1	2.4	4.37	0.05
5	6.0	7.4	9.27	0.18
6	14.2	21.0	5.66	0.38
7	14.9	218.9*	12.19	0.43*
8	23.4†	197.8*	2.72†	1.89*
9	11.3	1.4	8.49	0.02
10	33.5†	14.6	-1.06†	0.45

† measured at N=10,000, specimen failed afterwards
** measured at N=1,870, model failed afterwards*

Table 2.1 *Experimental and FEA interfacial creep damage displacements at N=50,000. There was a moderate correlation between these values (r^2=0.41). Relation between the total crack growth in the cement and crack volume fraction.*

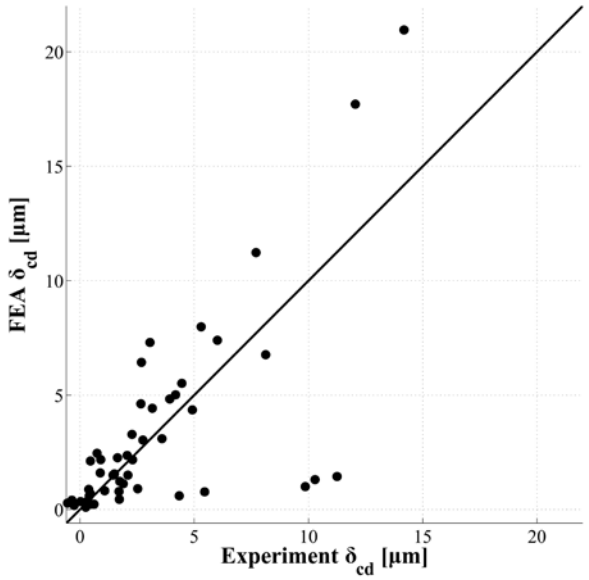

Figure 2.6 *Comparison of the FEA-predicted and experimental creep damage displacements at the various data-gathering points of the seven non-failed specimens (r^2=0.49). Note that the correlation is affected by the outliers of specimen 9; the seven measurement points parallel to the x-axis. The solid line represents 'Experiment δ_{cd}' = 'FEA δ_{cd}'.*

The experiments and FEA simulations displayed a permanent displacement at the cement-bone contact interface, which increased with time as a result of creep and crack accumulation in the cement (Figure 2.7). In most specimens, cracks were predicted to occur at locations where cracks were found in the experimental specimens (Figure 2.8). However, in the experimental specimens additional cracks were found at other locations in the cement. More cracks were predicted in models with a relatively high creep damage displacement. These simulated

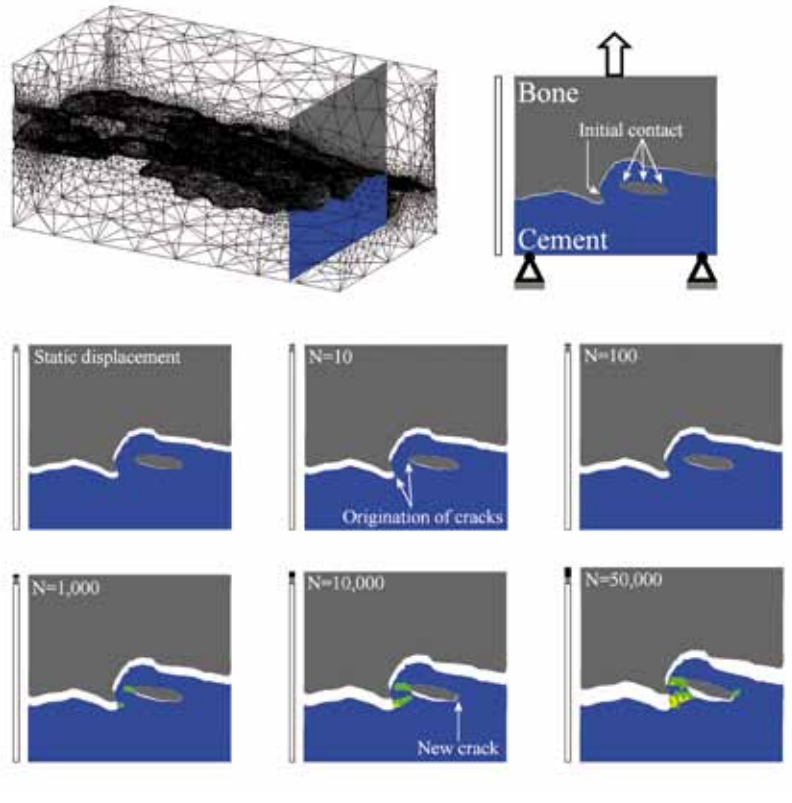

Figure 2.7 *Crack growth and deformation in a cutting plane of specimen 6. Cracks originated at the contact surface and grew into the bulk cement as the number of cycles increased. The bar next to each cutting plane presents the specimen's initial length (white), static displacement (grey) and creep damage displacement (black). The deformation scale was set to 10.*

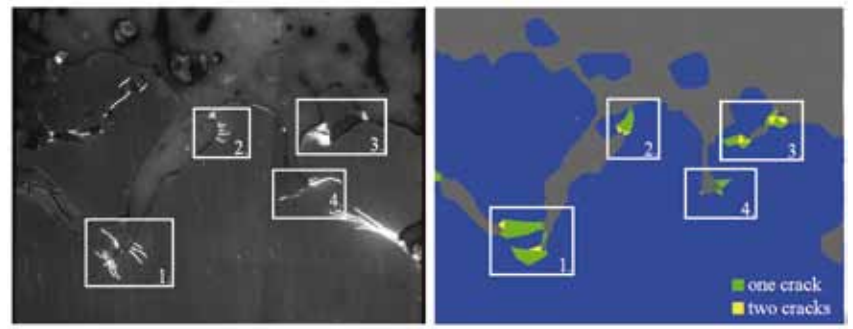

Figure 2.8 *Similarities in crack location at the surface of specimen 1 at the end of the loading history. The experiment (left) shows cracks emanating from pre-existing cracks (white) and new cracks (black). The simulation (right) shows elements with one or two cracks.*

In the experiments and in the simulations, the majority of the peak motion occurred at the contact interface. However, the experiments also showed some deformation in the bone and cement, while these deformations were negligible in the simulations (Table 2.2).

The average experimental cement crack growth and the FEA-predicted crack volume fraction of the seven non-failed specimens was 6.2mm (S.D. 3.4) and 0.17% (S.D. 0.13), respectively (Table 2.1). There appeared to be no correlation (r^2=0.06) between the experimental cement crack growth and the predicted crack volume fraction (Figure 2.9a). However, the correlation improved (r^2=0.43) when cracks generated at the surface of the FEA model were compared to the number of experimental cement crack growth (Figure 2.9b). In the experiment, cracks were also found in the bone, but to a much smaller extent (average=0.53 mm, S.D.=0.44). No correlation was found between the experimental total growth of cement and bone cracks (r^2=0.02).

	Average peak motion [µm] (S.D.)		
	Bone	*Interface*	*Cement*
Experiment	1.6 (2.8)	12.7 (5.7)	2.6 (2.8)
FEA	0.002 (0.24)	13.7 (9.62)	0.1 (0.62)

Table 2.2 *Average peak motion over the seven non-broken specimens in tension at N=50,000.*

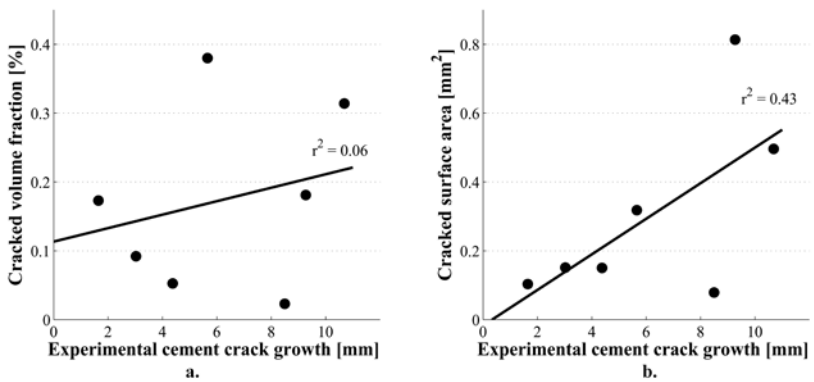

Figure 2.9 *a. Correlation between the experimental cement crack growth as measured on the surfaces of the specimens and the predicted crack volume fraction (r^2=0.06).*
b. Correlation between the experimental cement crack growth as measured on the surface of the specimens and the cracked surface area of the FEA model (r^2=0.43).

Discusion

The objective of the current study was to quantify the micromechanics of the cement-bone interface under tensile fatigue loading and determine if the fatigue creep damage response could be explained using µFEA models. The FEA modeling of the cement-bone interface was based on a newly developed erosion procedure to avoid peak stress artifacts that occurred previously[6,7]. This resulted in a gradual distributed load transfer over the contact interface. Additionally, it promoted gapping and sliding between the bone and cement.

The experimental and computational creep damage displacements both showed the typical phase I and II of the three-phase creep response. FEA simulated cracks localized at the contact interface and resulted in crack patterns similar to the experiments. Concurrent with the experiments, the majority of FEA-mesh displacement occurred at the contact interface. Only for specimen 9 the predicted displacement was much smaller than in the experiments. Analysis of the specimen's morphological parameters, FE-model and experiment could not clarify the discrepancy. Possibly, the specimen was damaged in the experiment before testing what resulted in high displacement response.

After 50,000 cycles, there appeared to be a very large variation in creep damage displacement for as well the experiments as the simulations (Table 2.1), despite the equal load-stiffness ratio for all the specimens. Therefore, the initial stiffness cannot be used as a prediction of the subsequent creep rate.

Obviously, there were limitations to both our experimental and computational study. Because the experiments were unable to capture biological phenomena, the creep damage behavior displayed would be representative of the immediate post-operative situation. Biological phenomena were also not included in the FEA simulations.

The geometrical accuracy of the FEA models was limited by the resolution of the µCT scan data. Morphological features below 12µm could therefore not be reproduced. In addition, the surface triangulation was based on an interpolation over six voxels in 3D and subsequently remeshed. However, this was necessary to reduce the computational costs.

An additional limitation of this study was that no bone damage was simulated, although the experiments did show limited crack formation in the bone. Previous studies have also demonstrated that trabecular and cortical bone do show some creep damage behavior in fatigue loading[3,16]. Bone damage was not simulated here because the phenomena of fatigue damage in bone has not been studied in sufficient detail to provide a basis for constitutive modeling[23]. Furthermore, the majority of the experimental cracks occurred in the cement rather than in the bone suggesting that our models should be able to capture most of the creep damage response seen experimentally.

The location of the cracks predicted by the FEA simulations corresponded to experimental crack locations, indicating the models were able to reproduce some of the fatigue crack formation phenomena. However, in other areas, additional cracks were found as well in the experimental specimens that were not predicted in the simulations. This discrepancy is likely due to pre-existing cracks present in the experimental specimens from polymerization

shrinkage or specimen preparation. These pre-cracks were not simulated because of lack of experimental guidance on distribution of pre-cracks in 3D.

There was a moderate correlation between the experimental total crack growth and the FE crack growth at the surfaces of the specimen for the seven specimens that did not fail, suggesting a reasonable validation of these types of models in terms of micro-crack predictions. The simulated cracked area of the outer surface was weakly correlated with the simulated crack volume fraction inside the simulated specimens (r^2=0.21). Hence, this indicates that the interpretation of surface crack measurements as typically done in experiments towards internal (volumetric) material damage is precarious. In addition, there appeared no correlation between the experimental creep damage displacement and the experimental total crack growth of the cement (r^2=0.07), while a strong correlation existed between the simulated creep damage displacement and the calculated crack volume fraction (r^2=0.76). This also emphasizes the importance of considering the total volumetric morphology, rather than relying solely on surface measurements.

From a clinical perspective, these results suggest that damage to the cement-bone interface from tensile fatigue loading will localize to the contact interface, thereby increasing micro-motion locally between the cement and bone. Greater amounts of creep damage displacement at the contact interface will also be associated with more localized damage to the cement in terms of cement cracking. Minimizing cement damage at the contact interface could reduce risk of failure of these interfaces and improve outcomes of cemented joint replacement procedures.

In conclusion, (1) non-linear micro-FEA models that incorporate the morphology of the contact interface, include friction of the interface, and allow for cement creep and cement damage due to fatigue loading can to a reasonable extent predict fatigue crack patterns similar to experimental findings, and are able to capture the general creep damage behavior of the cement-bone interface; (2) The majority of the motion took place at the contact interface, both in the experiments and in the FEA models; (3) There is no relationship between the experimental total length of cement crack growth found at the interface and the crack volume fraction in the FEA models, although there is a moderate correlation between experimental total length of cement cracks and FEA cracked area on the cement surface. Additionally, there is a strong relationship between the FEA creep damage displacement and the crack volume fraction calculated in FEA.

Acknowledgements

This work was funded by the NIH grant AR42017.

References

1. **Arola, D., Stoffel, K. A., Yang, D. T., (2006).**
Fatigue of the cement/bone interface: the surface texture of bone and loosening. J.Biomed.Mater.Res.B Appl.Biomater. 76, 287-297.
2. **Bean, D. J., Convery, F. R., Woo, S. L., Lieber, R. L., (1987).**
Regional variation in shear strength of the bone-polymethylmethacrylate interface. J.Arthroplasty 2, 293-298.
3. **Cotton, J. R., Winwood, K., Zioupos, P., Taylor, M., (2005).**
Damage rate is a predictor of fatigue life and creep strain rate in tensile fatigue of human cortical bone samples. J.Biomech.Eng 127, 213-219.
4. **Gardiner, R. C., Hozack, W. J., (1994).**
Failure of the cement-bone interface. A consequence of strengthening the cement-prosthesis interface? J.Bone Joint Surg.Br. 76, 49-52.
5. **Huiskes, R., (1993).**
Failed innovation in total hip replacement. Diagnosis and proposals for a cure. Acta Orthop.Scand. 64, 699-716.
6. **Janssen, D., Mann, K. A., Verdonschot, N., (2008).**
Micro-mechanical modeling of the cement-bone interface: The effect of friction, morphology and material properties on the micromechanical response. J.Biomech. 41, 3158-3163.
7. **Janssen, D., Mann, K. A., Verdonschot, N., (2009).**
Finite element simulation of cement-bone interface micromechanics: a comparison to experimental results. J.Orthop.Res. 27, 1312-1318.
8. **Jasty, M., Maloney, W. J., Bragdon, C. R., O'Connor, D. O., Haire, T., Harris, W. H., (1991).**
The initiation of failure in cemented femoral components of hip arthroplasties. J.Bone Joint Surg.Br. 73, 551-558.
9. **Kim, D. G., Miller, M. A., Mann, K. A., (2004).**
A fatigue damage model for the cement-bone interface. J.Biomech. 37, 1505-1512.
10. **Kim, D. G., Miller, M. A., Mann, K. A., (2004).**
Creep dominates tensile fatigue damage of the cement-bone interface. J.Orthop.Res. 22, 633-640.
11. **Lennon, A. B., Britton, J. R., MacNiocaill, R. F., Byrne, D. P., Kenny, P. J., Prendergast, P. J., (2007).**
Predicting revision risk for aseptic loosening of femoral components in total hip arthroplasty in individual patients--a finite element study. J.Orthop.Res. 25, 779-788.
12. **Lotz, J. C., Gerhart, T. N., Hayes, W. C., (1991).**
Mechanical properties of metaphyseal bone in the proximal femur. J.Biomech. 24, 317-329.
13. **Mann, K. A., Ayers, D. C., Werner, F. W., Nicoletta, R. J., Fortino, M. D., (1997).**
Tensile strength of the cement-bone interface depends on the amount of bone interdigitated with PMMA cement. J.Biomech. 30, 339-346.
14. **Mann, K. A., Miller, M. A., Cleary, R. J., Janssen, D., Verdonschot, N., (2008).**
Experimental micromechanics of the cement-bone interface. J.Orthop.Res. 26, 872-879.

15. **Mann, K. A., Miller, M. A., Race, A., Verdonschot, N., (2009).**
Shear fatigue micromechanics of the cement-bone interface: An in vitro study using digital image correlation techniques. J.Orthop.Res. 27, 340-346.
16. **Michel, M. C., Guo, X. D., Gibson, L. J., McMahon, T. A., Hayes, W. C., (1993).**
Compressive fatigue behavior of bovine trabecular bone. J.Biomech. 26, 453-463.
17. **Moreo, P., Perez, M. A., Garcia-Amar, J. M., Doblare, M., (2006).**
Modelling the mixed-mode failure of cement-bone interfaces.
Engineering Fracture Mechanics 73, 1379-1395.
18. **Race, A., Miller, M. A., Ayers, D. C., Mann, K. A., (2003).**
Early cement damage around a femoral stem is concentrated at the cement/bone interface. J.Biomech. 36, 489-496.
19. **Stoffel, K. A., Yang, D. T., Arola, D., (2008).**
The influence of surface topography on wear debris generation at the cement/bone interface under cyclic loading. J.Mater.Sci.Mater.Med. 19, 1935-1943.
20. **Stolk, J., Janssen, D., Huiskes, R., Verdonschot, N., (2007).**
Finite element-based preclinical testing of cemented total hip implants.
Clin. Orthop.Relat Res. 456, 138-147.
21. **Stolk, J., Verdonschot, N., Mann, K. A., Huiskes, R., (2003).**
Prevention of mesh-dependent damage growth in finite element simulations of crack formation in acrylic bone cement. J.Biomech. 36, 861-871.
22. **Stolk, J., Verdonschot, N., Murphy, B. P., Prendergast, P. J., Huiskes, R., (2004).**
Finite element simulation of anisotropic damage accumulation and creep in acrylic bone cement. Engineering Fracture Mechanics 71, 513-528.
23. **Stolken, J. S., Kinney, J. H., (2003).**
On the importance of geometric nonlinearity in finite-element simulations of trabecular bone failure. Bone 33, 494-504.
24. **Verdonschot, N., Huiskes, R., (1995).**
Dynamic creep behavior of acrylic bone cement. J.Biomed.Mater.Res. 29, 575-581.
25. **Verdonschot, N., Huiskes, R., (1996).**
Mechanical effects of stem cement interface characteristics in total hip replacement.
Clin.Orthop.Relat Res. 326-336.
26. **Zant, N. P., Heaton-Adegbile, P., Hussell, J. G., Tong, J., (2008).**
In vitro fatigue failure of cemented acetabular replacements: a hip simulator study.
J.Biomech.Eng 130, 021019.

Chapter 3

The effect of cement creep and cement fatigue damage on the micromechanics of the cement-bone interface

Journal of Biomechanics
(2010); 43(15):3028-34

Abstract

The cement-bone interface provides fixation for the cement mantle within the bone. The cement-bone interface is affected by fatigue loading in terms of fatigue damage, or micro cracks, and creep, both mostly in the cement. This study investigates how fatigue damage and cement creep separately affect the mechanical response of the cement-bone interface at various load levels in terms of plastic displacement and crack formation. Two FEA models were created, which were based on micro-computed tomography data of two physical cement-bone interface specimens. These models were subjected to tensile fatigue loads with four different magnitudes. Three deformation modes of the cement were considered; '*only creep*', '*only damage*' or '*creep and damage*'. The interfacial plastic deformation, the crack reduction as a result of creep and the interfacial stresses in the bone were monitored. The results demonstrate that, although some models failed early, the majority of plastic displacement was caused by fatigue damage, rather than cement creep. However, cement creep does decrease the crack formation in the cement up to 20%. Finally, while cement creep hardly influences the stress levels in the bone, fatigue damage of the cement considerably increases the stress levels in the bone. We conclude that at low load levels the plastic displacement is mainly caused by creep. At moderate to high load levels, however, the plastic displacement is dominated by fatigue damage and is hardly affected by creep, although creep reduced the number of cracks in moderate to high load region.

Introduction

The cement-bone interface provides fixation for cemented implants within bone. The interface is formed during polymethymethacrylate (PMMA) cement injection, when the cement is pressurized into the bone cavities. This results in a highly variable interlock between the bone and cement with a complex morphology and mechanical properties[15,16,30]. Experiments with cement-bone interface specimens have shown that the interface degrades over time by fatigue loading[7,17,29,31]. Under the influence of dynamic loading, creep and fatigue damage occurs in the cement and bone, causing a reduced stiffness and increased motion at the interface. Furthermore, experiments have shown that creep and fatigue cracking at the cement-bone interface occur mainly in the cement, rather than in the bone[8,17,29,31].

Studies on the creep behaviour of PMMA bulk cement have indicated that creep effectively attenuates stress peaks in the cement mantle[13,22,27], which reduces fatigue cracking of the cement. Since it is experimentally impossible to delineate how creep and fatigue damage interact at the cement-bone interface it is unknown which one affects the interface integrity the most. Finite Element Analysis (FEA) make this possible, but numerical studies in which fatigue failure of the cement-bone interface was investigated have not studied the relatively contribution of creep and fatigue damage[23,29].

In the current study, we assessed the relative effect of creep and fatigue in micromechanical FEA-models of cement-bone interface specimens and tried to answer the following questions: (1) How do cement creep and cement fatigue damage independently affect the micromechanical response of the cement-bone interface at various load levels, and how do these two phenomena interact in a combined model?; (2) Does cement creep influence fatigue crack formation in the cement? (3) How do cement creep, cement fatigue damage or a combination of both affect the stress levels in the bone?

Methods

Two rectangular-prism shaped FEA-models (~8x4x8mm^3) were created using micro-CT scans (12µm isotropic resolution) of two physical cement-bone interface specimens that were sectioned from laboratory-prepared cemented total hip replacements[29]. Each model comprised two components, bone and cement (Figure 3.1), and the two models had substantial differences regarding bone morphology. The bone model comprised the bony tissue of the cement-bone interface, the interfacial gaps and lacunar spaces. A voxel mesh of the bone model was automatically created by segmentation of the micro-CT data using MIMICS 11.0 (Materialise, Leuven, Belgium), based on the image grey scales, which ranged from -1,000 to 3,071 (bone 1,000 to 3,071; gaps -1,000 to 100)[6]. Grooves that were not selected during the first segmentation were segmented manually. Next, a triangular surface mesh was generated from the voxel mesh using a 6x6x6 voxel reduction with smoothing[9]. The smoothed meshes were assessed on their accuracy in which deficiencies were solved manually. The surface mesh was subsequently converted to a tetrahedral 3D solid mesh (PATRAN 2005r2, MSC Software

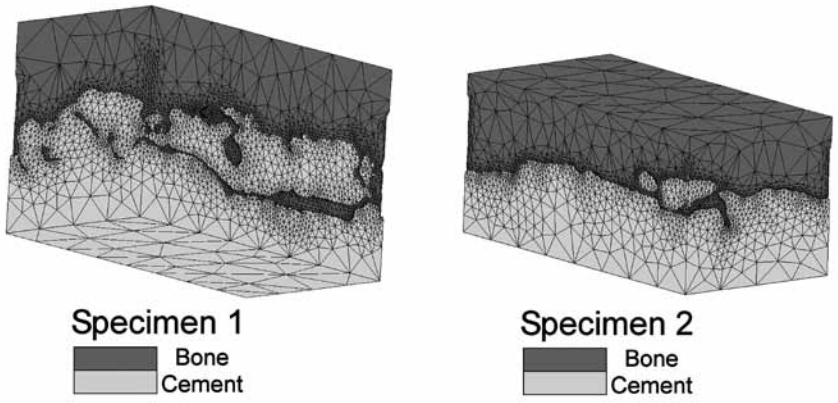

Figure 3.1 *The two cement-bone specimens were created from micro-CT data sets of laboratory-prepared cemented proximal femurs. Cement penetration into the bone varied over the two models; 2.2mm and 1.7mm for model 1 and model 2, respectively[28]. A tensile fatigue load was applied to one of the nodes in the top plane of the bone. All the other nodes in that particular plane were tied to that node to prevent the plane from tilting. The bottom of the cement was fixed.*

Corporation, Santa Ana, CA, USA) and mapped back into the micro-CT data, after which the weighted average of the grey scale was calculated for each element. Subsequently, an erosion algorithm was applied to the solid mesh to model the interfacial gaps between the bone and the cement[29]. The morphology of the cement was based on the non-eroded mesh of the bone.

The contact interface between the bone and cement was assumed to be unbonded[4,6,14]. Frictional contact between the bone and cement was modelled using a double-sided node-to-surface algorithm (MSC Marc 2007r1, MSC Software Corporation, Santa Ana, CA, USA) with a friction coefficient of 0.3[5]. In total, specimen 1 consisted of 462,102 elements and 109,568 nodes while specimen 2 consisted of 219,664 elements and 53,499 nodes.

The initial material properties of the bone and cement were considered to be linear elastic[10]. The averaged grey values of the bone elements were converted to HA-density values using a calibration phantom. Although some large BaSO4 particles resulted in local beam hardening artefacts in the cement, this did not affect the grey values in the bone. The Young's modulus (E) was assumed to be linearly dependent on the HA-density[12], resulting in Young's moduli ranging from 0.1 to 20,000MPa. The cement was assumed to have a constant Young's modulus of 3,000MPa[11]. The Poisson's ratio was set to 0.3 for both the bone and the cement.

Both specimens were virtually loaded for a total of 50,000 cycles, with an assumed

frequency of 1Hz, at four different tensile fatigue load levels: 0.1, 0.5, 1.0 and 2.0MPa. By means of a custom written FEA-algorithm that separately simulated fatigue damage and creep to the cement[25], we were able to simulate the time dependent behaviour of the cement. The bone was assumed to remain unimpaired, since previous studies have demonstrated that the majority of the damage occurs in the cement and not in the bone[17,29]. For each load level, we simulated either '*only fatigue damage*', '*only creep*', or both '*creep and fatigue damage*' occurring to the cement (total of 24 simulations).

The utilized FEA-algorithm[25] calculated the element deformation, {ε}, as: {ε}=[S]{σ}+{ε^c}. Fatigue damage was implemented in the compliance matrix [S] in which for each of the three principal stress directions a damage parameter (D) indicated whether an element was cracked (D=1). A crack was simulated by locally reducing the stiffness to 0.1MPa perpendicular to the corresponding maximum principal stress direction. Damage was calculated as:

$$D = \left(\frac{n}{Nf}\right)^{3.92}$$

where 0≤D≤1 in which n and Nf were the number of loading cycles and the fatigue life, respectively. The fatigue life (Nf) was determined based on the maximum principal stress:

$$\sigma = -4.736\log(Nf) + 37.8$$

Creep was implemented in the creep strain tensor {ε^c} which was dependent on the scalar {ε} defined as: $\varepsilon^c = 7.985\cdot10^{-7}.n^{0.4113-0.116\log(\sigma)}.\sigma^{1.9063}$ [24 26]

For each model the plastic displacement was determined to study the effect of creep and damage in the interface deformation. The plastic displacement was defined as the difference between the total displacement and elastic displacement. If the plastic displacement exceeded 0.1mm the interface was assumed to be failed[29].

During the simulations the total crack volume (V_{cr})of the cement was monitored. The total crack volume was defined as the ratio between total volume of cracked elements and the total cement volume:

$$V_{cr} = \frac{1}{3\cdot V_{tot}} \cdot \sum_{i=1}^{N_{els}} n_i \cdot V_i$$

In this definition V_{tot}, n_i and V_i were the total volume of the bulk cement, the number of cracks in each element {0≤n_i≤3} and the element volume, respectively.

To assess whether cement creep influences fatigue crack formation in the cement, the total crack volumes of the '*only damage*' and '*creep and damage*' were compared. For each load the reduction of cracks by creep was determined by:

$$\left(1 - \frac{V_{cr\&dam}}{V_{dam}}\right) \cdot 100\%$$

The stress levels in the bone were determined for the 0.1 and 1.0MPa loads of specimen 1, and the 0.1 and 0.5MPa loads for specimen 2. Different maximum stress levels for specimen 1 and 2 were chosen, since specimen 1 was approximately twice as stiff as specimen 2[29]. At the beginning and at the end of the simulation, Von Mises stresses were determined only for the group of elements that lied at the contact interface (Figure 3.2). All the stresses were normalized for this group of elements by dividing by the applied apparent stress, $\frac{\sigma_{VM}}{\sigma_{app}}$.

Subsequently, the normalized stresses were divided in 20 groups ranging from 0≤ $\frac{\sigma_{VM}}{\sigma_{app}}$ ≤10 [-] and one group $\frac{\sigma_{VM}}{\sigma_{app}}$ >10 [-].

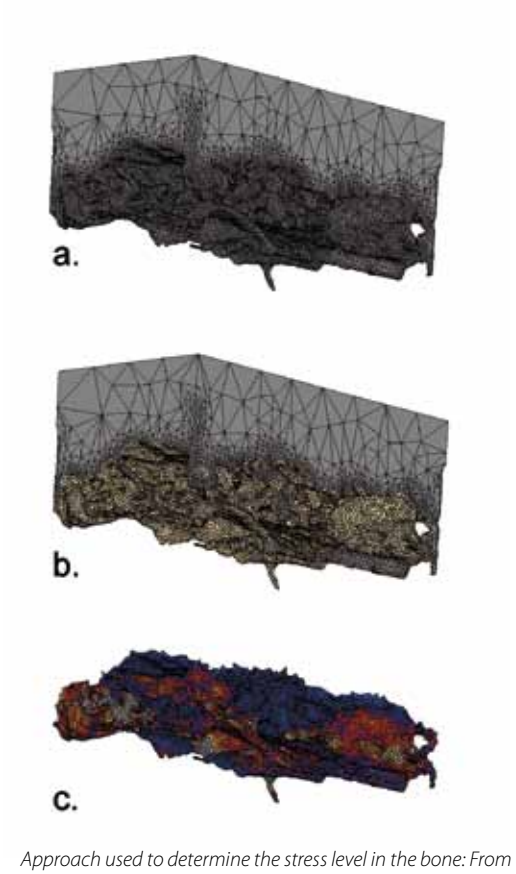

Figure 3.2 *Approach used to determine the stress level in the bone: From the bone model (a) all the nodes at the bone-cement contact interface were identified and the elements that shared one of the selected nodes was selected (b). The Von Mises stresses in those elements (c) were subsequently normalized by dividing them by the applied apparent stress,* $\frac{\sigma_{VM}}{\sigma_{app}}$

Results

There was a wide range of responses from the 24 tension fatigue simulations (Figure 3.3). Six simulations led to early failure of the specimens (plastic displacement>0.1mm). With the exception of the failed specimens, all the simulations showed the first two stages of the classical three-phase creep response. All simulations in which '*only creep*' was considered as a plastic deformation mode did not result in failed specimens.

For the specimens that were subjected to a 0.1MPa apparent load, creep was over the long term (N=50,000) the dominant factor in the time dependent plastic displacement (Figure 3.3, 3.4). At the higher load levels, damage contributed much more to interface deformation than creep. Simulations that included '*creep and fatigue damage*' always resulted in the greatest plastic displacement.

Figure 3.3

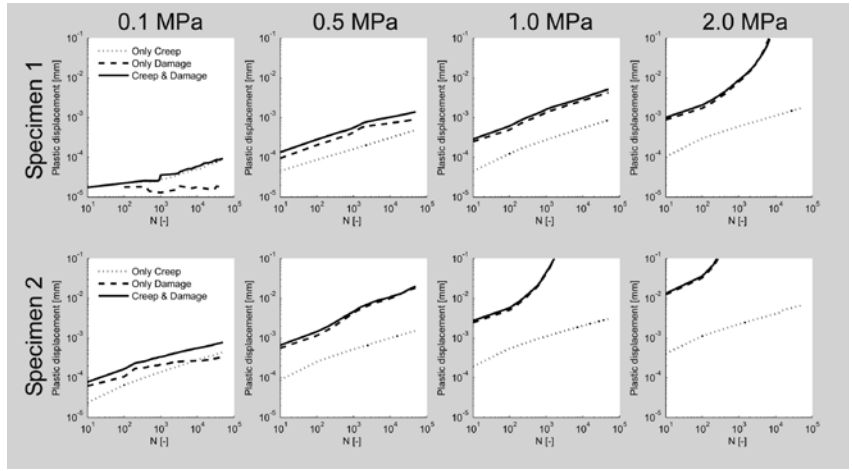

Tensile fatigue responses of all 24 simulations. With the exception of the failed specimens (plastic displacement > 0.1mm) all simulations showed a logarithmic behaviour in which the simulations with 'creep and damage' always resulted in the highest plastic displacement.

Figure 3.4

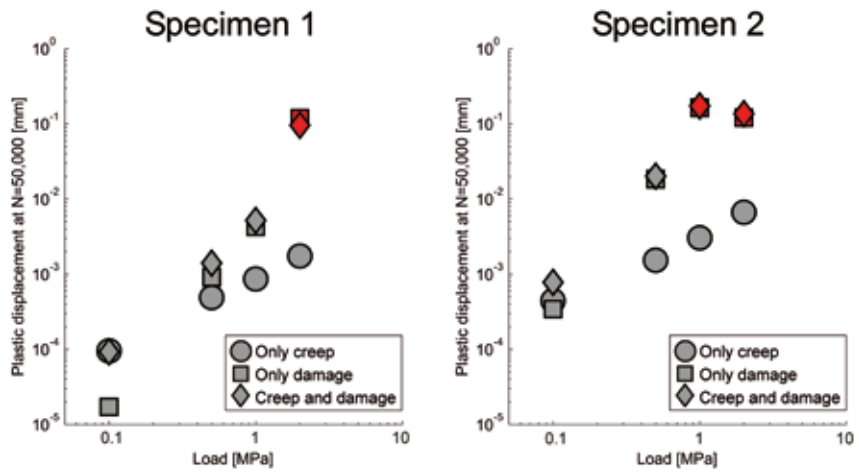

Plastic displacement at N=50,000 load cycles. Red markers indicate that the specimen failed before reaching N=50,000 load cycles. While specimen 1 only failed with a 2.0MPa apparent load, specimen 2 failed as well at 1.0 as at 2.0MPa. The simulations in which 'only creep' was considered remained intact.

Creep considerably reduced the formation of cracks in the cement (Figure 3.5). At N=50,000, the crack volume was reduced up to 20% with respect to the situation in which damage was considered to be the only deformation mode. Due to the low amount of cement damage, the simulations at a 0.1MPa load showed a very inconsistent response.

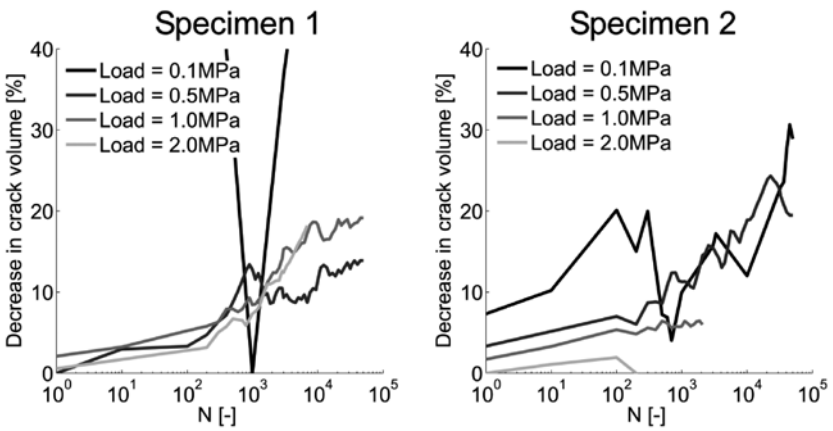

Figure 3.5 *The progression of decrease in cement crack volume due to cement creep in time (number of loading cycles) for both specimens. When 'creep and damage' were considered as deformation modes, the crack volume was reduced up to 20% with respect to 'only damage' situation. The unsteady response of the 0.1MPa simulations can be explained by the very low crack volume that occurred in the 'only damage' and 'creep and damage' response. For this stress level, a small change in crack volume resulted in relatively large decreases in crack volume. When specimen 2 was loaded to 2.0MPa, there was a very small effect of cement creep. However, at this load the specimen also failed in less than 200 loading cycles (Figure 3.3).*

There were distinct differences in Von Mises stresses in the bone. Directly after loading with an apparent stress of 0.1MPa, ~88% and ~80% of the total interface volume had a $\frac{\sigma_{VM}}{\sigma_{app}} \leq 1$, for specimen 1 and 2, respectively (Figure 3.6). When loaded to higher load levels, the relative stresses at the bony interface were much higher. When specimen 1 was loaded to 1.0MPa, ~35% of the interface volume had a $\frac{\sigma_{VM}}{\sigma_{app}} \leq 1$ and ~11% a $\frac{\sigma_{VM}}{\sigma_{app}} > 10$. When specimen 2 was loaded to 0.5MPa, ~53% of the interface volume had a $\frac{\sigma_{VM}}{\sigma_{app}} \leq 1$ and ~10% a $\frac{\sigma_{VM}}{\sigma_{app}} > 10$.

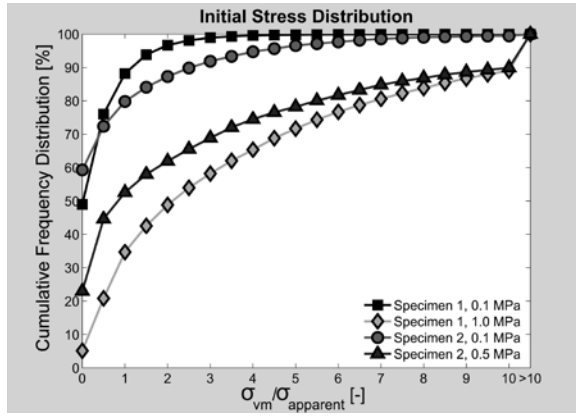

Figure 3.6 *Cumulative frequency distribution for $\frac{\sigma_{VM}}{\sigma_{app}}$ in the bone directly after loading (N=1) with different apparent stresses for specimen 1 and specimen 2. An apparent stress of 0.1 MPa resulted in ~88% and ~80% interface volume with $\frac{\sigma_{VM}}{\sigma_{app}} \leq 1$ for specimen 1 and specimen 2, respectively. When the two specimens were loaded to higher load levels, more than 10% of the total interface volume had a normalized stress of $\frac{\sigma_{VM}}{\sigma_{app}} > 10$.*

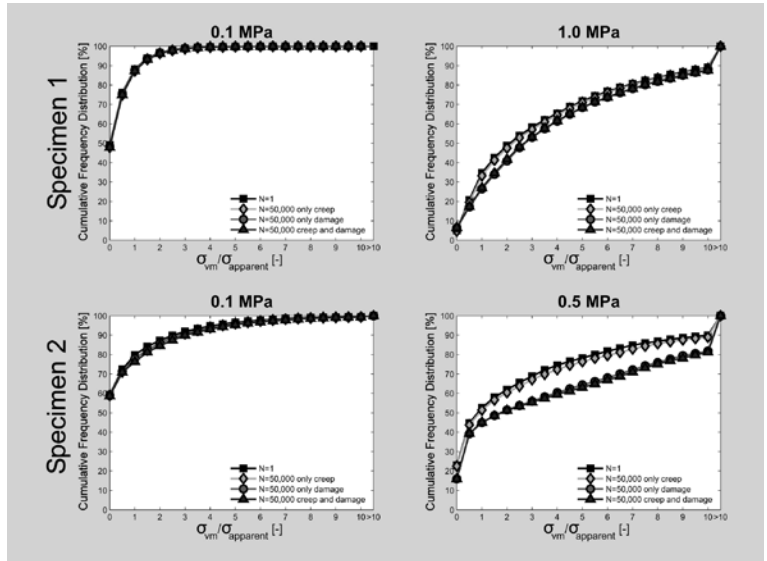

Figure 3.7 *Cumulative frequency distribution for $\frac{\sigma_{VM}}{\sigma_{app}}$ in the bone. When specimen 1 and specimen 2 were loaded to 0.1 MPa, the bone stress level hardly changed after 50,000 load cycles as a result of its deformation mode. When loaded to higher stress levels both specimens showed a decrease in low bone stresses, $\frac{\sigma_{VM}}{\sigma_{app}} \leq 1$. Furthermore, it shows that cement fatigue damage results in higher stresses in the bone and that cement creep has limited effect on the stress level.*

When loaded to 0.1MPa, cement creep and or fatigue damage had limited influence on the bone stress level for specimen 1 and specimen 2 after N=50,000 (Figure 3.7). However, when the specimens were subjected to higher loads there was a decrease in the volume with relative low bone stresses, $\frac{\sigma_{VM}}{\sigma_{app}}$ <1 and increase the volume with relative high bone stresses, $\frac{\sigma_{VM}}{\sigma_{app}}$ >1(Figure 3.7). While the situations in which '*only creep*' was considered showed minor increases in bone stress level compared to the initial bone stress level (N=1), fatigue damage resulted in a considerable increase in bone stress level. Comparison of the '*creep and damage*' with the '*only damage*' situations showed limited differences between the two; this demonstrates the minor influence of creep on the bone stress level (Figure 3.8).

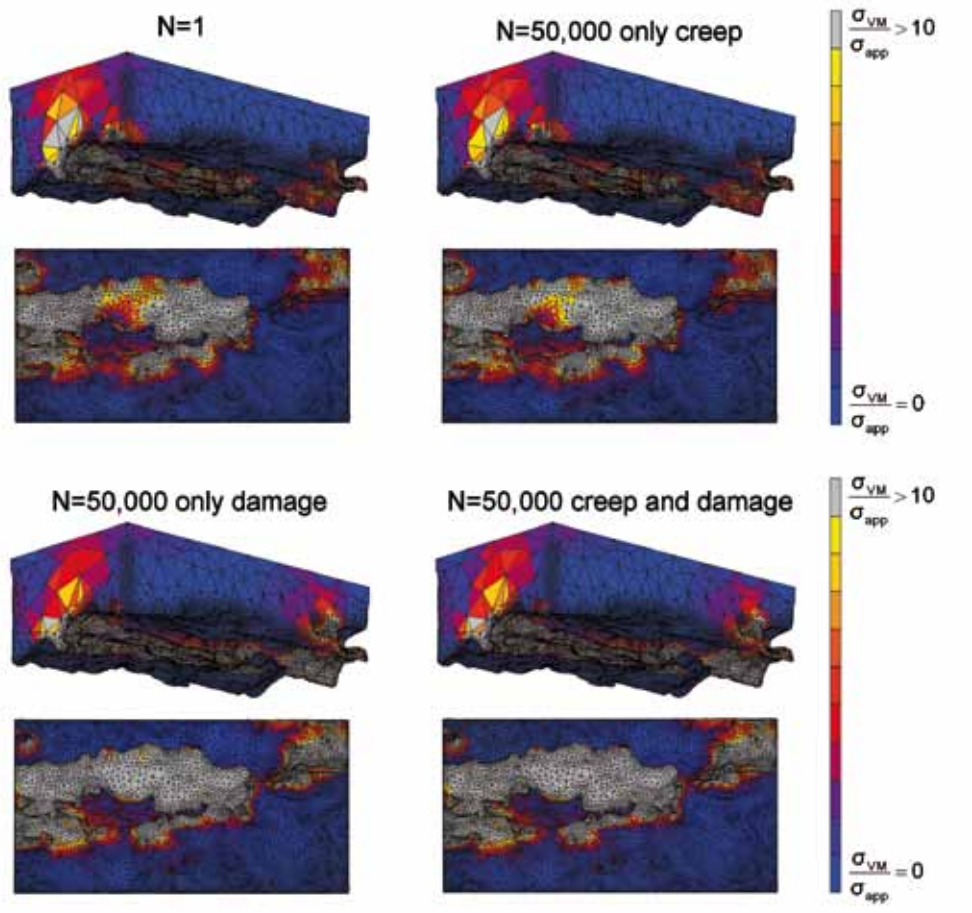

Figure 3.8 *Stress level patterns in the bone of specimen 2 loaded with 0.5 MPa.*

Discussion

In the current study we sought to gain insight in the relative contributions of cement creep and cement fatigue crack formation on the cement damage and micromechanical response of the cement-bone interface. We used these two deformation modes to study the consequences on the cement-bone interfacial plastic deformation, crack formation in the cement and interfacial stress levels in the bone.

Our results show that at almost all load levels, the majority of the time dependent plastic displacement found at the cement-bone interface was due to the formation of fatigue cracks which arose at the contact interface and subsequently progressed further into the bulk cement. When subjected to low stresses, however, the relative contribution of creep increased. The combined models in which both creep and fatigue cracking were simulated showed that creep had virtually no additional effect on the plastic response of the interface compared to the case with simulated cement fatigue cracking only.

Although the effect on the deformation of the interface was minimal, creep did reduce fatigue crack formation. The extent of this effect depended both on stress level and specimen morphology, but was most effective at lower stress levels since high stresses resulted in early failure of the specimen not giving creep the opportunity to decrease the crack formation effectively. This suggests that at higher external stresses, creep is not capable of relieving peak cement stresses to such an extent that fatigue crack formation is attenuated.

Fatigue cracking of the cement increased the stresses in the bone at the interface, while cement creep did not appear to have a considerable effect on bone stresses. Most likely the load transfer was altered due to cement cracking, enabling loads to be transferred over a different contact area, thereby increasing local bone stresses. Regardless, the increase of high stresses in the bone, the cracking of the cement will also reduce the global stiffness of the cement-bone interface[17,29]. This, subsequently, results in large motions at the cement-bone interface (Figure 3.3) and of the complete cement mantle within the femur[18].

While cement creep was able to reduce the number of fatigue cracks in the cement, it was not capable of reducing the stresses near the cement-bone interface. In contrast, previous studies have shown that creep does reduce the stresses at the stem-cement interface[13,22] and in the cement mantle[27]. Several phenomena might explain this discrepancy. First of all, the bone stresses might remain rather high due to the morphology of the cement-bone interface which is much more convoluted than the stem-cement interface in terms of more interfacial gaps[20], less relative contact area[16] and higher interdigitation[6]. This might subsequently result in much higher peak stresses in the cement which is more sensitive to cracking than creeping[25]. Cement cracking as a dominant failure type can also be seen at other convoluted interfaces such as the stem-cement interface where there is much more wear debris after debonding for rough stems than for polished stems[24]. Besides the physical morphology, the applied boundary conditions might also be responsible for the fact that the bone stresses did not reduce as a consequence of creep. In the current study, a constant apparent stress was applied which remained constant during the whole situation, basically not giving the local stresses the opportunity to decrease to zero. If initially a fixed displacement would have been applied, which would have been remained constant during the whole simulation, stresses would be able to spread and level out in time. Moreover, in the studies of Lu and McKellop (1997) and Verdon-

schot and Huiskes (1997) the stresses were analyzed utilizing models of complete cemented hip reconstructions. In contrast to the current micro models of the cement-bone interface, complete models of cemented hip reconstructions have restrictions in deformation of the interface. This makes stresses able to redistribute in time[21], due to for example creep.

Our study was limited with respect to material property assumptions, external loads, and interface morphology. The utilized FEA-models were idealized and focussed on the in-vitro failure of the cement-bone interface, hence biological responses were not considered, what is in conflict to what happens in-vivo[3,18,20]. The creep and fatigue properties were used for a single type of PMMA cement only, while the creep and fatigue damage response may vary over the different types of bone cements that are currently available on the orthopaedic market. Trabecular bone that is subjected to cyclic loads also shows fatigue damage[1,2]. However, since previous experiments have demonstrated that bone fatigue cracking was much lower in magnitude compared to cement damage[17,29], this was not simulated. How fatigue damage in the bone could affect the simulated plastic deformation in the cement bone interface is unknown. The plastic deformation could simply increase, but on the other hand, the stresses at the contact interface could also be distributed more evenly, resulting in less fatigue damage. In addition, although the effect of different load levels was analyzed, the models were loaded in the tensile direction only. Whether in shear the same quantitative findings would be obtained is unknown. Previous studies have shown that different loading directions can result in different mechanical responses, such as crack patterns[17,19,21,29,31]. Finally, only two interface morphologies were included in the current study. However, as previous studies have indicated that the micromechanical response depends on interface morphology (e.g. contact area, cement penetration depth)[16,28], we chose two specimens with substantial morphological differences. In-vivo phenomena that would influence the morphology of the cement-bone interface were also accounted for, since during the generation of the cement-bone interface specimens in-vivo conditions, like endosteal bleeding, were reproduced[16]. The thickness of the cement mantle adjacent to the cement-bone interface was modelled by a 1.0mm thick layer of cement at the bottom of the FEA-models. However, the adjacent layer of cement has negligible effects on the mechanical fatigue response of the cement-bone interface[17,29].

The current study is unique in the sense that cement creep and fatigue damage were separated to study their relative contributions to the micromechanical response of the cement-bone interface subjected to repetitive loads. The current results may be useful in the synthesis of new bone cement formulations. For instance, our finding that fatigue crack formation is responsible for the majority of the plastic deformation of the cement-bone interface indicates that, if one is interested in improving the dynamic response of the interface, the fatigue properties of cement should be improved upon, rather than modifying the creep properties. Moreover, improved fatigue resistance of the cement may confine the increase of interfacial stresses. If the goal is to reduce the quantity of fatigue cracks in the cement, one could consider modifying the cement to allow more creep.

Based on the findings in the current study we conclude that: (1) When the cement-bone interface is subjected to low stresses, the plastic interface displacement is mostly caused by cement creep, while at higher loads cement fatigue cracking is unambiguously the dominant factor; (2) cement creep is able to decrease the crack formation in the cement up to 20%; and (3) cement creep is not capable of decreasing the stress levels in the bone with respect to the initial state and cement fatigue damage only results in an increase in bone stresses.

Acknowledgements

This work was funded by the NIH grant AR42017.

References

1. **Cotton, J. R., Winwood, K., Zioupos, P., Taylor, M., (2005).**
   Damage rate is a predictor of fatigue life and creep strain rate in tensile fatigue of human cortical bone samples. J.Biomech.Eng 127, 213-219.
2. **Dendorfer, S., Maier, H. J., Hammer, J., (2009).**
   Fatigue damage in cancellous bone: an experimental approach from continuum to micro scale. J.Mech.Behav. Biomed. Mater. 2, 113-119.
3. **Gardiner, R. C., Hozack, W. J., (1994).**
   Failure of the cement-bone interface. A consequence of strengthening the cement-prosthesis interface? J.Bone Joint Surg.Br. 76, 49-52.
4. **Goto, K., Kawanabe, K., Kowalski, R., Baker, D., Nakamura, T., (2010).**
   Bonding ability evaluation of bone cement on the cortical surface of rabbit's tibia. J.Mater.Sci.Mater.Med. 21, 139-146.
5. **Janssen, D., Mann, K. A., Verdonschot, N., (2008).**
   Micro-mechanical modeling of the cement-bone interface: The effect of friction, morphology and material properties on the micromechanical response. J.Biomech. 41, 3158-3163.
6. **Janssen, D., Mann, K. A., Verdonschot, N., (2009).**
   Finite element simulation of cement-bone interface micromechanics: a comparison to experimental results. J.Orthop.Res. 27, 1312-1318.
7. **Kim, D. G., Miller, M. A., Mann, K. A., (2004).**
   A fatigue damage model for the cement-bone interface. J.Biomech. 37, 1505-1512.
8. **Kim, D. G., Miller, M. A., Mann, K. A., (2004).**
   Creep dominates tensile fatigue damage of the cement-bone interface. J.Orthop.Res. 22, 633-640.
9. **Leung, S. Y., Browne, M., New, A. M., (2008).**
   Smooth surface micro finite element modelling of a cancellous bone analogue material. Proc.Inst.Mech Eng H 222, 145-149.
10. **Leung, S. Y., New, A., Browne, M., (2006).**
    Modelling the mechanics of the cement-bone interface. J.Biomech. 39, S515.
11. **Lewis, G., (1997).**
    Properties of acrylic bone cement: state of the art review. J.Biomed.Mater.Res. 38, 155-182.
12. **Lotz, J. C., Gerhart, T. N., Hayes, W. C., (1991).**
    Mechanical properties of metaphyseal bone in the proximal femur. J.Biomech. 24, 317-329.
13. **Lu, Z., McKellop, H., (1997).**
    Effects of cement creep on stem subsidence and stresses in the cement mantle of a total hip replacement. J.Biomed.Mater.Res. 34, 221-226.
14. **Lucksanasombool, P., Higgs, W. A., Ignat, M., Higgs, R. J., Swain, M. V., (2003).**
    Comparison of failure characteristics of a range of cancellous bone-bone cement composites. J.Biomed.Mater.Res.A 64, 93-104.
15. **Maher, S. A., McCormack, B. A., (1999).**
    Quantification of interdigitation at bone cement/cancellous bone interfaces in cemented femoral reconstructions. Proc.Inst.Mech Eng H 213, 347-354.
16. **Mann, K. A., Miller, M. A., Cleary, R. J., Janssen, D., Verdonschot, N., (2008).**
    Experimental micromechanics of the cement-bone interface. J.Orthop.Res. 26, 872-879.

17. **Mann, K. A., Miller, M. A., Race, A., Verdonschot, N., (2009).**
    Shear fatigue micromechanics of the cement-bone interface: An in vitro study using digital image correlation techniques. J.Orthop.Res. 27, 340-346.
18. **Mann, K. A., Miller, M. A., Verdonschot, N., Izant, T. H., Race, A., (2010).**
    Functional interface micromechanics of 11 en-bloc retrieved cemented femoral hip replacements. Acta Orthop 81, 308-317.
19. **Mann, K. A., Mocarski, R., Damron, L. A., Allen, M. J., Ayers, D. C., (2001).**
    Mixed-mode failure response of the cement-bone interface. J.Orthop.Res. 19, 1153-1161.
20. **Miller, M. A., Eberhardt, A. W., Cleary, R. J., Verdonschot, N., Mann, K. A., (2010).**
    Micromechanics of postmortem-retrieved cement-bone interfaces. J.Orthop.Res. 28, 170-177.
21. **Moreo, P., Perez, M. A., Garcia-Amar, J. M., Doblare, M., (2006).**
    Modelling the mixed-mode failure of cement-bone interfaces. Engineering Fracture Mechanics 73, 1379-1395.
22. **Norman, T. L., Thyagarajan, G., Saligrama, V. C., Gruen, T. A., Blaha, J. D., (2001).**
    Stem surface roughness alters creep induced subsidence and 'taper-lock' in a cemented femoral hip prosthesis. J.Biomech. 34, 1325-1333.
23. **Perez, M. A., Palacios, J., (2010).**
    Comparative finite element analysis of the debonding process in different concepts of cemented hip implants. Ann.Biomed Eng 38, 2093-2106.
24. **Scheerlinck, T., Casteleyn, P. P., (2006).**
    The design features of cemented femoral hip implants. J.Bone Joint Surg.Br. 88, 1409-1418.
25. **Stolk, J., Verdonschot, N., Murphy, B. P., Prendergast, P. J., Huiskes, R., (2004).**
    Finite element simulation of anisotropic damage accumulation and creep in acrylic bone cement. Engineering Fracture Mechanics 71, 513-528.
26. **Verdonschot, N., Huiskes, R., (1995).**
    Dynamic creep behavior of acrylic bone cement. J.Biomed.Mater.Res. 29, 575-581.
27. **Verdonschot, N., Huiskes, R., (1997).**
    Acrylic cement creeps but does not allow much subsidence of femoral stems. J.Bone Joint Surg.Br. 79, 665-669.
28. **Waanders, D., Janssen, D., Mann, K. A., Verdonschot, N., (2010).**
    The mechanical effects of different levels of cement penetration at the cement-bone interface. J.Biomech. 43, 1167-1175.
29. **Waanders, D., Janssen, D., Miller, M. A., Mann, K. A., Verdonschot, N., (2009).**
    Fatigue creep damage at the cement-bone interface: an experimental and a micro-mechanical finite element study. J.Biomech. 42, 2513-2519.
30. **Wang, J. Y., Tozzi, G., Chen, J., Contal, F., Lupton, C., Tong, J., (2010).**
    Bone-cement interfacial behaviour under mixed mode loading conditions. J Mech Behav Biomed Mater 3, 392-398.
31. **Yang, D. T., Zhang, D., Arola, D., (2010).**
    Fatigue of the bone/cement interface and loosening of tatal joint replacements. International Journal of Fatigue 32, 1639-1649.

Chapter 4

The mechanical effects of different levels of cement penetration at the cement-bone interface

Journal of Biomechanics
(2010); 43(15):3028-34

Abstract

The mechanical effects of varying the depth of cement penetration in the cement-bone interface was investigated using finite element analysis (FEA) and validated using companion experimental data. Two FEA models of the cement-bone interface were created from micro-computed tomography data and the penetration of cement into the bone was varied over six levels each. The FEA models, consisting of the interdigitated cement-bone constructs with friction between cement and bone, were loaded to failure in tension and in shear. The cement and bone elements had provision for crack formation due to excessive stress. The interfacial strength showed a strong relationship with the average interdigitation (r^2=0.97 and r^2=0.93 in tension and shear, respectively). Also, the interface strength was strongly related with the contact area (r^2=0.98 and r^2=0.95 in tension and shear, respectively). The FEA results compared favorably to the stiffness-strength relationships determined experimentally. Overall, the cement-bone interface was 2.5 times stronger in shear than in tension and 1.15 times stiffer in tension than in shear, independent of the average interdigitation. More cracks occurred in the cement than in the bone, independent of the average interdigitation, consistent with the experimental results. In addition, more cracks were generated in shear than in tension. In conclusion, achieving and maintaining maximal infiltration of cement into the bone to obtain large interdigitation and contact area is key to optimizing the interfacial strength.

Introduction

In cemented total hip arthroplasty, the implant needs a mechanically stable cement-bone interface for long-term survival. Because there is no adhesive bonding between bone and conventional bone cement, such as polymethylmethacrylate (PMMA), fixation relies upon cement penetration to mechanically interlock the cement into the bone lacunar and trabecular spaces[5,6,11,16,34].

From a surgical perspective, the depth of cement penetration into the bone is dependent on several factors, including cement viscosity[32,36], bone preparation technique[3,19] and degree of cement pressurization[7,28]. These factors, combined with the quantity and morphology of the bone, contribute to a substantial variation in mechanical properties of the cement-bone interface[2,4].

Although previously the strength of the cement bone interface has been investigated as a single variable[20,24], the strength of the cement-bone interface has also been related to morphologic characteristics such as cement penetration depth and cement-bone contact area. While several studies found a positive relationship between the penetration depth and the strength of the cement-bone interface[1,8,13,17,21], others have not found such a relationship[18,27]. On the other hand, a strong relationship between the cement-bone contact area and the interfacial tensile strength was reported[22].

A major limitation of destructive mechanical tests such as those described above is that measurement of the failure response of a specimen to different loading directions is not possible. Because the cement-bone interface in total joint replacements is not only loaded in tension, but also in shear[29], it would be very useful to determine if strength-penetration depth relationships were the same under different loading regimes. Furthermore, the effect of penetration depth on mechanical response is confounded in experiments by the specimen-to-specimen variability. Finally, the cement penetration depth as previously been measured experimentally was often restricted to the specimen's outer surface, while it has recently been reported that the complete interdigitated volume should be analyzed instead of focusing on the outer surface only[37].

Micro-mechanical finite element analysis (FEA) in which the level of cement penetration is varied within a single specimen of bone allows for removal of bone morphology as a confounding variable. In this study, we developed computed tomography (CT) based micro-mechanical FEA models of the cement-bone interface, in which we only varied the penetration depth of the cement. These models had provision for failure of the cement and bone constituents via cracking of the bulk components. Using this modeling approach, we asked the following four research questions: (1) Is there a relationship between the average interdigitation of the cement, contact area between cement and bone, and the interface strength and stiffness?; (2) Is the cement-bone interface stronger in shear than in tension and does this depend on the average interdigitation?; (3) How valid are the FEA models when the mechanical responses of the different interdigitation depths of the cement-bone interface are compared with experimental findings?; (4) Do the majority of cracks occur in the bone or in the cement in these models and is this consistent with experimental results?

Methods

FEA models were created using micro-CT scans (12µm resolution) of two physical specimens containing the cement-bone interface that were sectioned (8x4x8mm³) from laboratory prepared cemented (PMMA) total hip replacements[37]. The FEA meshes (Figure 4.1) included the complex morphology of the cement-bone interface and were created by meshing the bone component and cement component using a custom algorithm to recreate an accurate representation of gaps between cement and bone[37]. Based on previous micro-FEA/experimental studies[10], contact between bone and cement was modeled using a double-sided node-to-surface contact algorithm with a friction coefficient of 0.3 (MSC.MARC 2007r1, MSC Software Corporation, Santa Ana, CA, USA).

The baseline (as cemented) models were constructed of four-noded tetrahedral elements (Specimen 1: 462,102 elements; Speciment 2: 219,664 elements). The initial material properties of the models were considered to be linear elastic. Young's modulus and Poisson's ratio (v) of the cement was set to 3,000MPa and 0.3, respectively. The bone properties were based upon micro-CT grayscale values, which were converted to equivalent HA-densities using a calibration phantom. The assumption of a linear relationship between the HA-density and the Young's modulus[15] resulted in Young's moduli ranging from 0.1 to 20,000MPa for the bone (v=0.3).

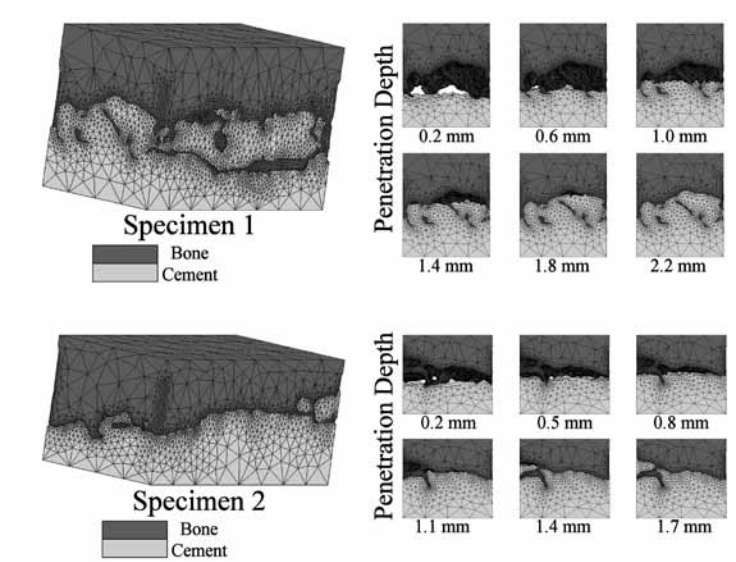

Figure 4.1 *Two finite element models were generated from micro-CT scans of the cement-bone interface. These two specimens were sectioned from total hip reconstructions, which were prepared using third generation cementing techniques using PMMA in a laboratory setting. From the initial FE-model of Specimen 1 (top), five other models were generated, each with a different penetration levels (the normal distance with respect to the transverse plane between the top of the bulk of the cement and the bottom of the bone). This resulted in six models of specimen 1 with penetration levels of 0.2, 0.6, 1.0, 1.4, 1.8 and 2.2mm. Same process was done for specimen 2 (bottom), resulting in levels of 0.2, 0.5, 0.8, 1.1, 1.4 and 1.7mm. The figures on the right are section views of the specimens for each penetration level.*

Approach to Modify Penetration Level

To simulate less cement penetration into the bone, the baseline models were modified by removing elements of cement beyond specific limits. The baseline models had maximum cement penetration levels of 2.2 and 1.7mm for specimen 1 and 2, respectively. The penetration level was defined as the normal distance with respect to the transverse plane between the top of the cement and the bottom of the bone (Figure 4.1). Five additional penetration levels were generated for both specimens by removing all cement elements above that particular penetration level, resulting in 12 unique FEA models (Figure 4.1). For each model a CT-based stereology approach was used to document the local cement interdigitation through the whole cement-bone specimen[26] (Figure 4.2). Subsequently, the average interdigitation was determined by averaging all the local interdigitations. The average interdigitation was subsequently used as a global measure of cement penetration (Table 1).

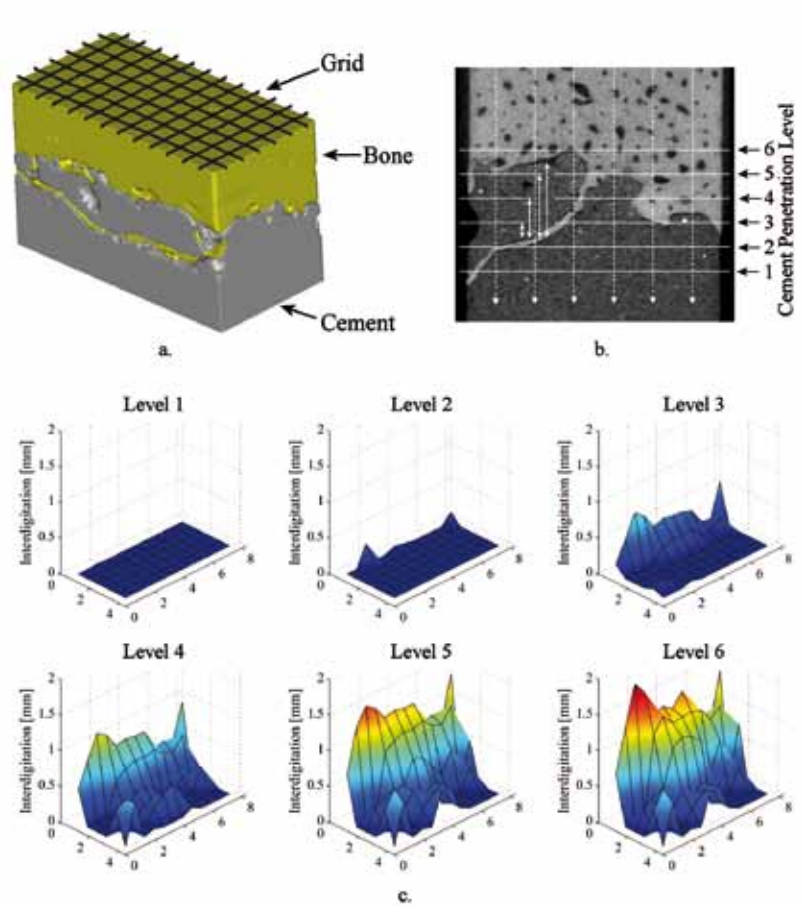

Figure 4.2 *A grid (12x6; 0.65mm spacing[25]) was constructed on the micro-CT scans and projected vertically through the image sets (a). For each vertical grid line and cement penetration level, the local cement penetration depth was measured (b), resulting in different distributions of interdigitation (c). The average of the 72 local interdigitation measurements was used as a measure of cement penetration depth.*

Cement and Bone Crack Formation

Previous experimental testing to failure in shear and tension indicates that cracks form in the cement and bone when loaded to failure[22]. Crack formation in the bulk bone and cement due to excessive local stresses was implemented in the models using a custom-written FEA algorithm to simulate static failure. An in-house fatigue failure algorithm[35] was adapted such that simulation of fatigue failure was disabled, while static failure was allowed to occur. Regardless of the type of load that was applied (tensile or shear), static failure was assumed when the local principal (tensile) stress of a cement or bone element exceeded its strength. A crack was simulated by setting the Young's modulus to 0.1MPa, perpendicular to the corresponding principal stress direction. The principal strength of the cement was set to 40MPa[9,14], while the strength of the bone (S) was based on its Young's modulus (E) and was derived from equations defined previously[12]:

$$E = 14{,}900 \cdot \rho_{ash}^{1.86}$$

$$S = 102 \cdot \rho_{ash}^{1.80}$$

Hence,

$$S = 102 \cdot \left(\frac{E}{14{,}900}\right)^{\frac{1.80}{1.86}}$$

All models were loaded until failure with displacement increments of 0.001mm in shear or tension. The bottom part of the cement was fixed, while the top part of the bone was displaced uniformly such that the bone did not tilt. The resultant reaction force was calculated and the resulting apparent stress-displacement responses were determined, subsequently resulting in the apparent strength and initial stiffness, both in tension and shear (Figure 4.3).

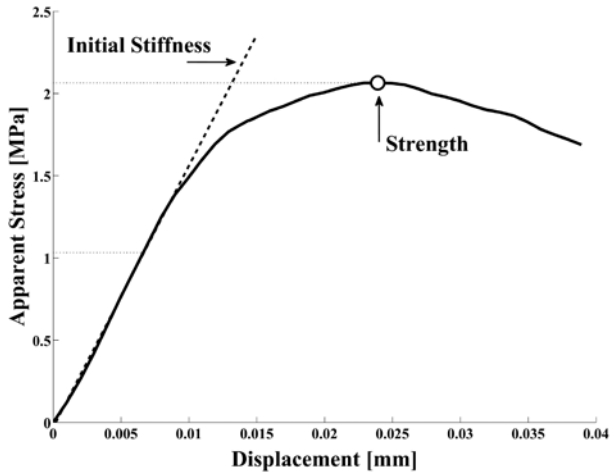

Figure 4.3 *The stress-displacement curve of a cement-bone specimen. The strength was defined as the maximum applied load divided by the nominal cross sectional area of the cement-bone interface. The initial stiffness was determined by a least-squares fit through the stress versus displacement response for applied stress levels less than 50% of the strength[21]. All cement-bone specimens were characterized by a linear slope followed by yielding till the strength was reached.*

Each element had one integration point, in which three cracks could occur (one in each principal direction). Hence, the crack volume was defined as[37]:

$$V_{cr_bone} = \frac{1}{3} \cdot \sum_{i=1}^{N_{bone}} n_i \cdot V_i$$

$$V_{cr_cement} = \frac{1}{3} \cdot \sum_{i=1}^{N_{cement}} n_i \cdot V_i$$

In which n_i and V_i are the number of cracks in a specific element and the element volume, respectively.

Outcome measures

As a validation, the results from the FEA simulations were compared with data obtained from experimental specimens[23,26]. These cement-bone specimens were fabricated from lab-prepared cemented hip reconstructions and post-mortem retrievals and were nominally the same size as the models. The acquired results comprised the apparent strength and stiffness of the specimens.

Because of interface and material discontinuities and differences in penetration levels, the apparent strain was not determined. Conversely, the stiffness was expressed as the ratio of the applied stress and the total deformation (MPa/mm)[11,22].

The contact area, an estimation of the interfacial contact between bone and cement, was estimated for each model/penetration level. Segmentation of the specimen's micro-CT data using MIMICS (MIMICS 11.1, Materialise, Leuven, Belgium) was followed by a dilation operation of the cement (Figure 4.4). Next, a Boolean intersection between the cement and bone resulted in the contact volume. This volume was subsequently divided by the dilation thickness giving the estimated contact area[22].

Linear regression analysis was used to determine relationships between average cement interdigitation, contact area, and interface strength and stiffness, and to compare the strength in tension and shear.

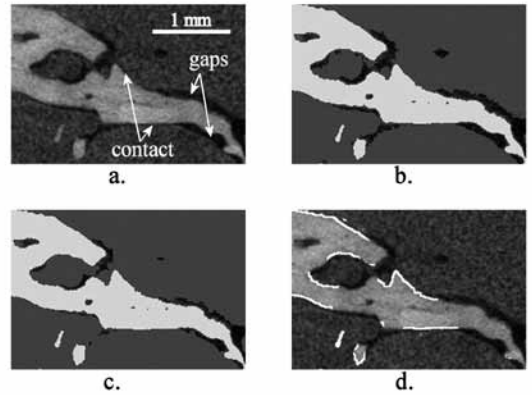

Figure 4.4 *Approach used to estimate the contact area between cement and bone[22]. The micro-CT scan (a) represented the gaps and initial contact between the bone and cement. Subsequently, the micro-CT scan was segmented into two 3D objects (b): cement (grey) and bone (white). Next, the 3D cement object was dilated by two voxels (24µm) (c). The Boolean intersection between the dilated cement and bone object was calculated (d). This volume was subsequently divided by the amount of cement dilation (24µm), resulting in an estimation of the contact area between cement and bone.*

Results

At the greater penetration levels, specimen 1 had a much larger contact area than specimen 2 (Table 1), while at the lesser penetration levels, the contact area of specimen 2 was larger than specimen 1. Overall, there was a very strong correlation between average interdigitation and contact area for the twelve models (r^2=0.99).

Very strong correlations were found between the tensile strength and the average interdigitation (r^2=0.97) and the shear strength and average interdigitation (r^2=0.93; Figure 4.5a-b). Surprising was the jump in strength specimen 2 with a small increase in average interdigitation at the lower average interdigitation level. The correlation between tensile and shear strength and the contact area was also very strong (r^2=0.98 and r^2=0.95, respectively; Figure 4.5c-d).

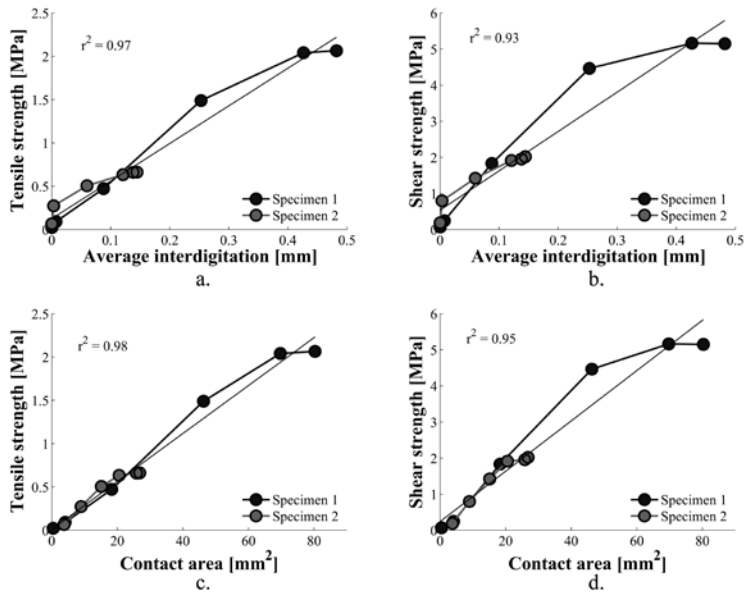

Figure 4.5 *Strong linear relationships existed between (a) the tensile strength and average interdigitation (r^2=0.97) as well as between (b) shear strength and average interdigitation (r^2=0.93). For specimen 2, there was a jump in strength with a small increase in the average interdigitation. The relationship between strength and contact area were also strong in tension (c) and shear (d) (r^2=0.98 and r^2=0.95, respectively. Note the different scales of the tensile and shear results.*

A comparison between the tensile and shear results showed that the cement-bone interface was about 2.5 times stronger in shear than in tension (r^2=0.98; Figure 4.6a).
The initial stiffness in tension and shear exhibited a similar behavior as the strength with regards to the effect of average interdigitation (Table 1). Penetration depth was less strongly correlated with tensile stiffness (r^2=0.91) and shear stiffness (r^2=0.89) than with contact area (r^2=0.93 and r^2=0.91, respectively). The cement-bone interface was 1.15 times stiffer in tension than in shear (r^2=0.98; Figure 4.6b).

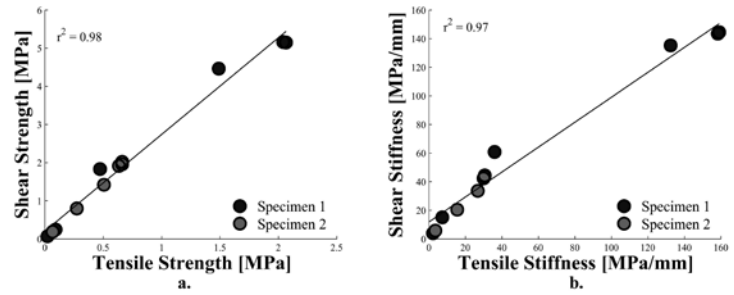

Figure 4.6 *a. The bone-cement interface was 2.5 times stronger in shear than in tension, independent of the penetration depth of the cement (r^2=0.98).*
b. The bone-cement interface was 1.15 times stiffer in tension than in shear, independent of the penetration depth of the cement (r^2=0.97).

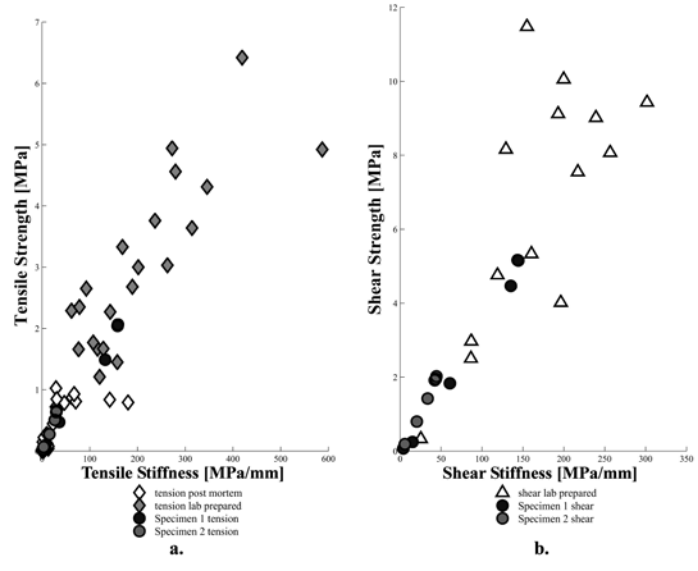

Figure 4.7 *Strength-stiffness relationships for tensile and shear loading. Lab-prepared specimens were loaded to failure in tension[22] and shear, while the post-mortem retrievals were loaded to failure only in tension[25]. For the strength-stiffness relation in tension (a), it is noted that even the higher penetrated models of specimen 2 have a strength-stiffness relation that corresponds with post-mortem interfaces. Like the strength-stiffness relation in tension, the strength-stiffness relation in shear compared satisfactorily with the experimental findings (b).*

For all models, there was a strong stiffness-strength relationship in tension (r^2=0.97) and shear (r^2=0.98). The FEA results compared favorably to the experimental stiffness-strength relationships of the lab-prepared and post-mortem specimens; all FEA results presented here fell within the distribution of the experimental data (Figure 4.7).

At the point of structural failure of the models, more cracks occurred in the cement than in the bone (Figure 4.8a-b). Also, more cracks occurred in shear than in tension. In shear, the amount of bone cracks of specimen 1 and bone and cement cracks of specimen 2 did not increase beyond a penetration depth of 1.4mm and 1.1mm, respectively. All cracks occurred in the interdigitated area (Figure 4.9).

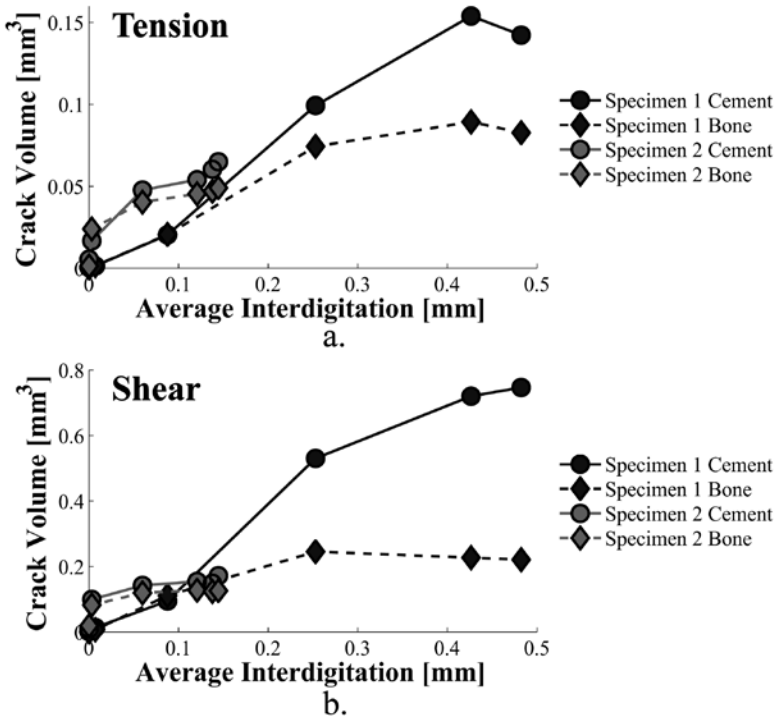

Figure 4.8 *a. Crack volume of the cement and bone for specimen 1 and 2 when the specimen's strength was reached in tension.*
b. Crack volume of the cement and bone for specimen 1 and 2 when the specimen's strength was reached in shear.

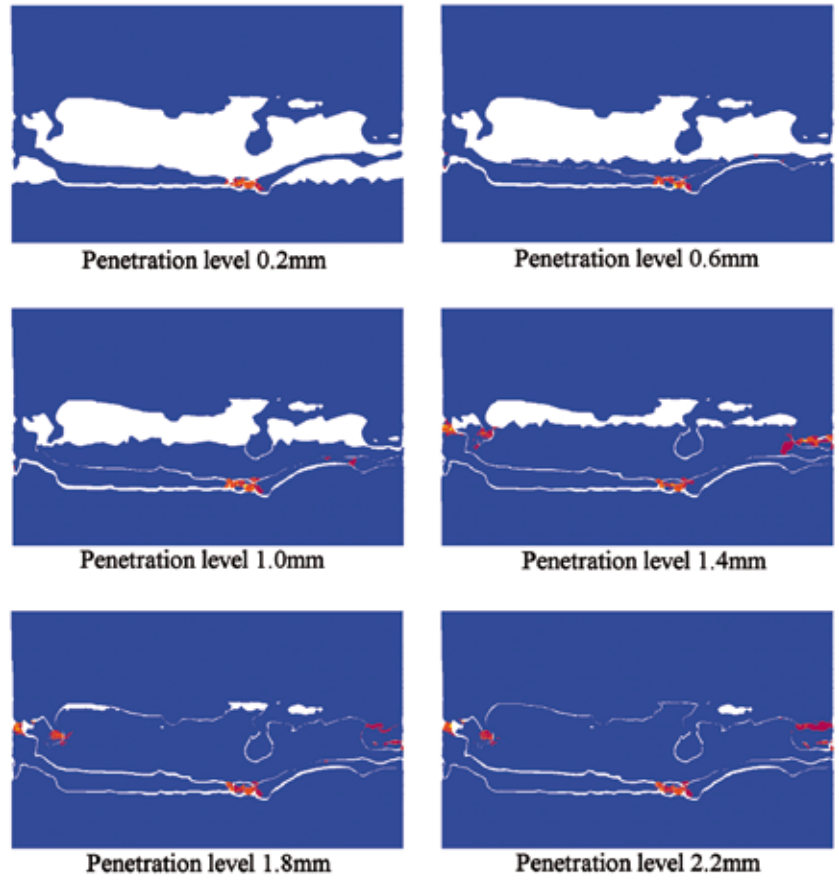

Figure 4.9 *Crack patterns for a cross-section of specimen 1 loaded in tension when the apparent strength was reached. Although the figure only shows one specific cross-section of the interface, it can be seen that the cement in the 1.4mm penetration level envelops several bony spurs which increases the average interdigitation and subsequently the apparent strength (Figure 4.4a-b). In shear, cracks generally at the same locations, but progressed in a different direction compared to the 'tensile cracks'. For all penetration levels and loading directions, all cracks were in the interdigitated area of the cement-bone interface and did not progress into the bulk of the bone or cement.*

Discussion

In this study, we investigated the difference in mechanical behavior of the cement-bone interface in response to tension and shear loading as a result of different cement penetration depths in a single bone morphology. The results show that the strength and stiffness of the cement-bone interface are linearly dependent on the average interdigitation and the contact area between the bone and cement, for both tensile and shear loading conditions. The cement-bone interface is 2.5 times stronger, but less stiff in shear than in tension, independent on the average interdigitation. As a validation, the FEA results were compared with experimental tests using post-mortem and lab-prepared cement-bone specimens. The FEA results compared favorably with these experiments. Finally, the majority of cracks occur in the cement which is consistent with what was found experimentally[22].

Our study was limited by the fact that the models of specimens with lower penetration depths may not have represented the actual physical morphology of that penetration depth. Due to the modeling approach of the different penetration depths, small cement fragments might have been present that enveloped bony spurs. It is unlikely that these situations occur physiologically.

The results of our analyses indicate that the strength of the cement-bone interface in the two models did not exceed 6MPa (Figure 4.5), while cracks occurred mainly in the cement, which had a tensile strength of 40MPa. This indicates that, although on an apparent level the applied loads were rather low, they had a substantial effect on the local stress distribution in the cement and bone.

As a validation, a direct comparison between the models and experiments is not possible because the cement penetration was varied numerically and failure was simulated in two loading directions. Therefore, we compared the FEA-simulation strength-stiffness relationships with experimental specimens that comprised a broad range of interdigitation levels. This approach provides a comparison between the models and experiments in terms of pre-yield (stiffness) and yielding behavior (strength). The crack patterns from the FE-simulations could also not be compared on a one-to-one basis. However, the finding that more cracks were present in the cement than the bone and all cracks occurred in the interdigitated region in these simulations is fully consistent to what has been reported for experimental specimens[22]. Further, micromechanical FEA-simulations of the cement-bone interface with fatigue loading resulted in similar crack patterns to those found experimentally[37].

Previously, it has been reported that the strength of the cement-bone interface does not increase when the cement penetration exceeded 3mm and 4mm[1,18]. This finding could not be affirmed, since the models as used in this study had relative low penetration levels, also compared with previous specimens (2.59±0.85mm)[37].

From previous experimental studies, an increase of penetration depth has been associated with an increase in strength of the cement-bone interface[1,8,13,17,21]. A likely confounding factor in these studies was that during the fabrication of the cement-bone specimens, the bone was not warmed to body temperature what does not represent the operative situation (although MacDonald did an in-vivo study). The difference in temperature gradient would alter the polymerization front of the curing cement and could affect the cement-bone morphology. On the other hand, studies that did not find a relationship between penetration depth and strength[18,27] did warm up the bone to body temperature. This is not consistent with the current study, since our results show a strong relationship while keeping the bone at body temperature during specimen generation[22]. However, the method used to measure penetration depth was different for the present study where the complete volume was sampled instead of measuring depth on a single exterior surface .

The results of the current study, in which the bone morphology was constant for each specimen, showed a strong relationship between the average interdigitation and tensile strength. However, in addition to the experimental literature detailed above, previous experiments of lab-prepared cement-bone specimens[22] showed no correlation (r^2=0.06) between stereology based measures of average interdigitation and tensile strength (unpublished data from co-author). This suggests that bone morphology plays an important role in the interface strength and one could expect a wide variety of interface strengths for the same average interdigitation in the in vivo environment. This finding is consistent with micro-CT based measurements of 21 different experimental specimens[22]; there was a poor correlation (r^2=0.06) between penetration depth, measured as the maximum distance between the bone and cement, and tensile strength of the cement-bone interface. The very high correlation between contact area and interface strength found for the models performed here has also been noted in experimental studies[22] of cement-bone specimens loaded to failure. Combining the FEA-findings with previous experimental tests suggests that achieving a maximal infiltration between the bone and cement is essential for increasing the interfacial strength. This suggests that efforts to maximize and maintain apposition between the cement and bone would be beneficial for implant fixation.

A large average interdigitation and contact area in trabecular bone can be achieved by preparing the bone with pulsatile lavage to allow for cement infiltration, but will be more difficult to achieve in cortical bone. Therefore, it might be beneficial to brush the cortical bone before cement insertion to increase the cement-bone contact area. The contact area can also be enlarged by reducing interfacial gaps, which can be obtained by reducing polymerization shrinkage and air and fluid inclusions[31,38].

Although the results of this study showed that the strength and stiffness of the cement-bone interface increased linearly with the average interdigitation, using excessive pressurization to obtain a large interdigitation may be deleterious for the surgical patient. Over pressurizing of the femoral canal can lead to a fat and bone-marrow embolism syndrome, which can cause complications and can sometimes even be fatal[30,33]. Secondly, as noted in several laboratory studies, excessive pressurization to achieve a large penetration has limited value[1,18].

An obvious limitation of this study was that that only the direct post-operative situation was considered. Over the long term, bone resorption may occur at the interface, which considerably weakens the interface[26]. From that point of view it might be advantageous to use a larger penetration depth, so that in the long term a large contact area can still be achieved to distribute the loads over the cement-bone interface.

In conclusion: (1) There are very strong positive relationships between the average interdigitation depth of the cement-bone interface and the strength and stiffness as well as the contact area and strength and stiffness. It is likely that this relationship depends on the morphology of the bone.; (2) The cement-bone interface is stronger in shear than in tension, independent of the average interdigitation.; (3) The stiffness-strength relationships of the FEA

simulations compared satisfactorily with experimental results.; (4) Upon structural failure of the cement-bone interface, the majority of cracks occurred in the cement.

Acknowledgements

This work was funded by the NIH grant AR42017.

References

1. **Askew, M. J., Steege, J. W., Lewis, J. L., Ranieri, J. R., Wixson, R. L., (1984).** Effect of cement pressure and bone strength on polymethylmethacrylate fixation. J.Orthop.Res. 1, 412-420.
2. **Bean, D. J., Convery, F. R., Woo, S. L., Lieber, R. L., (1987).** Regional variation in shear strength of the bone-polymethylmethacrylate interface. J.Arthroplasty 2, 293-298.
3. **Berry, D. J., (2004).** Cemented femoral stems: what matters most. J.Arthroplasty 19, 83-84.
4. **Bugbee, W. D., Barrera, D. L., Lee, A. C., Convery, F. R., (1992).** Variations in shear strength of the bone-cement interface in the proximal femur. Trans Orthop Res Soc 17:22.
5. **Freeman, M. A., Bradley, G. W., Revell, P. A., (1982).** Observations upon the interface between bone and polymethylmethacrylate cement. J.Bone Joint Surg.Br. 64, 489-493.
6. **Goto, K., Kawanabe, K., Kowalski, R., Baker, D., Nakamura, T., (2010).** Bonding ability evaluation of bone cement on the cortical surface of rabbit's tibia. J.Mater.Sci.Mater.Med. 21, 139-146.
7. **Gozzard, C., Gheduzzi, S., Miles, A. W., Learmonth, I. D., (2005).** An in-vitro investigation into the cement pressurization achieved during insertion of four different femoral stems. Proc.Inst.Mech.Eng [H.] 219, 407-413.
8. **Graham, J., Ries, M., Pruitt, L., (2003).** Effect of bone porosity on the mechanical integrity of the bone-cement interface. J.Bone Joint Surg.Am. 85-A, 1901-1908.
9. **Harper, E. J., Bonfield, W., (2000).** Tensile characteristics of ten commercial acrylic bone cements. J.Biomed.Mater.Res. 53, 605-616.
10. **Janssen, D., Mann, K. A., Verdonschot, N., (2008).** Micro-mechanical modeling of the cement-bone interface: The effect of friction, morphology and material properties on the micromechanical response. J.Biomech. 41, 3158-3163.
11. **Janssen, D., Mann, K. A., Verdonschot, N., (2009).** Finite element simulation of cement-bone interface micromechanics: a comparison to experimental results. J.Orthop.Res. 27, 1312-1318.
12. **Keyak, J. H., Kaneko, T. S., Tehranzadeh, J., Skinner, H. B., (2005).** Predicting proximal femoral strength using structural engineering models. Clin.Orthop.Relat Res. 437, 219-228.
13. **Krause, W. R., Krug, W., Miller, J., (1982).** Strength of the cement-bone interface. Clin.Orthop.Relat Res. 163, 290-299.
14. **Lewis, G., (1997).** Properties of acrylic bone cement: state of the art review. J.Biomed.Mater.Res. 38, 155-182.
15. **Lotz, J. C., Gerhart, T. N., Hayes, W. C., (1991).** Mechanical properties of metaphyseal bone in the proximal femur. J.Biomech. 24, 317-329.

16. **Lucksanasombool, P., Higgs, W. A., Ignat, M., Higgs, R. J., Swain, M. V., (2003).**
Comparison of failure characteristics of a range of cancellous bone-bone cement composites. J.Biomed.Mater.Res.A 64, 93-104.
17. **MacDonald, W., Swarts, E., Beaver, R., (1993).**
Penetration and shear strength of cement-bone interfaces in vivo. Clin.Orthop.Relat Res. 286, 283-288.
18. **Majkowski, R. S., Bannister, G. C., Miles, A. W., (1994).**
The effect of bleeding on the cement-bone interface. An experimental study. Clin.Orthop.Relat Res. 299, 293-297.
19. **Majkowski, R. S., Miles, A. W., Bannister, G. C., Perkins, J., Taylor, G. J., (1993).**
Bone surface preparation in cemented joint replacement. J.Bone Joint Surg.Br. 75, 459-463.
20. **Mann, K. A., Allen, M. J., Ayers, D. C., (1998).**
Pre-yield and post-yield shear behavior of the cement-bone interface. J.Orthop.Res. 16, 370-378.
21. **Mann, K. A., Ayers, D. C., Werner, F. W., Nicoletta, R. J., Fortino, M. D., (1997).**
Tensile strength of the cement-bone interface depends on the amount of bone interdigitated with PMMA cement. J.Biomech. 30, 339-346.
22. **Mann, K. A., Miller, M. A., Cleary, R. J., Janssen, D., Verdonschot, N., (2008).**
Experimental micromechanics of the cement-bone interface. J.Orthop.Res. 26, 872-879.
23. **Mann, K. A., Miller, M. A., Race, A., Verdonschot, N., (2009).**
Shear fatigue micromechanics of the cement-bone interface: An in vitro study using digital image correlation techniques. J.Orthop.Res. 27, 340-346.
24. **Mann, K. A., Werner, F. W., Ayers, D. C., (1999).**
Mechanical strength of the cement-bone interface is greater in shear than in tension. J.Biomech. 32, 1251-1254.
25. **Miller, M. A., Eberhardt, A. W., Cleary, R. J., Verdonschot, N., Mann, K. A., (2009).**
Micro-mechanics of Post-mortem Retrieved Cement-Bone Interface. J.Orthop.Res. in Press.
26. **Miller, M. A., Eberhardt, A. W., Cleary, R. J., Verdonschot, N., Mann, K. A., (2010).**
Micromechanics of postmortem-retrieved cement-bone interfaces. J.Orthop.Res. 28, 170-177.
27. **Miller, M. A., Race, A., Gupta, S., Higham, P., Clarke, M. T., Mann, K. A., (2007).**
The role of cement viscosity on cement-bone apposition and strength: an in vitro model with medullary bleeding. J.Arthroplasty 22, 109-116.
28. **Oates, K. M., Barrera, D. L., Tucker, W. N., Chau, C. C., Bugbee, W. D., Convery, F. R., (1995).**
In vivo effect of pressurization of polymethyl methacrylate bone-cement. Biomechanical and histologic analysis. J.Arthroplasty 10, 373-381.
29. **Perez, M. A., Garcia-Aznar, J. M., Doblare, M., Seral, B., Seral, F., (2006).**
A comparative FEA of the debonding process in different concepts of cemented hip implants. Med.Eng Phys. 28, 525-533.
30. **Pitto, R. P., Koessler, M., Kuehle, J. W., (1999).**
Comparison of fixation of the femoral component without cement and fixation with use of a bone-vacuum cementing technique for the prevention of fat embolism during total hip arthroplasty. A prospective, randomized clinical trial. J.Bone Joint Surg.Am. 81, 831-843.

31. **Race, A., Miller, M. A., Clarke, M. T., Mann, K. A., (2005).**
Cement-implant interface gaps explain the poor results of CMW3 for femoral stem fixation: A cadaver study of migration, fatigue and mantle morphology. Acta Orthop. 76, 679-687.
32. **Race, A., Miller, M. A., Clarke, M. T., Mann, K. A., Higham, P. A., (2006).**
The effect of low-viscosity cement on mantle morphology and femoral stem micromotion: a cadaver model with simulated blood flow. Acta Orthop. 77, 607-616.
33. **Sierra, R. J., Timperley, J. A., Gie, G. A., (2009).**
Contemporary cementing technique and mortality during and after exeter total hip arthroplasty. J.Arthroplasty 24, 325-332.
34. **Skripitz, R., Aspenberg, P., (1999).**
Attachment of PMMA cement to bone: force measurements in rats. Biomaterials 20, 351-356.
35. **Stolk, J., Verdonschot, N., Murphy, B. P., Prendergast, P. J., Huiskes, R., (2004).**
Finite element simulation of anisotropic damage accumulation and creep in acrylic bone cement. Engineering Fracture Mechanics 71, 513-528.
36. **Stone, J. J., Rand, J. A., Chiu, E. K., Grabowski, J. J., An, K. N., (1996).**
Cement viscosity affects the bone-cement interface in total hip arthroplasty. J.Orthop.Res. 14, 834-837.
37. **Waanders, D., Janssen, D., Miller, M. A., Mann, K. A., Verdonschot, N., (2009).**
Fatigue creep damage at the cement-bone interface: an experimental and a micro-mechanical finite element study. J.Biomech. 42, 2513-2519.
38. **Wang, J. S., Franzen, H., Lidgren, L., (1999).**
Interface gap after implantation of a cemented femoral stem in pigs. Acta Orthop.Scand. 70, 234-239.

Mixed-Mode Loading of the Cement-Bone Interface: a Finite Element Study

Chapter 5

Computer Methods in Biomechanics and Biomedical Engineering (2011); 14(2):145-55.

Abstract

While including the cement-bone interface of complete cemented hip reconstructions is crucial to correctly capture their response, its modeling is often overly simplified. In this study the mechanical mixed-mode response of the cement-bone interface is investigated taking into account the effects of the well-defined microstructure that characterizes the interface. CT-based plain strain FEA models of the cement-bone interface are built and loaded in multiple directions. Periodic boundaries are considered and the failure of the cement and bone fractions by cracking of the bulk components are included. The results compare favorably with experimental observations. Surprisingly, the analyses reveal that under shear loading no failure occurs and considerable normal compression is generated to prevent interface dilation. Reaction forces, crack patterns and stress fields provide more insight into the mixed-mode failure process. Moreover, the cement-bone interface analyses provides details which can serve as a basis for the development of a cohesive law.

Introduction

In Finite Element Analyses (FEA) of complete cemented total hip reconstructions, the mechanical response of the cement-bone interface is often overly simplified. In previous analyses the cement-bone interface has been uniformly modeled as infinitely stiff[5,9,33], as a layer of soft tissue elements[3,36] and as a frictional contact layer[14]. However, experiments with laboratory prepared cement-bone interface specimens demonstrate that the variety of the interfacial microstructure leads to a substantial variance in its mechanical compliance and strength[18]. Moreover, post-mortem retrievals show that the cement-bone interface is considerably degenerated making the interface even more compliant[2,22,30].

Micro-mechanical FEA models have recently been developed which are able to reproduce the static and fatigue behavior of the cement-bone interface in vitro[6,7,37,38]. However, such micro models cannot be implemented in complete FEA models of hip reconstructions due to their extremely large computational cost.

Cohesive zone models have attracted a growing interest in the scientific community to model the cement-bone interface in complete hip reconstructions[17,23,24,28]. In cohesive zone models a constitutive relation, or cohesive zone law, between the traction and opening displacement in both normal and tangential direction has to be defined. Moreover, the response of the interface to mixed-mode loading may be captured either by implementing an independent traction-opening displacement relationships in normal and tangential direction[17] or defining a mixed mode model with an interaction between normal and tangential opening displacements[23,24,28]. The responses of such mixed mode models can be fit to mixed-mode experimental observations[20,39]. However, a major limitation of these mixed-mode experiments is the wide range in mechanical responses as a result of specimen variety, since destructive mechanical testing in multiple directions with a single cement-bone interface specimen is not possible.

Several studies have focused on the relation between the mechanical response of the cement-bone interface and its interfacial morphology under tensile loading. It has been shown that the tensile strength of the interface is strongly related to the mineral density of the cement-bone interface obtained from quantitative computed tomography (CT) and the maximum cement penetration in the bone[15,16]. Moreover, unidirectional experiments and FEA analyses have successfully related the strength and stiffness of the cement-bone interface to the contact area between the bone and cement[18], the average level of cement penetration into the bone[37] and the fraction of cement-bone intersections over the complete interface[22]. However, no reports have been made to explore the relationship between strength of the interface and its morphology under different mixed loading conditions.

The goal of this study was to investigate in detail the mechanical mixed-mode response of the cement-bone interface. The acquired results, in terms of tractions and displacements, should subsequently serve as a basis for the implementation in cohesive elements. Using a multi-scale approach, CT based FEA models of the cement-bone interface were built and tested, under loading in multiple directions. The model accounted for the failure of both the cement and bone by cracking of the bulk components. We focused our analysis on the following key-aspects: (1) The relationship between the normal and tangential tractions during mixed-mode loading of the cement-bone interface, and (2) the relation between the interfacial response and morphology under mixed-mode loading.

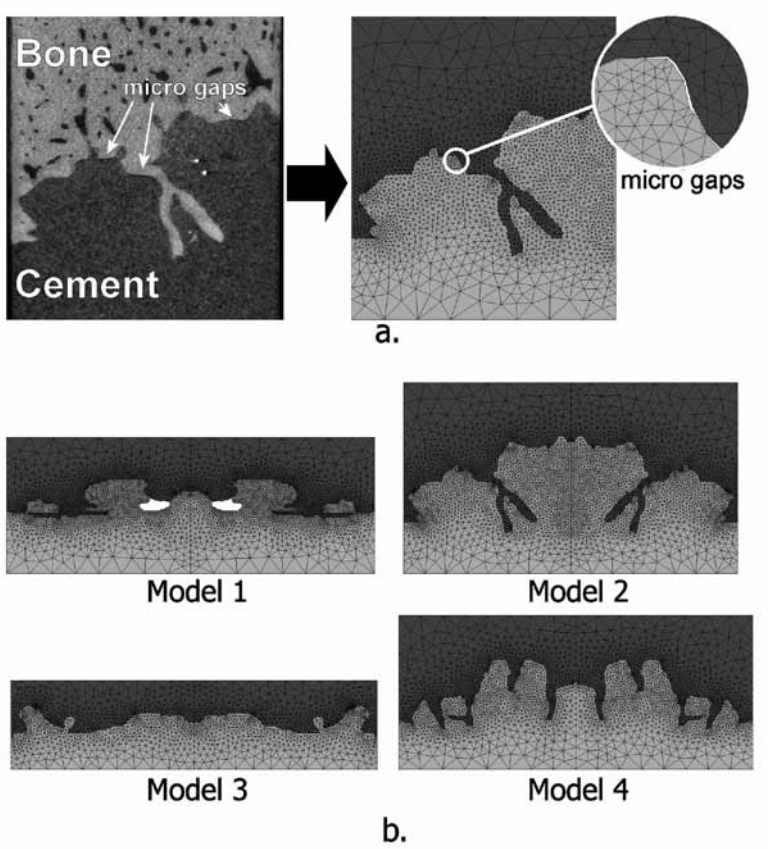

Figure 5.1 *a. Out of one slice of the micro-CT data of the cement-bone interface the generalized plain strain model was created. The micro-CT data contained only one bone and one cement body to avoid any redundant particles. Micro gaps between the bone and the cement were recreated using a custom algorithm[38].*
b. All models were mirrored what resulted in four models with distinct differences in dimensions and interface morphology (Table 5.1). The four mirrored models had an average width, 'w', and thickness, 't', of 9.43mm and 3.80mm, respectively.

Methods

Four generalized two-dimensional (2D) plane strain FEA models of the cement-bone interface were built, based on a single micro-CT slice (12 µm isotropic resolution, see Figure 5.1a) of four different physical specimens containing the cement-bone interface[38]. The selected slices contained only one bone and cement body to avoid floating particles. The FEA models included the complex morphology of the cement-bone interface and were meshed using a custom algorithm to recreate the gaps between the cement and bone[38]. The top edge of the bone and

bottom edge of the cement had an offset of ~1 mm relative to the contact interface to avoid mechanical boundary artifacts at the contact interface, since previous studies have shown that the majority of motion takes place at the contact interface and not in the surrounding materials[18,19,38,42]. Each model was mirrored to fulfill the periodic boundary conditions[25,26]; this will be clarified later (Figure 5.1b). The accuracy of the mesh was ascertained through a mesh refinement study and the resulting models contained on average 96,900 elements and 23,400 nodes. Contact between the bone and cement was modeled using a double-sided node to surface contact algorithm (MSC.MARC 2007r1, MSC Software Corporation, Santa Ana, CA, USA) with a friction coefficient of 0.3[6].

Both the bone and the cement were initially modeled as isotropic linear elastic materials. The Young's modulus (E) and Poisson's ratio (ν) of the cement were taken as 3000 MPa and 0.3, respectively[4,7]. The bone properties were based upon micro-CT grayscale values, which were converted to equivalent HA-densities using a calibration phantom. The assumption of a linear relationship between HA-density and Young's modulus[15] resulted in Young's modulus' $0.1 \leq E \leq 20{,}000$ MPa (ν=0.3).

Previous experiments showed the formation of cracks in the cement and bone when loaded to failure[18]. Crack formation in the bulk bone and cement due to excessive stresses was included in the models using an adapted custom-written FEA algorithm to simulate static failure[34]. Static failure occurred when the local principal tensile stress either in the cement or in the bone exceeded the strength of the material. The strength of the cement was taken as 40 MPa[4,13], while the strength of the bone was based on the local Young's modulus[10,37]:

$$S = 102 \cdot \left(\frac{E}{14{,}900} \right)^{\frac{1.80}{1.86}}$$

Cracks were simulated by setting the Young's modulus in the direction perpendicular to the corresponding principal stress direction to 0.1 MPa.

Periodic boundary conditions were applied to both sides of the model in order to establish a multi-scale representation of the cement-bone interface. In this way, the complete cement-bone interface was considered as a series of periodic micro structures[8]. The periodic boundary conditions were implemented constructing nodal links between nodes periodically located on the left and right side of the model (Figure 5.2a)[32]:

$$u_x(0,y) = u_x(w,y)$$
$$u_y(0,y) = u_y(w,y)$$

In these two equations 'ui' represents the displacement and 'w' the width. To avoid bone-to-cement nodes at the boundary between two different periodic cells, the models were mirrored. Moreover all nodes of the bottom edge were fixed in both directions (Figure 5.2b), while the nodes on the top edge uniformly displaced.

Figure 5.2

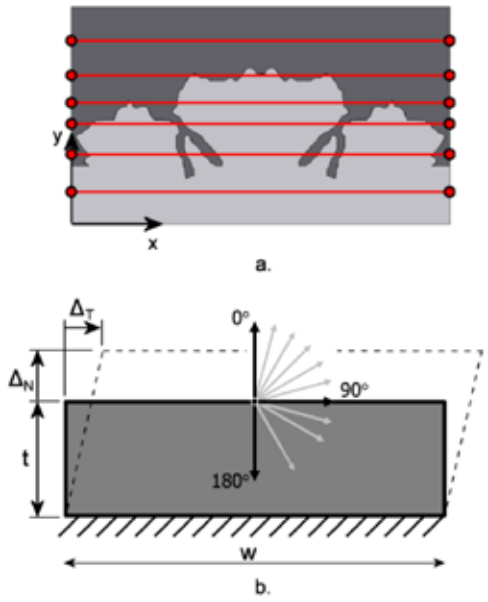

a. Periodic boundary conditions were applied to the left and right side of each model by applying links between each side. As a result of the mirroring of the models, only bone-to-bone and cement-to-cement links were created. Moreover, this subsequently resulted in a smooth 'infinite' contour of the contact interface between the bone and cement.

b. The bottom part of each model was fixated in as well x- as y-direction. The periodic boundary description resulted in equal motion of the nodes on the model's left and right side: $u_x(0,y)=u_x(w,y)$ $u_y(0,y)=u_y(w,y)$ *The nodes in top plane (y=t) were incrementally displaced under 11 different angles, α. Tangential displacements were consequently applied in positive x-direction.*

Each model was loaded until failure by applying an incremental displacement (Δ=0.001 mm) to the top edge. Eleven directions (α) were considered: 0° (pure tension), 15°, 30°, 45°, 60°, 75°, 90° (pure shear), 105°, 120°, 150° and 180° (pure compression) (Figure 5.2b). Hence, the incremental normal and tangential displacement, Δ_N and Δ_T, to applied to the nodes on the top edge were:

$$\Delta_N = \Delta \cdot \cos(\alpha)$$
$$\Delta_T = \Delta \cdot \sin(\alpha)$$

The resultant reaction force was calculated as well as its normal (T_N) and tangential (T_T) component.

The interface morphology was quantified using a CT-based stereology approach[22,37]. A 12x6 grid was spanned over the micro-CT scan of each model (Figure 5.3). For each of the 12 vertical and 6 horizontal lines the local normal and tangential cement interdigitation was measured, respectively. Local cement interdigitation was defined as the total amount of cement that was captured between two pieces of bone for the grid line. Subsequently, the average interdigitation was determined for both normal (int_N) and tangential direction, (int_T).

The tangential interdigitation was doubled to account for the interdigitation for the mirrored models. The average interdigitation in each direction was used as a global measure of cement penetration. Subsequently, for each loading angle (α) the average normal and tangential interdigitation was determined as:

$$int_{N,\alpha} = \left| int_N \cdot \cos(\alpha) \right|$$
$$int_{T,\alpha} = int_T \cdot \sin(\alpha)$$

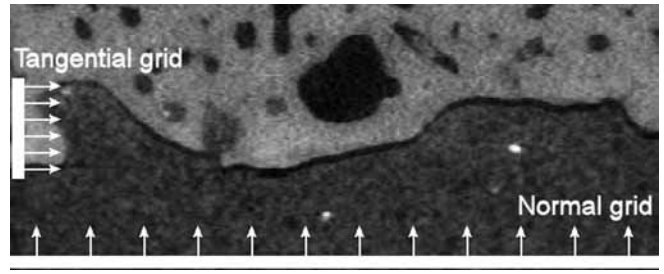

Figure 5.3 *A grid was superimposed over each specimen. Twelve vertical lines were subdivided over the complete specimen's width with equal spacing. For each line the local interdigitation was determined[22,37]. The twelve local interdigitations were averaged resulting in the average normal interdigitation, int_N, (Table 5.1). Similar approach was used to determine the cement interdigitation in tangential direction, int_T. The only difference was that the six horizontal lines were spanned over the height of interdigitation and not the specimen's complete height and that the tangential interdigitation was subsequently doubled.*

The influence of the choice of a ~1 mm offset dimension was explored by extending the cement and bone an additional 1 mm from the cement-bone interface in model 2. The extended model 2 was subsequently loaded in pure tension (0°) and pure shear (90°) and the results were compared with the original model 2.

During each simulation, the normal (T_N) and tangential tractions (T_T) as well as the normal (Δ_N) and tangential displacements (Δ_T) were monitored. For each simulation four traction-displacement (T-Δ) responses were analyzed: T_N-Δ_N, T_N-Δ_T, T_T-Δ_T and T_T-Δ_N. In normal and tangential direction the initial stiffness $\left(\frac{\partial T_N}{\partial \Delta_N} \text{ and } \frac{\partial T_T}{\partial \Delta_T}\right)$ and strength ($T_{N,ult}$ and $T_{T,ult}$) were determined. Linear regression analysis was used to determine relationships between the normalized cement interdigitation, $int_{N,\alpha}$ and $int_{T,\alpha}$, and interface initial stiffness and strength.

Figure 5.4

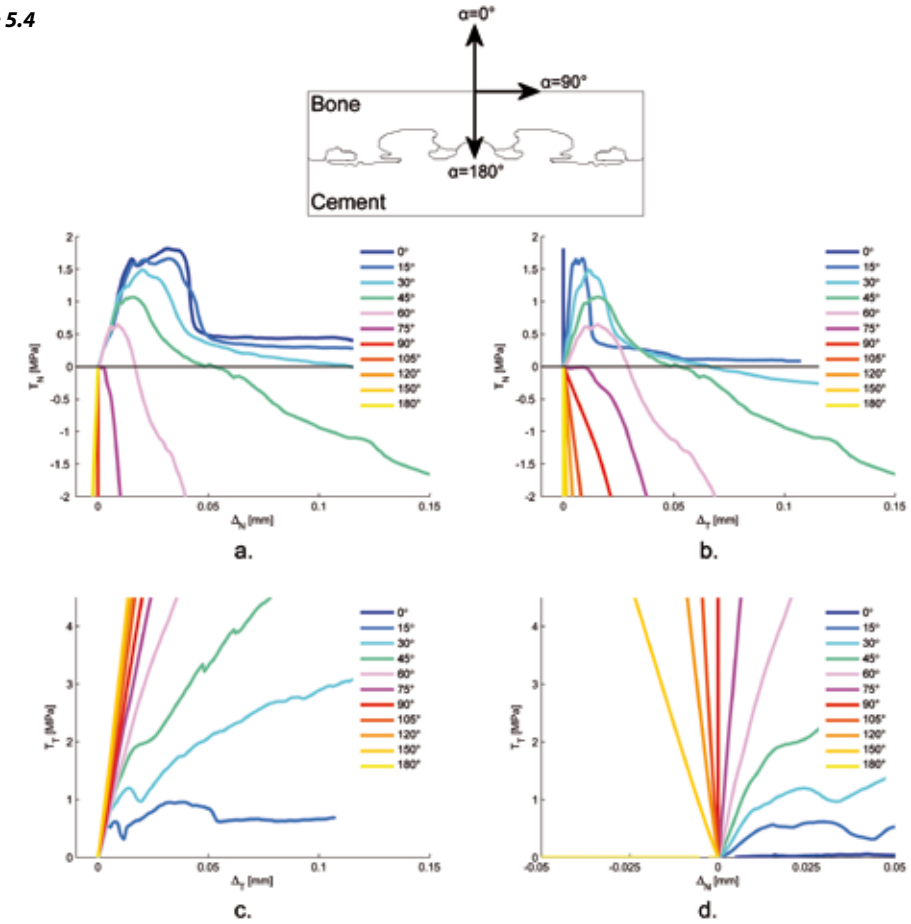

The traction-displacement relationships between T_N and Δ_N (a), T_N and Δ_T (b) , T_T and Δ_T (c) and T_T and Δ_N (d) of model 1 for 11 different angles. In pure tension (α=0°) the complete traction-displacement response is captured in subfigure (a). Obviously, no Δ_T took place in pure tension (b) and as a result of the symmetry no T_T occurred (d). In pure compression (α=180°) there was a very stiff T_N-Δ_N response (a), again without any Δ_T (b) and T_T (d). In pure shear (α=90°) no ultimate strength was found (c) and a considerable T_N was needed to prevent dilation of the bone (b). The mixed-mode responses showed a gradual decrease in ultimate T_N as the loading angle increased.

Results

All four models showed similar response under mixed-mode loading. In pure tension (α=0°) the cement-bone interface showed a traction-displacement response with an initial stiffness followed by initiation of damage and softening (Figure 5.4a). Moreover, under pure tension the tractions in the tangential direction (T_T) were found to be negligible (Figure 5.4d). Symmetric

crack patterns were characterized in breaking off bone and cement spurs (Figure 5.5). The ultimate strengths ($T_{N,ult}$) in pure tension for the four models ranged from 1.28 to 2.79MPa and the normal stiffness $\left(\frac{\partial T_N}{\partial \Delta_N}\right)$ from 123 to 251 MPa/mm (Table 5.1). In contrast, pure compressive loading (α=180°) resulted in a linear T_N-Δ_N relationship (Figure 5.4a), with stiffness ranging from 769 to 1538 MPa/mm (Table 5.1). Hardly any cracks occurred in pure compression (Figure 5.5).

In pure shear (α=90°) a linear increase of T_T as a function Δ_T was found; and none of the models reached failure (Figure 5.4c). The tangential stiffness $\left(\frac{\partial T_T}{\partial \Delta_T}\right)$ ranged from 222 to 332 MPa/mm for all models. Surprisingly, despite the lack of a softening phase in pure shear, cracks were observed which originated at the contact interface and progressed into the bone and cement bulk without breaking off spurs (Figure 5.5). Additionally, a considerable compressive traction was observed to prevent dilation of the interface (Figure 5.4b).

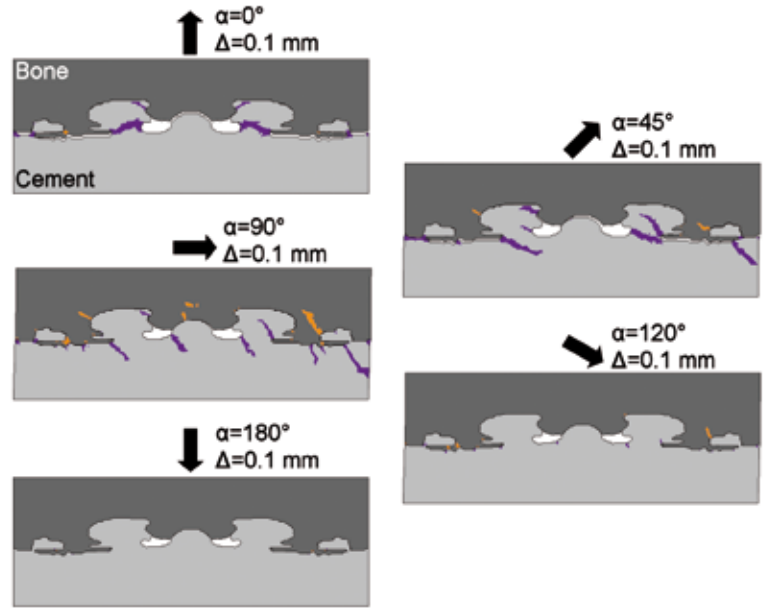

Figure 5.5 *Crack patterns in the cement (purple) and bone (orange) of model 1 after Δ=0.1 mm displacement under five different load angles. At α=0° the cement spurs were completely destructed what resulted in almost no T_N (Figure 5.4a). At α=90°, however, cracks traveled into the bulk of the bone and cement instead off breaking off spurs what resulted in no ultimate strength in shear (Figure 5.4c). The crack patterns that arose at α=45° showed a combination of the crack patterns in pure tension and shear. In pure compression (α=180°) hardly any cracks occurred.*

Model	int_N [mm]	int_T [mm]	0° $T_{N,ult}$ [MPa]	0° $\frac{\partial T_N}{\partial \Delta_N}\left[\frac{MPa}{mm}\right]$	180° $\frac{\partial T_N}{\partial \Delta_N}\left[\frac{MPa}{mm}\right]$	90° $\frac{\partial T_T}{\partial \Delta_T}\left[\frac{MPa}{mm}\right]$
1	0.21	5.84	1.82	123	888	217
2	0.26	5.14	2.79	251	975	241
3	0.03	3.08	1.28	149	769	294
4	0.48	4.36	2.19	172	1538	323
Experimental	0.14 - 0.48	No data	1.2 - 6.4	61.7 - 587	84 - 630	25.3 - 301

Table 5.1 *Morphological and mechanical parameters of the four models and experiments[18,37]. While the ultimate tensile strength, $T_{N,ult}$, and the stiffness at 0° and 90° fell in the range with what has been found previously, the compressive stiffness was over predicted.*

For all the considered intermediate values of α a smooth transition between responses described above was observed (Figure 5.4, 6). It is interesting to observe that for α=45°, 60° and 75° the normal tractions become eventually compressive. To better understand this counter intuitive response, we focused on model 3 where for α=45° the stress distribution at different points along the loading path was reported (Figure 5.7). We observed that for this value of α, the T_N-Δ_N response increased linearly until the ultimate strength ($T_{N,ult}$) was reached. At this point, all bone reaction forces acted in positive y-direction and few cracks were observed (Figure 5.7a). Nearly the whole stress field in normal direction (σ_{yy}) was positive and the stress field in tangential direction (σ_{xx}) revealed the first areas subjected to compression due to the bone-cement contact. After this point, T_N decreased and when T_N=0 both tensile and compressive contact forces were observed (Figure 5.7b). Cracks were present in both bone and cement and progressed into the bulk materials. Positive and negative values were found for the stress field σ_{yy}. The stress field σ_{xx} showed some areas of compression which were located between the contact area and the originated cracks. When displaced further T_N became negative, so that normal compression was induced even with the positive normal displacement. When T_N=-$T_{N,ult}$, almost all reaction forces acted in the negative y-direction (Figure 5.7c). The amount of cracks increased considerably and almost the whole area with bone-cement interlock was loaded in compression, σ_{xx}.

Comparison of all mixed mode responses showed that the normal traction (T_N) and displacements (Δ_N) at which the normal strength was reached $\left(\frac{\partial T_N}{\partial \Delta_N}=0\right)$ decreased when the loading angle increased (Figure 5.4, 5.6). Although loaded in different directions, the normal stiffness $\left(\frac{\partial T_N}{\partial \Delta_N}\right)$ remained constant (Figure 5.4, 5.6). On the other hand, the tangential stiffness $\left(\frac{\partial T_T}{\partial \Delta_T}\right)$

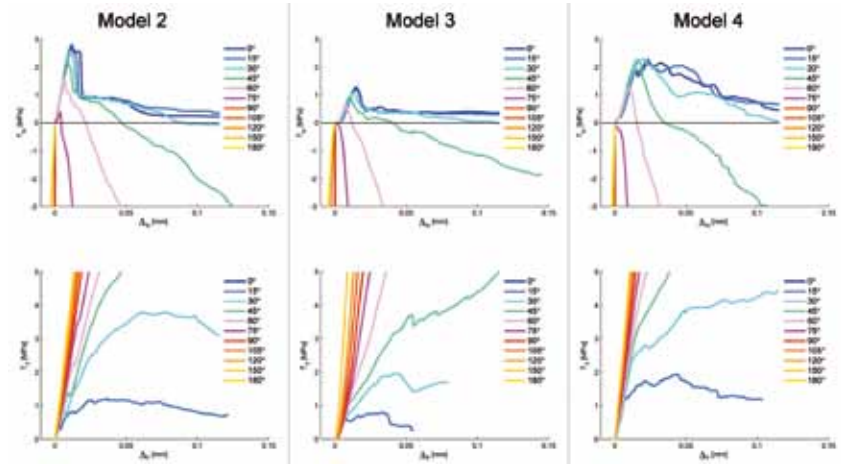

Figure 5.6 *The T_N-Δ_N and T_T-Δ_T relationships for the models 2, 3 and 4. The mixed-mode responses of model 1 was already shown in Figure 5.4. In pure tension the models 2 and 3 resulted in a rather 'brittle' response, while model 4 was more ductile.*

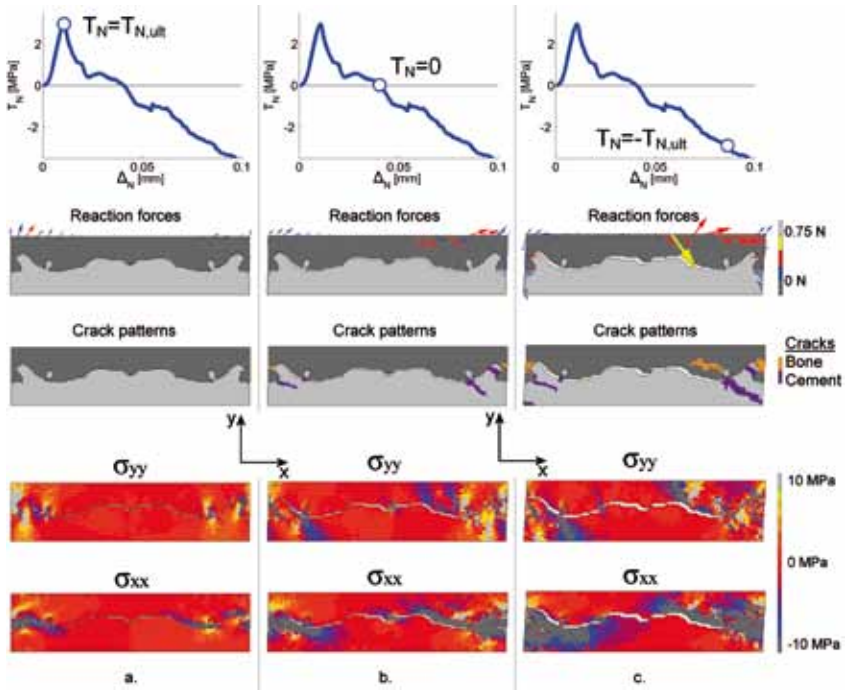

Figure 5.7 *Post-failure response of model 3 when loaded at 45°. Bone reaction forces, crack patterns and stress fields, σ_{xx} and σ_{yy}, at three different moments during the failure response: (1) T_N=$T_{N,ult}$, (2) T_N=0 and (3) T_N=-$T_{N,ult}$. The crack patterns at T_N=-$T_{N,ult}$ show bone and cement cracks that enter the model's right-hand side and continue progressing from the left side as a result of the periodic boundary conditions.*

For model 2, addition of an extra bone and cement layer did not affect the response in pure tension (0°) (Figure 5.8a). On the other hand, in pure shear (90°) the extra layers made the response in the tangential direction more compliant (Figure 5.8b); the tangential stiffness $\left(\frac{\partial T_T}{\partial \Delta_T}\right)$ decreased from 241 MPa/mm to 167 MPa/mm. However, when the same gage length in the extended model 2 was considered as in the original model, the difference in mechanical response was negligible. In contrast to the aforementioned phenomena, the coupled stiffness

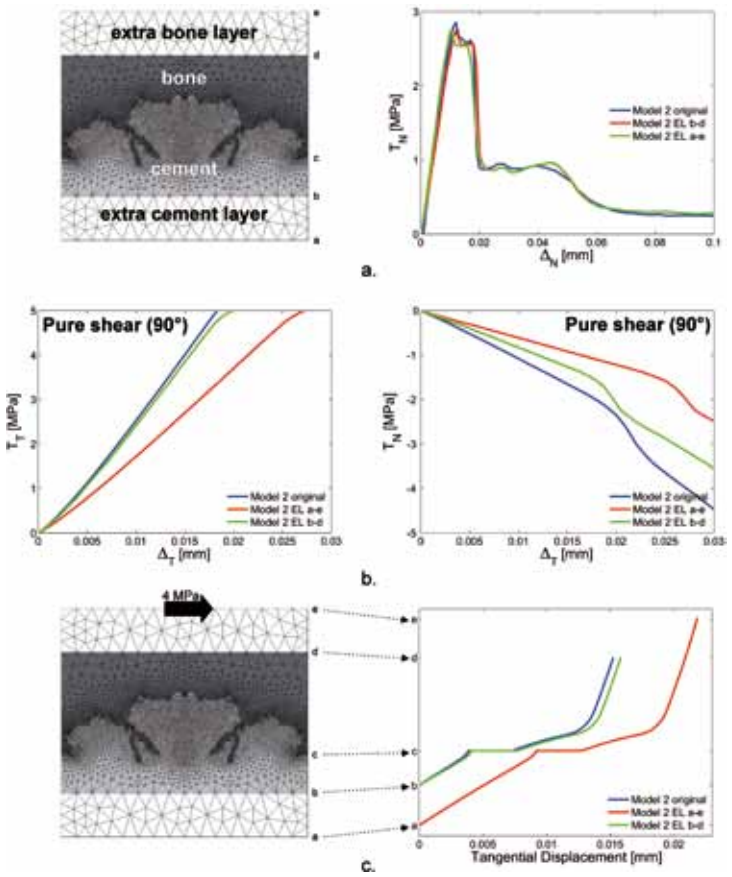

Figure 5.8

a There was negligible difference in tensile response (0°) between the original model 2 and the extended model 2 with a 1 mm extra layer (EL) of bone and cement.

b When loaded under a 90° angle, the response of the extended model 2 was more compliant in as well the tangential as normal direction. The tangential stiffness $\left(\frac{\partial T_T}{\partial \Delta_T}\right)$ decreased from 241 MPa/mm to 167 MPa/mm. However, considering the same area as the original model 2, here was hardly any difference in tangential stiffness.

c When loaded with 4 MPa in tangential direction there were only some small differences in tangential displacement between the original model 2 and the same area of the extended model 2. The extended model 2 resulted in more tangential displacement.

$\frac{\partial T_N}{\partial \Delta_T}$ based on the original gage length of the extended model did not match the $\frac{\partial T_N}{\partial \Delta_T}$ response of the original model 2 (Figure 5.8b). Considering an equal applied load, the extended model resulted in the largest tangential deformation (Figure 5.8c). Again when considering the same gage length in the extended model as the original model 2, the deformations were nearly identical.

Finally the relation between the mechanical response and the morphology was investigated. The maximum tensile traction (T_N) that occurred under tensile loading, $\left(\frac{\partial T_N}{\partial \Delta_N} = 0\right)$ was found to be moderately correlated with the average normal interdigitation ($int_{N,\alpha}$) (r^2=0.54; Figure 5.9a). Different loading directions did not strongly influence the normal stiffness $\left(\frac{\partial T_N}{\partial \Delta_N}\right)$ in tension and compression (Figure 5.4, 5.6) and could therefore not be related to the average normal interdigitation ($int_{N,\alpha}$) (r^2=0.00002 and r^2=0.21 for tension and compression, respectively; Figure 5.9b). The tangent stiffness at different load angles $\left(\frac{\partial T_T}{\partial \Delta_T}\right)$ showed no correlation with the average tangential interdigitation ($int_{T,\alpha}$) (r^2=0.03; Figure 5.9c).

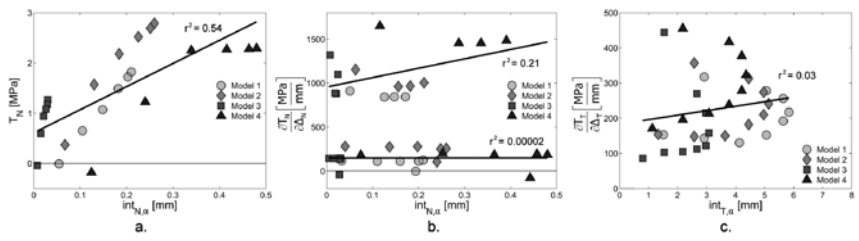

Figure 5.9

a. Relationship between the maximum tensile traction, T_N, and the average normal interdigitation, $int_{N,\alpha}$, (r^2=0.54).

b. Relationship between the normal stiffness, $\frac{\partial T_N}{\partial \Delta_N}$ and the average normal interdigitation, $int_{N,\alpha}$, resulted in no correlation in tension (r^2=0.00002) and a poor correlation in compression (r^2=0.21).

c. Relationship between the tangential stiffness, $\frac{\partial T_T}{\partial \Delta_T}$ and the average tangential interdigitation, $int_{T,\alpha}$, (r^2=0.03).

Discussion

In this study four generalized plain strain FEA models were used to investigate the mixed-mode response of the cement-bone interface. The analysis represented a basis for the implementation of an ad-hoc cohesive law.

The results show that the ultimate tensile strength ($T_{N,ult}$) and stiffness $\left(\frac{\partial T_N}{\partial \Delta_N}\right)$

determined for each model compare well with experimental observations, while the compressive stiffness is overestimated (Table 5.1). The response in shear also results in a satisfactorily stiffness $\left(\frac{\partial T_T}{\partial \Delta_T}\right)$ relative to experimental findings, but differs from the simulated tensile response as no ultimate strength is found. This can be explained by the crack patterns, which show that bone and cement spurs break off in tension, while in shear cracks progress into the bulk materials. Additionally, a considerable compressive traction is needed to prevent dilation of the interface. All mixed-mode responses show a gradual transition between the three 'principal' responses: tension, shear and compression.

The mechanical mixed-mode response cannot be related to the interface morphology in terms of cement interdigitation. The ultimate strength in normal direction for all mixed modes and the normal and tangential stiffness showed either a poor or no correlation with the average normal and tangential interdigitation of the cement.

In the original models, the top edge of the bone and bottom edge of the cement were modeled with an ~1 mm offset relative to the contact interface to avoid mechanical boundary artifacts, such as stress concentration and crack progression. To study the influence of such boundary conditions, the offset of model 2 was extended by adding an extra cement and bone layer. This extra layer appears not to affect the normal response, but makes the tangential response more compliant. However, when the same gage length as the original model 2 is considered, the response matches the response of the original model 2. This indicates that in the shear direction extending the boundary conditions does not have an effect on the near interface deformation field. However, the addition of the extra layers increases the compliance in the axial direction, which in turn reduces the amount of compression generated during shear loading. One would anticipate that additional extension of the cement and bone offset would further reduce the coupled stiffness, $\frac{\partial T_N}{\partial \Delta_T}$.

When loaded in pure tension (0°) fully symmetric crack patterns arise in the cement-bone interface as a result of the symmetric morphology (Figure 5.5). In pure shear (90°) the cracks progresses into the bulk material. This type of cracking at the cement- bone interface has been reported before[42]. The crack patterns that occur when loaded in 45° tend to be a combination of the crack patterns in 0° and 90°; spurs break off and cracks progress into the bulk (Figure 5.5).

In pure shear, a considerable compressive traction is generated which prevents dilation of the interface. Moreover, no ultimate strength was found in pure shear, which is different from experimental findings. This can be explained by the experimental setup used in these tests in which linear sliders were used, which result in no interfacial normal stresses when loaded in shear[11,20,21]. This allows the interface to open[12], but is neglected in the overall motion analysis[19], in contrast to the current study. However, recently, shear experiments of the cement-bone interface have been performed in which the interface was not allowed to dilate[42]. In this study, ultimate shear strengths were found which exceeded 20MPa; considerably larger compared to the studies in which interfacial dilation was allowed. FEA studies on other interfaces have demonstrated that normal compression stresses do occur in pure shear loading of interfaces[31]. It is believed that this is caused by the formation of micro cracks and shear hackles in the interlaced interface[29]. These features were also found in the current study

(Figure 5.5, 7).

By means of the implementation of periodic boundary conditions, one cement-bone interface model represents the complete cement-bone interface of a complete hip reconstruction. The periodic boundary conditions are applied using links, which provide equal displacements on both sides of the model[32]. The initial mirroring of the models consequently result in bone-to-bone and cement-to-cement links. The results show that the periodic boundary conditions result in stress distributions that are smoothly transferred from the model's left side to its right side (Figure 5.7). Also cracks that progressed into one of the model's sides continued progressing out of the opposite side (Figure 5.7) indicating that the boundary conditions functioned properly.

Our study limitations include the modeling of the cement-bone interface, which was considered as 2D plain strain models instead of complete 3D models of the interface. Although the plane strain models result in satisfactorily ultimate tensile strengths, the accompanying displacement at peak strength is rather low compared to experimental findings[18]. Whether this 'brittle response' could be ascribed to the fact that 2D models were used is not clear, but 2D models do prohibit local motions in the third degree of freedom, which could contribute to more interfacial friction. Furthermore, the models are very stiff in compression, which could be attributed to the absence of significant gaps and cavities at the interface. Moreover, the applied periodic boundary conditions prohibit the models to expand as a result of the compression.

During the generation of the models used in this study, the models were mirrored. Although this does not represent a cement-bone interface portion that would occur in vivo, utilizing symmetric models is commonly used in orthopaedic related FEA studies to apply the preferred boundary conditions[8,25,26]. Moreover, besides the boundary condition issue, mirroring is necessary to achieve the desired mechanical response. When the models would not have been mirrored, confounding tangential tractions would occur when loaded in pure tension.

To relate the mechanical mixed-mode response of the cement-bone interface to interface morphology we have focused on the cement penetration into the bone, which has been proven to be a reliable parameter for mechanical comparisons in tension and shear[37]. Other approaches, such as the quantitative CT-density and the contact area between the bone and cement have not been used, since these 'global' parameters could not be converted to a directional dependent value. To determine the angular-dependent cement penetration, we have used an approach that used the maximum normal and tangential cement penetration as a function of the loading angle. Quantifying the cement penetration for each loading angle would result in measurement difficulties, due to differences in grid distances and the interfacial with over which the grid is spanned.

Another limitation of our study is that the effect of damage occurring under a certain load/direction on the mechanical response in another direction has not been investigated. For example, it is not known how complete fracture, as a result of a pure tensile load, affects the mechanical response in tangential direction with respect to the undamaged tangential response. Additional simulations could be performed in which for each loading angle multiple damage stages are captured. Subsequently, these damaged cases would be loaded in other directions. However, this fell beyond the scope of the current study.

A similar limitation is the path dependency, which has not been investigated. In

this study, the top plane of the bone is consequently moved in one direction starting from the origin. Other paths, such as a normal displacement followed by a tangential displacement, have not been considered. However, it has previously been shown that the loading path has significant influence on the mechanical response[27,35].

The results show that the cement-bone interface is almost infinitely strong in pure shear. However, experimental tests have shown that this is not the case[20,21,42]. The discrepancy between these two findings can be explained by the rigid boundary conditions that have been applied to our micro-model, which are absent in reality. For example, the simulations do not allow any movement in normal direction if a pure shear was applied. In reality, the surrounding material will be compliant and allow deformation in normal direction. Therefore the information obtained with the micro-models in this study should be considered as describing the mechanical behavior of the cement-bone interface layer itself. If this behavior is implemented around cemented total joint reconstructions, the compliance of the surrounding material will govern the external boundary conditions. This will allow the interface to dilate and fail at realistic shear strength values.

The goal of this study was to generate data on the mixed-mode response of the cement-bone interface for implementation in cohesive elements. Cohesive models that have been developed in the past might not be applicable for the response found in this study, because these models assume separate fracture energies in tension and shear[1,27,41]. Our study, however, does not find a consistent value for the fracture energy in shear, because no failure is predicted. A possible solution is to include a cohesive model in which a global fracture energy is used instead of two separate fracture energies and the possibility to define an interface specific mechanical response in pure shear[40]. Besides the numerical implementation of cohesive failure models into cohesive elements it is also important to emphasize the physical implementation of the cohesive element into the mesh. This study demonstrated that the offset of the top and bottom edge relative to the contact area influences the shear properties of that specific portion of the cement-bone interface (Figure 5.8). Therefore, one should be aware that when implementing the reported mechanical response in complete models of cemented hip reconstructions, the cohesive element not only capture the interface, but also some adjacent material.

In conclusion: (1) This study revealed novel features of the cement-bone interface, such as considerable compressive tractions and no failure in shear. The predicted tensile strength and stiffness and the shear stiffness positively match previous experimental findings; (2) The mechanical response could not be related to the interfacial morphology in terms of cement penetration. Overall, we conclude that this study exhibited enough detail of the mechanical mixed-mode response of the cement-bone interface for implementation in cohesive elements.

Acknowledgements

This work was funded by the NIH grant AR42017.

References

1. **Alfano, G., Crisfield, M. A., (2001).**
Finite element interface models for the delamination analysis of laminated composites: Mechanical and computational issues.
International Journal for Numerical Methods in Engineering 50, 1701-1736.
2. **Bishop, N. E., Schoenwald, M., Schultz, P., Puschel, K., Morlock, M. M., (2009).**
The condition of the cement mantle in femoral hip prosthesis implantations--a post mortem retrieval study. Hip.Int. 19, 87-95.
3. **Colombi, P., (2002).**
Fatigue analysis of cemented hip prosthesis: model definition and damage evolution algorithms. International Journal of Fatigue 24, 895-901.
4. **Harper, E. J., Bonfield, W., (2000).**
Tensile characteristics of ten commercial acrylic bone cements. J.Biomed.Mater.Res. 53, 605-616.
5. **Hung, J. P., Chen, J. H., Chiang, H. L., Wu, J. S., (2004).**
Computer simulation on fatigue behavior of cemented hip prostheses: a physiological model. Comput.Methods Programs Biomed. 76, 103-113.
6. **Janssen, D., Mann, K. A., Verdonschot, N., (2008).**
Micro-mechanical modeling of the cement-bone interface: The effect of friction, morphology and material properties on the micromechanical response. J.Biomech. 41, 3158-3163.
7. **Janssen, D., Mann, K. A., Verdonschot, N., (2009).**
Finite element simulation of cement-bone interface micromechanics: a comparison to experimental results. J.Orthop.Res. 27, 1312-1318.
8. **Kadir, M. R., Syahrom, A., Ochsner, A., (2010).**
Finite element analysis of idealised unit cell cancellous structure based on morphological indices of cancellous bone. Med.Biol.Eng Comput. 48, 497-505.
9. **Katoozian, H., Davy, D. T., (2000).**
Effects of loading conditions and objective function on three-dimensional shape optimization of femoral components of hip endoprostheses. Med.Eng Phys. 22, 243-251.
10. **Keyak, J. H., Kaneko, T. S., Tehranzadeh, J., Skinner, H. B., (2005).**
Predicting proximal femoral strength using structural engineering models.
Clin.Orthop.Relat Res. 437, 219-228.
11. **Kim, D. G., Miller, M. A., Mann, K. A., (2004).**
A fatigue damage model for the cement-bone interface. J.Biomech. 37, 1505-1512.
12. **Lee, H. S., Park, Y. J., Cho, T. F., You, K. H., (2001).**
Influence of asperity degradation on the mechanical behavior of rough rock joints under cyclic shear loading. International Journal of Rock Mechanics and Mining Sciences 38, 967-980.
13. **Lewis, G., (1997).**
Properties of acrylic bone cement: state of the art review. J.Biomed.Mater.Res. 38, 155-182.
14. **Lewis, G., Duggineni, R., (2006).**
Finite element analysis of a three-dimensional model of a proximal femur-cemented femoral THJR component construct: Influence of assigned interface conditions on strain energy density. Bio-Medical Materials and Engineering 16, 319-327.

15. **Lotz, J. C., Gerhart, T. N., Hayes, W. C., (1991).**
Mechanical properties of metaphyseal bone in the proximal femur. J.Biomech. 24, 317-329.
16. **Mann, K. A., Ayers, D. C., Werner, F. W., Nicoletta, R. J., Fortino, M. D., (1997).**
Tensile strength of the cement-bone interface depends on the amount of bone interdigitated with PMMA cement. J.Biomech. 30, 339-346.
17. **Mann, K. A., Damron, L. A., (2002).**
Predicting the failure response of cement-bone constructs using a non-linear fracture mechanics approach. J.Biomech.Eng 124, 462-470.
18. **Mann, K. A., Miller, M. A., Cleary, R. J., Janssen, D., Verdonschot, N., (2008).**
Experimental micromechanics of the cement-bone interface. J.Orthop.Res. 26, 872-879.
19. **Mann, K. A., Miller, M. A., Race, A., Verdonschot, N., (2009).**
Shear fatigue micromechanics of the cement-bone interface: An in vitro study using digital image correlation techniques. J.Orthop.Res. 27, 340-346.
20. **Mann, K. A., Mocarski, R., Damron, L. A., Allen, M. J., Ayers, D. C., (2001).**
Mixed-mode failure response of the cement-bone interface. J.Orthop.Res. 19, 1153-1161.
21. **Mann, K. A., Werner, F. W., Ayers, D. C., (1999).**
Mechanical strength of the cement-bone interface is greater in shear than in tension. J.Biomech. 32, 1251-1254.
22. **Miller, M. A., Eberhardt, A. W., Cleary, R. J., Verdonschot, N., Mann, K. A., (2010).**
Micromechanics of postmortem-retrieved cement-bone interfaces. J.Orthop.Res. 28, 170-177.
23. **Moreo, P., Garcia-Aznar, J. M., Doblare, M., (2007).**
A coupled viscoplastic rate-dependent damage model for the simulation of fatigue failure of cement-bone interfaces. International Journal of Plasticity 23, 2058-2084.
24. **Moreo, P., Perez, M. A., Garcia-Amar, J. M., Doblare, M., (2006).**
Modelling the mixed-mode failure of cement-bone interfaces.
Engineering Fracture Mechanics 73, 1379-1395.
25. **Mullins, L. P., McGarry, J. P., Bruzzi, M. S., McHugh, P. E., (2007).**
Micromechanical modelling of cortical bone.
Comput.Methods Biomech.Biomed.Engin. 10, 159-169.
26. **Pahr, D. H., Zysset, P. K., (2008).**
Influence of boundary conditions on computed apparent elastic properties of cancellous bone. Biomech.Model Mechanobiol. 7, 463-476.
27. **Park, K., Paulino, G. H., Roesler, J. R., (2009).**
A unified potential-based cohesive model of mixed-mode fracture.
Journal of the Mechanics and Physics of Solids 57, 891-908.
28. **Perez, M. A., Garcia-Aznar, J. M., Doblare, M., (2009).**
Does increased bone-cement interface strength have negative consequences for bulk cement integrity? A finite element study. Ann.Biomed.Eng 37, 454-466.
29. **Pettersson, K. B., Neumeister, J. M., Gamstedt, E. K., Oberg, H., (2006).**
Stiffness reduction, creep, and irreversible strains in fiber composites tested in repeated interlaminar shear. Composite Structures 76, 151-161.
30. **Race, A., Miller, M. A., Mann, K. A., (2010).**
Novel methods to study functional loading micromechanics at the stem-cement and cement-bone interface in cemented femoral hip replacements. J.Biomech. 43, 788-791.

31. **Salomonsson, K., (2008).**
Mixed mode modeling of a thin adhesive layer using a meso-mechanical model.
Mechanics of Materials 40, 665-672.
32. **Salomonsson, K., Andersson, T., (2008).**
Modeling and parameter calibration of an adhesive layer at the meso level.
Mechanics of Materials 40, 48-65.
33. **Stolk, J., Janssen, D., Huiskes, R., Verdonschot, N., (2007).**
Finite element-based preclinical testing of cemented total hip implants.
Clin.Orthop.Relat Res. 456, 138-147.
34. **Stolk, J., Verdonschot, N., Murphy, B. P., Prendergast, P. J., Huiskes, R., (2004).**
Finite element simulation of anisotropic damage accumulation and creep in acrylic bone cement. Engineering Fracture Mechanics 71, 513-528.
35. **van den Bosch, M. J., Schreurs, P. J. G., Geers, M. G. D., (2006).**
An. improved description of the exponential Xu and Needleman cohesive zone law for mixed-mode decohesion. Engineering Fracture Mechanics 73, 1220-1234.
36. **Verdonschot, N., Huiskes, R., (1997).**
The effects of cement-stem debonding in THA on the long-term failure probability of cement. J.Biomech. 30, 795-802.
37. **Waanders, D., Janssen, D., Mann, K. A., Verdonschot, N., (2010).**
The mechanical effects of different levels of cement penetration at the cement-bone interface. J.Biomech. 43, 1167-1175.
38. **Waanders, D., Janssen, D., Miller, M. A., Mann, K. A., Verdonschot, N., (2009).**
Fatigue creep damage at the cement-bone interface: an experimental and a micro-mechanical finite element study. J.Biomech. 42, 2513-2519.
39. **Wang, J. Y., Tozzi, G., Chen, J., Contal, F., Lupton, C., Tong, J., (2010).**
Bone-cement interfacial behaviour under mixed mode loading conditions.
J Mech Behav Biomed Mater 3, 392-398.
40. **Wei, Y., Hutchinson, J. W., (2008).**
Toughness of Ni/Al2O3 interfaces as dependent on micron-scale plasticity and atomistic-scale separation. Philosophical Magazine 88, 3841-3859.
41. **Xu, X. P., Needleman, A., (1993).**
Void nucleation by inclusions debonding in a crystal matrix.
Model Simul Mater Sci Engng 1, 111-132.
42. **Yang, D. T., Zhang, D., Arola, D., (2010).**
Fatigue of the bone/cement interface and loosening of tatal joint replacements.
International Journal of Fatigue 32, 1639-1649.

Chapter

6

Multi-axial Loading Micromechanics of the Cement-Bone Interface in Post-Mortem Retrievals and Lab-Prepared Specimens

Journal of the Mechanical Behavior of Biomedical Materials (2011); 4(3):366-74.

Abstract

Maintaining adequate fixation between cement and bone is important for successful long term survival of cemented total joint replacements. Mixed-mode loading conditions (combination of tension/compression and shear) are present during in vivo loading, but the micromotion response of the interface to these conditions is not fully understood.

Non-destructive, multi-axial loading experiments were conducted on laboratory prepared (n=6) and post mortem (n=6) human cement-bone interfaces. Specimens were mounted in custom loading discs and loaded at 0, 30, 60, and 90° relative to the interface plane where 0° represents normal loading to the interface, and 90° represents shear loading along the longitudinal axis of the femur. Axial compliance did not depend on loading angle for laboratory prepared (p=0.96) or postmortem specimens (p=0.62). The cement-bone interface was more compliant under tensile than compressive loading at the 0° loading angle only (p=0.024). The coupled transverse to axial compliance ratio, which is a measure of the coupled motion, was small for laboratory prepared (0.115±0.115) and postmortem specimens (0.142±0.101). There was a moderately strong inverse relationship between interface compliance and contact index ($r^2 = 0.65$).

From a computational modeling perspective, the results of the current study support the concept that the cement-bone interface could be numerically implemented as a compliant layer with the same initial stiffness in tension and shear directions. The magnitude of the compliance could be modified to simulate immediate post-operative conditions (using laboratory prepared data set) or long-term remodeling (using postmortem data set).

Introduction

There is continued interest in understanding the role of the cement-bone interface in the loosening process of total joint replacements. Recent work has focused on improved characterization of the mechanics of the interface including mixed-mode loading experiment[14,17], modification of the interface to improve fatigue strength[1], evaluation of postmortem specimens in terms of morphology[2] and micromechanics[9], and development of micromechanical[15] and cohesive failure models[11,12].

Experimentally, the issue of mixed-mode loading of specimens remains a challenging one because a specimen can only be loaded in one direction to failure, and the failure response in other directions can obviously not be determined with the same specimen. One solution is to perform computational finite element analysis (FEA) of the test specimens, where it is possible to repeat loading and simulate subsequent failure on each model in all manner of loading directions[15]. However, there are several assumptions made with these models with regards to the elastic properties and material failure models used for the model constituents and the ability to accurately model the interface morphology between the cement and bone. These factors add a degree of uncertainty to the simulation results. Ideally, experiments that could be performed non-destructively, under a variety of mixed-mode loading conditions could provide new information regarding the micromechanics of the cement-bone interface. Data of this type is currently unavailable in the literature.

Recent experimental work on the cement-bone interface has found that the interface is quite compliant (~10 microns/MPa)[6] with sliding and opening occurring from shear and tensile loading conditions, respectively. In addition, this interface becomes more compliant following in vivo service (~50 microns/MPa)[9]. The question remains as to whether this micromotion is dependent on the loading direction. To address this question we performed multi-loading angle experiments on cement-bone interface specimens. We asked three research questions: (1) does interface compliance depend on loading angle?; (2) are there appreciable coupled transverse motions?; and (3) can interface compliance be explained by contact between cement and bone and source of bone (lab prepared or postmortem retrieval)?

Methods

Twelve cement-bone interface specimens were created from human cemented femoral hip replacements obtained as postmortem retrievals (n=6) and from laboratory prepared constructs (n=6). A total of eight fresh-frozen proximal femurs were obtained from the SUNY Upstate Medical University Anatomical Gift Program. Four donor bones had cemented femoral components in place (the retrieval group). An additional four donor femora without implants were prepared for cementing by broaching, brush lavage, and distal plugging followed by retrograde introduction of surgical PMMA cement with pressurization and introduction of a double-tapered acrylic stem (the laboratory prepared group). For the laboratory prepared group, bones were warmed to 37°C in a saline calcium buffered water bath prior to cementing. Specimen data, including donor age, sex, time in service (where appropriate), and anatomic location are shown in Table 6.1.

Specimen	Age	Sex	Years in Service	Distance from Calcar (mm)	Quadrant	Applied Stress (MPa)
LP1	80	Male	NA	50	Posterior	1.58
LP2	80	Male	NA	50	Lateral	1.02
LP3	90	Female	NA	80	Posterior	0.51
LP4	76	Female	NA	50	Anterior	0.45
LP5	75	Male	NA	100	Medial	0.48
LP6	80	Male	NA	90	Lateral	0.85
PM1	67	Female	14	100	Medial	0.04
PM2	67	Female	14	100	Posterior	0.39
PM3	67	Female	14	110	Lateral	0.14
PM4	76	Female	2	170	Lateral	0.17
PM5	93	Female	Unknown	70	Posterior	0.17
PM6	77	Female	Unknown	90	Lateral	0.18

Table 6.1 *Source of cement-bone specimens for lab prepared (LP) and postmortem retrieval specimens (PM). Distance from the calcar is measured distally with specimens taken from the distal half of the cemented stem construct.*

Specimens were obtained from both postmortem retrievals and laboratory prepared constructs to provide a sample population that spanned a wide range of interface morphologies and interface strengths. Specimen preparation followed a methodology described previously[6]. Briefly, transverse sections at 10mm intervals of the cemented construct were created. An acrylic side plate was attached between the cement and bone to protect the interface from untoward loading during subsequent handling. Rectangular prism-shaped specimens were then cut from the location of the side plate with 4x9mm cross section. Micro-CT scans (Scanco 40, SCANCO Medical AG, Bruttisellen, Switzerland) were obtained for each specimen to document interface morphology at 12 micron resolution. Specimens were screened to include only those with cement-bone interdigitation less than 3.2mm, to insure that they would fit the loading apparatus.

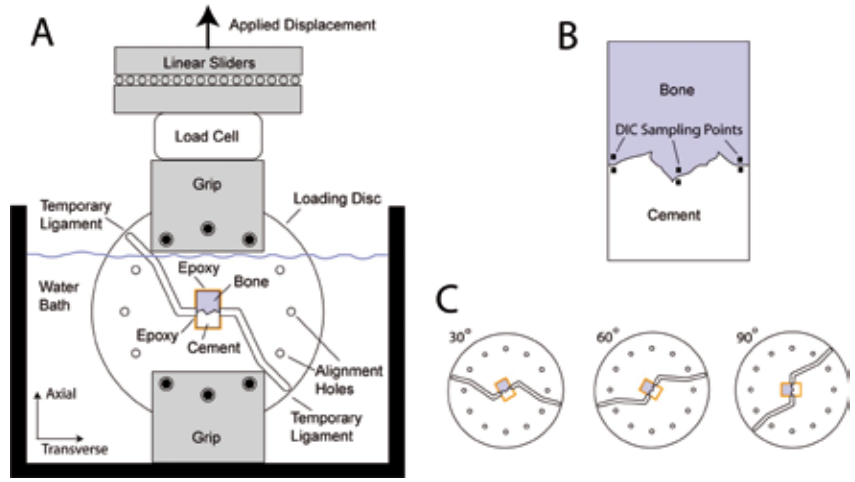

Figure 6.1 *Experimental apparatus used to apply axial loads to the loading disc in a water bath (a). The digital image correlation (DIC) sampling points were made at three pairs of points immediately adjacent to the cement-bone interface (b). The loading disc system was designed to allow testing at 0, 30, 60, and 90° loading directions (c).*

Specimens were mounted in a "Brazil nut"-type specimen loading disc with provision to load the interface at 0, 30, 60, or 90° relative to the cement-bone interface (Figure 6.1a). In terms of a cylindrical coordinate system of the cemented femoral component, 0° represents normal loading along the femoral radial axis, and 90° represents shear loading along the longitudinal axis of the femur. Loading discs were custom fabricated for each specimen from a 9.5mm thick polycarbonate sheet using a computer numerically controlled (CNC) mill. Instead of grips typically used to clamp the specimens, epoxy was used to bond the cement and bone to the loading disc. To achieve this, individual specimen shapes were cut out of the polycarbonate sheet using the CNC mill. A 3mm slot was milled in the loading disc to bisect the disc into two halves. Small temporary ligaments (Figure 6.1a) were used to maintain integrity of the two halves of the loading disc prior to insertion of the test specimen and to prevent loads from transferring across the cement-bone interface prior to mechanical testing. The epoxy was carefully applied to the cement and bone surfaces in situ, using an 18 gauge needle via small ports drilled through the loading disc. This ensured that epoxy did not contact the interface between cement and bone.

The loading discs were attached to custom grips using conical screws that aligned the specimen at the four different loading angles. Linear sliders were used above the top test grip to allow free out of plane displacement. Load (displacement) was applied using a screw driven mechanical load frame (Q-test, MTS Systems, Eden Prarie, MN) with an in-line load cell. Just prior to testing, the side plate connecting the cement and bone was severed, along with

the temporary ligaments in the loading disc, using a heated surgical blade. Specimens were tested in an acrylic water bath containing a calcium buffered saline solution at 37ºC.

To quantify interface motion during testing, a Digital Image Correlation (DIC) technique was used as described previously (Mann et al., 2008). Briefly, a black paint overspray was applied to the specimen surface to provide texture for the DIC process. A CCD camera with telecentric lens (0.0085 mm/pixel resolution) captured images during loading. Interface motion was measured at 3 pairs of points along the cement-bone interface (Figure 6.1b). The RMS error of the DIC system was 0.000395mm.

Because the measurement of interface micromotion using the DIC technique was performed as a post-processing step, after completion of mechanical loading, an initial loading procedure was performed on each specimen to determine limits that would result in measurable (on the order of 10 microns), but non-destructive loading. It was determined previously that the interface micromotion at failure in the tensile direction was 0.041±0.017 mm[6]. Hence, to be in the non-destructive range, 10 microns of global crosshead displacement was applied in the tensile direction, with the specimens oriented at the 30° loading angle. Note that application of global displacements of 10 microns should result in lower displacements at the interface, due to compliance at locations other than the cement-bone interface. The local interface micromotion was then calculated using DIC and the initial interface compliance was determined (inverse slope of the applied stress versus interface displacement curve). From this initial compliance estimate, the applied stress needed to displace the interface 8 microns (to ensure testing within the non destructive range) was calculated, and this applied stress was used as a limit for subsequent testing. The applied stress needed to displace the interface 8 microns was higher for the lab prepared specimens compared to the postmortem specimens (Table 6.1). This is expected because the tensile stiffness of lab prepared specimens (208±131 MPa/mm) has recently been shown to be much larger than postmortem retrieval (16±35 MPa/mm) specimens[9]. For the current data set, the estimated stiffness was 102±55 MPa/mm for the laboratory prepared specimens and 23±14 MPa/mm for postmortem retrieval specimens.

The main experiment consisted of loading the specimens to the prescribed stress level at 30°, 0°, 60°, and 90° test orientations, in that order (Figure 6.1c). We started with the 30° test orientation because preliminary testing suggested that this was the most compliant test direction; this was later proven to be not true, but for consistency the test was continued in that manner. Four tension-compression loading cycles were applied at each loading angle with DIC images captured during the fourth cycle; the first three cycles served as preconditioning cycles. *Axial compliance* (inverse of stiffness) in the direction of loading was defined as the inverse slope of the axial applied stress versus axial micromotion curve (Figure 6.2a) and was determined for tensile and compressive loading directions. *Coupled transverse compliance*, occurring perpendicular to the axis of loading was defined as the inverse slope of the axial applied stress versus transverse micromotion curve (Figure 6.2b). Conversion to local interface coordinates to document normal and shear components of micromotion was also performed (Figure 6.2c & d).

At the end of each test, the specimen was returned to the 30° and a confirmation compliance test was performed with results compared to the original 30° compliance test. For this purpose, the ratio of log compliance of the confirmation test was divided by the log compliance of the original test for both tension and compression loading directions. As noted below, the log compliance was used for all statistical tests to normalize data.

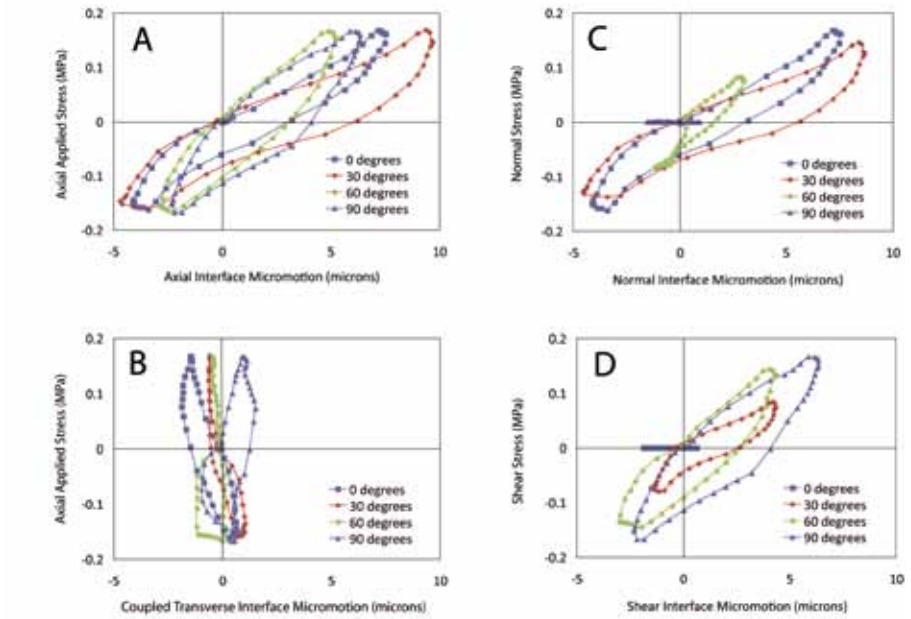

Figure 6.2 *The axial applied stress versus interface micro-motion response for specimen PM6 with loads applied at four different angles. The axial response (a) shows more micro-motion compared to the coupled transverse direction (b). Conversion to local coordinates is shown in panels c and d.*

Interface Morphology

A CT scan-based stereology approach was used to characterize the morphology of the interface for each specimen, and at each loading angle. Regularly spaced lines (0.38 to 0.53mm spacing) were projected through the specimen (Figure 6.3). At points where the projected lines crossed an interface between cement and bone, the status of the interface was designated as either in apposition, proximity, or gapped (>0.25mm). A *Contact Index* (CI) was calculated as the number of points of apposition, divided by the total number of projection lines that cross the interface. *Intersection Index* (II) was calculated as the total number points of apposition and proximity divided by total number of projection lines that cross the cement-bone interface. *Contact area* (CA) was calculated as the product of the Contact Index and the sampling area of the projection line. The sampling area of the projection line was defined as the square of the line spacing. The Interdigitation Depth (ID) was calculated along the projection lines using the same approach as described in Waanders et al. (2010). Considering a projection line that passed from the cement component to the bone (bottom to top in Figure 6.3), the distance from the first instance of contact with bone to the last instance of contact with cement would represent the interdigitation depth for that particular projection line. If the projection line crossed the cement-bone interface only once, the interdigitation depth was considered to be zero. The average of all projection line interdigitation depths was then determined. The interdigitation depth was only calculated at the 0° loading angle.

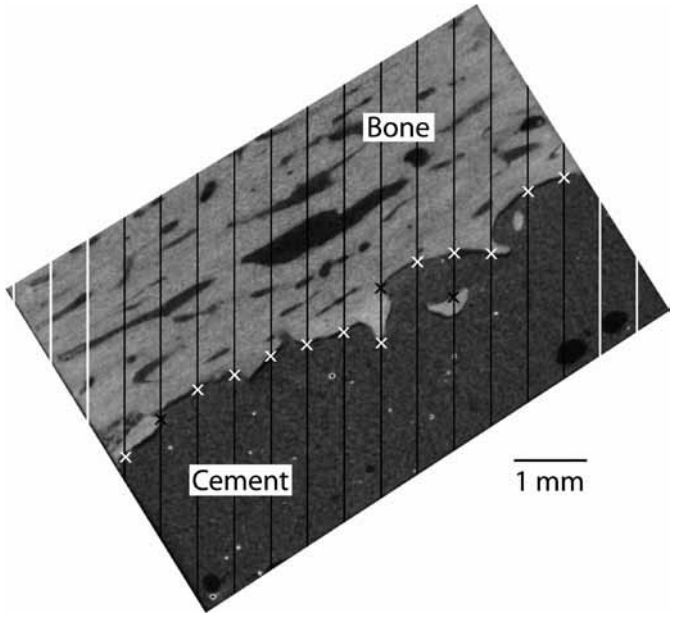

Figure 6.3 *Stereology grid lines was projected through the CT scan images of the specimens at the four different loading angles. A thirty degree loading angle case is shown here and lines that cross the cement-bone interface (black) are included in the total line count. Points of apposition (black x) and points of proximity (white x) at the cement-bone interface are shown for one plane of the interface.*

Statistical Analysis

To determine if compliance changed with loading angle, the slope of compliance versus loading angle was calculated for each specimen. From this, a t-test was performed to determine if the slope was different from zero. To determine if the interface was more compliant in the tensile direction compared to the compression direction for all loading angles, a tension to compression compliance ratio was calculated. A t-test with correction for multiple sampling was performed to determine if the ratio was greater than 1.0 for each loading angle. Similarly, a coupled transverse to axial compliance ratio was calculated to provide a relative measure of the magnitude of out of plane micro-motion. Simple linear regression analysis was used to assess the correlation of each of the morphology measurements with interface compliance. Following this, a step-wise regression was used to determine significant factors that contribute to interface compliance including morphological, source of bone, and loading angle. For all analyses, compliance was transformed with a log transformation to normalize distributions.

Parameter	*Laboratory Prepared (n=24)*		*Postmortem (n=23)*	
	Mean (SD)	Range	Mean (SD)	Range
Tensile axial compliance (mm/MPa)	0.0156 (0.008)	0.0033 – 0.037	0.052 (0.039)	0.0158 – 0.196
Compressive axial compliance (mm/MPa)	0.0146 (0.007)	0.0016 – 0.027	0.044 (0.028)	0.0133 – 0.109
Tension/Compression axial compliance ratio	1.108 (0.34)	0.68 – 2.12	1.140 (0.32)	0.77 – 1.86
Coupled Transverse compliance (mm/MPa)	0.0011 (0.0009)	$2.4x10^{-5}$ –0.0035	0.005 (0.006)	$1.12x10^{-5}$ – 0.027
Coupled Transverse/Axial compliance ratio	0.115 (0.115)	0.0157 – 0.48	0.142 (0.101)	0.0054 – 0.38
Contact Index (CI)	1.208 (0.61)	0.35 – 3.1	0.57 (0.31)	0.052 – 1.39
Contact Area (CA, mm^2)	22.97 (14.8)	6.5 – 53.8	10.8 (5.8)	2.02 – 21.6
Intersection index (II)	1.92 (0.65)	1.22 – 3.79	1.89 (0.69)	0.94 – 3.12
Interdigitation Depth (ID, mm)	0.234 (0.174)	0.062 – 0.43	0.375 (0.454)	0.009 – 0.990

Table 6.2 *Compliance and morphology data collected for the laboratory prepared and postmortem cement-bone interfaces. Results are shown for 24 laboratory prepared (4 loading angles x 6 specimens) and 23 postmortem (4 loading angles x 6 specimens, excluding PM1 loaded at 90°). The interdigitation depth was calculated for the 0° loading case only. Mean, standard deviation (SD) and range values are shown.*

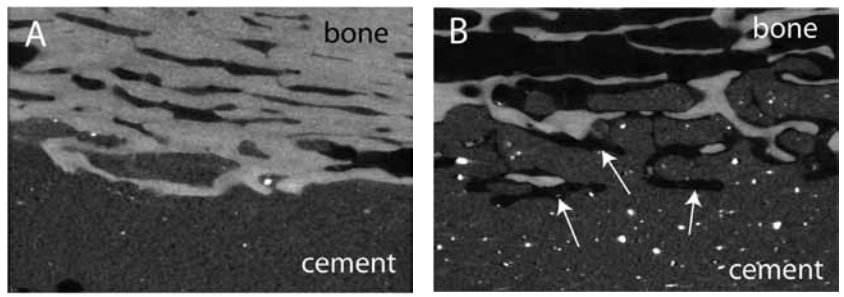

Figure 6.4 *Micro-CT images of the cement-bone interfaces from laboratory prepared (a, LP1) and postmortem retrieval (b, PM5) specimens. While the laboratory prepared specimen has extensive cement-bone contact at the interface, gaps are more prevalent between the cement and bone in the retrieval specimen. Regions indicative of bony resorption are designated by arrows.*

Results

Descriptive statistics for the mechanical and morphological outcome measures are presented as laboratory prepared and postmortem groups (Table 6.2). The morphology of the post-mortem specimens was substantially different from the laboratory prepared specimens. While the interdigitation depth ($p=0.50$) and intersection fraction ($p=0.87$) were not different between the two groups, there was significantly less contact index ($p<0.0001$) and contact area ($p<0.0001$) between cement and bone for the postmortem retrieval specimens. An example of these differences is shown in Figure 6.4 where there was similar interdigitation between the two specimen types but much less cement-bone contact for the post-mortem retrieval.

Tests were completed for all specimens at all loading angles except for PM1 that failed prior to completing the 90° loading angle configuration. It should be noted that PM1 had the lowest applied stress and was the most compliant of all the specimens, and thus was likely the weakest specimen. Axial compliance did not depend on loading angle (Figure 6.5a) for laboratory prepared ($p=0.96$) or postmortem specimens ($p=0.62$) (statistical analysis is shown in Table 6.3). The variance between specimens (0.78 coefficient of variation, calculated as the standard deviation divided by the mean) was much greater than the variance within specimens at the four different loading angles (0.28 average coefficient of variation, range: 0.036 to 0.92).

Specimen Source	*Mean (SD) ((mm/MPa)/degree)*	*Range ((mm/MPa)/degree)*	*P-value with Bonferroni Correction*
Laboratory Prepared (n=6)	6.1×10^{-5} (0.0027)	-0.0049 – 0.0026	0.96
Postmortem (n=6)	-0.0025 (0.0047)	-0.0113 – 0.0020	0.62
Combined (n=12)	-0.0011 (0.0039)	-0.0113 – 0.0026	0.62

Table 6.3 *The slope of the tensile compliance to loading angle response was calculated for laboratory prepared and postmortem specimens. A two-tailed t-test was performed to determine if the slope was different from 0. A zero slope would indicate that loading angle did not influence compliance. Mean, standard deviation (SD) and range values are shown.*

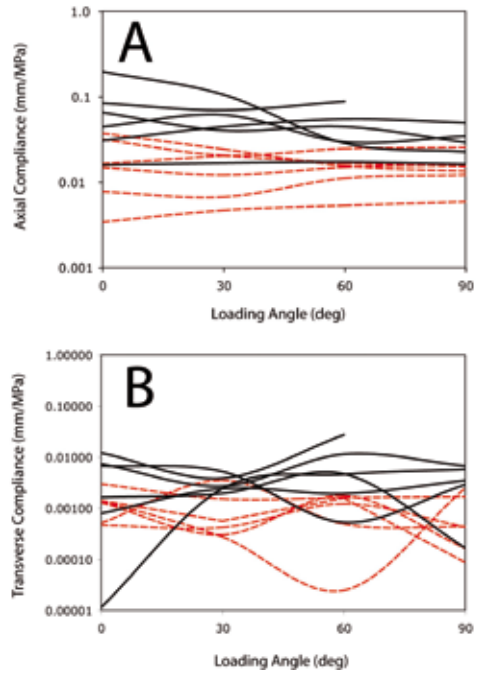

Figure 6.5 *Axial tensile compliance (a) and transverse compliance (b) of the cement-bone interface as a function of loading angle for postmortem (solid black lines) and laboratory prepared specimens (dashed red lines).*

The cement-bone interface was more compliant under tensile than compressive loading (Table 6.4) at the 0° loading angle only ($p=0.024$). The coupled transverse to axial compliance ratio, which is a measure of the coupled motion, was small for laboratory prepared (0.115±0.115) and postmortem specimens (0.142±0.101). The transverse compliance (Figure 6.5b) did not have any clear relationship with loading angle.

Compliance was inversely proportional to Contact Index ($r^2=0.50$, $p<0.0001$), Contact Area ($r^2=0.30$, $p<0.0001$), and Intersection Index ($r^2=0.12$, $p=0.018$). Using a stepwise regression model, both Contact Index ($p<0.0001$), and bone source (lab prepared or postmortem) ($p=0.0017$) contributed to estimates of interface compliance ($r^2 = 0.65$). Interestingly, for the same Contact Index, the postmortem specimens were more compliant than the laboratory prepared specimens (Figure 6.6). The interdigitation depth did not correlate with axial compliance ($r^2=0.08$, $p=0.36$).

The confirmation compliance test at 30° degrees was compared to the initial 30° compliance test for both tension and compression loading (22 total tests from 11 specimens with full runs with both tensile and compressive compliance measurements). Overall, the confirmation to original compliance ratio was 1.03 (0.15 SD) with 19 of the 22 tests having confirmation to original compliance ratios of less than 110%. Interestingly, half of the tests had confirmation compliances that were less than the original compliance. Two specimens with confirmation to original compliance ratios greater than 110% (115% in the compression direction and 129% and 152% in the tension direction) were from the most compliant specimens.

Loading Angle (deg)	Mean (SD)	Range	P-value with Bonferroni Correction
0	1.36 (0.43)	0.89 – 2.12	0.024
30	1.17 (0.32)	0.68 – 1.86	0.134
60	0.99 (0.18)	0.82 – 1.51	0.97
90	0.94 (0.09)	0.77 – 1.08	0.97

Table 6.4 *The ratio of axial tensile to axial compressive compliance of the cement-bone interface as a function of loading angle for the 12 test specimens. A one-tailed t-test was performed to determine if mean value was greater than 1.0. Mean, standard deviation (SD) and range values are shown.*

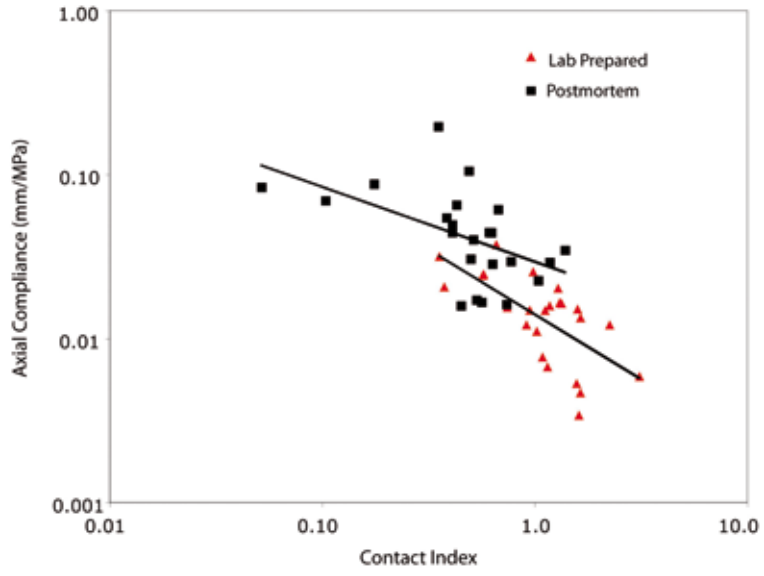

Figure 6.6 *Axial tensile compliance as a function of Contact Index for lab prepared and post mortem specimens.*

Discussion

The results of this study suggest that the magnitude of interface micromotion from an externally applied load does not depend on the angle at which that load is applied. Further, coupled transverse micromotions are small. As described previously[8,10], there is local sliding and opening of the interface between the interdigitated cement and bone that is responsible for this micromotion. The finding that interface compliance (inverse stiffness) is invariant

to loading direction might seem in conflict with previous reports that indicated that interface strength is greater in shear than in tension[8]. However, if we compare the stiffness versus strength response in tension[6] with that from the shear direction[7] (Figure 6.7), we find that for the same stiffness (or compliance), the interface is stronger in shear than in tension. For the data presented in Figure 6.7, the ratio of slopes of the strength versus stiffness linear regression is 4.02:1 (shear to tension) indicating that for the same interface stiffness, a specimen would be 4 times stronger in shear than in tension. It should be noted that the shear loading experiments were from a relatively small sample population and that more data should be collected to provide a more complete description of the strength to stiffness response in the shear direction using both lab prepared and postmortem retrieved specimens.

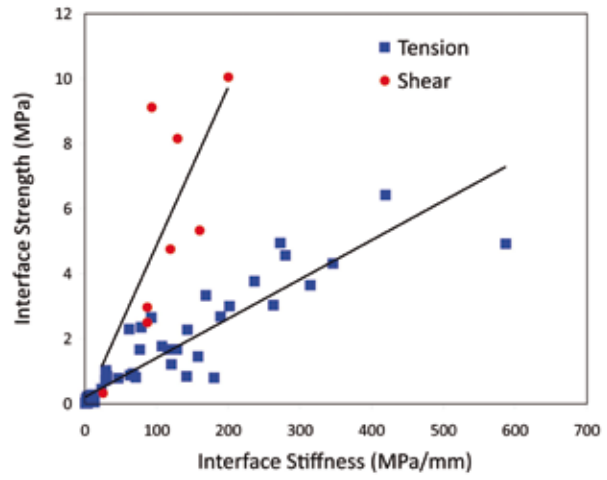

Figure 6.7 *Relationship between interface stiffness and interface strength compiled from previously reported data[6,7].*

An alternative approach to determine the multi-axial response of the cement-bone interface is to perform micromechanical finite element analyses. With this approach detailed finite element models of the cement and bone are created that capture the local interface morphology. In addition, a failure criterion for the cement and bone can be used such that tests to failure tests on the same specimen can be conducted in tension and shear. Using this approach for two finite element meshes with different levels of interdigitation based on laboratory prepared specimens, Waanders et al. (2010) found that the cement-bone interface was, on average, slightly less compliant (tension:shear ratio of 0.87) in 0° (tension) than 90° (shear) loading angles. In the current experimental study, we found that for 12 different specimens that the ratio of 0° to 90° loading angle compliance was 0.998.

Modeling of the cement-bone interface in cemented hip replacement has evolved substantially over the last several decades. Initial work focused on the effects of decoupling of the cement from the bone through inclusion of a fibrous tissue layer at the cement-bone interface[3,16]. The addition of fibrous tissue in these models resulted in changes in distribution and magnitude of bone and cement stresses from the standard bonded condition at the

cement-bone interface. However, these models were not capable of simulating the actual failure process at the interface. More recently, efforts have been made to model the failure response of the cement-bone interface using damage mechanics approaches[10,11,12,13]. These studies showed that the cement-bone interface plays an important role in the failure process of the cemented stem construct. The results from the present study could be used to improve the accuracy of these damage models through implementation of a high compliance layer with isotropic deformation properties (invariant to loading direction for the same applied stress). The magnitude of compliance could be modified from a highly interdigitated state with relatively low compliance to a state where there is little cement-bone contact with relatively high compliance. The evolution of the interface from a highly interdigitated state, to a loose state could also be explored[4,5].

The main limitation to this study is that specimens were not loaded to failure, so that the full failure response in each loading direction was not determined. As described above, one approach to generate a full failure response is to perform finite element (FE) simulations to failure of the same specimen with different loading directions. However, FE simulations are limited by the ability to capture all features of the failure response. The concurrence between the experimental findings here and the micromechanical FE results to failure suggests that the models are capable of capturing the primary failure mechanisms. In addition to single cycle loading limitations, the multi-axial fatigue loading response cannot be addressed with this experimental approach. There is the possibility that the weakest (most compliance) specimens could have been damaged during the rotation to the different loading angle. Removal of the two most compliant specimens from the data set did not affect the overall conclusion that compliance did not depend on loading angle.

Recently, our group showed that postmortem retrieval specimens have much less contact between cement and bone when compared to laboratory prepared specimens[9]. However, in the previous testing of laboratory prepared specimens, a side plate was not used to support the interface prior to loading. In some cases, weak specimens would fail during set up in the loading grips. In the current study, because side plates were attached between the cement and bone during preparation, the weaker laboratory prepared specimens remained intact during the experimental setup and could be tested. As such, data is now presented that indicates that for the same interface Contact Index, postmortem retrieval specimens are more compliant than laboratory prepared specimens. The reason for this is unclear but could be due to changes in the stiffness (modulus) of the bone in contact with the cement or some other morphology parameters not captured by the Contact Index. Additional work is needed to determine the cause of this discrepancy.

Interdigitation depth was not found to correlate with interface compliance in the present study. Performing mixed-mode tests on cement-bovine bone interfaces with an average interdigitation depth of 0.51 mm, Wang et al. (2010) found a poor correlation (r^2=0.16) between interdigitation depth and interface strength. In the current study, the average interdigitation depth was also small (0.3 mm). It is possible that a much wider range of interdigitation depth would reveal a relationship between interface compliance and strength.

Postmortem retrieval specimens are more compliant and have less contact between cement and bone when compared to laboratory prepared specimens. While laboratory prepared specimens can be more easily obtained, they appear to only represent behavior that would exist in the immediate post-operative condition. The biological response to implantation clearly changes the morphology of fixation with reduced contact between cement and bone. There is also clear evidence of bony resorption from regions that had originally been interdigitated (Figure 6.4). In the development of bench-top preclinical models for evaluation of new implant designs, conditions that simulated the *in vivo* situation would be preferable, but also may be harder to achieve with experimental models.

In terms of clinical relevance, these results indicate that interface compliance increases following *in vivo* service. This is due to a loss of contact between cement and bone. In addition, there appears to be an additional increase in compliance for postmortem specimens for the same amount of contact between cement and bone. The mechanism for this is unclear, but could be due to other changes at the bone-cement interface.

Acknowledgements

This work was funded by the National Insititutes of Health (NIH AR42017).

References

1. **Arola, D., Stoffel, K.A., Yang, D.T., 2006.**
   Fatigue of the cement/bone interface: the surface texture of bone and loosening.
   J. Biomed. Mater. Res. B: Appl. Biomat. 76, 287-297.
2. **Bishop, N.E., Schoenwald, M., Schultz, P., Puschel, K., Morlock, M.M., 2009.**
   The condition of the cement mantle in femoral hip prosthesis implantations--a post mortem retrieval study. Hip Int. 19, 87-95.
3. **Brown, T.D., Pedersen, D.R., Radin, E.L., Rose, R.M., 1988.**
   Global mechanical consequences of reduced cement/bone coupling rigidity in proximal femoral arthroplasty: A three-dimensional finite element analysis. J. Biomech. 21, 115-129.
4. **Giori, N.J., Ryd, L., Carter, D.R., 1995.**
   Mechanical influences on tissue differentiation at bone-cement interfaces. J. Arthroplasty 10, 514-522.
5. **Lennon, A.B., Prendergast, P.J., 2009.**
   The cement-bone interface: Is it susceptible to damage adaptive remodeling?, 4th European Conference of the International Federation for Medical and Biologicial Engineering.
   Springer Verlag, pp. 1990-1993.
6. **Mann, K.A., Miller, M.A., Cleary, R.J., Janssen, D., Verdonschot, N., 2008.**
   Experimental micromechanics of the cement-bone interface. J. Orthop. Res. 26, 872-879.
7. **Mann, K.A., Miller, M.A., Race, A., Verdonschot, N., 2009.**
   Shear fatigue micromechanics of the cement-bone interface: An in vitro study using digital image correlation techniques. J. Orthop. Res. 27, 340-346.
8. **Mann, K.A., Werner, F.W., Ayers, D.C., 1999.**
   Mechanical strength of the cement-bone interface is greater in shear than in tension.
   J. Biomech. 32, 1251-1254.
9. **Miller, M.A., Eberhardt, A., Cleary, R.J., Verdonschot, N., Mann, K.A., 2010.**
   Micro-mechanics of post-mortem retrieved cement-bone interfaces. J. Orthop. Res. 28, 170-177.
10. **Moreo, P., Garcia-Aznar, J.M., Doblare, M., 2007.**
    A coupled viscoplastic rate-dependent damage model for the simulation of fatigue of cement-bone interfaces. Int. J. Plasticity 23, 2058-2084.
11. **Moreo, P., Pérez, M.A., García-Aznar, J.M., Doblaré, M., 2006.**
    Modelling the mixed-mode failure of cement-bone interfaces Eng. Fract. Mech. 73, 1379-1395.
12. **Perez, M.A., Garcia-Aznar, J.M., Doblare, M., 2009.**
    Does increased bone-cement interface strength have negative consequences for bulk cement integrity? A finite element study. Ann. Biomed. Eng. 37, 454-466.
13. **Perez, M.A., Palacios, J., 2010.**
    Comparative finite element analysis of the debonding process in different concepts of cemented hip implants. Ann. Biomed. Eng. 38, 2093-2106.
14. **Tong, J., Wong, K.Y., Lupton, C., 2007**
    Determination of interfacial fracture toughness of bone-cement interface using sandwich Brazilian disks. Eng. Fract. Mech .74, 1904-1916.
15. **Waanders, D., Janssen, D., Mann, K.A., Verdonschot, N., 2010.**
    The mechanical effects of different levels of cement penetration at the cement-bone interface. J. Biomech. 43, 1167-1175.
16. **Waide, V., Cristofolini, L., Stolk, J., Verdonschot, N., Boogaard, G.J., Toni, A., 2004.**
    Modeling the fibrous tissue layer in cemented hip replacements: experimental and finite element methods. J. Biomech. 37, 13-26.
17. **Wang, J.Y., Tozzi, G., Chen, J., Contal, F., Lupton, C., Tong, J., 2010.**
    Bone-cement interfacial behaviour under mixed mode loading conditions.
    J Mech. Beh. Biomed. Mat. 3, 392-398.

Chapter 7

Morphology Based Cohesive Zone Modeling of the Cement-Bone Interface from Postmortem Retrievals

Journal of the Mechanical Behavior of Biomedical Materials (2011); 4(7):1492-503

Abstract

In cemented total hip arthroplasty, the cement-bone interface can be considerably degenerated after less than one year in-vivo service; this makes the interface much weaker relative to the direct post-operative situation. It is, however, still unknown how these degenerated interfaces behave under mixed-mode loading and how this is related to the morphology of the interface. In this study, we used a finite element approach to analyze the mixed-mode response of the cement-bone interface taken from postmortem retrievals and we investigated whether it was feasible to generate a fully elastic and a failure cohesive model based on only morphological input parameters.

Computed tomography-based finite element analysis models of the postmortem cement-bone interface were generated and the interface morphology was determined. The models were loaded until failure in multiple directions by allowing cracking of the bone and cement components and including periodic boundary conditions. The resulting stiffness was related to the interface morphology. A closed form mixed-mode cohesive model that included failure was determined and related to the interface morphology.

The responses of the finite element simulations compare satisfactorily with experimental observations, albeit the magnitude of the strength and stiffness are somewhat overestimated. Surprisingly, the finite element simulations predict no failure under shear loading and a considerable normal compression is generated which prevents dilation of the interface. The obtained mixed-mode stiffness response could subsequently be related to the interface morphology and subsequently be formulated into an elastic cohesive zone model. Finally, the acquired data could be used as an input for a cohesive model that also includes interface failure.

Introduction

In cemented total hip arthroplasty, the fixation at the cement-bone interface is one of the critical factors in the longevity of the cemented hip reconstruction. Since bone cement is not osteoconductive, physicochemical bonding cannot be expected[26], and therefore, interface fixation relies on cement interdigitation into the bone[17]. However, recent research has indicated that after less than one year *in vivo* service the cement-bone interface can be considerably degenerated due to bone resorption[19,37]. This subsequently makes the interface considerably weaker relative to the immediate post-operative situation[21].

The implementation of the mechanical behavior of the cement-bone interface into Finite Element Analysis (FEA) of cemented hip reconstructions has often been over-simplified. Over the years, the cement-bone interface has frequently been implemented either as an infinitely stiff interface[7,13,35], a uniform layer of soft tissue elements[3,38] or as a frictional contact layer[16]. The main limitation of these methods is that the interface behavior may not capture the true physics of the cement-bone interface.

Recently, the mechanical mixed-mode behavior of the cement-bone interface has been modeled utilizing sophisticated cohesive zone models[24,28]. The mechanical characteristics of these cohesive models were based on experimental data acquired from lab-prepared cement-bone interfaces that represent the immediate post-operative situation. It has recently also been reported that the increased compliance of these lab-prepared interfaces, relative to an assumed infinitely stiff interface also increases the overall cement mantle damage[41]. However, it is still unknown how increased compliance and reduced strength of the cement-bone interface following *in vivo* service influences the mixed-mode loading response and subsequent cement mantle damage.

In order to understand the behavior of the cement-bone interface derived from postmortem retrievals, from which cohesive models could be generated, information on the mixed-mode failure response of the interface is necessary. A possible method to obtain this information could be to load multiple postmortem specimens to failure under different directions, like has previously been done with lab-prepared specimens[20,43]. However, postmortem retrievals can be highly variable in terms of the amount of interdigitation due to biological changes at the interface, so that a consistent failure response as a function of different loading directions would be difficult to develop using an experimental approach. We have previously shown that micromechanical finite element models can be used to predict the failure response of lab-prepared specimens[39]. Here we propose to extend this concept to postmortem retrievals using an *in silico* approach; specimens will be loaded to failure in multiple loading directions and the mechanical response quantified.

Around the cement mantle, the degenerated cement-bone interface does not exhibit a homogenous morphology[1]. To account for variable morphology in cohesive zone modeling of the cement-bone interface, interface properties have previously been based on the quantity of cement interdigitation into the bone[29]. However, the quantity of cement interdigitation into the bone has been based on lab-prepared cement-bone interfaces[20] and it is therefore unknown whether it can also be applied to postmortem retrievals. Moreover, the quantity of cement interdigitation into the bone does not provide insight into the micromechanics that cause the mechanical properties of the interface.

The goal of this study is to investigate the mechanical mixed-mode response of the cement-bone interface from radiographically well-fixed postmortem retrievals and relate this response to their morphology. A subsequent goal is to generate an elastic and failure cohesive model with only morphological factors as an input. From quantitative computed tomography (CT) data of postmortem retrievals, micromechanical FEA models were generated using a multi-scale approach. These models were subsequently loaded in multiple directions while failure could occur by allowing both the bone and cement components to crack. Using this approach, we addressed three research questions: (1) what are the mixed-mode characteristics of the postmortem cement-bone interface and how do these simulations compare to experimental findings?; (2) can the initial elastic stiffness in multiple directions be related to the interfacial morphology?; and (3) can a (I) fully linear elastic or (II) nonlinear elastic cohesive failure model reproduce the mechanical response of the in silico experiments using the interface morphology as the input parameters?

Methods

Specimen preparation

Four cement-bone interface specimens were retrieved from the proximal femurs of two donors with cemented hip components at autopsy (Table 7.1) through the anatomical donor programs at SUNY Upstate Medical University and the University of Alabama at Birmingham. Donations to the anatomical donor programs were made between 1 and 2 days of death and frozen at -20°C prior to tissue harvest. The specimen size, age, gender, cause of death and number of years in service were documented. Specimen source locations were documented including distance from the calcar and anterior/posterior-medial/lateral quadrant. By observation of the cement mantle porosity it was assessed whether the utilized bone cement was vacuum mixed prior to insertion. All specimens were micro-CT scanned at 12-micron isotropic resolution (Scanco 40, SCANCO Medical AG, Brüttisellen, Switzerland). Based on planar x-rays of the cemented femur construct, the quality of the cement-bone interface fixation was assessed and specified as radiographically *'definitely loose'*, *'possibly loose'*, or *'not loose'*.

	Specimen 1	*Specimen 2*	*Specimen 3*	*Specimen 4*
Specimen size (lxbxh mm³)	3.98x2.06x2.70	3.41x2.42x3.00	4.04x2.00x3.20	3.65x2.06x3.40
Age	67	93	93	67
Gender	Female	Female	Female	Female
Cause of death	Alzheimer's disease	Renal insufficiency	Renal insufficiency	Alzheimer's disease
Years in service	14	Not available	Not available	14
Distance from calcar [mm]	100	70	70	110
A/P-M/L quadrant	Medial	Medial	Lateral	Lateral
Vacuum-mixed	Yes	Yes	Yes	Yes
Fixation quality	Not loose	Possibly loose	Not loose	Not loose
	Model 1	*Model 2*	*Model 3*	*Model 4*
FEA model size (lxbxh mm³)	7.97x4.13x2.70	6.82x4.85x3.00	8.08x4.01x3.20	7.30x4.13x3.40
Number of elements	343,988	357,236	468,308	367,160
Number of nodes	80,804	83,589	106,473	81,078

Table 7.1 *Donor and FEA model information for the four models.*

FEA modeling

From each specimen a FEA model was generated. Each model consisted of two parts: bone and cement. The FEA meshes were created from the micro-CT data of the cement-bone interface using MIMICS 11.0 (Materialize, Leuven, Belgium). After segmentation of the micro-CT data, the 3D voxel meshes of the bone and cement were transformed to triangular surface meshes, using a 6x6x6 voxel interpolation with smoothing. Next, these surface meshes were remeshed to reduce the number of triangles and to remove low quality triangles. To avoid intersecting elements, the mesh of the cement was subtracted from the bone mesh. The resulting low quality elements of the bone were subsequently remeshed. Finally, an erosion (2.0 µm) was applied to the bone interface to ensure that the two meshes were not intersecting[42]. Next, both surface meshes were meshed as a tetrahedral 3D solid mesh (Patran 2005r2, MSC Software Corporation, Santa Ana, CA, USA). The solid mesh of the bone was mapped back into the micro-CT data set, after which the weighted average of the grayscale was calculated for each solid element using MIMICS.

In order to avoid off axis tractions during loading in normal directions and to apply periodic boundary conditions (see section '*Material propterties*'), the initial meshes were mirrored[25,27,39]. First, the initial mesh was mirrored in the y-z plane (Figure 7.1a). Subsequently, this mirrored mesh was mirrored in the x-z plane. The resulting models contained on average 384,000 elements and 88,000 nodes (Table 7.1; Figure 7.1b). Contact between the bone and cement was modeled using a double-sided node to surface contact algorithm (MSC.MARC 2007r1, MSC Software Corporation, Santa Ana, CA, USA) with a friction coefficient of 0.3[9].

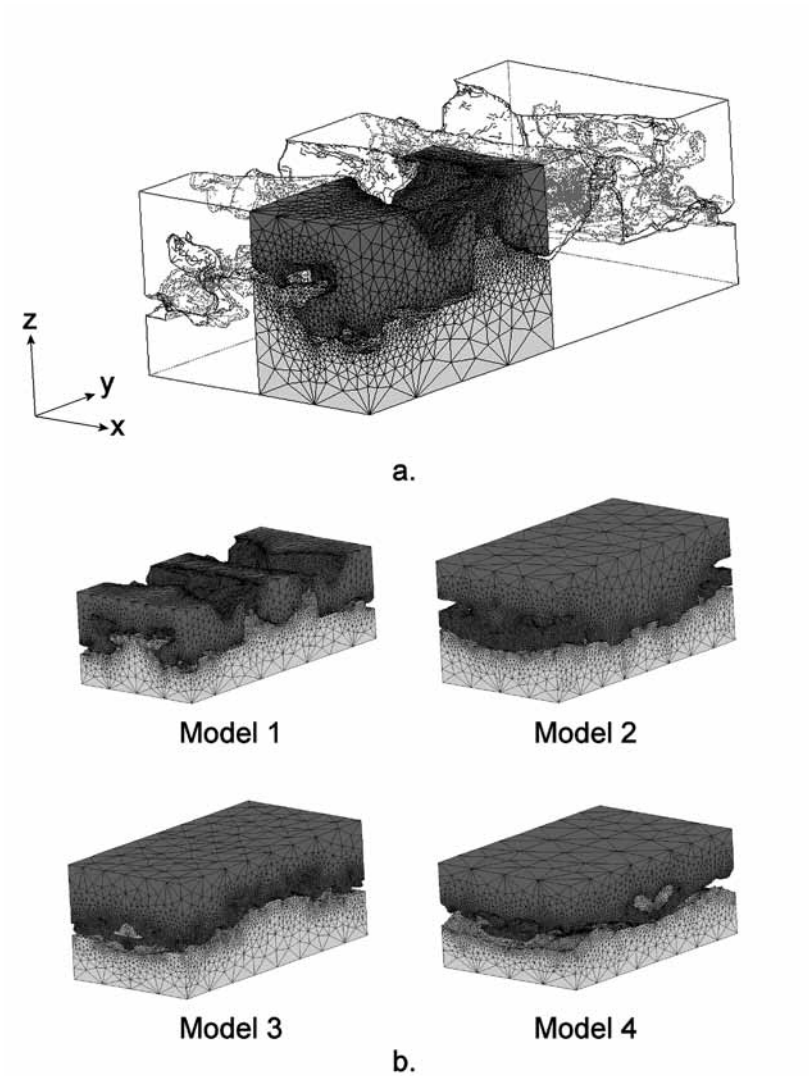

Figure 7.1 *a. The initial mesh was first mirrored in the y-z plane and subsequently mirrored in the x-z plane.*
b. The four models as used in this study.
The dimensions of the four models were on average ~4.2 x 7.2 x 3.0 mm3.

Material properties

Both bone and cement were initially modeled as isotropic linear elastic materials. Since the exact material properties of the cement were unknown, Young's modulus (E) and Poisson's ratio (v) of the cement were taken as 3000 MPa and 0.3, respectively[6,9,15]. The bone elastic properties were based upon micro-CT greyscale values, which were converted to equivalent HA-densities using a calibration phantom. The Young's modulus was assumed to be linearly dependent on the HA-density[10], resulting in bone modulus values ranging from 0.1 to 20,000 MPa.

Previous experiments showed that when the cement-bone interface was loaded until failure, cracks initiated in both the cement and bone[18]. Therefore, crack formation in the bulk bone and cement was simulated using an adapted custom-written FEA algorithm to simulate static failure[36]. Static failure in either bone or cement occurred when the local principal tensile stress exceeded the material strength. The strength of the cement was taken as 40 MPa[6,15], while the strength of the bone was derived from the Young's modulus[14,40]:

$$S = 102 \cdot \left(\frac{E}{14{,}900} \right)^{\frac{1.80}{1.86}} \qquad (1)$$

Cracks were simulated by setting the Young's modulus to 0.1 MPa in the direction perpendicular to the corresponding principal stress direction.

Boundary conditions

In order to establish a multi-scale representation of the cement-bone interface, periodic boundary conditions were applied. In this way, one single model of the cement-bone interface was considered as an infinite series of periodic microstructures[12]. The periodic boundary conditions were implemented by constructing nodal links between nodes periodically located on the left (y=0) and right side (y=w) of the model (Figure 7.2)[32] and were defined as:

$$u_i(x,0,z) = u_i(x,w,z) \qquad (2)$$

In this equation, 'u_i' represents the displacement in the x, y and z-direction. As a result of the mirroring of the meshes, no bone-to-cement links at the boundary between two different periodic cells occurred.

While all nodes in the bottom plane (z=0) were fixed in all directions (Figure 7.2), the nodes in the top plane (z=h) were uniformly displaced until failure. Seven different angles (α) were considered: 0° (pure tension), 30°, 60°, 90° (pure shear), 120°, 150° and 180° (pure compression) (Figure 7.2). The incremental displacement in normal and tangential direction, Δ_N and Δ_T, could hence be calculated as $\Delta_N = \Delta\cos(\alpha)$ and $\Delta_T = \Delta\sin(\alpha)$, respectively. The resultant nodal reaction force [N] was calculated and subsequently decomposed and converted to tractions $\left[\frac{MPa}{mm}\right]$ in normal and tangential direction, T_N and T_T respectively.

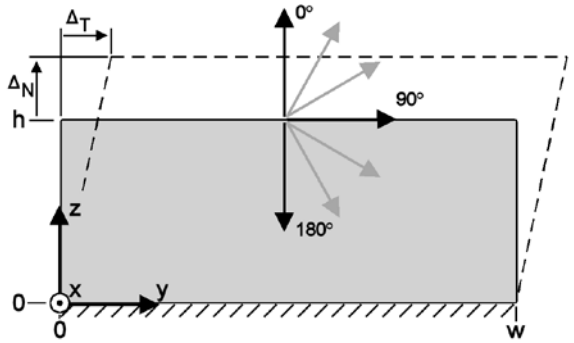

Figure 7.2 *The boundary conditions as applied in this study: all nodes at z=0 were fixated in all degrees of freedom, while all nodes at z=h were uniformly displaced in seven different directions. Periodic boundary conditions were applied on the model's left and right side using nodal ties and were defined as: $u_i(x,0,z)=u_i(x,w,z)$. In this equation, 'u_i' represents the displacement in the x, y and z-direction. Tangential displacements were consequently displaced in positive y-direction.*

Morphology

In order to capture the morphology of the cement-bone interface, a CT-based stereology approach was used[21]. A grid (0.3 x 0.3 mm spacing) was placed over the micro-CT data and lines were projected vertically through the specimen (Figure 7.3). At the points where the projection lines crossed the interface, the status was designated as either apposition or proximity (gap < 0.25 mm). From this, the *Contact Index* (CI) was calculated as the number of points of apposition divided by the total number of projection lines. The *Intersection Index* (II) was calculated as the total number of points in apposition and proximity divided by the total number of projection lines. Finally, the gap between the cement and bone was measured for each projection line. Subsequently, the average of all the local gaps was determined what resulted in the *Gap Thickness* (GT).

Figure 7.3 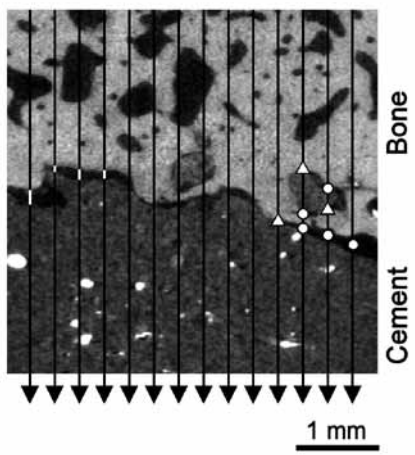

The micro-CT data set consisted of the bone (top) and cement (bottom). At various locations, there was cement penetration into the cavities of the bone. The white spots in the bulk cement can be attributed to the presence of $BaSO_4$ particles. A grid (0.3 x 0.3 mm spacing) was placed over the micro-CT data and lines were projected vertically through the specimen. At those locations where a projection line crossed the interface, the interface status was designated as either apposition (triangle) or proximity (circle). Also, the gap thickness between the bone and cement (white lines) was measured for projection line. From this, the Contact Index (CI), Intersection Index (II) and Gap Thickness (GT) could be determined. It has previously been show that these parameters can be used to clarify the cement-bone interface response[21,22].

Cohesive modeling

The interface stiffness as a result of multi-axial loading was, like in physical experiments, determined in the direction of the interface displacement. In physical experiments, where off-axis loads usually do not occur as a result of the experimental setup such as use of linear sliders or a universal joint, the load vector (**T**) always points in the same direction as the displacement vector (**Δ**)[18,22]. However, as a result of the boundary conditions as applied in the current study, the load vector (**T**) and the displacement vector (**Δ**) do not necessarily point in the same direction (Figure 7.4)[39]. Therefore, the orthogonal projection of **T** onto **Δ** was determined (**T'**) to obtain the stiffness in the direction of the displacement (Figure 7.4). The vector **z** was defined as the component of **T** perpendicular to **Δ**. From this, the stiffness in the direction of the applied displacement $\left(\frac{\partial T'}{\partial \Delta}\right)$ and its perpendicular stiffness $\left(\frac{\partial z}{\partial \Delta}\right)$ could be determined.

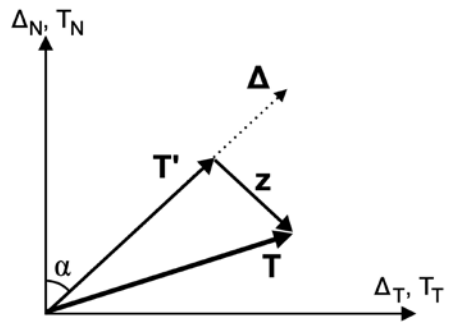

Figure 7.4 *The load vector (**T**) was decomposed into **T'** and **z**. The vector **T'** was defined as the orthogonal projection of **T** onto **Δ**. The vector **z** was defined as the component of **T** orthogonal to **Δ**.*

Elastic cohesive model

In order to generate an elastic model for postmortem cement-bone interfaces, a step-wise regression model was used to determine the relationship between $\left(\frac{\partial T'}{\partial \Delta}\right)$ and the three morphological factors (CI, II and GT) as well as the loading angle (α). In order to incorporate the number of variables in the correlation, the adjusted correlation coefficient, $\overline{r}$, was used. It was assumed that $\left(\frac{\partial z}{\partial \Delta}\right)$ could be determined as:

$$\frac{\partial z}{\partial \Delta} = A \cdot \sin(\alpha) \cdot \frac{\partial T'}{\partial \Delta} \qquad (3)$$

in which 'A' is a constant to be determined and $\left(\frac{\partial T'}{\partial \Delta}\right)$ as predicted by the morphological factors and the loading angle. Linear regression analysis was used to assess the correlation between the predicted $\left(\frac{\partial T'}{\partial \Delta}\right)$ and $\left(\frac{\partial z}{\partial \Delta}\right)$.

Failure cohesive model

A mixed-mode model which also included interfacial failure was determined utilizing the following cohesive model[44]:

$$T_N(\Delta_N,\Delta_T)=\frac{\Gamma_0}{\delta_N}\left[\frac{\Delta_N}{\delta_N}-\left((1+\beta)\frac{\Delta_N}{\delta_N}-\beta\right)f(\Delta_T)\right]\exp\left(-\frac{\Delta_N}{\delta_N}\right) \qquad (4a)$$

$$T_T(\Delta_N,\Delta_T)=\Gamma_0\frac{df(\Delta_T)}{d\Delta_T}\left[1+(1+\beta)\frac{\Delta_N}{\delta_N}\right]\exp\left(-\frac{\Delta_N}{\delta_N}\right) \qquad (4b)$$

In this set of equations, the normal and tangential tractions (T_N and T_T) were defined as a function of the normal and tangential displacements (Δ_N and Δ_T) and four parameters which can partly be linked to the morphology. The parameter Γ_0 denotes the total fracture energy in pure tension (Δ_T=0), which was therefore calculated from equation 4a as:

$$\Gamma_0 = T_{N,ult}\cdot\delta_N\cdot\exp(1) \qquad (5)$$

where $T_{N,ult}$ is the tensile strength of the cement-bone interface. Since for postmortem retrievals there is a positive relationship (r^2=0.57) between the tensile strength and stiffness, $T_{N,ult}$ was determined as[21,40]:

$$T_{N,ult} = 0.0069\frac{\partial T_N}{\partial \Delta_N}+0.093 \qquad (6)$$

where the normal stiffness $\left(\frac{\partial T_N}{\partial \Delta_N}\right)$ was determined from the morphological based stiffness $\frac{\partial T}{\partial \Delta}$ from section '*Elastic cohesive model*'. The variable δ_N was defined as the displacement at the tensile strength and was determined as a function of $T_{N,ult}$ and $\frac{\partial T_N}{\partial \Delta_N}$ utilizing the data of Mann et al. (2008) and was therefore also morphology dependent. The function $f(\Delta_T)$ was used to define the response in pure shear:

$$T_T(0,\Delta_T)=\Gamma_0\frac{df(\Delta_T)}{d\Delta_T} \qquad (7)$$

Since a previous mixed-mode study suggested a linear relationship between T_T and Δ_T[39], this function resulted in:

$$f(\Delta_T)=\frac{1}{2\Gamma_0}\frac{\partial T_T}{\partial \Delta_T}\Delta_T^2 \qquad (8)$$

The parameter $\left(\frac{\partial T_T}{\partial \Delta_T}\right)$ was defined as the tangential stiffness in pure shear, which was also determined from the morphological based stiffness $\frac{\partial T}{\partial \Delta}$ Finally, the fitting coefficient β was set to -0.8[41]. This value had to be negative in order to reproduce normal compression when loaded in pure shear.

The generated elastic and failure cohesive models were subsequently compared with the responses as found by the mixed-mode simulations. From this it was assessed whether the generated cohesive fit was satisfactory.

Results

Mixed-mode response

A similar mixed-mode response was found for all four models. In pure tension (α=0°), the response showed a traction-displacement response with an initial stiffness followed by yielding and softening (Figure 7.5a). The ultimate tensile strengths ($T_{N,ult}$) ranged from 0.10 to 0.81 MPa and the normal stiffness $\left(\frac{\partial T_N}{\partial \Delta_N}\right)$ from 5.4 to 93.0 MPa/mm (Table 7.2). In pure compression (α=180°), a linear T_N-Δ_N relationship was found with stiffness ranging from 21.4 to 441.2 MPa/mm (Table 7.2).

In pure tension and compression, the tangential tractions (T_T) were found to be negligible (Figure 7.5d). In pure shear (α=90°), the tangential traction (T_T) increased linearly with the applied tangential displacement (Δ_T) (Figure 7.5c) and none of the models reached failure. The four models had a tangential stiffness $\left(\frac{\partial T_T}{\partial \Delta_T}\right)$ ranging from 10.1 to 184.3 MPa/mm (Table 7.2). Remarkably, a considerable compressive traction was needed to prevent dilation of the interface (Figure 7.5b).

For all the intermediate values of α, all the responses showed a smooth transition between the aforementioned three 'principal' responses. It is interesting to note that although interfaces are loaded in mixed-mode tension (30° and 60° cases), normal compression occurred in the softening phase (Figure 7.5a-b).

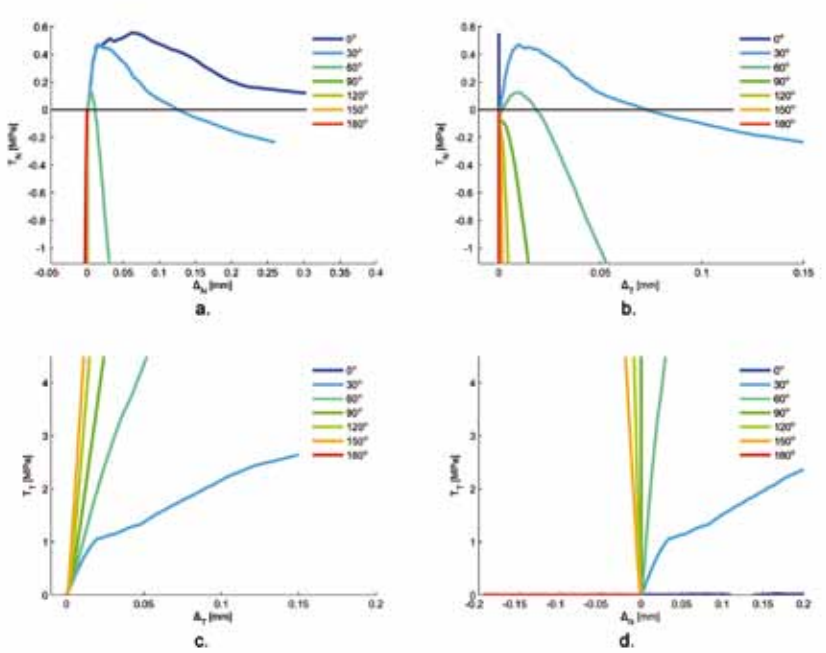

Figure 7.5 *The traction-displacement relationships between (a) T_N and Δ_N, (b) T_N and Δ_T, (c) T_T and Δ_T, and (d) T_T and Δ_N of model 4. In pure tension (α =0°), the complete traction-displacement response is captured in subfigure (a). As a result of the symmetry, no tangential tractions occurred in pure tension (d). In pure shear (α =0°), no ultimate strength was found (c) and a considerable normal compression was needed to prevent dilation of the interface (b).*

Model	0° $T_{N,ult}$ [MPa]	0° $\frac{\partial T_N}{\partial \Delta_N}$ [MPa/mm]	180° $\frac{\partial T_N}{\partial \Delta_N}$ [MPa/mm]	90° $\frac{\partial T_T}{\partial \Delta_T}$ [MPa/mm]	CI [-]	II [-]	GT [mm]
1	0.55	21.7	248.1	154.4	0.18	1.01	0.101
2	0.10	5.4	21.4	10.1	0.13	1.34	0.231
3	0.81	93.0	258.6	139.4	0.29	1.26	0.076
4	0.56	37.7	441.2	184.3	0.74	1.20	0.015
Mean (SD)	0.51 (0.30)	39.5 (38.1)	242.3 (171.9)	122.1 (76.9)	0.34 (0.28)	1.20 (0.14)	0.11 (0.09)
Miller et al., 2010 Mean (SD)	0.21 (0.32)	16 (35)	47 (61)	-	0.11 (0.17)	0.72 (0.62)	0.33 (0.28)
Miller et al. 2011 Mean (SD)	-	19.2 (25.6)	22.7 (35.7)	-	0.57 (0.31)	1.89 (0.69)	-

Table 7.2 *Mechanical and morphological parameters of the four models and experimental findings utilizing postmortem retrievals[21,22]. Unfortunately, no experimental postmortem retrieval data in pure shear was available.*

Cohesive model

When the logarithmic value of the interfacial stiffness in the direction of the applied displacement $\left(\log\left(\frac{\partial T'}{\partial \Delta}\right)\right)$ was used in the regression model, the morphological variables *Contact Index, Gap Thickness* and cos(α) showed a significant contribution to the predicted stiffness ($\bar{r}^2$ =0.91, p<0.0001; Table 7.3; Regression model 1). The *Intersection Index* did not significantly contribute to the regression (p=0.72). With this regression model, a negative estimate for the *Contact Index* coefficient was found. A physical interpretation would be that increasing the *Contact Index* would result in a lower interface stiffness (holding all other parameters constant). This conflicts with previous experimental findings, but can be attributed to the fact that *Contact Index* and *Gap Thickness* are not independent; there is an inversely proportional relationship between the *Contact Index* and the *Gap Thickness* (r^2=0.63). Since the *Contact Index* was the least significant estimate, it was, like the *Intersection Index*, ignored in the second regression model (Table 7.3; Regression model 2). Considering only the *Gap Thickness* and cos(α), the predicted stiffness $\log\left(\frac{\partial T'}{\partial \Delta}\right)$ still showed a strong correlation with the estimates (r^2 =0.81, p<0.0001) (Figure 7.6a). There was also a strong correlation (r^2=0.73, p<0.0001) between $\frac{\partial z}{\partial \Delta}$ and $A \cdot \sin(\Delta) \cdot \frac{\partial T'}{\partial \Delta}$, in which 'A' was estimated to be 0.316 and $\left(\frac{\partial T'}{\partial \Delta}\right)$ the aforementioned predicted stiffness from Regression model 2 (Figure 7.6b).

Regression Model Term	Regression model 1 Estimate	SE	p-Value	Regression model 2 Estimate	SE	p-Value
CI [-] (a_1)	-1.346	0.242	<0.0001	-	-	-
II [-] (a_2)	-0.140	0.390	0.72	-	-	-
GT [mm] (a_3)	-9.646	0.735	<0.0001	-6.369	0.649	<0.0001
cos(α) [-] (a_4)	-0.289	0.046	<0.0001	-0.289	0.068	<0.0001
Constant [-](a_5)	3.233	0.154	<0.0001	2.439	0.086	<0.0001

Table 7.3 *The logarithmic value of the interfacial stiffness in the direction of the applied displacement log was linearly related to the Contact Index (CI), Intersection Index (II), Gap Thickness (GT) and the cosine of the loading angle (cos(α)) (2 r =0.91, p<0.0001) (Regression model 1): 1 2 3 4 5 a CI a II a GT a cos α a With GT as the only morphology parameter (Regression model 2), there is still a strong correlation between log and the predicted estimates (2 r =0.81, p<0.0001).*

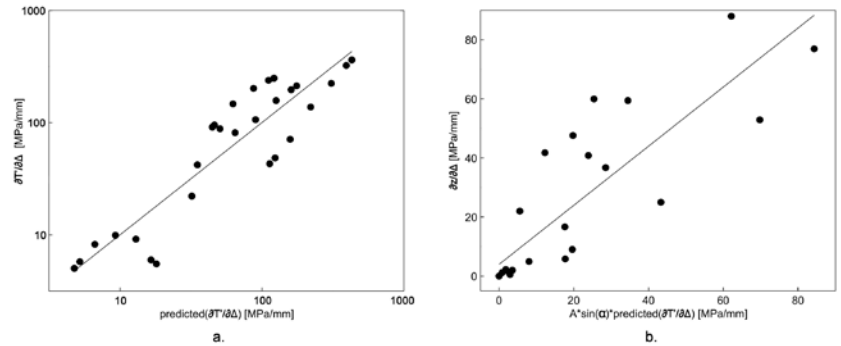

Figure 7.6 *a. There was a strong correlation ($\bar{r}$=0.81, p<0.0001) between the logarithmic value of the stiffness $\frac{\partial T'}{\partial \Delta}$ and the Gap Thickness and cos(α): $\log\left(\frac{\partial T'}{\partial \Delta}\right) = a_3 GT + a_4 \cos(\alpha) + a_5$ (Table 7.3; Regression model 2).*
b. A strong correlation (r_2=0.72, p<0.0001) was found between $\frac{\partial z}{\partial \Delta}$ as measured from the simulations and $\frac{\partial T'}{\partial \Delta}$, in which $\frac{\partial T'}{\partial \Delta}$ was the aforementioned predicted stiffness by Regression model 2. The variable 'A' was estimated to be 0.316.

Elastic cohesive model

Hence, using the predictions as mentioned above, the interfacial normal and tangential tractions (T_N and T_T) could be determined:

$$\begin{bmatrix} T_N \\ T_T \end{bmatrix} = \frac{\partial T'}{\partial \Delta} \cdot \Delta \cdot \begin{bmatrix} \cos(\alpha) \\ \sin(\alpha) \end{bmatrix} + 0.316 \cdot \sin(\Delta) \cdot \frac{\partial T'}{\partial \Delta} \cdot \Delta \cdot \begin{bmatrix} -\sin(\alpha) \\ \cos(\alpha) \end{bmatrix} \qquad (9)$$

Knowing that $\cos(\alpha) = \frac{\Delta_N}{\Delta}$, $\sin(\alpha) = \frac{\Delta_T}{\Delta}$, and $\frac{\partial T'}{\partial \Delta} = 10^{-6.369GT - 0.289\frac{\Delta_N}{\Delta} + 2.439}$ the previous equation can be re-written in terms of Δ, Δ_N and Δ_T, in which $\Delta = \sqrt{\Delta_N^2 + \Delta_T^2}$:

$$\begin{bmatrix} T_N \\ T_T \end{bmatrix} = 10^{-6.369GT-0.289\frac{\Delta_N}{\Delta}+2.439} \begin{bmatrix} \Delta_N - 0.316 \cdot \frac{\Delta_T^2}{\Delta} \\ \Delta_T \left(1 + 0.316 \cdot \frac{\Delta_N}{\Delta}\right) \end{bmatrix} \qquad (10)$$

This model resulted in a generally satisfactory fit between the simulated and the predicted elastic responses for all four models (Figure 7.7). Of note for the T_N-Δ_N responses was that when the tensile or compressive direction was predicted nicely, the opposite direction was rather under or over predicted. The tangential elastic stiffness for model 2 and 3 was predicted with good fidelity, while the stiffness of model 1 and 4 was a rather under and over predicted, respectively.

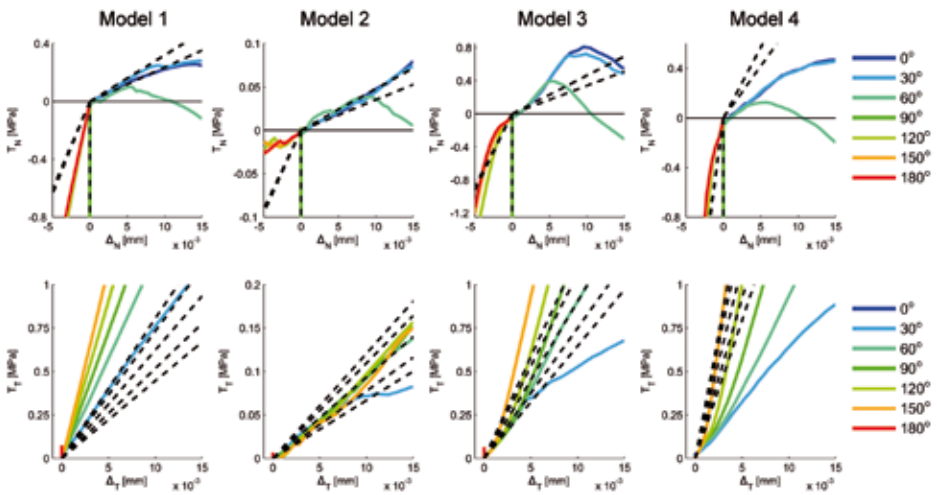

Figure 7.7 *Comparison between the finite element simulated responses (solid lines) to mixed-mode loading and the predicted elastic responses (dashed lines) using the Regression Model 2 for the four finite element models. The top and bottom rows show the responses the in normal and shear directions, respectively. For each model, 0º, 90º, and 180º indicates loading in tension, shear, and compression, respectively.*

Failure cohesive model

When the mixed-mode model as proposed by Wei and Hutchinson (2008) was considered, the responses showed some artifacts in the normal direction (Figure 7.8; top row), particularly for the post-yield response. The mixed-mode model had some difficulties with predicting the ultimate tensile strength ($T_{N,ult}$) and its corresponding displacement (δ_N). The RMS difference between $T_{N,ult}$ as determined by the simulations and the predicted mixed-mode model was 0.28 MPa. For δ_N the RMS difference was 64µm. However, the responses in normal compression were predicted with fewer artifacts than the elastic cohesive model. In the tangential direction, the mixed-mode responses were predicted satisfactorily for model 2 and 3 (Figure 7.8; lower row). As was found in the elastic cohesive model (Figure 7.7), the stiffness of model 1 and 4 was slightly under and over predicted, respectively.

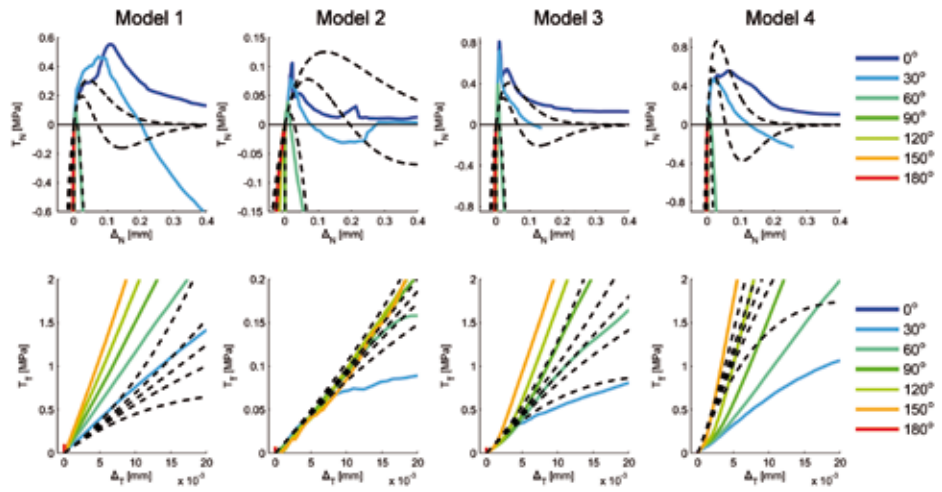

Figure 7.8 *Comparison between the finite element simulations (solid lines) and the responses using the mixed-mode model (dashed lines) as proposed by Wei and Hutchinson (2008). The top and bottom rows show the responses the in normal and shear directions, respectively. For each model, 0º, 90º, and 180º indicates loading in tension, shear, and compression, respectively.*

Discussion

The aim of this study was to investigate the mixed-mode behavior of cement-bone interfaces from postmortem retrievals utilizing micromechanical FEA models and, subsequently, generate an elastic and failure cohesive model based on the determined mixed-mode response and the interfacial morphology. This study distinguishes itself from physical experiments because one single interface morphology could be loaded until failure in multiple directions instead of one single direction.

The results show that the tensile strength ($T_{N,ult}$) and stiffness $\left(\frac{\partial T_N}{\partial \Delta_N}\right)$ as obtained by the FEA models compare well with experimental observations. However, the normal stiffness $\left(\frac{\partial T_N}{\partial \Delta_N}\right)$ at 0° is rather stiff compared to the mean normal stiffness as obtained by experimental findings (Table 7.2). This overestimation can be explained by the origin of the specimens; specimens 1 and 4 were harvested from the stiffest donor as used in the study of Mann et al., 2010 (model K). Although it is known that in compression the interface is stiffer than in

tension[18,22] the compressive stiffness as determined with the FEA models seems to be overestimated. In pure shear, a considerable compressive traction is needed to prevent dilation of the interface. This phenomenon has been described before in other interface studies[31,39]. All mixed-mode responses show a gradual transition between the three 'principal' responses (tension, shear and compression).

The boundary conditions as applied in the current study are different from the boundary conditions that occur in physical experiments. In the current study, no relative motions between the top and the bottom plane were possible, whereas they can occur in experiments as a result of the experimental setup[22]. As a result of this restriction, the mechanical stiffness can increase since the "path of least resistance" cannot be followed. This could also be an explanation of the overestimated stiffness in pure compression. Furthermore, the applied periodic boundary conditions result in a multi-scale representation of the interface which is not possible to validate experimentally. In order to assess the effect of the periodic boundary conditions, additional simulations have been executed in which the periodic boundary conditions were removed. It appears that the interface with periodic boundary conditions is stronger and stiffer relative to the interface without, but the differences are small (Figure 7.9). However, a considerable difference can be observed in the distribution of the Von Mises stresses; the interface with periodic boundary conditions presents a smooth transition of the stresses over the two sides, where the interface without periodic boundary conditions does not (Figure 7.9).

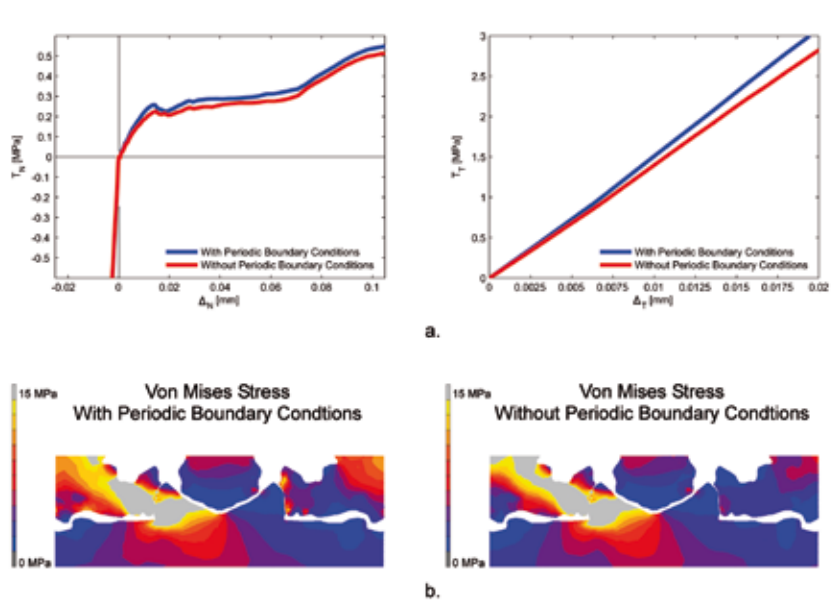

Figure 7.9 *a. The mixed-mode response of Model 1 with and without periodic boundary conditions. When periodic boundary are considered, the interface was about 6% stronger in tension. The periodic boundary conditions also make the interface stiffer; 18%, 4% and 9% in tension, compression and shear, respectively.*
b. Von Mises stress in Model 1 after a tangential displacement, Δ_T, of 15μm. When periodic boundary conditions are considered, there is a smooth stress distribution between the left and right side of the model. Without periodic boundary conditions, the stresses are truncated.

In order to generate an elastic mixed-mode cohesive model, the stiffness in line with the applied displacement, Δ, was determined $\left(\frac{\partial T}{\partial \Delta}\right)$. This stiffness was successfully related to the *Contact Index* (CI), *Gap Thickness* (GT) and loading angle (cos(α)) (Table 7.3; Regression model 1). However, the estimate of CI was found to be negative. This is counterintuitive, since it implies that a decrease of CI increases the interface stiffness. This conflicting finding can be attributed to the inversely proportional relationship between CI and GT for the four models (r^2=0.63); an increase of gaps as a result of bone resorption decreases the amount of cement-bone contact. Considering 50 postmortem specimens, Miller et al. (2010) also found an inverse proportional relationship between GT and CI (r^2=0.42). Since CI was the least significant estimate in the fit, CI was disregarded in further step-wise regression in generating a morphological based model to describe $\frac{\partial T}{\partial \Delta}$. This resulted in a fit for $\frac{\partial T}{\partial \Delta}$ which only considered GT as a morphological input and the loading angle, cos(α) ($\bar{r}$ =0.81, p<0.0001) (Table 7.3; Regression model 2). The estimate of GT was found to be negative, indicating that an increase of the *Gap Thickness* decreases the interface stiffness. Surprisingly, the estimate of cos(α) was the same for both Regression model 1 and 2. When CI would have been used in the fit to describe instead of GT, the estimate of CI would be positive (CI=1.174, p=0.008). This is consistent with what has been found previously[21]. However, a fit which only includes CI, cos(α) and a constant reduces the correlation considerably relative to a fit with GT ($\bar{r}$ =0.30, p=0.0005).

A mixed-mode cohesive model which also includes failure was determined based on the model as proposed by Wei and Hutchinson (2008). This model has, besides Δ_N and Δ_T, four different input parameters: the normal strength ($T_{N,ult}$) and its corresponding displacement (δ_c), the tangential stiffness in pure shear $\left(\frac{\partial T_T}{\partial \Delta_T}\right)$ and a fitting coefficient (β). The normal strength ($T_{N,ult}$) is calculated based on a positive linear relationship between $T_{N,ult}$ and $\left(\frac{\partial T_N}{\partial \Delta_N}\right)$. It would also be possible to calculate $T_{N,ult}$ according to a morphological fit as proposed by Miller et al. (2010). However, when we applied this relationship we found the same RMS difference between $T_{N,ult}$ of the simulations and the predicted mixed-mode model, but the relative difference, especially for the weak model 2, was much higher. Additionally, the RMS difference for δ_c was increased by a factor of 2.5 when the model of Miller et al. (2010) was considered. The variable δ_c was calculated based on the data of Mann et al. (2008) where the interface displacements at yield and the ultimate strength were determined relative to their corresponding stresses. Using this approach, δ_c could be determined as a function of $T_{N,ult}$ and $\left(\frac{\partial T_N}{\partial \Delta_N}\right)$. Although the data reported by Mann et al. (2008) was from lab-prepared specimens, we believe the same function of $T_{N,ult}$ and $\left(\frac{\partial T_N}{\partial \Delta_N}\right)$ will be found for postmortem responses. Finally, we believe it is more accurate than simply assuming δ_c to be the division of $T_{N,ult}$ with $\left(\frac{\partial T_N}{\partial \Delta_N}\right)$, although the T_N-Δ_N responses of model 2 and 3 might presume so.

The main limitation of this study is the absence of a direct quantitative validation. However, the methodology used to model the micromechanical FEA models has previously been used in studies in which the FEA models were successfully validated to experimental results[8,10,42]. Although these studies involved lab-prepared specimens, we believe the same methodology was applicable for postmortem specimens. Furthermore, a direct validation was not possible since within physical experiments the specimens could be tested until failure in one direction only and not in multiple directions. We were therefore forced to do a quantitative validation of previously published data. Unfortunately, the amount of quantitative mechanical data of postmortem cement-bone interface specimens is, in contrast to lab-prepared data, also limited[19,21,22]. In the past, studies to postmortem cement-bone interfaces mainly

focused on the histology rather than the mechanical behavior of the interface[1,2,11,33]. Finally, the FEA models used in this study do not directly match the geometry of the postmortem specimens as a result of the mirroring. However, the mirroring was necessary in order to avoid off-axis tractions in the cohesive model. It is more than likely that these off-axis tractions occur in experiments in which asymmetric postmortem specimens are used.

Another big limitation is the small sample that was used. The step-wise regression analysis in which the stiffness $\frac{\partial T}{\partial \Delta}$ was related to the *Contact Index*, *Intersection Index*, *Gap Thickness* and cos(α) could be improved through use of a larger sample. However, it is unknown whether a larger number of samples would change the outcome of the significance of each morphological parameter. Consistent with the present study it has recently been shown that the *Contact Index*, and thus the *Gap Thickness*, influences the interface stiffness and the *Intersection Index* does not[22]. It is questionable whether a larger sample would disapprove this finding.

The penetration depth of the cement into the bone was not considered as a morphological factor. Although a larger penetration depth correlates nicely with the interface strength in unidirectional loading[40], no correlation was found when considering the strength under multiple loading directions[43]. Moreover, two other studies have shown that there is no correlation between the amount of cement penetration and the interface stiffness in mixed-mode loading[22,39].

From a clinical perspective, the results of the current study implicate that minimizing the gap between the cement and the bone enhances the mechanical properties of the cement-bone interface. From a surgical point of view the gap could be minimized by the degree of cement pressurization[5], although over pressurizing of the femoral canal can lead to fat and bone-marrow embolism syndrome, which can sometimes even be fatal[34]. However, gaps could also be created due to heat necrosis as a result of cement polymerization[23], bone remodeling[4] or cement shrinkage[30].

The cohesive models as derived in this study are applicable to multiple applications in the research to cemented hip implants. One could even consider whether this method could be applicable to any cemented orthopaedic device, such as tibial trays or glenoid components. A possible application of the derived cohesive model involves FEA simulations for macroscopic pre-clinical testing of newly developed orthopaedic implants or cement-bone interface optimization. Even *in vivo* studies in which bone degeneration at the cement-bone interface is monitored on a microscale might be considered. The cohesive models could possibly indicate what the mechanical consequences of such remodeling are or explain the cause of remodeling based on local stress intensities.

We conclude that the simulated mixed-mode behavior of the cement-bone interface from postmortem retrieved cemented hip replacements satisfactorily match experimental findings with similar specimens, albeit the stiffness is somewhat overestimated in compression. The obtained mixed-mode stiffness response can subsequently be related to the interface morphology and can be formulated in an elastic cohesive model. Finally, the acquired data can be used as an input for a cohesive model which also includes interface failure.

Acknowledgements

This work was funded by the National Institutes of Health (NIH AR42017).

References

1. **Bishop, N. E., Schoenwald, M., Schultz, P., Puschel, K., Morlock, M. M., (2009).** The condition of the cement mantle in femoral hip prosthesis implantations--a post mortem retrieval study. Hip.Int. 19, 87-95.
2. **Clauss, M., Ilchmann, T., Zimmermann, P., Ochsner, P. E., (2010).** The histology around the cemented Muller straight stem: A post-mortem analysis of eight well-fixed stems with a mean follow-up of 12.1 years. J Bone Joint Surg.Br. 92, 1515-1521.
3. **Colombi, P., (2002).** Fatigue analysis of cemented hip prosthesis: model definition and damage evolution algorithms. International Journal of Fatigue 24, 895-901.
4. **Goodman, S. B., Huie, P., Song, Y., Lee, K., Doshi, A., Rushdieh, B., Woolson, S., Maloney, W., Schurman, D., Sibley, R., (1997).** Loosening and osteolysis of cemented joint arthroplasties. A biologic spectrum. Clin. Orthop Relat Res 149-163.
5. **Gozzard, C., Gheduzzi, S., Miles, A. W., Learmonth, I. D., (2005).** An in-vitro investigation into the cement pressurization achieved during insertion of four different femoral stems. Proc.Inst.Mech.Eng [H.] 219, 407-413.
6. **Harper, E. J., Bonfield, W., (2000).** Tensile characteristics of ten commercial acrylic bone cements. J.Biomed.Mater.Res. 53, 605-616.
7. **Hung, J. P., Chen, J. H., Chiang, H. L., Wu, J. S., (2004).** Computer simulation on fatigue behavior of cemented hip prostheses: a physiological model. Comput.Methods Programs Biomed. 76, 103-113.
8. **Janssen, D., Mann, K. A., Verdonschot, N., (2008).** Finite Element Simulation of cement-bone interface micro-mechanics., 16th ESB Congress.
9. **Janssen, D., Mann, K. A., Verdonschot, N., (2008).** Micro-mechanical modeling of the cement-bone interface: The effect of friction, morphology and material properties on the micromechanical response. J.Biomech. 41, 3158-3163.
10. **Janssen, D., Mann, K. A., Verdonschot, N., (2009).** Finite element simulation of cement-bone interface micromechanics: a comparison to experimental results. J.Orthop.Res. 27, 1312-1318.
11. **Jasty, M., Maloney, W. J., Bragdon, C. R., O'Connor, D. O., Haire, T., Harris, W. H., (1991).** The initiation of failure in cemented femoral components of hip arthroplasties. J.Bone Joint Surg.Br. 73, 551-558.
12. **Kadir, M. R., Syahrom, A., Ochsner, A., (2010).** Finite element analysis of idealised unit cell cancellous structure based on morphological indices of cancellous bone. Med.Biol.Eng Comput. 48, 497-505.

13. **Katoozian, H., Davy, D. T., (2000).**
Effects of loading conditions and objective function on three-dimensional shape optimization of femoral components of hip endoprostheses. Med.Eng Phys. 22, 243-251.
14. **Keyak, J. H., Kaneko, T. S., Tehranzadeh, J., Skinner, H. B., (2005).**
Predicting proximal femoral strength using structural engineering models. Clin.Orthop.Relat Res. 437, 219-228.
15. **Lewis, G., (1997).**
Properties of acrylic bone cement: state of the art review. J.Biomed.Mater.Res. 38, 155-182.
16. **Lewis, G., Duggineni, R., (2006).**
Finite element analysis of a three-dimensional model of a proximal femur-cemented femoral THJR component construct: Influence of assigned interface conditions on strain energy density. Bio-Medical Materials and Engineering 16, 319-327.
17. **Lucksanasombool, P., Higgs, W. A., Ignat, M., Higgs, R. J., Swain, M. V., (200**3).
Comparison of failure characteristics of a range of cancellous bone-bone cement composites. J.Biomed.Mater.Res.A 64, 93-104.
18. **Mann, K. A., Miller, M. A., Cleary, R. J., Janssen, D., Verdonschot, N., (2008**).
Experimental micromechanics of the cement-bone interface. J.Orthop.Res. 26, 872-879.
19. **Mann, K. A., Miller, M. A., Verdonschot, N., Izant, T. H., Race, A., (2010).**
Functional interface micromechanics of 11 en-bloc retrieved cemented femoral hip replacements. Acta Orthop 81, 308-317.
20. **Mann, K. A., Mocarski, R., Damron, L. A., Allen, M. J., Ayers, D. C., (2001).**
Mixed-mode failure response of the cement-bone interface. J.Orthop.Res. 19, 1153-1161.
21. **Miller, M. A., Eberhardt, A. W., Cleary, R. J., Verdonschot, N., Man**n, K. A., (2010).
Micromechanics of postmortem-retrieved cement-bone interfaces. J.Orthop.Res. 28, 170-177.
22. **Miller, M. A., Race, A., Waanders, D., Cleary, R. J., Janssen, D., Verdonschot, N., Mann, K. A., (2011).**
Multi-axial loading micromechanics of the cement-bone interface in post-mortem retrievals and lab-prepared specimens. Journal of the Mechanical Behavior of Biomedical Materials 4, 366-374.
23. **Mjoberg, B., (1986).**
Loosening of the cemented hip prosthesis. The importance of heat injury. Acta Orthop Scand.Suppl 221, 1-40.
24. **Moreo, P., Perez, M. A., Garcia-Amar, J. M., Doblare, M., (2006).**
Modelling the mixed-mode failure of cement-bone interfaces. Engineering Fracture Mechanics 73, 1379-1395.
25. **Mullins, L. P., McGarry, J. P., Bruzzi, M. S., McHugh, P. E., (2007).**
Micromechanical modelling of cortical bone. Comput.Methods Biomech.Biomed.Engin. 10, 159-169.
26. **Oonishi, H., Ohashi, H., Oonishi, H., Jr., Kim, S. C., (2008).**
THA with hydroxyapatite granules at cement-bone interface: 15- to 20-year results. Clin.Orthop Relat Res 466, 373-379.
27. **Pahr, D. H., Zysset, P. K., (2008).**
Influence of boundary conditions on computed apparent elastic properties of cancellous bone. Biomech.Model Mechanobiol. 7, 463-476.

28. **Perez, M. A., Garcia-Aznar, J. M., Doblare, M., (2009).**
Does increased bone-cement interface strength have negative consequences for bulk cement integrity? A finite element study. Ann.Biomed.Eng 37, 454-466.
29. **Perez, M. A., Palacios, J., (2010).**
Comparative finite element analysis of the debonding process in different concepts of cemented hip implants. Ann.Biomed Eng 38, 2093-2106.
30. **Roques, A., Browne, M., Taylor, A., New, A., Baker, D., (2004).**
Quantitative measurement of the stresses induced during polymerisation of bone cement. Biomaterials 25, 4415-4424.
31. **Salomonsson, K., (2008).**
Mixed mode modeling of a thin adhesive layer using a meso-mechanical model. Mechanics of Materials 40, 665-672.
32. **Salomonsson, K., Andersson, T., (2008).**
Modeling and parameter calibration of an adhesive layer at the meso level. Mechanics of Materials 40, 48-65.
33. **Schmalzried, T. P., Maloney, W. J., Jasty, M., Kwong, L. M., Harris, W. H., (1993).**
Autopsy studies of the bone-cement interface in well-fixed cemented total hip arthroplasties. J Arthroplasty 8, 179-188.
34. **Sierra, R. J., Timperley, J. A., Gie, G. A., (2009).**
Contemporary cementing technique and mortality during and after exeter total hip arthroplasty. J.Arthroplasty 24, 325-332.
35. **Stolk, J., Janssen, D., Huiskes, R., Verdonschot, N., (2007).**
Finite element-based preclinical testing of cemented total hip implants. Clin.Orthop.Relat Res. 456, 138-147.
36. **Stolk, J., Verdonschot, N., Murphy, B. P., Prendergast, P. J., Huiskes, R., (2004).**
Finite element simulation of anisotropic damage accumulation and creep in acrylic bone cement. Engineering Fracture Mechanics 71, 513-528.
37. **Venesmaa, P. K., Kroger, H. P., Jurvelin, J. S., Miettinen, H. J., Suomalainen, O. T., Alhava, E. M., (2003).**
Periprosthetic bone loss after cemented total hip arthroplasty: a prospective 5-year dual energy radiographic absorptiometry study of 15 patients. Acta Orthop Scand. 74, 31-36.
38. **Verdonschot, N., Huiskes, R., (1997).**
The effects of cement-stem debonding in THA on the long-term failure probability of cement. J.Biomech. 30, 795-802.
39. **Waanders, D., Janssen, D., Bertoldi, K., Mann, K. A., Verdonschot, N., (2011).**
Mixed-mode loading of the cement-bone interface: a finite element study. Comput.Methods Biomech.Biomed.Engin. 14, 145-155.
40. **Waanders, D., Janssen, D., Mann, K. A., Verdonschot, N., (2010).**
The mechanical effects of different levels of cement penetration at the cementbone interface. J.Biomech. 43, 1167-1175.

41. **Waanders, D., Janssen, D., Mann, K. A., Verdonschot, N., (2011).**
The behavior of the micro-mechanical cement-bone interface affects the cement failure in total hip replacement. J Biomech. 44, 228-234.
42. **Waanders, D., Janssen, D., Miller, M. A., Mann, K. A., Verdonschot, N., (2009).**
Fatigue creep damage at the cement-bone interface: an experimental and a micro-mechanical finite element study. J.Biomech. 42, 2513-2519.
43. **Wang, J. Y., Tozzi, G., Chen, J., Contal, F., Lupton, C., Tong, J., (2010).**
Bone-cement interfacial behaviour under mixed mode loading conditions. J Mech Behav Biomed Mater 3, 392-398.
44. **Wei, Y., Hutchinson, J. W., (2008).**
Toughness of Ni/Al2O3 interfaces as dependent on micron-scale plasticity and atomistic-scale separation. Philosophical Magazine 88, 3841-3859.

Chapter 8

The behavior of the micro-mechanical cement-bone interface affects the cement failure in total hip replacement

Journal of Biomechanics
(2011); 44(2):228-34

Abstract

In the current study, the effects of different ways to implement the complex micro-mechanical behavior of the cement-bone interface on the fatigue failure of the cement mantle was investigated. In an FEA-model of a cemented hip reconstruction the cement-bone interface was modeled and numerically implemented in four different ways: (I) as infinitely stiff, (II) as infinitely strong with a constant stiffness, (III) a mixed-mode failure response with failure in tension and shear, and (IV) realistic mixed mode behavior obtained from micro FEA-models. Case II, III and IV were analyzed using data from a stiff and a compliant micro-FEA model and their effects on cement failure were analyzed. The data used for Case IV was derived from experimental specimens that were tested previously. Although the total number of cement cracks was low for all cases, the compliant Case II resulted in twice as many cracks as Case I. All cases caused similar stress distributions at the interface. In all cases, the interface did not display interfacial softening; all stayed the elastic zone. Fatigue failure of the cement mantle resulted in a more favorable stress distribution at the cement-bone interface in terms of less tension and lower shear tractions. We conclude that immediate cement-bone interface failure is not likely to occur, but its local compliancy does affect the formation of cement cracks. This means that at a macro-level the cement-bone interface should be modeled as a compliant layer. However, implementation of interfacial post-yield softening does seem to be necessary.

Introduction

Fatigue failure of the cement mantle in terms of cement cracking is one of the failure mechanisms that leads to aseptic loosening in cemented hip reconstructions[7]. Finite element analysis (FEA) has been proven successful in simulating the fatigue failure process of the cement mantle in complete hip reconstructions and is therefore a good tool to predict implant survival[8,21,24].

It has previously been demonstrated that the stem-cement interface is a debonded interface, which enables gapping and sliding between the stem and cement[4,23]. This has widely been implemented in FEA-models in which the stem-cement interface was invoked as a frictional contact layer[5,20,29]. Recently, however, experiments have demonstrated that the movements at the cement-bone interface are also substantial[16,22]. It can therefore be suggested that the compliance of the cement-bone interface may have substantial influence on the fatigue failure of the cement mantle and should therefore be incorporated into computational models of complete cemented hip reconstructions.

The cement-bone interface has previously been modeled in basically three different manners, as: (1) An infinitely stiff interface between the cement and bone[6,8,9,24]; (2) a layer of soft tissue elements with a constant stiffness[3,29,33], which represented osteolysis around the cement mantle[2]; and (3) a layer of cohesive elements in which the mixed-mode behavior of the cement-bone interface is implemented[13,19,20]. The experimental validation of these three aforementioned methods is, however, debatable. Experiments with laboratory prepared cement-bone interface specimens demonstrate a significant variation in compliance and strength[14] which does not match the infinitely stiff (1) or soft tissue layer (2) assumption. Input for the cohesive elements was experimental mixed-mode data: linear increase followed by softening, for the tension and shear direction[17]. A considerable deviation in stiffness and strength was reported. Theoretical mixed-mode models[1] were used to fit the stiffness and strength while accurate modeling of the softening phase was neglected.

Recently, the mixed-mode behavior of the cement-bone interface has been studied utilizing four micro FEA-models (Figure 8.1a)[30]. These FEA-models included simulation of cement and bone cracking and were loaded in 11 different directions, while monitoring tractions (T_N and T_T) and displacements (Δ_N and Δ_T) in normal and tangential direction. Only frictional contact was assumed at the complex interdigitated interface between cement and bone. Because no bonding was assumed, failure (cracking) of the interface on an apparent level could only occur through failure of the bulk cement and bone; no failure could occur at the actual contact interface between cement and bone. Depending on the micro-structure of the interface, considerable different magnitudes in strength and stiffness were found (Table 8.1), which compared favorably with experiments[14]. Innovative observations included (i) a considerable compression generated during the softening phase at mixed-mode angles larger than 45°; and (ii) lack of failure under pure shear loading (Figure 8.1b). This could be explained by the presence of crack patterns (Figure 8.1c) and applied the boundary conditions. This new information allows the implementation of the validated micro-mechanical behavior into macro-models of cemented hip reconstructions. However, implementation of this more realistic behavior of the cement-bone interface is rather complex and increases computational time. It is therefore worthwhile to assess whether it is truly necessary to represent the compliancy and post-yield mechanical behavior of the cement-bone interface.

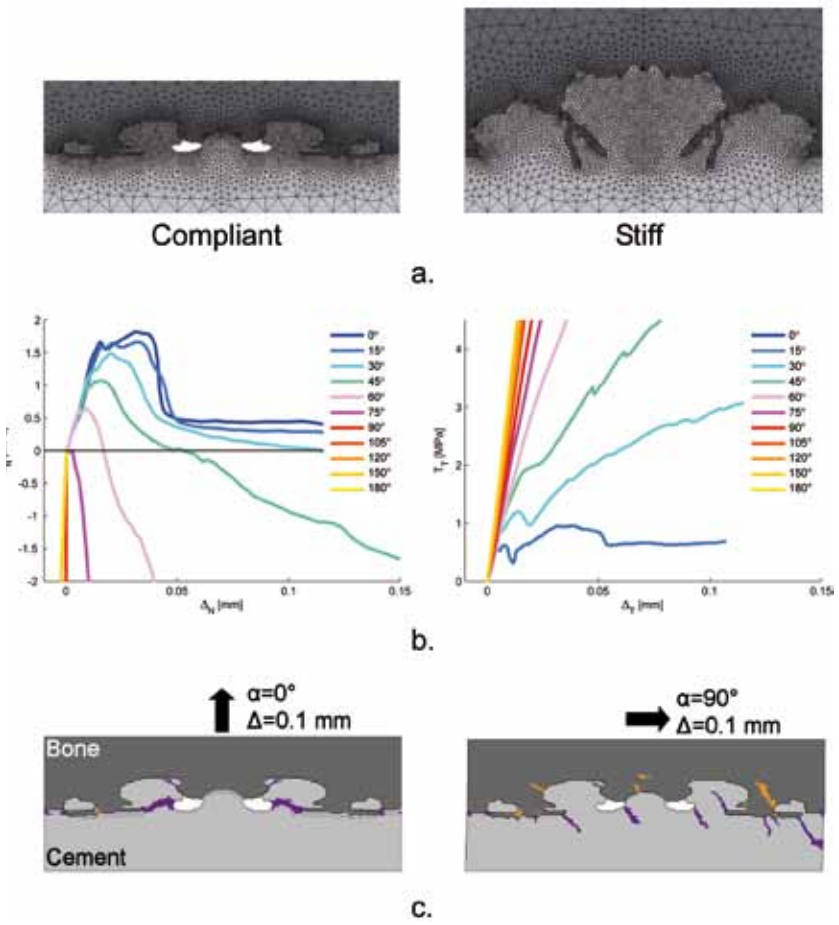

Figure 8.1 *a. The compliant and stiff generated plain strain micro FEA-model of the cement-bone interface used to determine the mixed-mode behaviour of the cement-bone interface30. All models were mirrored to facilitate the application of periodic boundary conditions to both sides of the models. The bottom part of the cement was fixed for all degrees of freedom, while the top part of the bone was uniformly displaced under eleven different angles without allowing transverse motions. In each model, both the bone and cement had provision for element cracking.*

b. Mechanical mixed-mode response of the compliant micro FEA-model: on the left, the normal traction versus normal displacement response, TN-ΔN, and on the right the tangential traction versus tangential displacement response, TT-ΔT, for the eleven different directions. For the mixed-mode responses in which tension was involved, compressive stresses were generated in the softening phase.
Also, the mixed-mode responses showed a gradual decrease in ultimate TN as the loading angle increased. The TT-ΔT-response showed no failure in pure shear (α=90°).

c. Crack patterns predicted in the bone and cement. Because of the mirroring of the models, symmetric crack patterns occurred in pure tension (α=0°). In pure shear, (α=90°), cracks progresses into the bulk material without breaking off cement or bone spurs. This could clarify the feature that was found of no failure in shear.

We therefore assessed in this study the added value of the cement-bone interface mechanics in an increasingly complex fashion using four steps. Four different cement-bone interface behaviors were considered: (I) infinitely stiff interface; (II) compliant interface with infinite strength; (III) mixed-mode failure response according to experimental findings including post-yield softening under tensile and shear conditions; and (IV) mixed-mode behavior as obtained with the aforementioned micro FEA-models. Each case was analyzed with the most compliant and most stiff cement-bone interface as found in the aforementioned micro FEA-study (Table 8.1)[30]. An FEA-model of a complete cemented hip reconstruction utilizing a Lubinus SPII prosthesis, in which the cement-bone interface was macroscopically implemented using the micro FEA-data, was subjected to a loading configuration simulating normal walking. Crack formation in the cement mantle and load distribution at the cement-bone interface were monitored. We asked: (1) How do cement-bone interface variations of stiffness and strength influence number and distribution of cracks in the cement mantle? (2) Does failure of the cement-bone interface occur during cyclic loading of normal walking? (3) Does fatigue failure of the cement mantle influence the probability of failure of the cement-bone interface?

Response	*Tensile strength, T_{Nmax} [MPa]*	*Tensile stiffness, $\frac{\partial T_N}{\partial \Delta_N}, \left[\frac{MPa}{mm}\right]$*	*Displacement at T_{Nmax}, δ_N [mm]*	*Shear stiffness, $\frac{\partial T_T}{\partial \Delta_T}, \left[\frac{MPa}{mm}\right]$*
Stiff	2.79	251	0.012	241
Compliant	1.82	123	0.030	217

Table 8.1 *Interface properties of the most stiff and most compliant responses obtained from micro FEAmodels 30. The tensile strength and stiffness of the most stiff model differed approximately a factor 2 compared to the compliant model. The displacement at the tensile strength, δN, was much larger for the compliant model. The difference in shear stiffness was not comparable to the difference in tensile stiffness.*

Methods

We used a complete 3D FEA-model of a cemented hip reconstruction utilizing a Lubinus LPII stem from a previous study (Figure 8.2)[24]. This model was based on a laboratory implantation of the stem in a composite femur whose stem orientation was based on radiographs and CT-data of the reconstruction. The complete reconstruction was meshed with eight-node isoparametric brick elements. The cortex was modeled as transversely isotropic, with a higher stiffness in axial direction of the femur (Table 8.2). Trabecular bone, cement mantle, and stem were modeled as isotropic (Table 8.2). For this study, an additional layer of cohesive elements was modeled between cement and bone, to represent the cement-bone interface (Figure 8.2). To maintain the initial mesh, the cohesive elements were physically modeled with zero thickness. The stem-cement interface was considered to be debonded and contact was modeled utilizing a node-to-surface algorithm with a friction coefficient of 0.25 (MSC.MARC 2007r1, MSC Software Corporation, Santa Ana, CA, USA).

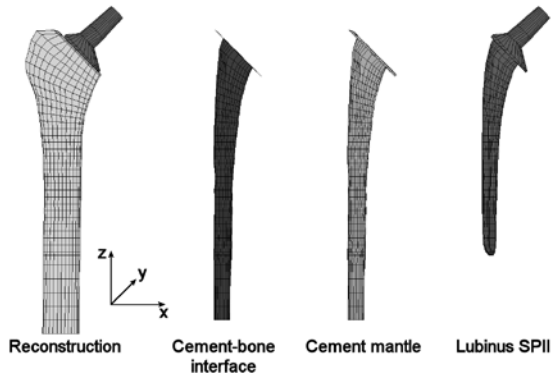

Figure 8.2 *The complete cemented hip reconstruction implanted with a Lubinus SPII stem. Between the cement mantle and the bone, a layer of cohesive elements was modeled that represented the cement-bone interface.*

Part	*Young's Modulus, E, [MPa]*	*Poisson's ratio, ν, [-]*
Stem	210,000	0.3
Cement	2,400	0.3
Trabecular bone	400	0.3
Cortical bone	$E_x = E_y = 7{,}000$; $E_z = 11{,}500$ $G_{xy} = 2{,}600$; $G_{yz} = G_{zx} = 3{,}500$	$\nu_{xy} = \nu_{yz} = \nu_{zx} = 0.4$

Table 8.2 *Material properties of the hip reconstruction. Stem, cement and trabecular bone were modeled as isotropic materials, while cortical bone was modeled as transversely isotropic. All material properties were based on Stolk et al. (2007).*

The models were subjected to a loading history of 20 million cycles of walking. The loading configuration included the hip contact force and two muscle forces (abductors and vastus lateralis[25]), all based on 700N body weight. Fatigue failure of the bulk cement was calculated by means of a custom-written FEA-algorithm that simulated creep and damage accumulation[26]. This method calculated the element's deformation as $\{\varepsilon\}=[S]\cdot\{\sigma\}+\{\varepsilon^c\}$. The compliance matrix [S] incorporated the damage by reduction of stiffness to 0.1MPa perpendicular to corresponding maximum principal stress direction. Each component of the creep strain tensor $\{\varepsilon^c\}$ was dependent on the scalar ε^c defined as $\varepsilon^c=7.985\cdot10^{-7}\cdot\eta^{0.4113-0.116\log(\sigma)}\cdot\sigma^{1.9063}$ [28].

The cement-bone interface was numerically implemented with four different cases (Figure 8.3):

I: An infinitely stiff interface with infinite strength

II: A compliant interface with infinite strength

III: A mixed-mode failure response according to experimental findings

IV: A mixed-mode failure response according to micro-FEA mixed-mode models

The interface in Case I was assumed to be completely bonded without the possibility for deformations at the cement-bone interface. Case II represented a constant stiffness without interfacial failure and represented a soft tissue layer as implemented previously[3,29]. Case III represented failure in tension and shear; a behavior widely observed experimentally[18,34]. Case IV represented the behavior obtained from a previous micro FEA-study[30]. Case II to IV were each analyzed at high and low stiffness and referred to as "stiff" and "compliant". The magnitudes of stiffness and strength were based on the stiffest and most compliant response of the micro-FEA study (Table 8.1).

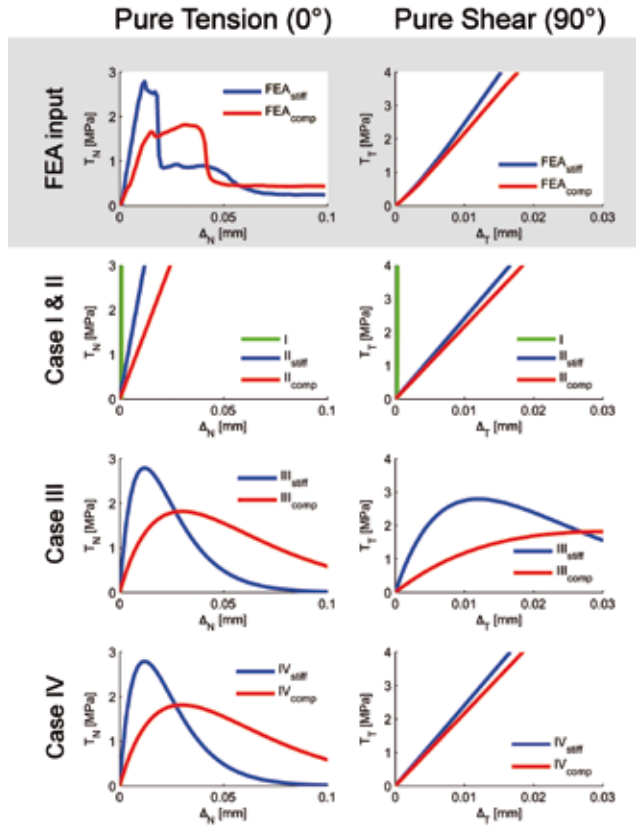

Figure 8.3 *The mechanical behaviors in pure tension (0°) and pure shear (90°) of the micro FEA-model (in grey) and the four different cases. Note that only the responses in pure tension and pure shear are presented and not the mixed mode responses. In pure tension, the micro FEA-models resulted in a linear increase of TN followed by yielding and softening. In pure shear, a linear increase of TT was found without any softening. Case I and II were modeled as a constant stiffness in tension and shear in which Case I was assumed to be infinitely stiff. Case III had a similar behavior as has been found in experiments: yielding and softening in tension and shear with a equal stiffness in tension as in shear[14,18]. Case IV had the same mixed mode behavior as the micro FEA-models. For Case III and IV, the parameters of the cohesive model were set according to the interfacial strength (TN and TT) and its corresponding displacement (δN and δT) (Table 8.3).*

All cases were numerically implemented using a cohesive model which defined the normal and tangential traction (T_N and T_T) as a function of normal and tangential displacements (Δ_N and Δ_T)[35]:

$$T_N = \frac{\Gamma_0}{\delta_N}\left[\frac{\Delta_N}{\delta_N} - \left((1+\beta)\frac{\Delta_N}{\delta_N} - \beta\right) f(\Delta_T)\right] \exp\left(-\frac{\Delta_N}{\delta_N}\right)$$

$$T_T = \Gamma_0 \frac{df(\Delta_T)}{d\Delta_T}\left[1 + (1+\beta)\frac{\Delta_N}{\delta_N}\right] \exp\left(-\frac{\Delta_N}{\delta_N}\right)$$

where Γ_0 denotes the total fracture energy and δ_N the displacement at the tensile strength. The function f (Δ_T) was used to define the response in pure shear: $T_T(0,\Delta_T) = \Gamma_0 \frac{df(\Delta_T)}{d\Delta_T}$

Case I, II and IV were assumed to have a constant stiffness in pure shear without interfacial failure (Figure 8.3). Hence: $\frac{df(\Delta_t)}{d\Delta_t} = \frac{1}{\Gamma_0}\frac{\partial T_t}{\partial \Delta_t}\cdot\Delta_t$, where $\frac{\partial T_t}{\partial \Delta_t}$ is the tangential stiffness in shear (Table 8.1). Case III assumed interfacial failure in shear (Figure 8.3) and was defined as: $\frac{df(\Delta_t)}{d\Delta_t} = \frac{\Delta_t}{\delta_t^2}\exp\left(-\frac{\Delta_t}{\delta_t}\right)$ The values of all parameters are listed in Table 8.3.

To investigate how cement-bone interface variations influence cement cracking, we monitored the number of cracks formed in the cement and analyzed the distribution of the cracks. We monitored whether failure occurs during cyclic walking simulation by tracking whether cohesive elements at the interface entered the softening phase. Finally, we analyzed whether fatigue failure of the cement mantle influenced failure of the cement-bone interface by comparing interfacial failure directly after loading and after 20 million cycles of normal walking.

Case	Γ_0	$\delta_N[mm]$	$\frac{df(\Delta_T)}{d\Delta_T}$	β	$\delta_T[mm]$
I	400,000	2.0	$\frac{100,000}{\Gamma_0}\cdot\Delta_t$	0.0	-
II_{stiff}	1,004	2.0	$\frac{241}{\Gamma_0}\cdot\Delta_t$	0.0	-
$II_{compliant}$	492	2.0	$\frac{217}{\Gamma_0}\cdot\Delta_t$	0.0	-
III_{stiff}	0.091	0.012	$\frac{\Delta_t}{\delta_t^2}\exp\left(-\frac{\Delta_t}{\delta_t}\right)$	0.0	0.012
$III_{compliant}$	0.148	0.030	$\frac{\Delta_t}{\delta_t^2}\exp\left(-\frac{\Delta_t}{\delta_t}\right)$	0.0	0.030
IV_{stiff}	0.091	0.012	$\frac{241}{\Gamma_0}\cdot\Delta_t$	-0.8	-
$IV_{compliant}$	0.148	0.030	$\frac{217}{\Gamma_0}\cdot\Delta_t$	-0.8	-

Table 8.3 *The values of all parameters used by the cohesive model35. 0 was the total fracture energy and N the displacement which corresponded to the displacement at the tensile strength. The function was used to define the behaviour in pure shear. The parameter was used to model the compressive normal tractions which occurred in the softening phase. A negative value of resulted in compression in the softening phase. Finally, T corresponded to the displacement at the shear strength and was therefore only used for Case III.*

Results

The number of bulk cement cracks that were predicted varied considerably over the seven different simulations, although the total number of cracks was always <1% of the complete cement mantle (Figure 8.4). After 20 million cycles, the compliant Case II showed a number of cracks twice as large as Case I. For each case, the compliant cement-bone interface resulted in more cracks than the stiff interface. Remarkable are the normalized number of cracks of the stiff Case III and the stiff Case IV, which hardly resulted in any differences. On the other hand, the compliant Case III and compliant Case IV do show some differences. Qualitatively, the differences between the crack patterns of all simulations were negligible.

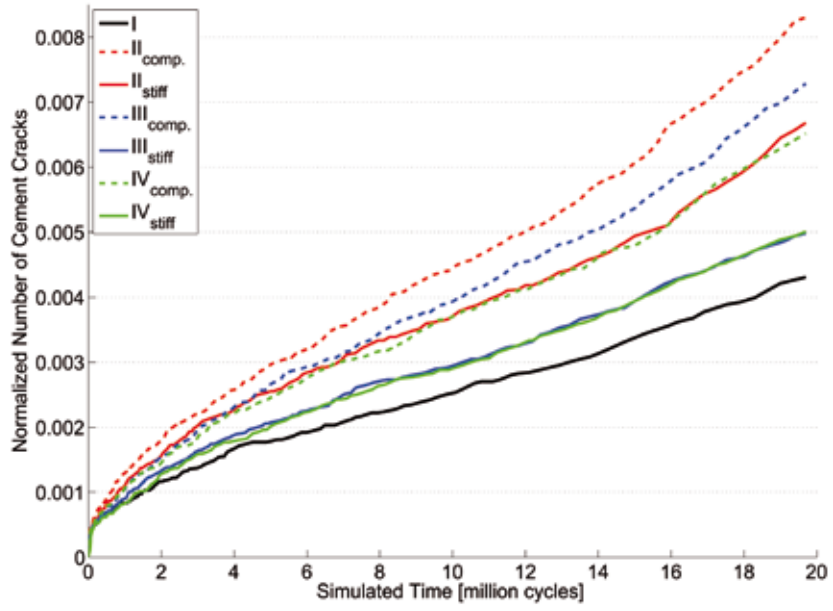

Figure 8.4 *Normalized number of cement cracks in the cement mantle with respect to the number of loading cycles of the 7 different simulations. The cracks were normalized by dividing the predicted number of cracks by the maximum number of cracks possible, which was equal to three time the number of integration points of the cement mantle. Case I, the infinitely stiff interface, resulted in the smallest number of cement cracks. The compliant Case II resulted in almost double number of cement cracks compared to Case I.*

In none of the simulations in which failure of the cement-bone interface could occur, interfacial failure was predicted. The normal and tangential tractions (T_N and T_T) stayed below the interfacial strength during the entire loading history. Furthermore, after 20 million cycles the maximum normal traction (T_N) at the cement-bone interface decreased for Case II,

Case	N=100 min T_N	N=100 max T_N	N=100 max T_T	N=20 million min T_N	N=20 million max T_N	N=20 million max T_T
I	-10.1	2.76	2.93	-10.5	3.15	3.19
II_{stiff}	-2.17	1.23	2.10	-3.27	0.67	2.53
$II_{compliant}$	-3.16	1.62	1.94	-4.42	0.72	2.04
III_{stiff}	-3.41	1.12	1.40	-5.08	0.65	1.55
$III_{compliant}$	-6.44	1.77	1.95	-8.48	1.00	2.12
IV_{stiff}	-3.34	1.03	1.93	-5.21	0.64	2.27
$IV_{compliant}$	-6.70	1.66	1.66	-8.70	0.99	2.16

Table 8.4 *The minimum and maximum tractions that occurred at the cement-bone interface at N=100 and N=20 million cycles. For all cases, the maximum normal compression traction, min TN, increased and the maximum normal tensile traction decreased, with respect to Case I. Surprisingly, the maximum tangential traction increased, while it was also shown that overall the tangential tractions decreased (Figure 8.6b).*

The distribution of normal tractions (T_N) at the cement-bone interface was qualitatively the same for all simulations. Initially, considerable normal compression (T_N <0) was observed below the medial implant collar and lateral at tip level (Figure 8.5a). The stem tip also resulted in some areas with tension at the medial side of the cement-bone interface, which almost disappeared after 20 million cycles. At the end of the simulations, more areas with compression were visible as a result of stem subsidence. Overall, the total area with tensile tractions decreased as a result of cement failure (Figure 8.5b).

The initial distribution of tangential tractions (T_T) revealed high tangential tractions at the medial side of the collar and at the stem tip level of the cement-bone interface (Figure 8.6a). After 20 million cycles the area with high tangential tractions at the stem tip level had moved from the posterior to the lateral side. Overall, the tangential tractions decreased in time (Figure 8.6b), although the maximum peak tangential traction at the cement-bone interface increased (Table 8.4).

Figure 8.5 *a. Distribution of normal tractions, TN, at the cement-bone interface for Case I. There were hardly any differences regarding TN-distribution over the 7 different cases. As a result of stem subsidence, a larger area of the cement bone interface was loaded under compression.*
b. The percentage cement-bone interface area under different ranges of normal traction, TN.
The amount of area of the cement-bone interface that was loaded under tension decreased considerably after 20 million cycles.
On the other hand, more area was loaded under compression.

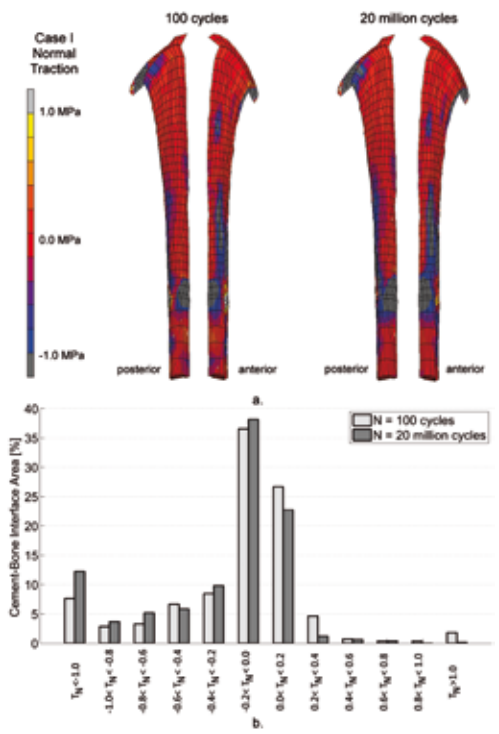

Figure 8.6 *a. Distribution of tangential tractions, TT, at the cement-bone interface. After 20 million loading cycles, the tangential tractions decreased. However, the maximum tangential peak traction increased (Table 8.4).*
b. The percentage cement-bone interface area under different ranges of tangential traction, TT.
The magnitude of the tangential tractions, TT, decreased considerable after 20 million cycles.

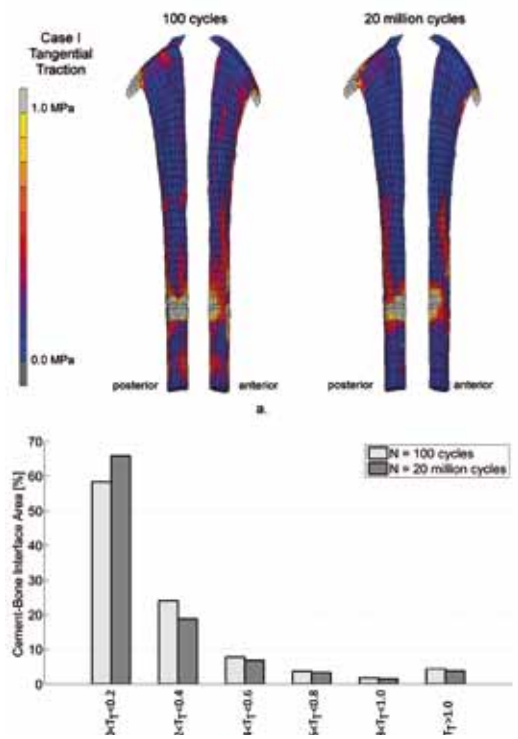

Discussion

We investigated the effect of various behaviors of the cement-bone interface on the fatigue failure of the cement mantle. We find that compliant cement-bone interfaces results in more cement cracking than a stiff interface. The investigated interfacial behaviors did not influence the distribution and magnitude of normal and tangential tractions at the cement-bone interface. Fatigue failure of the cement mantle resulted in increased compression at the cement-bone interface and in decreased tangential tractions. We find also that the tractions stayed in the elastic zone for the cases in which failure of the interface was allowed.

The finding that increased compression was found at the interface after fatigue crack formation of the interface may be attributed to the fact that the cement cracks may create room for the implant to subside or rotate, causing a redistribution of the load transfer. Although the shift from tangential to compression tractions at the cement-bone interface seems beneficial, the underlying mechanism may not be, as more room for implant motion would also entail increased micromotions at the implant-cement interface, possibly leading to the generation of wear debris and particle-induced osteolysis.

Our finding that failure did not occur at the cement-bone interface may be explained by the simulation of normal walking and by the well-functioning of the majority of the cemented hip reconstructions, without evidence of interface gapping or formation of fibrous tissue layers. The lack of failure, even in the compliant case, is consistent with analyses of post-mortem en-bloc specimens[16]. Indeed, some en-bloc specimens displayed a compliant response despite the fact that the reconstructions were well-functioning.

The predicted amount of cracks in the cement mantle was less than 1% of the bulk. This is a low percentage in comparison to the ~6% and ~8% found for a Charnley and Exeter stem, respectively[21]. This difference could be attributed to the fact that in the current study only simulated walking was considered. However, it has previously also been shown that a Lubinus SPII stem results in the fewest number of cement cracks compared with three other stems[24]. Furthermore, from a clinical point of view, the clinical results of the Lubinus SPII stem are excellent[12].

One might expect that the reconstruction with the compliant interface at lower strength would fail earlier than the stiff case. However, in none of the simulated cases failure was predicted, in terms of interfacial softening. Hence, the entire cement-bone interface was only elastically stimulated for both compliant and stiff cases. This can be explained by the interfacial elastic energy in pure tension, which can be determined as: $W(\delta_N,0)=\int_0^{\delta_N} T_N \partial\Delta_N = \Gamma_0 \cdot [1-2\exp(-1)]$ and is larger for the compliant than for the stiff interface (Table 8.3).

Although simulations referred to the elastic phase, differences were predicted in the number of cracks. A possible explanation for this difference can be related to the definition of the normal traction (T_N) in the utilized numerical model[35]. The input parameters of this model for Case II were set to match the constant normal stiffness $\left(\frac{\partial T_N}{\partial \Delta_N}\right)$ to the normal stiffness of our previous micro FEA-study[30]. Instead, Case III and IV were fit to the tensile strength ($T_{N,max}$) and its corresponding displacement (δ_N). This resulted in a decreasing normal stiffness $\left(\frac{\partial T_N}{\partial \Delta_N}\right)$ in the elastic phase for Case III and IV (Figure 8.3) and therefore a different T_N-Δ_N-response compared to the normal stiffness of Case II. For example, the normal stiffness at zero displacement (Δ_N = Δ_T = 0.0 mm) matches $\frac{\partial T_N}{\partial \Delta_N}=\frac{\Gamma_0}{\delta_N^2}$. For Case II and Case III or IV, this results in a $\frac{\partial T_N}{\partial \Delta_N}$ of 251 $\frac{MPa}{mm}$ and 631.9 $\frac{MPa}{mm}$, respectively. This considerable difference is also visible in the T_N-Δ_N-responses (Figure 8.3). The difference in $\frac{\partial T_N}{\partial \Delta_N}$ has hardly any influence on the traction distribution at the cement-bone interface (Figure 8.5), but does result in differences of interfacial displacement, which are significantly higher for the compliant cases.

Apart from the fact that only one stem type in one bone was considered, one of the main limitations of this study was that fatigue failure of the cement-bone interface was not considered. It can be expected that, although all the deformations were elastic, fatigue failure is likely to occur and to affect the mechanical situation at the local level. Fatigue failure will result in a mechanical degradation of the cement-bone interface and a further increase of cement cracks in the cement mantle.

It was previously found that fatigue failure of the cement-bone interface includes a decay of the interfacial stiffness[10,15,32]. Furthermore, the number of cycles to failure, N_f, was determined as: $N_f = 12.581 \cdot \left(\frac{\sigma}{\sigma_{ult}}\right)^{-13.43}$ [11]. This finding can be related to a damage parameter, *d*, as $\dot{d}^{cyc} = \frac{1}{N_f}$ which linearly influences the stiffness, $K = (1-d)K_0$ (with $0 \le d \le 1$)[19]. Also, the stiffness of the cement-bone interface can be defined as: $K = 10^{0.52}\delta_c^{-0.46}CA^{0.63}$, in which CA is the interface contact area and δ_c the interface creep: $\delta_c = 10^{0.57} \cdot \left(\frac{\tau_{max}}{K}\right)^{1.35} n^{0.24} CA^{-0.40}$ with *n* represents the number of loading cycles[15]. Assuming that the interface always shows an elastic behavior, mixed-mode traction-displacement responses are not a necessary input and the initial stiffness in tension $\left(\frac{\partial T_N}{\partial \Delta_N}\right)$ and shear $\left(\frac{\partial T_T}{\partial \Delta_T}\right)$ would already be sufficient.

Only two micromechanical models were used as input for the cohesive models of Case IV. This is a limitation to our study considering the wide spread of micromechanical response that has been shown experimentally[14,15]. Because the extraction of multi-axial data from micromechanical FEA models requires a substantial amount of computational power, the number of calculations that can be performed is limited. In order to still provide representative data for the cohesive models, we selected the two extremes (stiffest and most compliant) of the four experimental specimens with distinct differences in terms of interface morphology and mechanical response[30].

A homogenous distribution of the cement-bone interface characteristics around the cement mantle is assumed even though that the cement penetration of a cemented hip reconstruction is much higher proximally than elsewhere[27]. This is because no reliable data exist on the distribution of the mechanical properties of the cement-bone interface affected by the non-homogenous distribution[21,31].

Although the above mechanical descriptions of the cement-bone interface are rather sophisticated, they still lack the major influence of the biological component. Indeed, biological processes govern the micro-biomechanical behavior of the interface16 in terms of considerable soft-tissue formation around the cement, which reduces strength and stiffness roughly by a factor of 10. Hence, this biological response (and its subsequent mechanical deterioration) should be taken into account in the implementation of long-term degradation of cement-bone properties on the survival of cemented total hip arthroplasty.

With reference to the research questions as posed in the introduction, we conclude that: (1) A compliant cement-bone interface results in more cracks in the cement mantle than

a stiff interface. Therefore the compliancy of the cement-bone interface should be included in models that focus on the prediction of failure of the cement mantle. (2) The cement-bone interface does not show immediate failure under the loading conditions as utilized in this study. Hence, it does not seem to be necessary to implement complex softening of the cement-bone interface. (3) Fatigue failure of the cement mantle results in more compression at the cement-bone interface and a decrease in tangential tractions. Finally, we conclude that failure of the cement-bone interface relies on fatigue damage, which can be based on decay of the interfacial stiffness as has been found experimentally. Therefore, use of complex mixed-mode models are unnecessary. Finally, we conclude that failure of the cement-bone interface in the direct post-operative situation does not occur, in agreement with clinical data. However, the compliancy of the cement-bone interface does have an accelerating effect on the formation of cement cracks and should be considered, without the necessity of the implementation of post-yield softening. For a realistic description of the cement-bone interface behavior on the longer-term, the mechanical representation of soft-tissue interpositioning at the interface should be represented. In that circumstance, post-yield softening may acquire importance, and require more complex descriptions to represent the mechanical behavior of the cement-bone interface accurately.

Acknowledgements

This work was funded by the NIH grant AR42017.

References

1. **Alfano, G., Crisfield, M. A., (2001).**
Finite element interface models for the delamination analysis of laminated composites: Mechanical and computational issues.
International Journal for Numerical Methods in Engineering 50, 1701-1736.
2. **Bauer, T. W., Schils, J., (1999).**
The pathology of total joint arthroplasty.II. Mechanisms of implant failure.
Skeletal Radiol. 28, 483-497.
3. **Colombi, P., (2002).**
Fatigue analysis of cemented hip prosthesis: model definition and damage evolution algorithms.
International Journal of Fatigue 24, 895-901.
4. **Gravius, S., Wirtz, D. C., Siebert, C. H., Andereya, S., Mueller-Rath, R., Maus, U., Mumme, T., (2008).**
In vitro interface and cement mantle analysis of different femur stem designs.
J Biomech. 41, 2021-2028.
5. **Hertzler, J., Miller, M. A., Mann, K. A., (2002).**
Fatigue crack growth rate does not depend on mantle thickness: an idealized cemented stem construct under torsional loading. J Orthop.Res. 20, 676-682.
6. **Hung, J. P., Chen, J. H., Chiang, H. L., Wu, J. S., (2004).**
Computer simulation on fatigue behavior of cemented hip prostheses: a physiological model.
Comput.Methods Programs Biomed. 76, 103-113.
7. **Jasty, M., Maloney, W. J., Bragdon, C. R., O'Connor, D. O., Haire, T., Harris, W. H., (1991).**
The initiation of failure in cemented femoral components of hip arthroplasties.
J.Bone Joint Surg.Br. 73, 551-558.
8. **Jeffers, J. R., Browne, M., Lennon, A. B., Prendergast, P. J., Taylor, M., (2007).**
Cement mantle fatigue failure in total hip replacement: experimental and computational testing.
J Biomech. 40, 1525-1533.
9. **Katoozian, H., Davy, D. T., (2000).**
Effects of loading conditions and objective function on three-dimensional shape optimization of femoral components of hip endoprostheses. Med.Eng Phys. 22, 243-251.
10. **Kim, D. G., Miller, M. A., Mann, K. A., (2004).**
A fatigue damage model for the cement-bone interface. J.Biomech. 37, 1505-1512.
11. **Kim, D. G., Miller, M. A., Mann, K. A., (2004).**
Creep dominates tensile fatigue damage of the cement-bone interface. J.Orthop.Res. 22, 633-640.
12. **Malchau H, Herberts P, Garellick G, Soderman P, Eisler T, (2006).**
Prognosis of total hip replacement. Available at: http://www.jru.orthop.gu.se.
13. **Mann, K. A., Damron, L. A., (2002).**
Predicting the failure response of cement-bone constructs using a non-linear fracture mechanics approach. J.Biomech.Eng 124, 462-470.
14. **Mann, K. A., Miller, M. A., Cleary, R. J., Janssen, D., Verdonschot, N., (2008).**
Experimental micromechanics of the cement-bone interface. J.Orthop.Res. 26, 872-879.

15. **Mann, K. A., Miller, M. A., Race, A., Verdonschot, N., (2009).**
Shear fatigue micromechanics of the cement-bone interface: An in vitro study using digital image correlation techniques. J.Orthop.Res. 27, 340-346.
16. **Mann, K. A., Miller, M. A., Verdonschot, N., Izant, T. H., Race, A., (2010).**
Functional interface micromechanics of 11 en-bloc retrieved cemented femoral hip replacements. Acta Orthop 81, 308-317.
17. **Mann, K. A., Mocarski, R., Damron, L. A., Allen, M. J., Ayers, D. C., (2001).**
Mixed-mode failure response of the cement-bone interface. J.Orthop.Res. 19, 1153-1161.
18. **Mann, K. A., Werner, F. W., Ayers, D. C., (1999).**
Mechanical strength of the cement-bone interface is greater in shear than in tension. J.Biomech. 32, 1251-1254.
19. **Moreo, P., Perez, M. A., Garcia-Amar, J. M., Doblare, M., (2006).**
Modelling the mixed-mode failure of cement-bone interfaces.
Engineering Fracture Mechanics 73, 1379-1395.
20. **Perez, M. A., Garcia-Aznar, J. M., Doblare, M., (2009).**
Does increased bone-cement interface strength have negative consequences for bulk cement integrity? A finite element study. Ann.Biomed.Eng 37, 454-466.
21. **Perez, M. A., Palacios, J., (2010).**
Comparative finite element analysis of the debonding process in different concepts of cemented hip implants. Ann.Biomed Eng 38, 2093-2106.
22. **Race, A., Miller, M. A., Mann, K. A., (2010).**
Novel methods to study functional loading micromechanics at the stem-cement and cement-bone interface in cemented femoral hip replacements. J.Biomech. 43, 788-791.
23. **Ramos, A., Simoes, J. A., (2009).**
The influence of cement mantle thickness and stem geometry on fatigue damage in two different cemented hip femoral prostheses. J Biomech. 42, 2602-2610.
24. **Stolk, J., Janssen, D., Huiskes, R., Verdonschot, N., (2007).**
Finite element-based preclinical testing of cemented total hip implants.
Clin.Orthop.Relat Res. 456, 138-147.
25. **Stolk, J., Verdonschot, N., Huiskes, R., (2002).**
Stair climbing is more detrimental to the cement in hip replacement than walking.
Clin.Orthop Relat Res 294-305.
26. **Stolk, J., Verdonschot, N., Murphy, B. P., Prendergast, P. J., Huiskes, R., (2004).**
Finite element simulation of anisotropic damage accumulation and creep in acrylic bone cement. Engineering Fracture Mechanics 71, 513-528.
27. **Stone, J. J., Rand, J. A., Chiu, E. K., Grabowski, J. J., An, K. N., (1996).**
Cement viscosity affects the bone-cement interface in total hip arthroplasty.
J.Orthop.Res. 14, 834-837.
28. **Verdonschot, N., Huiskes, R., (1995).**
Dynamic creep behavior of acrylic bone cement. J.Biomed.Mater.Res. 29, 575-581.

29. **Verdonschot, N., Huiskes, R., (1997).**
The effects of cement-stem debonding in THA on the long-term failure probability of cement. J.Biomech. 30, 795-802.
30. **Waanders, D., Janssen, D., Mann, K. A., Verdonschot, N., (2010).**
Mixed-Mode Behavior of the Cement-Bone Interface. Trans pre-Orthop Res Soc.
31. **Waanders, D., Janssen, D., Mann, K. A., Verdonschot, N., (2010).**
The mechanical effects of different levels of cement penetration at the cement-bone interface. J.Biomech. 43, 1167-1175.
32. **Waanders, D., Janssen, D., Miller, M. A., Mann, K. A., Verdonschot, N., (2009).**
Fatigue creep damage at the cement-bone interface: an experimental and a micro-mechanical finite element study. J.Biomech. 42, 2513-2519.
33. **Waide, V., Cristofolini, L., Stolk, J., Verdonschot, N., Boogaard, G. J., Toni, A., (2004).**
Modelling the fibrous tissue layer in cemented hip replacements: experimental and finite element methods. J Biomech. 37, 13-26.
34. **Wang, J. Y., Tozzi, G., Chen, J., Contal, F., Lupton, C., Tong, J., (2010).**
Bone-cement interfacial behaviour under mixed mode loading conditions.
J Mech Behav Biomed Mater 3, 392-398.
35. **Wei, Y., Hutchinson, J. W., (2008).**
Toughness of Ni/Al2O3 interfaces as dependent on micron-scale plasticity and atomistic-scale separation. Philosophical Magazine 88, 3841-3859.

Chapter

9

Interface micromechanics of transverse sections from retrieved cemented hip reconstructions: An experimental and finite element comparison

Submitted

Abstract

In finite element analysis (FEA) models of complete cemented hip reconstructions, it is crucial to include the mechanics of the cement-bone interface, although the interface modeling itself has often been overly simplified. Recently, however, a micromechanical morphology-based cohesive model has been generated to reproduce the mixed-mode behavior of the cement-bone interface. The goal of this study was to investigate whether this micromechanical cohesive model, of which the behavior was dependent on the gap thickness between the bone and cement, was directly applicable on a macro level to reproduce the micromotions of the cement-bone interface.

From transverse sections of retrieved cemented hip reconstructions, two FEA models were generated in which the cement-bone interface was modeled with cohesive elements having properties as reported in the literature. A torsional loading regime was applied and the micromotions at the cement-bone interface were monitored. A sensitivity analysis was performed to investigate whether the cohesive model could be adapted. Furthermore, two different gap interpretations were considered. From the complete transverse section, the global stiffness and stem translation were determined. All results were compared with experimental findings. The results showed that the original cohesive model resulted in a too compliant macromechanical response; the interfacial motions were too large and the global stiffness too small. However, when the cohesive model was adapted to also incorporate larger interface gaps, the match with the experimental response improved considerably.

Introduction

Stable fixation at the cement-bone interface is essential for the longevity of cemented components used in cemented total hip arthroplasty, since aseptic loosening at the cement-bone interface is the main reason for revision surgery[8]. The polymethymethacrylate (PMMA) bone cement used in cemented hip reconstructions is usually not osteoconductive and therefore physicochemical bonding between the bone and cement cannot be expected[7,25]. As a result, fixation between the bone and cement relies upon cement penetration into the bone[16] which results in a complex mechanical interlock between the two constituents[35]. However, this mechanical interlock can be considerably degraded after only one year in vivo service as a result of bone resorption[4,20,32]. This degradation weakens the cement-bone interface considerably relative to the direct post-operative situation[22] making the cement-bone interface one of the most compliant regions in cemented hip reconstructions[20].

In previous finite element analyses (FEA) of cemented hip reconstructions, the mechanical characteristics of the cement-bone interface have often been overly simplified. In several analyses the cement-bone interface was considered to act as (1) an infinitely stiff interface[10,13,29]; (2) a frictional contact layer[1,15]; or (3) as a layer of soft tissue elements which represented osteolysis around the cement mantle[5,33]. However, the validity of these three approaches to represent the interface mechanics is debatable. Experiments with laboratory prepared cement-bone interface specimens[19] showed a huge variation in stiffness and strength, which was not consistent with the three aforementioned assumptions.

A more appropriate approach to model the actual mechanical response of the cement-bone interface is through use of using cohesive zone models[17,24,27,37]. In these cohesive zone models a constitutive relationship has to be defined, which describes the interaction between the interface tractions and displacements in normal and shear direction[2]. Experiments in which cement-bone interface specimens are loaded in multiple directions could serve as an input for the cohesive zone models[21,38]. However, the huge variation in mechanical responses due to interfacial variations makes it very difficult to develop a comprehensive cohesive zone model using an experimental approach. This is because each experimental specimen can only be loaded to failure in one direction, and the cohesive zone model requires a full description of the mixed-model failiure response. An elegant alternative to study the mixed-mode failure response is the use of micromechanical FEA models[34]. Using this approach, a cohesive zone model has recently been developed in which the interfacial morphology was incorporated[36].

The cement-bone interface does not exhibit a homogenous morphology around the cement mantle[4], which subsequently results in local differences in mechanical characteristics. However, these local mechanical differences at the cement-bone interface have never been included in previous FEA studies. Moreover, previous macro FEA studies of cemented hip reconstructions which included cohesive zone models have never been directly validated with physical experiments. It has never been investigated whether a cohesive zone model of the cement-bone interface as determined on a micro level is directly applicable and yields appropriate results on a macro level.

The goal of this study was to investigate whether the micromechanical response of the cement-bone interface could be reproduced on a macro level by simulating macromechanical experiments[20]. A subsequent goal was to investigate how the micromechanical char-

acteristics of the cement-bone interface influence the mechanical properties on a macro level. From two transverse sections of cemented hip reconstructions with considerable mechanical differences[20] FEA models were generated. The FEA models consisted of bone, the cement-bone interface, which was modeled by cohesive elements, a cement mantle and a stem. Like in the experiments, a torsional loading regime was applied to the stem while monitoring the motions at the cement-bone interface. Using this approach, we asked the following three research questions: (1) Can the motions that occurred experimentally at the cement-bone interface be reproduced? (2) Is the previously derived micromechanical mixed-mode formulation of the cement-bone interface directly applicable on a macro level? and (3) How do the micromechanics of the cement-bone interface influence the macromechanical properties of the complete reconstruction?

Methods

Specimen preparation

Two postmortem retrieved transverse sections of cemented hip reconstructions were considered for this study. The specimens were selected based on their mechanical response as determined by Mann et al. (2010): donor 1 and 2 (Table 9.1) were the most torsionally compliant and the stiffest specimen analyzed, respectively[20]. The considered transverse sections had a thickness of 10 mm and were retrieved from two different donors at autopsy (Table 9.1). The two donors were provided by the Anatomical Gift Program at SUNY Upstate Medical University[20]. Donations were made between 1 and 2 days after death and frozen at -20°C prior to tissue harvest. Age, sex, number of years in service, cause of death, implant type and distance of the cut section from the calcar were documented. After mechanical testing of each transverse section, the surface roughness (Ra) of the stem was determined. By observing the porosity of the mid-mantle on the sectioned surface, it was assessed whether the cement was vacuum mixed. Planar x-rays of the cemented femur construct were made, after which it was assessed whether the cement-bone interface fixation loose or not loose (Table 9.1). A high-resolution image (pixel size: 5.7 µm) was made of each transverse section to document the morphology at the surface of the section (Figure 9.1; High Resolution Image).

	Donor 1	*Donor 2*
Age	85	67
Sex	Female	Female
Years in service	8	14
Cause of death	Bacterial endocarditis	Alzheimer's disease
Implant type	Versys cemented - Zimmer	Harris precoat - Zimmer
Distance from calcar (mm)	40	30
Stem roughness (Ra, µm)	2.5	1.3
Vacuum-mixed	Yes	Yes
Radiographically loose	Yes	No
	FEA model dimensions	
Number of elements	13,215	9,425
Number of nodes	7,271	5,234
Assumed friction coefficient at stem-cement interface	0.3	2.0

Table 9.1 *Donor information for the two investigated cemented implants.*

Experimental testing

The protocol used for experimental testing of the transverse sections has been documented before[20] and will therefore only be described in brief. The outer surface of each transverse section was fixed in a custom-machined block. Subsequently, the stem of each transverse section was loaded by a torsional loading regime. The torque limits were set to 0.22 Nm and 0.73 Nm in anteversion and retroversion, respectively, what represented torques that occur during normal walking[3]. During each loading cycle a digital image correlation (DIC) technique was used to quantify the motions at the cement-bone interface. The DIC sampling locations were placed at a distance of 0.25 mm from the interface to prevent errors in the DIC sampling at the material discontinuities. The angular rotation of the stem was also measured using DIC.

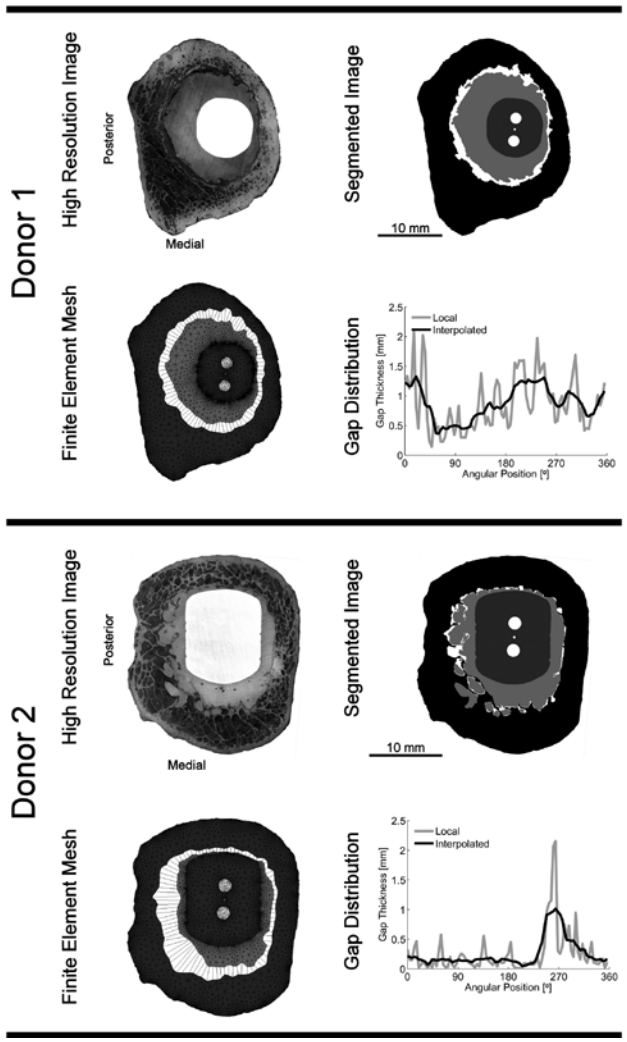

Figure 9.1 *FEA modeling procedure of the two donors. High Resolution Image: In order to capture the morphology at the surface of each transverse section, a high-resolution image with pixel size of 5.7 µm was taken. The images were re-orientated such that the left side and bottom were the posterior and medial side, respectively. Segmentation: The high resolution images were segmented into six parts: (I) bone, (II) cement-bone gaps, (III) cement, (IV) stem-cement gaps, (V) stem and (VI) screw holes. The small dot between Finite Element Mesh: From each segmented transverse section an FEA mesh was generated. The bone, cement and stem were meshed with 2D plain strain triangles, while the complete cement-bone interface was meshed with 2D quad cohesive elements. All elements had an assumed thickness of 10 mm. Gap distribution: For each cohesive element of the cement-bone interface the average local gap thickness was calculated. Subsequently, the interpolated gap thickness was calculated by taking the average local gap thickness of the four adjacent elements on both sides of the considered element. Note that the mean gap thickness is the same for both cases.*

FEA modeling

From each transverse slab a FEA model was generated. First, the high-resolution image was segmented into six parts: (I) bone, (II) cement-bone gaps, (III) cement, (IV) stem-cement gaps, (V) stem and (VI) screw holes (Figure 9.1; Segmentation). The screw holes in the stem indentify the locations where the torque was applied. Next, the contours of the segmented bone, cement and stem were determined by a Moore Neighborhood algorithm. A Douglas-Peucker line simplification was subsequently applied to reduce the number of line segments of each contour[6]. The simplified contours were subsequently meshed with 2D plain strain triangles with an assumed thickness of 10 mm (Figure 9.1; Finite Element Mesh). The cement-bone interface was meshed with 90 2D quad cohesive elements with a fixed 4 degrees of angular spacing. The cohesive elements captured the complete interdigitated zone of the cement-bone interface. The nodes of the cohesive elements matched the experimental DIC locations, which had an offset of 0.25 mm relative to the contact interface. The resulting models contained on average 11,700 elements and 6,500 nodes (Table 9.1). Contact between the stem and the cement was modeled using a double-sided node-to-surface contact algorithm (MSC.MARC 2007r1, MSC Software Corporation, Santa Ana, CA, USA). The assumed friction coefficient of the stem-cement interface of donor 1 was set to 0.3[1] and the precoated interface of donor 2 to 2.0.

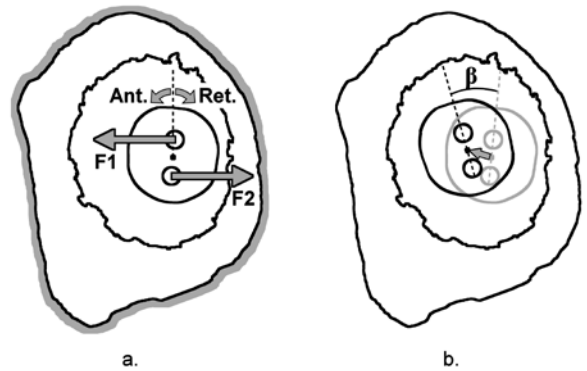

Figure 9.2 *a. The outside of the bone was fixed in all degrees of freedom. Two point loads, F1 and F2, were applied to the nodes in the middle of the two screw holes in order to rotate the stem in anteverion and retroversion.*
b. The center of the stem was not fixed. The resulting displacement of the center of the stem was monitored as well as the angular rotation, β.

Boundary conditions

To simulate the experimental setup, all the nodes on the outside of the bone were fixed in all degrees of freedom (Figure 9.2a). Furthermore, an incremental point load was applied to the nodes in the centroid of the two screw holes to reproduce the torque (Figure 9.2a). The resulting total torque was calculated for each increment. Like in the experiments, the FEA models were loaded up to 0.22 Nm and 0.73 Nm in anteversion and retroversion, respectively. Although in the experiment the stem was only meant to rotate[20], small planar movements were measured during the loading cycles. Hence, in the current study the center of the stem was not fixed and had therefore the freedom to translate (Figure 9.2b).

Material properties

The stem, cement and bone were modeled as isotropic linear elastic materials. The stem was given an assumed Young's modulus (E) and Poisson's ratio (v) of 210,000 MPa and 0.3, respectively[29]. Since the exact material properties of the cement were unknown, E and v were taken as 3000 MPa and 0.3, respectively[9,11,14]. In order to determine the material properties of the bone, the 2D FEA mesh of the bone was mapped back onto the high resolution image. Next, for each triangular element the average gray value was determined based on a 8-bit grayscale. The material properties of the bone were assumed to be linearly dependent on the average gray value[12]. The elements with the lowest and highest gray value were assigned a Young's modulus 0.1 and 20,000 MPa, respectively.

Cohesive modeling cement-bone interface

The mechanics of the cement-bone interface were modeled using a recently developed cohesive model[36]. This cohesive model determined the tractions [MPa] in normal and tangential direction (T_N and T_T) based on the displacements [mm] in normal and tangential direction (Δ_N and Δ_T) and the interface morphology. The interface morphology was expressed by the gap thickness, GT, which defined the average gap between the cement and the bone. The tractions in normal and tangential direction were defined as:

$$\begin{bmatrix} T_N \\ T_T \end{bmatrix} = 10^{A\cdot GT+B\frac{\Delta_N}{\Delta}+C} \cdot \begin{bmatrix} \Delta_N - D\cdot\frac{\Delta_T^2}{\Delta} \\ \Delta_T\left(1+D\cdot\frac{\Delta_N}{\Delta}\right) \end{bmatrix}$$

in which $\Delta = \sqrt{\Delta_N^2+\Delta_T^2}$. In this set of equations the term $10^{A\cdot GT+B\frac{\Delta_N}{\Delta}+C}$ was defined as the stiffness parallel to the loading direction. The parameter values 'A', 'B', 'C' and 'D' were estimated from a series of computational cement-bone interface models which were loaded to failure in multiple directions while monitoring the interfacial tractions[36]. In the ***original description*** of the cohesive model, the estimated parameters 'A' and 'C' were used to express the response in pure tension and were estimated to equal -6.369 and 2.439, respectively. Parameter 'B' was used to incorporate the effect of the loading angle and was estimated to equal -0.298. Finally, parameter 'D' was used to define tractions perpendicular to the loading direction and was estimated to equal 0.316.

Local gaps and interpolated gaps

In order to use the cohesive model properly, the gap thickness of each cohesive element in the cement-bone interface had to be determined. Therefore, each cohesive element was mapped back onto the segmented image, after which the average *local gap* thickness was calculated (Figure 9.1; Gap Distribution). However, the width of the cohesive elements as used in the current study was on average a factor 9 smaller (0.79 mm) relative to the average width of the models used to determine the cohesive model (7.54 mm)[36]. The local gap thickness was therefore interpolated such that the *interpolated gap* thickness of each element, IGT, was based on the average local gap thickness, LGT, of the four adjacent elements on both sides of the considered element: $IGT_N = \frac{1}{9}\sum_{i=-4}^{4} LGT_{N+i}$ (Figure 9.1; Gap Distribution). This resulted in a gap thickness for each element bases on an imaginary width similar to the models of Waanders et al (2011b). Note that the mean gap thickness over the whole cement-bone interface is the same for both the interpolated as the local gap description.

Sensitivity analysis

Limitation from the previously developed cohesive model was that it was based on four micromechanical FEA models with an average gap thickness of 0.106 mm (SD = 0.091 mm). When the gap thickness becomes considerably larger, like donor 1, the estimated stiffness might become too small relative to experimental findings[19,22] (Figure 9.3). Furthermore, the developed cohesive model resulted in a tensile stiffness of 141.3 MPa/mm when a gap thickness of 0 mm was considered. This was much lower than what has been found experimentally: 229.5 MPa/mm (SD = 144.7; Figure 9.3). Therefore, in the current study an additional sensitivity analysis was performed in which the parameters 'A' and 'C' were varied. Parameter 'A' was considered to be -6.369, -5.0, -4.0, -3.0 and -2.0, while for parameter 'C' the values 2.439 and 2.650 were taken, which corresponded to an initial tensile stiffness of 141.3 and 229.5 MPa/mm.

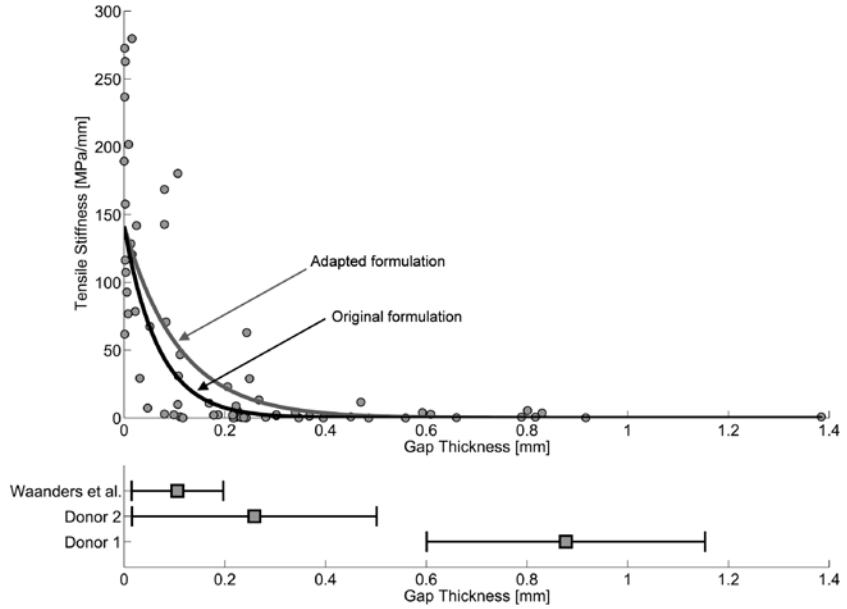

Figure 9.3 *The gray dots in the upper graph presents the relationship between tensile stiffness and gap thickness as previously been found experimentally[19,22]. The solid black line represents the tensile stiffness as a function of the gap thickness as determined by the developed cohesive model in pure tension (A = -6.369; C = 2.439; Δ_T=0; Δ/Δ_N=1)[36]. When a gap thickness of 0 mm was considered the cohesive model resulted in a tensile stiffness of 141.3 MPa/mm, which was much smaller than the average 229.5 MPa/mm (SD = 144.7) as found experimentally. The gray line represents the adapted formulation of the cement-bone interface (A = -4.000; C = 2.439). Note that the adapted formulation results in a higher tensile stiffness for larger gaps.*
The lower graph presents the variation in gap thickness over the two donors and the study of Waanders et al. (2011b) Note that the gap thickness of donor 1 is very large relative to the considered range in gap thickness of Waanders et al. (2011b).

Output measures

Throughout the whole simulation the interface micromotions at the cement-bone interface were calculated. The micromotions consisted of a normal and shear component and the total interface micromotions were calculated as the vector sum of both components. Cumulative frequency distributions of the micromotions were generated for each donor specimen.

In order to study the effect of the utilization of interpolated gaps relative to local gaps, the total interface micromotions were analyzed for both cases. Additionally, the interfacial work of separation, W_{sep}, at the cement-bone interface was determined. The work of separation was defined as the total amount of energy dissipated due to deformation of the interface: $W_{sep} = \int T_N(\Delta_N,\Delta_T)\partial\Delta_N + \int T_T(\Delta_N,\Delta_T)\partial\Delta_T$ [26]. The first term in this work of separation expression was the work done by the normal traction, while the second term was the work done by the tangential traction.

As mentioned in the previous section, the center of the stem was not fixed in the FEA simulations what subsequently could result in a ***stem translation*** (Figure 9.3b). Translations of the center of the stem in x- and y-direction were monitored and the total translation of the stem was calculated as the vector sum of both components. Finally, the ***global stiffness***, K_{glob}, [Nm/deg] of the whole FEA-model was calculated: $K_{glob} = \left|\frac{M_{ant} - M_{ret}}{\beta_{ant} - \beta_{ret}}\right|$, where M_{ant} and M_{ret} are the torques at full anteversion and retroversion, respectively, and β the corresponding angular rotations of the stem[20].

Quantification micromotions cement-bone interface

In order to quantify the spatial dispersion of micromotions at the cement-bone interface for each transverse section, circular statistics was used[39]. Using circular statistics, the mean angle of micromotions on the circumference of the cement-bone interface could be determined, as well as a measure for the concentration of the micromotions. A circular statistics approach was used because the nature of the angular position data results in a repeating pattern such that a 0° angular position is the same as a 360° angular position.

A so-called second-order analysis was performed in which the total micromotion, Δ, at each angular position was used as a weight factor for all the data points[18]. In this case, the mean angle with the concentration of largest micromotions, θ, and the measure of dispersion of the micromotions, *r*, were determinable as:

$$\theta = \tan^{-1}\frac{Y}{X} \text{ and } r = \sqrt{X^2 + Y^2}$$

Where X and Y were weighted using the total micromotion at angle a_i:

$$X = \frac{1}{n}\sum_{i=1}^{n}\Delta_i \cdot \cos(a_i) \text{ and } Y = \frac{1}{n}\sum_{i=1}^{n}\Delta_i \cdot \sin(a_i)$$

Note that *r* is dependent on the micromotions and should therefore be interpreted relative to the magnitude of the micromotions. Furthermore, it should be noticed that θ and *r* do not give an indication about the average magnitude of the micromotion at the cement-bone interface. Therefore the mean micromotion of all 90 data points, $\overline{\Delta}$, was determined additionally. In order to find the optimal cohesive description of the cement-bone interface based on the output of the sensitivity analysis, the relative difference between the FEA predicted and experimental value of *r* and $\overline{\Delta}$ were determined as $Dr = \frac{|r_{fea} - r_{exp}|}{r_{fea}}$ and $D\overline{\Delta} = \frac{|\overline{\Delta}_{fea} - \overline{\Delta}_{exp}|}{\overline{\Delta}_{fea}}$, respectively. Finally, a measure of the overall difference, D, was determined as:

$$D = \frac{1}{2}\sum_{i=1}^{2} Dr_i + D\overline{\Delta}_i + Dr_i D\overline{\Delta}_i$$

in which 'i' represents the donor.

Results

Original description cement-bone interface; interpolated gaps

Using the original description of the mixed-mode mechanical response of the cement-bone interface (A = -6.369; C = 2.439; *interpolated gaps*), the responses of donor 1 and 2 were both too compliant relative to the experiments (Figure 9.4a-b). Donor 1 could even not be loaded up to 0.73 Nm in retroversion and was therefore loaded with 0.4 Nm in this particular direction. Despite this torque reduction, donor 1 showed a considerable difference in the mean micromotion, $\overline{\Delta}$, relative to the experiment which was overestimated by a factor 10 ($\overline{\Delta}$= 0.90; Table 9.2). There was a considerable difference in angle with the concentration of largest micromotions, θ, between the experimental and FEA response for donor 1 (Figure 9.4a). However, for the experiment the value of *r* was relatively low indicating that θ could not be properly determined. Although the distribution of the micromotions of donor 2 was qualitatively reasonable, there was a phase shift visible in the difference in θ between the experiment and FEA simulation (Figure 9.4b).

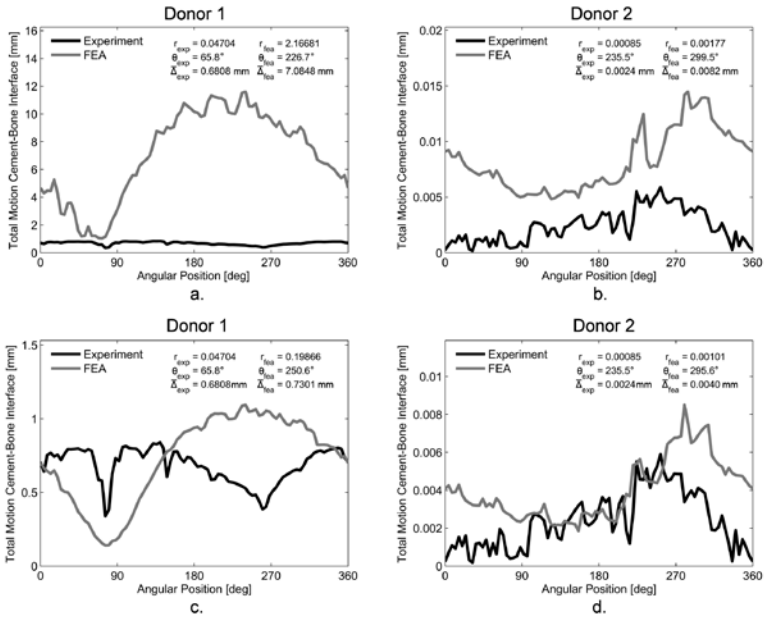

Figure 9.4 *Distributions of the total motion along the circumference of the cement-bone interface when interpolated gaps were considered.*

a. The response of donor 1 with the original description of the cement-bone interface (A = - 6.369; C = 2.439) resulted in a too compliant interface. Both the dispersion of the micromotions, r, as the mean micromotion, $\overline{\Delta}$, were overestimated. Note that for the experiment the value of r is relatively low and the significance of θ is debatable.

b. The response of donor 2 with the original description of the cement-bone interface (A = - 6.369; C = 2.439) was also too compliant, but not as severe as donor 1. The distribution of micromotions showed the same trend, although there was a phase shift in θ relative to the experiment.

c. For donor 1, the adapted description of the cement-bone interface (A = -4.000; C = 2.439) showed a much better fit relative to the experiment. Note that the value of r for the FEA simulation is relatively large, which means that its dispersion of micromotions along the interface is not as arbitrary as in the experiment.

d. Also for donor 2 showed the adapted description of the cement-bone interface (A = -4.000; C = 2.439) a better fit with the experiment. Also here, there was no considerable change in θ.

Original description; interpolated versus local gaps

When the stiffness of the cement-bone interface (A = -6.369; C = 2.439) was based on *local gaps*, the magnitude of the simulated micromotions improved relative to interpolated gaps; the average motion, $\overline{\Delta}$, of donor 1 and 2 both decreased from 7.0848 mm and 0.0082 mm (interpolated gaps; Figure 9.4a) to 1.1245 mm and 0.0038 mm (local gaps), respectively. A considerable difference in the work of separation, W_{sep}, was determined between the two gap interpretations when the transverse section was loaded in full retroversion. For donor 1, W_{sep} was determined as 39.9378 and 2.4198 MPa·mm for the interpolated and local gaps, respectively. For the interpolated and local gap interpretation of donor 2, W_{sep} was respectively determined as 0.0585 and 0.0264 MPa·mm (Figure 9.5a). Furthermore, the distribution of local work of separation was smooth when considering interpolated gaps and irregular when considering local gaps. This implies that when considering local gaps, the load transfer from the cement to the bone was concentrated on very specific locations.

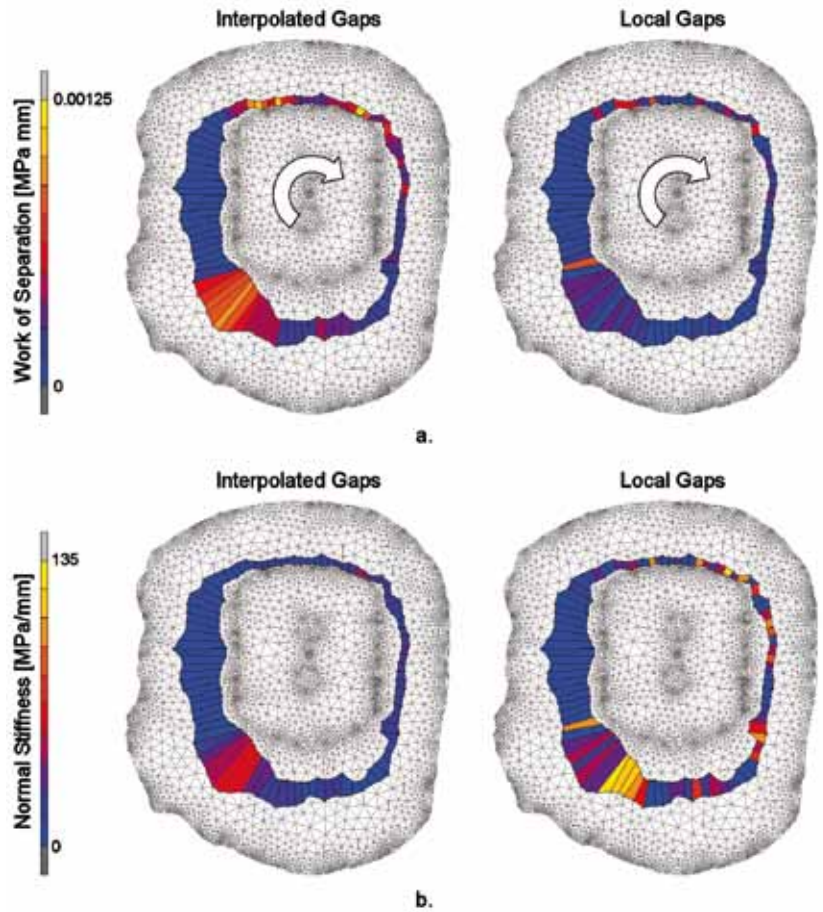

Figure 9.5 *a. When donor 2 was loaded to 0.73 Nm in retroversion, the simulation with interpolated gaps resulted in a smooth distribution of local work of separations at the cement-bone interface. When the stiffness of the cohesive elements was based on the local gaps, the distribution of local work of separations was irregular. Moreover, when local gaps were considered the total work of separation, W_{sep}, was more than half the work of separation with interpolated gaps; 0.0264 versus 0.0585 MPa·mm, respectively.*

b. The distribution of the normal stiffness differed considerably between the two gap interpretations. This was a result of the stiffness formulation, which was exponentially dependent on the gap thickness.

Sensitivity analysis

The sensitivity analysis showed that the angle with the concentration of largest micromotions, θ, hardly changed for both donor 1 (244.0° ± 9.2) and donor 2 (295.5° ± 3.7) (Table 9.2). Although Test 4 (A = -3.000; C = 2.439) showed the best responses for both donors in terms of Dr, the corresponding $D\overline{\Delta}$ for donor 1 was very large, subsequently making the overall difference, D, large too (Table 9.2). The parameters of Test 3 and 8 only differed in the value of C and they resulted in the smallest difference of all 10 tests. Since Test 3 was slightly better than Test 8, the parameters of Test 3 (A = -4.000; C = 2.439) were used for the adapted description of the cement-bone interface (Figure 9.3). The main difference between the original and the adapted description of the cement-bone interface for donor 1 was the reduction of *r* and $\overline{\Delta}$ (Figure 9.4c) and for donor 2 the reduction of $\overline{\Delta}$ (Figure 9.4d). Independent on the angular position at the cement-bone interface, the distribution of total micromotions of the adapted description matched the experimental findings much better than the original distribution (Figure 9.6).

	Parameter		θ [deg]		Dr [-]		$D\overline{\Delta}$ [-]		D [-]
Test	*A*	*C*	*Donor 1*	*Donor 2*	*Donor 1*	*Donor 2*	*Donor 1*	*Donor 2*	
1*	-6.369	2.439	226.7	299.5	0.98	0.52	0.90	0.71	2.18
2	-5.000	2.439	238.2	296.3	0.93	0.35	0.73	0.56	1.73
3	-4.000	2.439	250.6	295.6	0.76	0.16	0.07	0.40	0.75
4	-3.000	2.439	252.1	293.6	0.15	0.12	3.24	0.17	2.10
5	-2.000	2.439	248.7	290.4	6.42	0.67	22.00	0.20	85.32
6	-6.369	2.650	230.5	300.5	0.98	0.38	0.92	0.55	1.96
7	-5.000	2.650	244.1	298.4	0.90	0.12	0.60	0.31	1.25
8	-4.000	2.650	251.0	297.3	0.62	0.09	0.50	0.08	0.80
9	-3.000	2.650	251.6	293.7	0.86	0.52	5.88	0.26	6.35
10	-2.000	2.650	246.3	289.4	10.88	1.18	36.41	0.85	223.18
		MEAN	244.0	295.5	2.35	0.41	7.12	0.41	32.56
		STD	9.2	3.7	3.49	0.34	12.25	0.25	71.92

* For Test 1 donor 1 was loaded to 0.40 Nm in retroversion instead of 0.73 Nm.

Table 9.2 *Results of the sensitivity analysis in order to improve the mechanical response of the cementbone interface. In this table, θ was the mean angle with the concentration of largest micromotions. Dr and $D\overline{\Delta}$ were the relative difference between the FEA predicted and experimental value of r and $\overline{\Delta}$, respectively:*
Regarding parameter
C: the value 2.439 was determined by Waanders et al. (2011b) and the value 2.650 based on experimental findings (Figure 9.3). The best values for the parameters A and C were found to be -4.000 and 2.439, respectively (Test 3). Note that the magnitude of the differences does not indicate whether the response was under or overestimated. If the FEA response was overestimated, the values of Dr and $D\overline{\Delta}$ could never exceed 1.00. On the other hand, an underestimation of the FEA response could result in differences much larger than 1.0 (Test 5 and 10). Furthermore, not that for Test 5 and 10 the error $D\overline{\Delta}$ was much larger for donor 1 than for donor 2, indicating that the decrease of parameter A has more influence on the stiffness of large gaps.

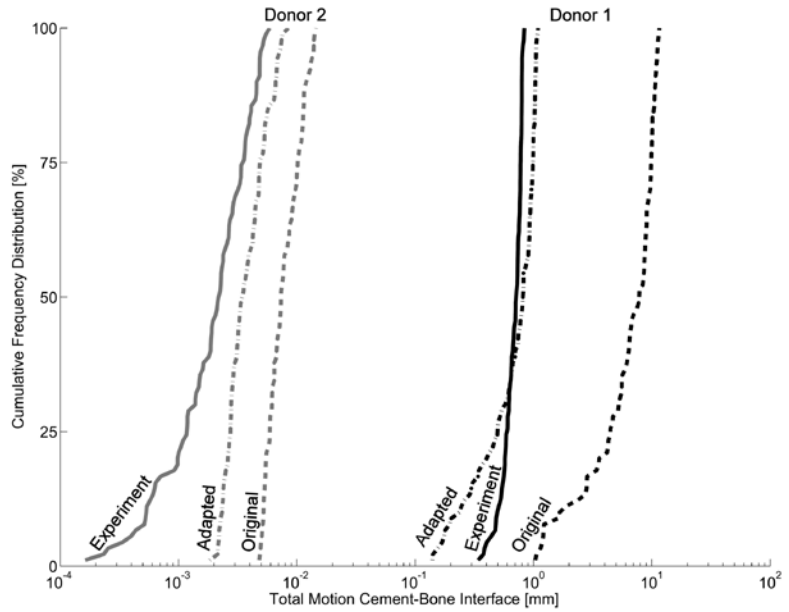

Figure 9.6 *Cumulative Frequency Distribution of the total motion at the cement-bone interface are shown for donor 1 (black) and donor 2 (gray). The experimental distribution is indicated by a solid line, the original FEA (A = -6.369; C = 2.439) by a dashed line and the adapted FEA (A = -4.000; C = 2.439) by the dash-dot line.*

Stem translation

The original description of the cement-bone interface (A = -6.369; C = 2.439) resulted in an excessive stem translation in donor 1 (3.757 mm; Figure 9.7a). The adapted description (A = -4.000; C = 2.439) reduced the stem translation considerably (0.331 mm), but was still larger than in the experiment (0.063 mm). For donor 2, the stem translation of the original cement-bone interface description (0.0017 mm) was three times the translation when considering the adapted description (0.0005 mm), but both much smaller than measured experimentally (0.0035 mm; Figure 9.7b). However, the experimentally measured stem translations almost equal the RMS error of the DIC system (0.0026 mm)[20] and can therefore be misleading.

Global stiffness

As a result of the large motions at the cement-bone interface of donor 1, the global stiffness with the original description of the cement-bone interface was extremely underestimated (12 Nm/deg) relative to the experiment (1374 Nm/deg; Figure 9.7c). After adaption of the interface, the global stiffness still did not reach the experimental global stiffness (265 Nm/deg). For donor 2 the predicted global stiffness fluctuated around the experimentally estimated stiffness (17916 Nm/deg); 13232 Nm/deg and 21380 Nm/deg for the original and adapted description, respectively (Figure 9.7d).

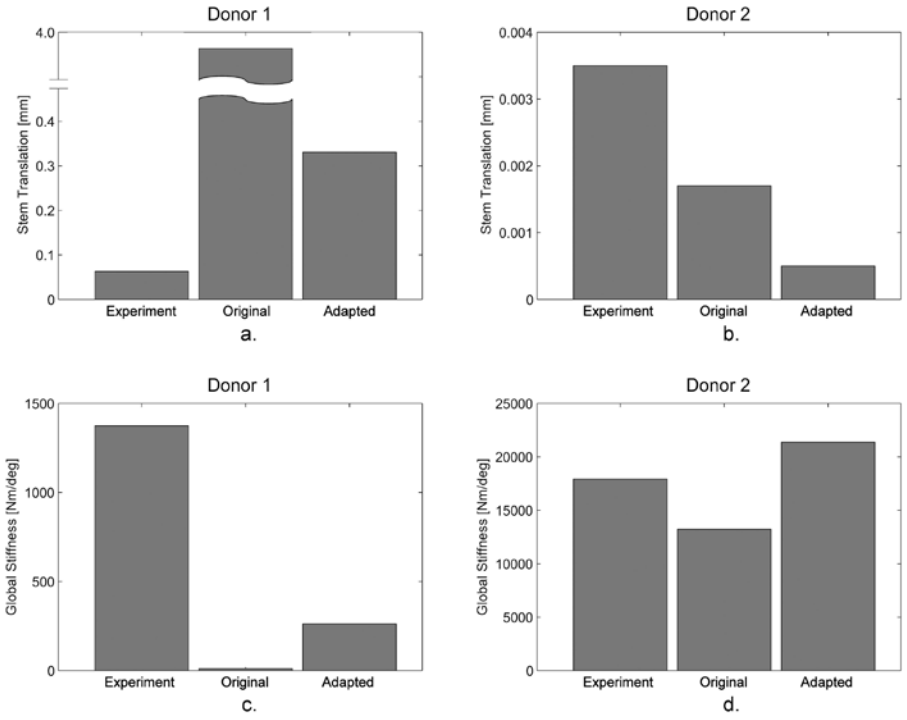

Figure 9.7

a. *The original description of the cement-bone interface (A = -6.369; C = 2.439) resulted in a excessive translation of the stem relative to the experiment. The translation of the stem of the adapted description (A = -4.000; C = 2.439) was much smaller, but still larger than in the experiment.*
b. *The translations of the stem were experimentally larger than in the FEA simulations. Also here, the adapted description of the cement-bone interface resulted in a smaller translation than the original description. However, the translation measured experimentally almost have the same magnitude as the RMS error of the DIC system (0.0026 mm) so the experimental translation could be misleading.*
c. *As a result of the large motions at the cement-bone interface of donor 1, the global stiffness with the original description of the cement-bone interface was extremely underestimated. The adapted description of the cement-bone interface did increase the global stiffness, but was still not in the range as determined experimentally.*
d. *The global stiffness of the original and the adapted description of donor 2 were under and over predicted, respectively.*

Description	*r* [-]		$\overline{\Delta}$ [mm]		D [-]
	Donor 1	Donor 2	Donor 1	Donor 2	
Experiment	0.04704	0.00085	0.6808	0.0024	-
Original: interpolated gaps	2.16681*	0.00177	7.0848*	0.0082	2.18
Original: local gaps	0.33676*	0.00096	1.1245*	0.0038	1.06
Adapted	0.19866	0.00101	0.7301	0.0040	0.75

* Loaded to 0.40 Nm in retroversion instead of 0.73 Nm.

Table 9.3 *Summary of the different descriptions. The original (A = -6.369; C = 2.439) with interpolated gaps resulted in a larger overall difference, D, than considering local gaps. The smallest overall difference, D, was obtained when considering the adapted description (A = -4.000; C = 2.439; interpolated gaps).*

Discussion

The main goal of the current study was to investigate whether the micromechanical response of the cement-bone interface could be reproduced on a macro level by the utilization of cohesive elements which were implemented in FEA models of transverse sections of postmortem retrieved cemented hip reconstructions. This study distinguishes itself from other FEA studies in which cohesive zone modeling was applied, because this is the first time the micromechanical based cohesive zone was directly compared to experiments on a macro level.

When the cohesive zone formulation as determined by Waanders et al. (2011b) was considered, the displacements at the cement-bone interface were too large for both donors (Table 9.3; Figure 9.4). Donor 1 could not even be loaded up to the required 0.73 Nm in retroversion because of excessive interfacial deformations. Furthermore, not the exact micromotion distribution was found along the circumference of the cement-bone interface, with donor 1 in particular (Figure 9.4).

With respect to the second research question in which we asked whether the cohesive formulation as determined by Waanders et al. (2011b) was directly applicable on a macro level we conclude that: (I) The determined cohesive formulation is too compliant, especially for gaps that are considerably larger than the gaps which were included in the original study[36], and (II) The way of gap implementation results in considerable mechanical differences.

Regarding (I) the underestimated stiffness for large gaps: The sensitivity analysis indicated that when the exponent which defined the reduction in stiffness as a result of an growing gap was decreased from -6.369 to -4.000, it matched the experiments considerably better (Table 9.3). Furthermore, we found that an increase of the stiffness considering a 0 mm gap thickness did not improve the response. This emphasizes that the imperfection of the original formulation lies in the range for large gaps. Additionally, the adapted cohesive model

(A = -4.000; C = 2.439) has been re-analyzed in the regression model used by Waanders et al. (2011b). It was found that the adapted cohesive model is still correlated to the mixed-mode responses as reported by Waanders et al. (2011b) ($r^2 = 0.79$; $p < 0.001$), hence it is still applicable for models with smaller gaps.

Regarding (II) the gap implementation: When the mechanics of the cement-bone interface were based on *local gaps*, rather than *interpolated gaps*, the motions at the cement-bone interface decreased considerably. This might be found remarkable since the average gap thickness was the same for both cases. However, the interpolated gap description was a general smoothing of the coarse local gap distribution, leveling out all the local minimum and maximum gaps. The small local peak gaps had a substantial effect on the magnitude of the element stiffness, since it was exponentially dependent on the gap thickness (Figure 9.5b). This can be seen in the work of separation, which was considerably smaller for the local gap description than for the interpolated description, although the local differences are much larger considering local gaps (Figure 9.5a). Moreover, note that a refined cohesive mesh (e.g. 180 elements instead of 90) will stiffen the interface even more considering local gaps. As a result of the stiffening of the interface, the response with a local gap description matched the experimental response better than considering a interpolated gap description. However, we believe it is better to work with the interpolated description, provided that the adapted description of the cement-bone interface is used (Table 9.3). In the micromechanical mixed-mode study on which the cohesive zone formulation was based[36], local interface phenomena were neither taken into account. Only the apparent response of the complete structure was considered, making the formulation mesh size dependent.

With respect to the third research question, the mechanics of the cement-bone interface had a considerable effect on the macromechanical properties of the whole transverse section. The adapted description of the cement-bone interface decreased the stem translations considerably and increased the global stiffness, relative to the original description. The stem translation of donor 1 was overestimated for both the original as the adapted description. This can be explained by the center of the stem which was not fixed in the FEA simulations. The overestimation of these stem translations in donor 1 might also have contributed to the underestimation of the corresponding global stiffness; the limited freedom of the stem in the experimental environment might not only have affected its translation, but also its rotation. However, the differences found in global stiffness might also be a result of the motions at the stem-cement interface, which have not been assessed.

The cement-bone interface was modeled by 90 cohesive elements with 4 degrees of angular spacing which captured the complete interdigitated region of the cement-bone interface. This was done in order to match the DIC measurement locations of the experiment. This modeling approach resulted in cohesive elements which all had approximately the same width, but differed considerably in height. This does not affect the mechanical response of the interface since cohesive elements are, in contrast to 'regular' elements, displacement driven and not strain driven. The element height is therefore a redundant parameter in the cohesive element description. This also makes cohesive element suitable to be implemented as zero thickness elements[28,31].

No failure of the cement-bone interface was considered, because the transverse torque limits that were applied were based on torques that occur during normal walking[3,20]. Since recent research has shown that no instant failure of the cement-bone interface occurs during walking[37], interfacial failure was not included.

Because of the small stem-cement motions that were found experimentally[20], the stem-cement interface was assumed to be not bonded, although other studies have assumed the opposite[40]. Since the friction coefficient at the stem-cement interface was unknown for both donors, they had to be assumed. Donor 1 was implanted with a Versys cemented stem which was assumed to have the same surface texture as a Charnley stem. Therefore, the friction coefficient was set to 0.3 for this donor[1]. Donor 2 was implanted with a Harris Precoat stem. During a post-experimental evaluation of the stem-cement interface no debonding was seen and, moreover, a considerable force was required to remove the stem from the cement mantle. However, since motions were found experimentally, the stem-cement interface was assumed to be not bonded and, therefore, was assigned a high friction coefficient of 2.0. To what extent the experimental reported motions could be assigned to material deformation is unknown. As mentioned before, misinterpretations at this interface could have affected the global stiffness of the transverse section.

There were several limitations that need to be acknowledged and addressed regarding this study. Firstly, only surface information of the specimens was available. The transverse sections were too large for micro-CT scanning devices in order to document the internal micro-morphology of the cement-bone interface. It was therefore assumed that the morphology of the cement-bone interface was homogenously distributed into the depth of the transverse section with the same gap distribution as visible on the outer surface. However, we realize that the 'hidden' internal morphology may weaken or stiffen the interface locally. This might also be an explanation why the micromotion distribution along the circumference of the cement-bone interface did not nicely match the experimental distribution. A second limitation was that only two transverse sections were considered in this study, because the FEA modeling of the transverse sections was a highly time consuming process. However, the two analyzed transverse sections were selected based on their mechanical characteristics, which were the two most extreme as analyzed by Mann et al. (2010). We realize that more analyzed specimens would have strengthened the current study. A third limitation was that only the gap thickness was considered as a morphological parameter which influenced the stiffness of the cement-bone interface. Previous studies have shown that also other factors contribute to the mechanical response, such as a normalized cement-bone contact index or the contact area between the bone and the cement[23,35].

From a clinical perspective, the results of the current study implicate that the currently developed cohesive zone models can be used for multiple applications in the research to cemented hip implants. Applications one could think of are patient specific FEA models to investigate causes of early failure of the cemented reconstruction or pre-clinical testing of newly developed orthopaedic implants. It has recently been reported that the behavior of the cement-bone interface affects cement-mantle failure[37]. Also the degeneration of the cement-bone interface can be analyzed, since this can ultimately lead to aseptic loosening of the implant[30]. However, a possible restriction could be that it is currently difficult to document the micro gap distribution at the cement-bone interface of a complete cemented hip reconstruction.

Based on the findings in the current study we conclude that with the current methods: (1) Only the mean micromotion and dispersion of micromotions as measured experimentally can be reproduced, but not the exact distribution of micromotions along the circumfer-

ence of the cement-bone interface. (2) The previously derived micromechanical mixed-mode formulation is not directly applicable on a macro level. We also found that (3) the micromechanics of the cement-bone interface have a considerable influence on the macromechanical properties of the complete reconstruction. We finally conclude that, although the current study contributes to a better understanding of interfacial micromechanics on a macro level, there is still lots to improve in terms of consistency of the cohesive formulation and modeling issues.

Acknowledgements

This work was funded by the National Institutes of Health (NIH AR42017).

References

1. **Afsharpoya, B., Barton, D. C., Fisher, J., Purbach, B., Wroblewski, M., Stewart, T. D., (2009).**
Cement mantle stress under retroversion torque at heel-strike. Med.Eng Phys. 31, 1323-1330.
2. **Alfano, G., Crisfield, M. A., (2001).**
Finite element interface models for the delamination analysis of laminated composites: Mechanical and computational issues.
International Journal for Numerical Methods in Engineering 50, 1701-1736.
3. **Bergmann, G., Graichen, F., Rohlmann, A., (1995).**
Is staircase walking a risk for the fixation of hip implants? J Biomech. 28, 535-553.
4. **Bishop, N. E., Schoenwald, M., Schultz, P., Puschel, K., Morlock, M. M., (2009).**
The condition of the cement mantle in femoral hip prosthesis implantations--a post mortem retrieval study. Hip.Int. 19, 87-95.
5. **Colombi, P., (2002).**
Fatigue analysis of cemented hip prosthesis: model definition and damage evolution algorithms. International Journal of Fatigue 24, 895-901.
6. **Douglas, D., Peucker, T., (1973).**
Algorithms for the reduction of the number of points required to represent a digitized line or its caricature. The Canadian Cartographer 10, 112-122.
7. **Goto, K., Kawanabe, K., Kowalski, R., Baker, D., Nakamura, T., (2010).**
Bonding ability evaluation of bone cement on the cortical surface of rabbit's tibia. J.Mater.Sci.Mater.Med. 21, 139-146.
8. **Hailer, N. P., Garellick, G., Karrholm, J., (2010).**
Uncemented and cemented primary total hip arthroplasty in the Swedish Hip Arthroplasty Register. Acta Orthop 81, 34-41.
9. **Harper, E. J., Bonfield, W., (2000).**
Tensile characteristics of ten commercial acrylic bone cements. J.Biomed.Mater.Res. 53, 605-616.
10. **Hung, J. P., Chen, J. H., Chiang, H. L., Wu, J. S., (2004).**
Computer simulation on fatigue behavior of cemented hip prostheses: a physiological model. Comput.Methods Programs Biomed. 76, 103-113.
11. **Janssen, D., Mann, K. A., Verdonschot, N., (2008).**
Micro-mechanical modeling of the cement-bone interface: The effect of friction, morphology and material properties on the micromechanical response. J.Biomech. 41, 3158-3163.
12. **Janssen, D., van, A. J., Scheerlinck, T., Verdonschot, N., (2009).**
Finite element analysis of the effect of cementing concepts on implant stability and cement fatigue failure. Acta Orthop. 80, 319-324.
13. **Katoozian, H., Davy, D. T., (2000).**
Effects of loading conditions and objective function on three-dimensional shape optimization of femoral components of hip endoprostheses. Med.Eng Phys. 22, 243-251.
14. **Lewis, G., (1997).**
Properties of acrylic bone cement: state of the art review. J.Biomed.Mater.Res. 38, 155-182.

15. **Lewis, G., Duggineni, R., (2006).**
Finite element analysis of a three-dimensional model of a proximal femur-cemented femoral THJR component construct: Influence of assigned interface conditions on strain energy density. Bio-Medical Materials and Engineering 16, 319-327.
16. **Lucksanasombool, P., Higgs, W. A., Ignat, M., Higgs, R. J., Swain, M. V., (2003).**
Comparison of failure characteristics of a range of cancellous bone-bone cement composites. J.Biomed.Mater.Res.A 64, 93-104.
17. **Mann, K. A., Damron, L. A., (2002).**
Predicting the failure response of cement-bone constructs using a non-linear fracture mechanics approach. J.Biomech.Eng 124, 462-470.
18. **Mann, K. A., Gupta, S., Race, A., Miller, M. A., Cleary, R. J., (2003).**
Application of circular statistics in the study of crack distribution around cemented femoral components. J Biomech. 36, 1231-1234.
19. **Mann, K. A., Miller, M. A., Cleary, R. J., Janssen, D., Verdonschot, N., (2008).**
Experimental micromechanics of the cement-bone interface. J.Orthop.Res. 26, 872-879.
20. **Mann, K. A., Miller, M. A., Verdonschot, N., Izant, T. H., Race, A., (2010).**
Functional interface micromechanics of 11 en-bloc retrieved cemented femoral hip replacements. Acta Orthop 81, 308-317.
21. **Mann, K. A., Mocarski, R., Damron, L. A., Allen, M. J., Ayers, D. C., (2001).**
Mixed-mode failure response of the cement-bone interface. J.Orthop.Res. 19, 1153-1161.
22. **Miller, M. A., Eberhardt, A. W., Cleary, R. J., Verdonschot, N., Mann, K. A., (2010).**
Micromechanics of postmortem-retrieved cement-bone interfaces. J.Orthop.Res. 28, 170-177.
23. **Miller, M. A., Race, A., Waanders, D., Cleary, R. J., Janssen, D., Verdonschot, N., Mann, K. A., (2011).**
Multi-axial loading micromechanics of the cement-bone interface in post-mortem retrievals and lab-prepared specimens.
Journal of the Mechanical Behavior of Biomedical Materials 4, 366-374.
24. **Moreo, P., Perez, M. A., Garcia-Amar, J. M., Doblare, M., (2006).**
Modelling the mixed-mode failure of cement-bone interfaces.
Engineering Fracture Mechanics 73, 1379-1395.
25. **Oonishi, H., Ohashi, H., Oonishi, H., Jr., Kim, S. C., (2008).**
THA with hydroxyapatite granules at cement-bone interface: 15- to 20-year results.
Clin.Orthop Relat Res 466, 373-379.
26. **Park, K., Paulino, G. H., Roesler, J. R., (2009).**
A unified potential-based cohesive model of mixed-mode fracture.
Journal of the Mechanics and Physics of Solids 57, 891-908.
27. **Perez, M. A., Palacios, J., (2010).**
Comparative finite element analysis of the debonding process in different concepts of cemented hip implants. Ann.Biomed Eng 38, 2093-2106.
28. **Salomonsson, K., Andersson, T., (2008).**
Modeling and parameter calibration of an adhesive layer at the meso level.
Mechanics of Materials 40, 48-65.
29. **Stolk, J., Janssen, D., Huiskes, R., Verdonschot, N., (2007).**
Finite element-based preclinical testing of cemented total hip implants.
Clin.Orthop.Relat Res. 456, 138-147.

30. **Sundfeldt, M., Carlsson, L. V., Johansson, C. B., Thomsen, P., Gretzer, C., (2006).**
Aseptic loosening, not only a question of wear: a review of different theories.
Acta Orthop 77, 177-197.
31. **Ural, A., (2009).**
Prediction of Colles' fracture load in human radius using cohesive finite element modeling. J Biomech. 42, 22-28.
32. **Venesmaa, P. K., Kroger, H. P., Jurvelin, J. S., Miettinen, H. J., Suomalainen, O. T., Alhava, E. M., (2003).**
Periprosthetic bone loss after cemented total hip arthroplasty: a prospective 5-year dual energy radiographic absorptiometry study of 15 patients. Acta Orthop Scand. 74, 31-36.
33. **Verdonschot, N., Huiskes, R., (1997).**
The effects of cement-stem debonding in THA on the long-term failure probability of cement. J.Biomech. 30, 795-802.
34. **Waanders, D., Janssen, D., Bertoldi, K., Mann, K. A., Verdonschot, N., (2011a).**
Mixed-mode loading of the cement-bone interface: a finite element study.
Comput.Methods Biomech.Biomed.Engin. 14, 145-155.
35. **Waanders, D., Janssen, D., Mann, K. A., Verdonschot, N., (2010).**
The mechanical effects of different levels of cement penetration at the cement-bone interface. J.Biomech. 43, 1167-1175.
36. **Waanders, D., Janssen, D., Mann, K. A., Verdonschot, N., (2011b).**
Morphology Based Cohesive Zone Modeling of the Cement-Bone Interface from Postmortem Retrievals. Journal of the Mechanical Behavior of Biomedical Materials. in press.
37. **Waanders, D., Janssen, D., Mann, K. A., Verdonschot, N., (2011c).**
The behavior of the micro-mechanical cement-bone interface affects the cement failure in total hip replacement. J Biomech. 44, 228-234.
38. **Wang, J. Y., Tozzi, G., Chen, J., Contal, F., Lupton, C., Tong, J., (2010).**
Bone-cement interfacial behaviour under mixed mode loading conditions.
J Mech Behav Biomed Mater 3, 392-398.
39. **Zar J.H., (2010).**
Biostatistical Analysis, Fifth Edition. Pearson Prentice Hall, Upper Saddle River, NJ.
40. **Zelle, J., Janssen, D., Peeters, S., Brouwer, C., Verdonschot, N., (2011).**
Mixed-mode failure strength of implant-cement interface specimens with varying surface roughness. J Biomech. 44, 780-783.

Discussion

Chapter

10

This thesis described a number of studies in which several fundamental mechanical aspects of the cement-bone interface were investigated by the utilization and combination of finite element analysis (FEA) and experimental techniques. The overall goal was to provide more insight into the micromechanical fatigue and static response of the cement-bone interface of cemented total hip arthroplasty (THA) reconstructions. Furthermore, it was investigated how this micromechanical behavior affects the mechanics of cemented THA reconstructions on a macro scale. The outcomes of these studies have contributed to a much better understanding of cement-bone interface mechanics, also with respect to its morphology, and its effect of the cemented reconstruction. However, one question that still remains is how this fundamental work relates to clinical reality. In this Discussion the acquired fundamental contributions of this thesis will be put into a more clinical context.

Main findings

It has to be noted that the fatigue studies as presented in the Chapters 2 and 3 do not represent the long term *in vivo* situation since the biological response to implantation has neither been incorporated in the laboratory experiments nor in the FEA simulations. In both the FEA simulations as the laboratory experiments it is unknown how the bone reacts to a repetitive load from a biological point of view. Moreover, in the FEA simulations, mechanical failure of the bone was not considered. This assumption was based on the fact that in the *in vitro* experiments hardly any bone damage was found. In addition, no constitutive model of fatigue failure of bone was available by then, although *in vitro* studies had gathered reasonable amounts of data regarding fatigue failure of trabecular bone[8,9]. To date, improvements have been made regarding this matter[22]. Despite these limitations, these studies have contributed to a much better understanding of the role of cement failure at the cement-bone interface. It has been shown that the role of cement cracking in the fatigue failure process of the cement-bone interface is much more important than cement creep. In the study as described in Chapter 2 it was found that cement cracking decreases the stiffness of the interface, but subsequently also increases the stresses in the periprosthetic bone (Chapter 3). Moreover, it has been shown that despite the finding that cement creep reduces crack formation up to 20%, it hardly influences the permanent plastic deformation of the cement-bone interface. Improvements of the cement toughness with respect to fatigue cracking could therefore help to prevent, or at least reduce, local failure of the cement-bone interface.

In studies in which postmortem cement-bone interfaces were analyzed, it was found that the strength and stiffness were considerably lower than in lab-prepared specimens[28,34]. It can, however, not simply be stated that this is solely caused by fatigue cracking of the cement. Although postmortem retrieved transverse sections of cemented hip reconstructions, like in Chapter 9, showed some severe cement cracks (Figure 1.2), the micro computed tomography (μCT) scans did neither reveal any loose cement particles nor cracks in the cement itself. The latter could, however, be invisible on the μCT scans as a result of closing of the cracks and the relative coarse resolution of the scans. It is therefore very likely that the substantial difference in mechanical properties between the postmortem and lab-prepared cement-bone interface specimens is a result of another factor, namely the considerable difference in interface morphology as a result of bone remodeling and subsequently resorption.

Many morphological parameters have been considered in this thesis in order to acquire a relationship between the morphology and the mechanical characteristics of the cement-bone interface, such as cement penetration depth, contact area between the cement and bone, or the amount of gaps between the two constituents. Based on all the analyses that we have performed, it can be concluded that the amount of cement-bone apposition is essential in order to achieve a strong and stiff interface. But how can a good apposition between the bone and cement be realized? And, moreover, how can it be maintained?

Based on the results as presented in this thesis, a good apposition between the bone and cement can be realized by maximizing the amount of contact between the two constituents. Intuitively, the solution would be to simply increase the amount of cement interdigitation; the more cement fills up the bone lacunar and trabecular spaces, the more contact will be achieved. Another way to approach this issue is by decreasing the gaps at the

cement-bone interface. Decreasing the gaps at the interface implicitly increases the amount of interfacial apposition. This can be verified by the inverse proportional relationship that was found between the quantity of contact and the size of interface gaps (Chapter 7). Whether the *depth* of cement interdigitation into the bone is also an important factor is debatable. While unidirectional tests of the cement-bone interface have shown that there is, at least to a certain level, a positive relationship between the cement interdigitation depth and the mechanical strength (Chapter 4), multidirectional tests did not find such a relationship (Chapter 5 and 6). A minimal penetration depth is of course necessary to achieve the required cement-bone apposition, but this morphological feature is not the one that drives the mechanical response of the interface. One might, however, be confused by a surgical technique developed in France, which has the intension to remove as much trabecular bone in the intramedullary canal as feasible in combination with the Charnley-Kerboull prosthesis[23,44]. The 'old-fashioned' cement interdigitation into trabecular bone with a large cement penetration depth is not possible with this technique, although a micro interlock between the endosteal bone surface and cement might be still possible by cement penetrating the canaliculi of the cortical bone. This technique, consequently, results in a cement-bone fixation that generally relies on a macro locking between the cement and bone. Despite the excellent survival rates of this technique[20,44], it cannot simply be stated that, based on the results of this thesis, the macro interlock can only be stable when a large contact area is pursued. This thesis solely concentrated on a fixation with trabecular and not with cortical bone. Moreover, it is more than likely that this French technique relies on a different locking mechanism, such as shape-closed mechanism between the cement mantle and endosteal bone. Except for this particular example, achieving a maximum infiltration of cement into the bone might be the key to generate a large contact area between the bone and cement what consequently results in a mechanically stable cement-bone interface.

Several laboratory studies have shown that the cement interdigitation into bone can be maximized, and thus the amount of cement-bone apposition, by using a low-viscosity cement[41,42,47]. Although this should result in a stable cement-bone interface and thus improved survival rates, clinical studies show the contrary; much poorer survival rates were reported when low-viscosity cement was used[15]. It was found that THA reconstructions using a low-viscosity cement resulted in inferior cement-bone interfaces[14,40]. Endosteal bleeding in the femoral canal could be an explanation of this phenomenon, since it has the capability to displace the cement before it has cured[17,27]. Low viscosity cement is obviously more sensitive to this phenomenon than regular viscocity cement what subsequently results in less apposition between the bone and cement and hence more and larger interfacial gaps[35]. But also the curing process of the cement itself results in interface gaps between the cement and bone due to cement shrinkage[40]. This is, however, not only an issue at the cement-bone interface, but also the integrity of the stem-cement interface is affected by gap formation as a result of cement shrinkage. One way to reduce the interfacial gaps and subsequently increase the contact area between bone and cement is by pressurization of the cement. However, one should keep in mind that excessive pressurization of the cement to obtain can lead to fat and bone-marrow embolism what can cause complications to the patient and can sometimes even be fatal[39,45].

Maintaining good apposition between the bone and cement is another issue. Directly after cement insertion, the periprosthetic bone at the cement-bone interface has to resist the hot temperatures due to the exothermal cement polymerization and the toxicity of the cement monomer. This could possibly result in direct bone necrosis, but it could also affect the bone's blood supply what subsequently induces bone necrosis. Moreover, it has neither been investigated how the periprosthetic bone of a cemented THA reconstruction reacts as a result of the non-natural mechanical loading at the micro level. It is more than likely that the cement mantle locally induces stress shielding due to the non-physiological loading of the bone. All these phenomena could possibly affect the cement-bone apposition and eventually result in aseptic loosening of the cement-bone interface. In the late eighties, however, a surgical technique was developed that stimulates cement-bone bonding in cemented THA[37]. This technique is better known as the 'interface bioactive bone cement' (IBBC) technique and it consists of smearing 2 to 5 grams of hydroxyapatite (HA) granules onto the endosteal bone surface just before cement insertion. The HA granules provide bioactivity on the surface of the cement mantle for prosthetic fixation. The clinical follow-up results indicate that IBBC results in low incidences of radiolucent lines and osteolysis after 15 to 20 years *in vivo* service[21,37,38,43]. Also animal studies show the presence HA at the cement-bone interface enhances cement-bone apposition[48]. HA granules at the cement-bone interface may therefore increase the longevity of the cemented reconstruction.

Proposed failure scenario in cemented THA

In the mid 90's, Verdonschot presented a flowchart which described the failure scenario of femoral cemented hip reconstructions from a mechanical point of view[49]. This flowchart showed that the most probable site for the initiation of cemented THA failure was the implant-cement interface (Figure 10.1). This was subsequently followed by failure of the cement mantle and the cement-bone interface what eventually resulted in gross loosening of the complete reconstruction. Verdonschot also stated that it was highly unlikely that the mechanical failure process was initiated at the cement-bone interface[49]. However, to date we know that this is not the case, since retrieval studies have shown that the cement-bone interface can be considerably degraded while the implant-cement interface still intact and very well bonded[2,29]. Moreover, even in the most ideal situation of a cemented reconstruction where no abrasive particles arise at the implant-cement interface, it is not excluded that the bone will remain unaffected. Besides bone resorption, however, the cement-bone interface also suffers from fatigue cracking of the cement (Chapter 2 and 3). As shown in the Chapters 6, 7 and 9, both bone resorption and fatigue cement cracking make the cement-bone interface considerably more compliant. This in turn promotes fatigue cracking of the cement-mantle (Chapter 8).

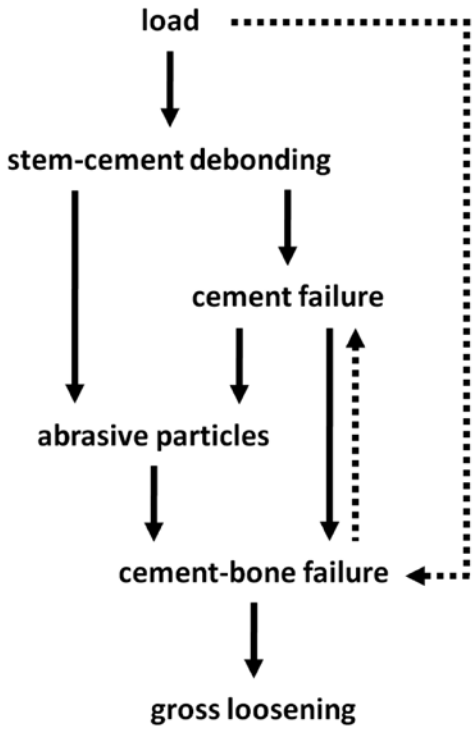

Figure 10.1 *The failure process of a femoral THA reconstruction as proposed by Verdonschot (solid lines) and modified based on the results as presented in this thesis (dashed lines). The cement-bone interface is the end-stage of the failure process. Degradation of the cement-bone interface is better known as aseptic loosening and can often be indentified on radiographs which can subsequently serve as an indication of the necessity of a revision surgery.*

The findings as presented in this thesis justify a modification of the flowchart of the failure scenario of cemented hip reconstructions as proposed by Verdonschot (Figure 10.1). Firstly, the flowchart has been modified such that also the load is able to induce cement-bone interface failure (Chapter 2 and 3). Secondly, it has now been indicated in the flowchart that cement-bone failure also promotes cement failure, as shown in Chapter 8. Notice that Verdonschot already found that cement failure provokes cement-bone failure. Hence, the cement failure and cement-bone failure appear to attenuate each other.

According to Verdonschot, failure of the cement-bone interface results in gross loosening of the cemented reconstruction and is the end-stage of the failure process. This phenomenon of a degraded cement-bone interface, often termed as aseptic loosening, is the most common complication causing failure of the cemented THA reconstruction. It should be noted, however, that other failure mechanisms, such as wear, severe cement cracks in the cement mantle (like in Figure 1.2 from Chapter 1), luxation of the joint or serious loosening of the implant-cement interface, can also lead to complications to the patient and subsequently make a revision surgery necessary. But also biological issues, such as infections, which have not been incorporated in the flowchart, can lead to serious problems to the patient. It should be accentuated that even despite a considerably degraded cement-bone interface patients may still perform very well, what excludes a revision surgery[2,29]. However, a mechanically stable cement-bone interface still remains one of the goals in order to improve the longevity of cemented THA components.

Improving the quality of cemented THA using computer simulations

The quality of THA can be defined as the longtime durability of the reconstruction without the occurrence of complications to the patient. Considering the clinical outcomes of THA replacements over the past decades, it can be concluded that the quality of THA has improved considerably. Overall, the durability has increased and many patients with a THA replacement do not have to undergo a revision surgery in their lifetime. Hence, one could conclude that the current quality of hip implants is sufficient. However, one should also focus on the future. The current trend shows that patients are undergoing THA at an increasingly younger age and the patient population is becoming more and more active. Furthermore, also the health care systems demand long-term solutions in order to reduce costs. Hence, it is obvious that the quality of THA has to improve in the near future.

In order to improve the quality of THA, inferior implants and bone cements, and surgical techniques with moderate clinical outcomes should be excluded from the orthopaedic market. Ideally, and perhaps even more importantly, inferior implants should be excluded prior to entering the orthopaedic market. This requires pre-clinical testing, since pre-clinical testing has the potential to estimate the durability, and thus the quality, of the THA reconstruction containing the newly developed implant. Within orthopaedic research, there is a general pre-clinical testing sequence of four different methods that could be used to assess the quality

of implants: FEA simulations, laboratory tests, animal experiments and clinical studies. Previous studies have shown that FEA can be a very valuable tool in the initial pre-clinical testing procedure, since it can provide information about the probability of failure of the THA reconstruction[6,46,56]. However, it should also be noted that the FEA simulations have to become more accurate to have a real predictive value.

The Chapters 5 to 7 of this thesis have also contributed to new insights and techniques which can be used for the pre-clinical testing phase of newly developed orthopaedic devices. In these three studies, FEA and bench-top experiments were used to investigate the mixed-mode response of lab-prepared and postmortem retrieved cement-bone interfaces. The primary goal was not to investigate whether the cement-bone interface properties differed between the tensile and shear direction, but the development of a cohesive zone model which describes the complete multi-axial mechanical behavior of the cement-bone interface. This cohesive zone model should subsequently be implementable in FEA models. The results show that we have been able to develop a cohesive zone model of the cement-bone interface of which the mechanical response is dependent on its micro morphology (Chapter 7). This model has subsequently successfully been tuned and validated in macro models of cemented THA reconstructions (Chapter 9). It has also been shown how the cohesive zone model of the cement-bone interface can be used in FEA simulations in order to demonstrate how the cement mantle failure depends on the cement-bone interface stiffness (Chapter 8) and how it influences the macro mechanics of cemented THA reconstructions (Chapter 9). These findings emphasize the need of including the mechanical characteristics of the cement-bone interface into FEA-based pre-clinical testing models of cemented hip reconstructions.

The strength of FEA relative to laboratory tests, animal experiments and clinical studies lies in the fact that FEA has the ability to determine the effect of isolating and modifying one single parameter, while keeping all the other parameters constant. Hence, in contrast to laboratory tests or animal experiments, which are often obscured by uncontrollable experimental adverse effects, there is absolute control in the FEA environment. This is also reflected in the Chapters 5 and 7, where a novel way was used to *in-silico* load the cement-bone interface to failure in multiple directions. As a result of this novel way, confounding issues that would occur in laboratory experiments were made redundant. When the specimens were loaded in pure tension, for instance, no out of axis movements and tractions occurred. However, in pure shear something remarkable occurred relative to previous studies in which cement-bone interface specimens were loaded in pure shear. The two FEA mixed-mode studies showed that the shear response of the cement-bone interface was almost infinitely strong in pure shear. However, previous physical experimental tests and, moreover, another study in this thesis (Chapter 4) have shown that this is not the case[30,31,34,51,53]. The discrepancy between these cases can be explained by the differences in applied boundary conditions. In laboratory experiments of cement-bone interfaces, the experimental setup is usually such that it allows some interfacial movements perpendicular to the loading direction. This means that, when loaded in pure shear, the interface deformation is able to follow the path of least resistance and therefore dilates. In the experiments performed by Yang et al.[53], the cement-bone interfaces were not allowed to dilate when loaded in pure shear. This resulted in shear strengths that were approximately 10 times larger than in other laboratory experiments. It has to be noted, however, that this thesis has shown that when loaded in pure shear dilation of the interface is hardly the case when the loading response remains elastic (Chapter 6). In the FEA mixed-mode studies, it was chosen not to allow any out of loading axis movements, since the responses of these mixed-mode simulations would be used as an input for a cohesive zone model. Because the utilized cohesive models have displacements as an input and tractions as an output, it was not practical to develop a cohesive model in which the out of loading axis displacements and tractions were unknown and zero, respectively.

The absolute control in FEA is probably also its main downside when applied in the pre-clinical testing phase. It implies that the accuracy of the modeled THA reconstruction strongly depends on the model's input data. Nowadays, there is unfortunately often a huge lack of relevant input data in the FEA models. An example are the bone material properties, which are frequently considered to be completely homogenous isotropic and its failure, either static or fatigue, is often not included. Other examples are the implant-cement and cement-bone interface behavior that are frequently not incorporated. Furthermore, biological responses of the periprosthetic tissue are often not included and the load cases which are applied are overly simplified and do not match the real *in vivo* loading. But most importantly, the variability between patient, but also surgeons, is ignored in generic FEA pre-clinical testing models. It should, however, be noted that for probabilistic modeling the complexity of an FEA model can be reduced to a minimum. When the global transitions of forces in a hip reconstruction have to be modeled, it is superfluous to include the biological and fatigue properties. When the lifetime of a reconstruction has to be modeled, or to reproduce a patient specific case, one has to include all the mechanical and biological phenomena that occur *in vivo*. Since most FEA simulations do not capture all these clinical phenomena, one of the most frequently cited arguments is that numerical output cannot be valid, because they simply cannot be validated.

Validation of computer simulations

The limited validation of several *in-silico* studies as described in this thesis is a major shortcoming (Chapter 4, 5 and 7). A direct quantitative validation was unfortunately not possible as a result of geometrical discrepancies. Although the FEA-models were based on a physiological morphology of the cement-bone interface, they were manipulated such that the achieved geometry did not match the physiological situation anymore. In the Chapters 5 and 7, for instance, the initial models were mirrored what resulted in a fully symmetric geometry. It is obvious that these models cannot be directly validated by experimental tests. However, these geometrical assumptions had to be made in order to reduce the complexity of the geometrical situation to a minimum and to generate an unaffected mechanical response. But also the FEA simulations of Chapter 4, where the mechanical effect of different cement penetration depths in a single bone morphology was investigated, are hard to execute with experimental testing. If one wants to know using experiments how the penetration depth affects the mechanical response one needs many cement-bone interface specimens. But for that case the bone morphology is still a confounding variable. As an alternative, the FEA simulations, which were impossible to validate directly, were qualitatively compared with previously obtained experimental findings. The studies from Chapter 3 and 8 are even a different story. Here, the FEA simulations were used as a sensitivity analysis where the material properties of the ce-

ment (Chapter 3) and cement-bone interface (Chapter 8) were modified such that it did not represent the physical situation anymore, making a direct validation impossible.

Over the years, considerable improvements have been made within orthopaedic research regarding FEA modeling. The newest scanning devices, like CT and Magnetic Resonance Imaging (MRI), allow us to generate FEA models that accurately match the physiological situation[3,10,54]. Thanks to musculoskeletal models, loads can be applied that would also occur in the in vivo situation[3,11,12]. Laboratory experiments have provided lots of data regarding, for instance, the anisotropic bone material properties[19,26,32], cement properties[13,24,50], and implant-cement[55] and cement-bone interface properties (this thesis). These data can be converted to numerical formulations, which can subsequently be implemented into FEA simulations. When similar laboratory studies are compared with FEA simulations in which the numerical formulations are implemented, the numerical formulations can be validated. A similar approach has been used in the Chapters 7 and 9 of this thesis.

Future perspective and concluding remarks

With respect to the cement-bone interface, this thesis has provided some unique insights, but it is obvious that there is still a lot to investigate. For instance: How does the bone adapt to the toxicity and the exothermal reaction of the cement directly after cement insertion? What is the biological response of the cement-bone interface as a result of fatigue loading? Will it in the future be possible to document the micro morphology of the cement-bone interface on a macro level, so an accurate representation of the mechanical characteristics around e.g. a complete cement mantle is feasible? Is it possible to develop a bone cement or a surgical treatment which counteracts the inflammation reaction due to wear particles or fatigue craking? But perhaps the most serious subject that we do not know, and what is critical in pre-clinical testing utilizing FEA, is the sequence of failure events and how these events influence and accelerate each other. We are able to simulate many failure mechanisms independent from each other, but to date we are not able to put all the failure mechanisms in a realistic time-frame due to a lack of comprehension of the integrated failure mechanics that occur at different areas within the reconstruction. This is very challenging, but also essential to know in order to provide an accurate prediction.

It can therefore be concluded that generating and maintaining a mechanically stable cement-bone interface is easier said than done. Although the *in vitro* and *in silico* studies from this thesis have shown which morphological factors are essential to achieve a stable cement-bone interface, the surgeon faces many challenges in order to optimize these factors. The surgeon is trained to obtain a suitable femoral canal preparation, avoiding over pressurization and the appropriate timing of cement and stem insertion. The skills of the surgeon are, however, also challenged by patient variables, such as excessive bleeding or limited endosteal trabecular bone for fixation, what is especially the case in revision arthroplasty. This makes the surgical procedure more challenging. It would therefore be very valuable if future research focuses on the possibilities to overcome all the aforementioned clinical issues or to come up with methods that aim to prevent complications. Possible research areas to focus on are for instance the optimization of the cement properties. Laboratory studies have indicated that for example the fatigue toughness of the cement can be improved by highly cross-linking[1] or by adding zirconia fibers to the cement[18]. The cement could also be equipped with self-healing capacities[5,25,52]. If micro cracks arise in the cement, then the cement has the ability to restore itself, what also improves its fatigue properties. When micro encapsulated paraffin based phase change material is incorporated into the cement, then the peak temperatures that arise during the curing process are reduced[7]. This might be beneficial for the initial cement-bone apposition, since this will reduce the chance of bone necrosis due to overheating. Another way to augment the cement-bone apposition is to have no or at least a reduction of cement shrinkage during the curing process. One could also think of adding a bioactive component to the cement that enhances bone apposition, such as a bone morphogenic protein (BMP). Several animal studies have shown bone formation at periprosthetic tissues utilizing BMPs[4,16,33,36]. In these studies, however, the BMPs were implemented as an allograft directly at the interface with the bone. It would be worth to investigate whether it is possible to add the BMP to the cement. When a crack arises in the cement, the BMP comes free what could give a boost of bone formation at the surrounding tissue. Besides the developments of new bone cement, the development of new surgical techniques is also one of the options to improve the longevity of the cement-bone interface. One could think of placing a mesh-like resorbable socket prior to cement insertion. This socket should be placed directly onto the endosteal bone of the reamed medulary canal and be equipped with for instance HA granules and BMPs, which are released when the socket is resorbed. As a result of the mesh texture of the socket, the cement is still able to penetrate the trabecular bone. Although this figment might sound impossible on beforehand, unique ideas, possibly combined with techniques that never have been applied in orthopaedics, will be the key to improve the longevity of the cement-bone interface in cemented THA.

It can be concluded that the quality of the cement-bone interface can theoretically be considerably improved. Thanks to the latest techniques, the actual physical construct can be tested and simulated more and more realistically, both in a pre-clinical state, but also following *in vivo* service. However, one should realize that the ultimate test is still taking place in the patient.

References

1. **Atwood, S. A., Van Citters, D. W., Patten, E. W., Furmanski, J., Ries, M. D., Pruitt, L. A., (2011).**
   Tradeoffs amongst fatigue, wear, and oxidation resistance of cross-linked ultra-high molecular weight polyethylene. J Mech Behav Biomed Mater 4, 1033-1045.
2. **Bishop, N. E., Schoenwald, M., Schultz, P., Puschel, K., Morlock, M. M., (2009).**
   The condition of the cement mantle in femoral hip prosthesis implantations--a post mortem retrieval study. Hip.Int. 19, 87-95.
3. **Blemker, S. S., Asakawa, D. S., Gold, G. E., Delp, S. L., (2007).**
   Image-based musculoskeletal modeling: applications, advances, and future opportunities. J Magn Reson.Imaging 25, 441-451.
4. **Bragdon, C. R., Doherty, A. M., Rubash, H. E., Jasty, M., Li, X. J., Seeherman, H., Harris, W. H., (2003).**
   The efficacy of BMP-2 to induce bone ingrowth in a total hip replacement model. Clin.Orthop Relat Res 50-61.
5. **Brochu, A. B., Craig, S. L., Reichert, W. M., (2011).**
   Self-healing biomaterials. J Biomed Mater Res A 96, 492-506.
6. **Chong, D. Y., Hansen, U. N., van, d., V, Verdonschot, N., Amis, A. A., (2011).**
   The influence of tibial component fixation techniques on resorption of supporting bone stock after total knee replacement. J Biomech. 44, 948-954.
7. **De, S. R., Ambrogi, V., Carfagna, C., Ambrosio, L., Nicolais, L., (2006).**
   Effect of microencapsulated phase change materials on the thermo-mechanical properties of poly(methyl-methacrylate) based biomaterials. J Mater Sci Mater Med. 17, 1219-1226.
8. **Dendorfer, S., Maier, H. J., Hammer, J., (2009).**
   Fatigue damage in cancellous bone: an experimental approach from continuum to micro scale. J.Mech.Behav.Biomed.Mater. 2, 113-119.
9. **Dendorfer, S., Maier, H. J., Taylor, D., Hammer, J., (2008).**
   Anisotropy of the fatigue behaviour of cancellous bone. J Biomech. 41, 636-641.
10. **Derikx, L. C., Vis, R., Meinders, T., Verdonschot, N., Tanck, E., (2011).**
    Implementation of asymmetric yielding in case-specific finite element models improves the prediction of femoral fractures. Comput.Methods Biomech.Biomed Engin. 14, 183-193.
11. **Dugailly, P. M., Sobczak, S., Moiseev, F., Sholukha, V., Salvia, P., Feipel, V., Rooze, M., Van Sint, J. S., (2011).**
    Musculoskeletal modeling of the suboccipital spine: kinematics analysis, muscle lengths, and muscle moment arms during axial rotation and flexion extension. Spine (Phila Pa 1976.) 36, E413-E422.
12. **Hansen, L., de, Z. M., Rasmussen, J., Andersen, T. B., Wong, C., Simonsen, E. B., (2006).**
    Anatomy and biomechanics of the back muscles in the lumbar spine with reference to biomechanical modeling. Spine (Phila Pa 1976.) 31, 1888-1899.
13. **Harper, E. J., Bonfield, W., (2000).**
    Tensile characteristics of ten commercial acrylic bone cements. J.Biomed.Mater.Res. 53, 605-616.
14. **Havelin, L. I., Espehaug, B., Vollset, S. E., Engesaeter, L. B., (1995).**
    The effect of the type of cement on early revision of Charnley total hip prostheses. A review of eight thousand five hundred and seventy-nine primary arthroplasties from the Norwegian Arthroplasty Register. J Bone Joint Surg.Am. 77, 1543-1550.

15. **Herberts, P., Malchau, H., (2000).**
    Long-term registration has improved the quality of hip replacement: a review of the Swedish THR Register comparing 160,000 cases. Acta Orthop Scand. 71, 111-121.
16. **Hoshino, M., Namikawa, T., Kato, M., Terai, H., Taguchi, S., Takaoka, K., (2007).**
    Repair of bone defects in revision hip arthroplasty by implantation of a new bone-inducing material comprised of recombinant human BMP-2, Beta-TCP powder, and a biodegradable polymer: an experimental study in dogs. J Orthop Res 25, 1042-1051.
17. **Juliusson, R., Flivik, G., Nilsson, J., Ryd, L., Onnerfalt, R., (1995).**
    Circulating blood diminishes cement penetration into cancellous bone. In vivo studies of 21 arthrotic femoral heads. Acta Orthop Scand. 66, 234-238.
18. **Kane, R. J., Yue, W., Mason, J. J., Roeder, R. K., (2010).**
    Improved fatigue life of acrylic bone cements reinforced with zirconia fibers. J Mech Behav Biomed Mater 3, 504-511.
19. **Keaveny, T. M., Yeh, O. C., (2002).**
    Architecture and trabecular bone - toward an improved understanding of the biomechanical effects of age, sex and osteoporosis. J Musculoskelet.Neuronal.Interact. 2, 205-208.
20. **Kerboull, L., Hamadouche, M., Courpied, J. P., Kerboull, M., (2004).**
    Long-term results of Charnley-Kerboull hip arthroplasty in patients younger than 50 years. Clin.Orthop Relat Res 112-118.
21. **Kim, S. C., Ohashi, H., Oonishi, H., Jr., Oonishi, H., (2007).**
    Histologic findings at 14 and 18 years after cemented total hip arthroplasty with interface bioactive bone cement technique. J Arthroplasty 22, 1067-1069.
22. **Kosmopoulos, V., Schizas, C., Keller, T. S., (2008).**
    Modeling the onset and propagation of trabecular bone microdamage during low-cycle fatigue. J Biomech. 41, 515-522.
23. **Langlais, F., Kerboull, M., Sedel, L., Ling, R. S., (2003).**
    The 'French paradox'. J Bone Joint Surg.Br. 85, 17-20.
24. **Lewis, G., (1997).**
    Properties of acrylic bone cement: state of the art review. J.Biomed.Mater.Res. 38, 155-182.
25. **Lewis, G., Wellborn, B., Jones, I. L., Biggs, P., (2009).**
    A room-temperature autonomically-healing PMMA bone cement: influence of composition on fatigue crack propagation rate. J Appl.Biomater.Biomech. 7, 90-96.
26. **Liu, X. S., Sajda, P., Saha, P. K., Wehrli, F. W., Bevill, G., Keaveny, T. M., Guo, X. E., (2008).**
    Complete volumetric decomposition of individual trabecular plates and rods and its morphological correlations with anisotropic elastic moduli in human trabecular bone. J Bone Miner.Res 23, 223-235.
27. **Majkowski, R. S., Bannister, G. C., Miles, A. W., (1994).**
    The effect of bleeding on the cement-bone interface. An experimental study. Clin.Orthop.Relat Res. 299, 293-297.

28. **Mann, K. A., Miller, M. A., Cleary, R. J., Janssen, D., Verdonschot, N., (2008).**
Experimental micromechanics of the cement-bone interface. J.Orthop.Res. 26, 872-879.
29. **Mann, K. A., Miller, M. A., Verdonschot, N., Izant, T. H., Race, A., (2010).**
Functional interface micromechanics of 11 en-bloc retrieved cemented femoral hip replacements. Acta Orthop 81, 308-317.
30. **Mann, K. A., Mocarski, R., Damron, L. A., Allen, M. J., Ayers, D. C., (2001).**
Mixed-mode failure response of the cement-bone interface. J.Orthop.Res. 19, 1153-1161.
31. **Mann, K. A., Werner, F. W., Ayers, D. C., (1999).**
Mechanical strength of the cement-bone interface is greater in shear than in tension. J.Biomech. 32, 1251-1254.
32. **McBride, S. H., Evans, S. F., Knothe Tate, M. L., (2011).**
Anisotropic mechanical properties of ovine femoral periosteum and the effects of cryopreservation. J Biomech. 44, 1954-1959.
33. **McGee, M. A., Findlay, D. M., Howie, D. W., Carbone, A., Ward, P., Stamenkov, R., Page, T. T., Bruce, W. J., Wildenauer, C. I., Toth, C., (2004).**
The use of OP-1 in femoral impaction grafting in a sheep model. J Orthop Res 22, 1008-1015.
34. **Miller, M. A., Eberhardt, A. W., Cleary, R. J., Verdonschot, N., Mann, K. A., (2010).**
Micromechanics of postmortem-retrieved cement-bone interfaces. J.Orthop.Res. 28, 170-177.
35. **Miller, M. A., Race, A., Gupta, S., Higham, P., Clarke, M. T., Mann, K. A., (2007).**
The role of cement viscosity on cement-bone apposition and strength: an in vitro model with medullary bleeding. J.Arthroplasty 22, 109-116.
36. **Murakami, N., Saito, N., Takahashi, J., Ota, H., Horiuchi, H., Nawata, M., Okada, T., Nozaki, K., Takaoka, K., (2003).**
Repair of a proximal femoral bone defect in dogs using a porous surfaced prosthesis in combination with recombinant BMP-2 and a synthetic polymer carrier. Biomaterials 24, 2153-2159.
37. **Oonishi, H., Kadoya, Y., Iwaki, H., Kin, N., (2001).**
Total hip arthroplasty with a modified cementing technique using hydroxyapatite granules. J Arthroplasty 16, 784-789.
38. **Oonishi, H., Ohashi, H., Oonishi, H., Jr., Kim, S. C., (2008).**
THA with hydroxyapatite granules at cement-bone interface: 15- to 20-year results. Clin.Orthop Relat Res 466, 373-379.
39. **Pitto, R. P., Koessler, M., Kuehle, J. W., (1999).**
Comparison of fixation of the femoral component without cement and fixation with use of a bone-vacuum cementing technique for the prevention of fat embolism during total hip arthroplasty. A prospective, randomized clinical trial. J.Bone Joint Surg.Am. 81, 831-843.
40. **Race, A., Miller, M. A., Clarke, M. T., Mann, K. A., Higham, P. A., (2006).**
The effect of low-viscosity cement on mantle morphology and femoral stem micromotion: a cadaver model with simulated blood flow. Acta Orthop. 77, 607-616.
41. **Reading, A. D., McCaskie, A. W., Barnes, M. R., Gregg, P. J., (2000).**
A comparison of 2 modern femoral cementing techniques: analysis by cement-bone interface pressure measurements, computerized image analysis, and static mechanical testing. J Arthroplasty 15, 479-487.
42. **Rey, R. M., Jr., Paiement, G. D., McGann, W. M., Jasty, M., Harrigan, T. P., Burke, D. W., Harris, W. H., (1987).**
A study of intrusion characteristics of low viscosity cement Simplex-P and Palacos cements in a bovine cancellous bone model. Clin.Orthop Relat Res 272-278.
43. **Sakai, T., Ohzono, K., Nishii, T., Miki, H., Takao, M., Sugano, N., (2010).**
Grafting with hydroxyapatite granules for defects of acetabular bone at revision total hip replacement: a minimum ten-year follow-up. J Bone Joint Surg.Br. 92, 1215-1221.
44. **Scheerlinck, T., Casteleyn, P. P., (2006).**
The design features of cemented femoral hip implants. J.Bone Joint Surg.Br. 88, 1409-1418.
45. **Sierra, R. J., Timperley, J. A., Gie, G. A., (2009).**
Contemporary cementing technique and mortality during and after exeter total hip arthroplasty. J.Arthroplasty 24, 325-332.
46. **Stolk, J., Janssen, D., Huiskes, R., Verdonschot, N., (2007).**
Finite element-based preclinical testing of cemented total hip implants. Clin.Orthop.Relat Res. 456, 138-147.
47. **Stone, J. J., Rand, J. A., Chiu, E. K., Grabowski, J. J., An, K. N., (1996).**
Cement viscosity affects the bone-cement interface in total hip arthroplasty. J.Orthop.Res. 14, 834-837.
48. **Timperley, A. J., Nusem, I., Wilson, K., Whitehouse, S. L., Buma, P., Crawford, R. W., (2010).**
A modified cementing technique using BoneSource to augment fixation of the acetabulum in a sheep model. Acta Orthop 81, 503-507.
49. **Verdonschot, N., (1995).**
Biomechanical failure scenarios for cemented total hip replacement, PhD thesis, Radboud University Nijmegen Medical Centre.
50. **Verdonschot, N., Huiskes, R., (1995).**
Dynamic creep behavior of acrylic bone cement. J.Biomed.Mater.Res. 29, 575-581.
51. **Wang, J. Y., Tozzi, G., Chen, J., Contal, F., Lupton, C., Tong, J., (2010).**
Bone-cement interfacial behaviour under mixed mode loading conditions. J Mech Behav Biomed Mater 3, 392-398.
52. **White, S. R., Sottos, N. R., Geubelle, P. H., Moore, J. S., Kessler, M. R., Sriram, S. R., Brown, E. N., Viswanathan, S., (2001).**
Autonomic healing of polymer composites. Nature 409, 794-797.
53. **Yang, D. T., Zhang, D., Arola, D., (2010).**
Fatigue of the bone/cement interface and loosening of total joint replacements. International Journal of Fatigue 32, 1639-1649.
54. **Yang, N. H., Canavan, P. K., Nayeb-Hashemi, H., Najafi, B., Vaziri, A., (2010).**
Protocol for constructing subject-specific biomechanical models of knee joint. Comput. Methods Biomech.Biomed Engin. 13, 589-603.
55. **Zelle, J., Janssen, D., Peeters, S., Brouwer, C., Verdonschot, N., (2011).**
Mixed-mode failure strength of implant-cement interface specimens with varying surface roughness. J Biomech. 44, 780-783.
56. **Zelle, J., Janssen, D., Van, E. J., De Waal, M. M., Verdonschot, N., (2011).**
Does high-flexion total knee arthroplasty promote early loosening of the femoral component? J Orthop Res 29, 976-983.

Summary

Chapter

11

Introduction *(Chapter 1)*

Cemented total hip artrhoplasty (THA) is one of the most successful and reliable surgical procedures in orthopaedics. However, 5 to 10% of all the cemented THA reconstructions fail within 10 years of *in vivo* service[4]. The most common reason for failure of cemented reconstructions is periprosthetic osteolysis at the cement-bone interface, usually termed as aseptic loosening. This interfacial degradation mechanically weakens the cement-bone interface relative to the direct post-operative situation. The true micromechanics of the cement-bone interface, both direct post-operative and after longer term, are not well understood. The main issue addressed in this thesis, therefore, is to investigate how the cement-bone interface behaves on a micro scale and how this micro behavior affects the macro mechanics of the cemented reconstruction. In order to achieve this goal, laboratory experiments and Finite Element Analysis (FEA) techniques were used to analyze the static and fatigue response of the interface.

In Chapter 1, backgrounds of cemented THA are presented and the current state of the our understanding of cement-bone interface mechanics are discussed. It is also discussed how FEA can contribute to a better understanding of the cement-bone interface.

Fatigue response *(Chapter 2 and 3)*

It has previously been indicated that in cemented THA fatigue failure of the cement mantle initiates at the cement-bone interface[20]. Previous research on the fatigue response of the cement-bone interface has primarily focused on documenting the overall structural response, such as permanent creep damage[2,8]. A more detailed fatigue study, however, showed that fatigue cracking arose at the contact interface and occurred mainly in the cement, leaving the bone almost unaffected[15]. It was also found that the creep damage deformation was presumed to manifest as gapping and sliding between the cement and the bone. However, it is also commonly known that, due to fatigue loading, the bone cement itself will creep, what subsequently effectively attenuates stress peaks and as a result decreases fatigue crack formation[22]. A limitation of these laboratory experiments is that the mechanism of failure cannot be attributed to a particular mechanical feature. However, FEA can be a useful tool to provide more insight into this failure mechanism.

In Chapter 2 the micromechanics of the cement-bone interface under tensile fatigue loading were investigated. In this particular study, laboratory-prepared cement-bone specimens were subjected to a tensile fatigue load, while the local displacements and crack growth on the specimen's surface were monitored. In order to explain the fatigue response, FEA models were created from micro-computed tomography (μCT) data of the same specimens. A new erosion procedure was developed to model the complex morphology at the contact interface between the bone and cement. As a result of this procedure, a gradual distributed load transfer was created and peak stress artifacts that occurred in previous studies were avoided[5,6]. The results showed that the FEA simulations were able to capture the general experimental

creep damage behavior of the cement-bone interface as occurred experimentally. Consistent with the experiments, the majority of the deformation took place at the contact interface and not in the bulk bone or cement. The FEA simulations could also, to a reasonable extent, predict fatigue crack patterns on the specimen's surface which were similar to experimental findings. Although the cracks that were found experimentally on the specimen's surface correlated moderately with FEA surface cracks, they did not correlate with the simulated crack volume fraction. This indicates that the specimen's surface information does not necessarily represent the behavior of the complete volume. Moreover, the FEA creep damage displacement showed a strong relationship with the cracked volume fraction, but no correlation with the surface cracks.

The aim of Chapter 3 was to gain more insight into the relative contributions of cement creep and cement fatigue crack formation on the micromechanical fatigue response of the cement-bone interface. Utilizing two of the micromechanical FEA models created in the previous chapter, we found that when the cement-bone interface is subjected to rather low stresses, the plastic interface displacement is mostly caused by cement creep. For higher loads, however, cement fatigue cracking was unambiguously the dominant factor. Although cement creep was able to reduce the crack formation in the cement up to 20%, it had virtually no additional effect on the plastic deformation of the interface, nor did it decrease the stress levels at the contact interface in het bone.

Effect of cement penetration *(Chapter 4)*

Since conventional bone cement, such as polymethylmethacrylate (PMMA), is not osteoconductive, physicochemical bonding between the bone and cement cannot be expected18. Therefore, the interface fixation relies on cement penetration into the bone lacunar and trabecular spaces, which provides an interlock between the two constituents[5,10]. While several studies found that the strength of the cement-bone interface is dependent on the depth of the cement penetration[11,13], others did not find such a relationship[12,16].

In this chapter it was investigated what the mechanical responses of the cement-bone interface were during tension and shear loading in case of different cement penetration depths. It was also investigated whether the mechanical responses could be related to the contact area between the bone and cement, since it was previously shown that this might also influence the mechanical response[14]. Simulations were performed with micromechanical FEA models of the cement-bone interface with one single bone morphology in order to eliminate specimen-to-specimen variability as a confounding factor. There were very strong correlations between the penetration depth and the interfacial tensile and shear strength. Also the contact area showed a very strong correlation with the strength in both tension and shear. Overall, the cement-bone interface was more than twice as strong in shear than in tension and slightly stiffer in tension than in shear.

Mixed-mode response *(Chapter 5 to 7)*

Since the cement-bone interface is a compliant interface[14,24], it is essential to include this interface in FEA models of cemented hip reconstructions. An elegant method to model the cement-bone interface within FEA models is the utilization of cohesive elements[17,19]. In these cohesive elements, a cohesive zone model has to be implemented, which describes the interfacial normal response, tangential response and a combination of the two; the mixed-mode response. A good understanding of the mixed-mode response is therefore essential. Experimentally, acquiring the mixed-mode response of cement-bone interface specimens remains challenging, because a specimen can only be loaded to failure once. One solution is to generate FEA models of the test specimens, which obviously can be loaded to failure in multiple directions in the virtual environment. The goal of the Chapters 5 to 7 was to investigate the micromechanical mixed-mode response of the cement-bone interface in detail. Additionally, it was investigated whether the mixed-mode response could be related to multiple morphological parameters and subsequently fit into a cohesive zone model.

In Chapter 5, FEA was used to look into the mixed-mode response of lab-prepared cement-bone interfaces. The simulations showed that when loaded in pure tension, the response was characterized by a linear elastic phase, followed by yielding and softening of the interface. A remarkable finding was the response in pure shear, which did not indicate interfacial failure despite considerable crack formation in the cement and bone. Moreover, a considerable normal compression was generated in pure shear to prevent dilation of the interface. The mechanical mixed-mode response could not be related to the cement interdigitation depth into the bone.

In Chapter 6, the mixed-mode response of laboratory prepared and postmortem retrieved cement-bone interfaces were investigated by *in vitro* experiments. This was only possible since the deformation to which the specimens were subjected remained in the elastic phase and was therefore non-destructive. The experiments showed that the compliance did not depend on the loading angle for both lab-prepared and postmortem interfaces. From a FEA modeling perspective, this suggests that the cement-bone interface could be numerically implemented as a compliant layer with the linear isotropic material properties. Like in Chapter 5, but in contrast with Chapter 4, the interfacial compliance did not correlate with the cement interdigitation depth. On the other hand, the interfacial compliance was inversely proportional to the amount of contact between the cement and the bone. Interestingly, for the same amount of interfacial contact, the postmortem specimens were much more compliant than the lab-prepared specimens.

In Chapter 7, the mixed-mode response of postmortem retrieved cement-bone interfaces was investigated by *in silico* experiments. Due to in vivo service, these specimens were considerably degraded in terms of bone resorption, what resulted in large gaps between the bone and cement. The mixed-mode responses were similar to those as reported in Chapter 5, although the strength and stiffness were considerably weaker, what can be explained by the interfacial degradation. This study distinguished itself from the one in Chapter 5, since the mixed-mode response was successfully converted to two cohesive zone models; a fully elastic model and one that included failure. Both cohesive zone models were depending on the gap thickness between the bone and cement, which will weaken the interface for larger gaps.

Cement mantle failure *(Chapter 8)*

In order to implement the mechanics of the cement-bone interface in FEA models of cemented hip reconstructions, the cement-bone interface has frequently been modeled as either an infinitely stiff interface[7,21], a uniform layer of soft tissue elements[3,23], a frictional contact layer[1,9] or by cohesive zone elements[17,19]. It is, however, unknown how different descriptions of the cement-bone interface affect other failure mechanisms in the cemented hip reconstruction. This chapter describes how the fatigue failure of the cement mantle is affected by considering four different models of the cement-bone interface: (I) infinitely stiff interface; (II) compliant interface with infinite strength; (III) mixed-mode failure response according to experimental findings; and (IV) mixed-mode failure response according to FEA models. Additionally, in order to include the effect of interfacial compliancy, each model was considered as a stiff or a compliant case. When a loading regime equal to walking was applied to the reconstruction, a considerable difference in crack formation in the cement mantle was found between an infinitely stiff and a compliant case, in which the former showed the least amount of cement cracks. Hence, the compliancy of the cement-bone interface has a considerable effect on the fatigue failure of the cement mantle. Furthermore, all stresses remained below the interface strength considering a load case equal to walking. This suggests that under these loading conditions the cement-bone interface could be modeled as an elastic layer without any softening properties. On the long term, it was found that fatigue failure resulted in a redistribution of stresses at the cement-bone interface as lower tension and shear tractions and the removal of peak stresses.

Micromechanics of transverse sections of cemented THA *(Chapter 9)*

In previous FEA studies of cemented hip reconstructions in which the cement-bone interface was modeled by cohesive elements, the cohesive zone model as derived on a micro level was directly implemented on a macro level[17,19]. The simulated interfacial responses were taken for granted, although it has never been verified whether this predicted behavior is still reliable. The main issue addressed in Chapter 9, therefore, was whether the mechanical response of the cement-bone interface as determined on a micro level could be reproduced on a macro level by the utilization of cohesive elements. From transverse sections of postmortem retrieved cemented hip reconstructions, FEA models were generated in which the cement-bone interface was modeled by cohesive elements. It appeared that the cohesive zone model, as derived in Chapter 7, was not fully applicable on a macro level. Firstly, the distribution of gaps along the circumference of the cement-bone interface needed to be interpolated in order to tackle the mesh dependent artifacts. Secondly, the cohesive model needed to be adapted such to make it applicable for larger interface gaps. After this adaption the mean magnitude of the micro motions along the circumference of the cement-bone interface could be reproduced. However, reproducing the exact distribution of micro motions remains challenging. The micromechanics of the cement-bone interface also appeared to have a considerable effect on the macromechanical properties of the complete reconstruction. This emphasizes that a correct description of the cement-bone interface is essential in the modeling of cemented hip reconstructions.

References

1. **Afsharpoya, B., Barton, D. C., Fisher, J., Purbach, B., Wroblewski, M., Stewart, T. D., (2009).**
   Cement mantle stress under retroversion torque at heel-strike. Med.Eng Phys. 31, 1323-1330.
2. **Arola, D., Stoffel, K. A., Yang, D. T., (2006).**
   Fatigue of the cement/bone interface: the surface texture of bone and loosening.
   J.Biomed.Mater.Res.B Appl.Biomater. 76, 287-297.
3. **Colombi, P., (2002).**
   Fatigue analysis of cemented hip prosthesis: model definition and damage evolution algorithms.
   International Journal of Fatigue 24, 895-901.
4. **Espehaug, B., Furnes, O., Engesaeter, L. B., Havelin, L. I., (2009).**
   18 years of results with cemented primary hip prostheses in the Norwegian Arthroplasty
   Register: concerns about some newer implants. Acta Orthop 80, 402-412.
5. **Janssen, D., Mann, K. A., Verdonschot, N., (2008).**
   Micro-mechanical modeling of the cement-bone interface: The effect of friction, morphology
   and material properties on the micromechanical response. J.Biomech. 41, 3158-3163.
6. **Janssen, D., Mann, K. A., Verdonschot, N., (2009).**
   Finite element simulation of cement-bone interface micromechanics: a comparison to
   experimental results. J.Orthop.Res. 27, 1312-1318.
7. **Jeffers, J. R., Browne, M., Lennon, A. B., Prendergast, P. J., Taylor, M., (2007).**
   Cement mantle fatigue failure in total hip replacement: experimental and computational testing.
   J Biomech. 40, 1525-1533.
8. **Kim, D. G., Miller, M. A., Mann, K. A., (2004).**
   Creep dominates tensile fatigue damage of the cement-bone interface. J.Orthop.Res. 22, 633-640.
9. **Lewis, G., Duggineni, R., (2006).**
   Finite element analysis of a three-dimensional model of a proximal femur-cemented femoral
   THJR component construct: Influence of assigned interface conditions on strain energy density.
   Bio-Medical Materials and Engineering 16, 319-327.
10. **Lucksanasombool, P., Higgs, W. A., Ignat, M., Higgs, R. J., Swain, M. V., (2003).**
    Comparison of failure characteristics of a range of cancellous bone-bone cement composites.
    J.Biomed.Mater.Res.A 64, 93-104.
11. **MacDonald, W., Swarts, E., Beaver, R., (1993).**
    Penetration and shear strength of cement-bone interfaces in vivo. Clin.Orthop.Relat Res. 286, 283-288.
12. **Majkowski, R. S., Bannister, G. C., Miles, A. W., (1994).**
    The effect of bleeding on the cement-bone interface. An experimental study.
    Clin.Orthop.Relat Res. 299, 293-297.
13. **Mann, K. A., Ayers, D. C., Werner, F. W., Nicoletta, R. J., Fortino, M. D., (1997).**
    Tensile strength of the cement-bone interface depends on the amount of bone interdigitated
    with PMMA cement. J.Biomech. 30, 339-346.
14. **Mann, K. A., Miller, M. A., Cleary, R. J., Janssen, D., Verdonschot, N., (2008).**
    Experimental micromechanics of the cement-bone interface. J.Orthop.Res. 26, 872-879.
15. **Mann, K. A., Miller, M. A., Race, A., Verdonschot, N., (2009).**
    Shear fatigue micromechanics of the cement-bone interface: An in vitro study using
    digital image correlation techniques. J.Orthop.Res. 27, 340-346.
16. **Miller, M. A., Race, A., Gupta, S., Higham, P., Clarke, M. T., Mann, K. A., (2007).**
    The role of cement viscosity on cement-bone apposition and strength: an in vitro model
    with medullary bleeding. J.Arthroplasty 22, 109-116.
17. **Moreo, P., Perez, M. A., Garcia-Amar, J. M., Doblare, M., (2006).**
    Modelling the mixed-mode failure of cement-bone interfaces.
    Engineering Fracture Mechanics 73, 1379-1395.
18. **Oonishi, H., Ohashi, H., Oonishi, H., Jr., Kim, S. C., (2008).**
    THA with hydroxyapatite granules at cement-bone interface: 15- to 20-year results.
    Clin.Orthop Relat Res 466, 373-379.
19. **Perez, M. A., Garcia-Aznar, J. M., Doblare, M., (2009).**
    Does increased bone-cement interface strength have negative consequences for bulk
    cement integrity? A finite element study. Ann.Biomed.Eng 37, 454-466.
20. **Race, A., Miller, M. A., Ayers, D. C., Mann, K. A., (2003).**
    Early cement damage around a femoral stem is concentrated at the cement/bone
    interface. J.Biomech. 36, 489-496.
21. **Stolk, J., Janssen, D., Huiskes, R., Verdonschot, N., (2007).**
    Finite element-based preclinical testing of cemented total hip implants.
    Clin.Orthop.Relat Res. 456, 138-147.
22. **Verdonschot, N., Huiskes, R., (1997).**
    Acrylic cement creeps but does not allow much subsidence of femoral stems.
    J.Bone Joint Surg.Br. 79, 665-669.
23. **Verdonschot, N., Huiskes, R., (1997).**
    The effects of cement-stem debonding in THA on the long-term failure probability of
    cement. J.Biomech. 30, 795-802.
24. **Wang, J. Y., Tozzi, G., Chen, J., Contal, F., Lupton, C., Tong, J., (2010).**
    Bone-cement interfacial behaviour under mixed mode loading conditions.
    J Mech Behav Biomed Mater 3, 392-398.

Chapter

12

Introductie *(Hoofdstuk 1)*

De gecementeerde totale heupvervanging (THV) is één van de meest succesvolle en betrouwbare chirurgische ingrepen binnen de orthopedie. Echter, 5 tot 10% van alle gecementeerde THV reconstructies faalt binnen 10 jaar na de operatie[4]. De meest voorkomende complicatie die het falen van een gecementeerde reconstructie veroorzaakt is osteolyse van het bot in het gebied rondom de cementmantel. Deze verbinding tussen het femur en de cementmantel wordt de 'cement-bot interface' genoemd. Het fenomeen van osteolyse rondom de cementmantel staat bekend als aseptische loslating. Deze degeneratie van de cement-bot interface verzwakt de interface in vergelijking met de situatie direct postoperatief. Het mechanische gedrag van de cement-bot interface op microniveau, van zowel de direct postoperatieve als de gedegenereerde situatie, is nog niet goed begrepen. Het belangrijkste doel van dit proefschrift is daarom te onderzoeken hoe de cement-bot interface zich gedraagt op microniveau en hoe dit microgedrag de macromechanica van de gecementeerde reconstructie beïnvloedt. Teneinde dit doel te bereiken zijn de statische en vermoeiingseigenschappen van de cement-bot interface onderzocht door middel van de Eindige Elementen Methode (EEM) en laboratorium experimenten.

In Hoofdstuk 1 worden zowel de achtergronden van gecementeerde THV gepresenteerd als de huidige stand van zaken wat betreft de mechanica van de cement-bot interface. Verder wordt besproken hoe de EEM kan bijdragen om een beter inzicht te krijgen in de mechanische eigenschappen van de cement-bot interface.

Vermoeiingsgedrag *(Hoofdstuk 2 en 3)*

In het verleden heeft onderzoek aangetoond dat het falen van de cementmantel van een gecementeerde THV begint in de cement-bot interface door scheurvorming ten gevolge van vermoeiing[20]. Eerdere onderzoeken naar het vermoeiingsgedrag van de cement-bot interface concentreerden zich meestal op de globale respons, zoals blijvende vervorming door kruip[2,8]. Een meer gedetailleerde vermoeiingsstudie, uitgevoerd door Mann et al.[15], heeft echter aangetoond dat scheurvorming door vermoeiing ontstaat bij de contactinterface en voornamelijk optreedt in het cement en niet in het bot. Een andere bevinding van Mann et al. was dat de deformatie door kruip in feite het gevolg was van het openen en glijden van het cement ten opzichte van het bot. Het is algemeen bekend dat door de vermoeiingsbelasting het botcement zelf gaat kruipen, wat vervolgens de spanningspieken in het cement verlaagd en dus scheurvorming door de vermoeiing verminderd[22]. Een beperking van deze laboratorium experimenten is dat het werkelijke faalmechanisme door een vermoeiingsbelasting niet kan worden toegeschreven aan één specifiek mechanisch fenomeen. De EEM is een handige methode om meer inzicht in dit faalmechanisme te verschaffen.

In Hoofdstuk 2 is de micromechanica van de cement-bot interface onderzocht bij

een vermoeiingsbelasting in trek. In deze studie zijn testmonsters van de cement-bot interface gemaakt (zogenoemde *lab-geprepareerde specimens*) en vervolgens onderworpen aan een vermoeiingsbelasting in trek. Tijdens het experiment werden lokale vervormingen en scheurgroei op het oppervlak van het specimen gevolgd. Om het vermoeiingsgedrag van de experimenten te verklaren werden EEM modellen gemaakt van dezelfde specimens als in het experiment door middel van micro-computed tomograhpy (µCT) scans. Teneinde de contactinterface tussen het bot en het cement goed te kunnen modelleren is er een erosie procedure ontwikkeld. Door deze erosie procedure wordt de belastingsoverdracht tussen cement en bot geleidelijke verdeeld en worden piekspanningen, die optraden in vorige studies, tevens ontweken[5,6]. De resultaten tonen aan dat de EEM simulaties in staat zijn het algemene kruip schade gedrag van de cement-bot interface, zoals die experimenteel optrad, te reproduceren. Net als bij de experimenten trad de meerderheid van de vervorming op bij de contactinterface en niet in het bot of cement zelf. De EEM simulaties konden de experimentele patronen van vermoeiingsscheuren op de oppervlakten van de speciemens voorspellen. De oppervlaktescheuren van de specimens toonden geen relatie met het gesimuleerde scheurvolume. Dit houdt in dat de informatie van het oppervalk van het specimen niet direct voor het complete volume geldt. De gesimuleerde kruip verplaatsingen toonden een sterke relatie met het gesimuleerde scheurvolume, maar niet met de oppervlakte scheuren.

Het doel van Hoofdstuk 3 is om meer inzicht te krijgen in de relatieve bijdragen van enerzijds kruip deformatie van het cement en anderzijds de formatie van vermoeiingsscheuren in het cement ten gevolge van de vermoeiingsrespons van de cement-bot interface. Twee van de EEM modellen uit Hoofdstuk 2 werden hiervoor gebruikt. Aangetoond werd dat wanneer de cement-bot interface wordt onderworpen aan een relatief lage belasting de plastische deformatie van de interface vooral wordt veroorzaakt door kruip van het cement. Echter, voor hogere belastingen zijn vermoeiingsscheuren zonder twijfel de dominante factor. Kruip van het cement was in staat om de scheurvorming in het cement tot 20% te reduceren. Daarentegen had kruip van het cement nagenoeg geen effect op de plastische deformatie van de interface, noch verlaagde het de spanningen op de contact interface in het bot.

Effect van cement penetratie *(Hoofdstuk 4)*

Aangezien conventioneel botcement, zoals Polymethylmethacrylaat (PMMA), geen botingroei stimuleert, kan er geen directe vaste verbinding tussen het bot en cement worden verwacht[18]. De fixatie van de interface hangt derhalve af van cement penetratie in het trabeculaire bot, wat resulteert in een interlock tussen de twee bestanddelen[5,10]. Verscheidene studies toonden een sterke relatie tussen de sterkte van de cement-bot interface en de diepte van cementpenetratie in het bot aan[11,13], doch andere vonden een dergelijke relatie niet[12,16].

In Hoofdstuk 4 is de mechanische respons van de cement-bot interface onderzocht bij een trek en schuif belasting bij een interface met verschillende cement penetratiedieptes. Er werd onderzocht of de mechanische respons kon worden gerelateerd aan zowel de penetratiediepte van het cement als aan het contactoppervlak tussen het bot en cement, dit omdat het contactoppervlak de mechanische respons kan beïnvloeden[14]. Simulaties met ver-

schillende penetratiedieptes van het cement werden uitgevoerd met EEM modellen van de cement-bot interface waarbij het bot een unieke morfologie had. Dit werd gedaan om een 'speciment-to-specimen' variabiliteit tegen te gaan. Zeer sterke correlaties werden gevonden tussen de penetratie diepte en de sterkte van de interface in trek en schuif. Ook het contact-toppervlak toonde een zeer sterke correlatie met de sterkte van de interface. De cement-bot interface was meer dan twee keer zo sterk in schuif dan in trek en maar nauwelijks stijver in trek dan in schuif.

Mixed-mode respons *(Hoofdstuk 5 tot en met 7)*

Omdat de cement-bot interface geen stijve, maar een *compliante* interface is[14,24], is het essentieel deze interface te modelleren in EEM studies van gecementeerde heup reconstructies. Een elegante manier deze cement-bot interface te modelleren in een EEM omgeving is door gebruik te maken van zogenaamde *cohesive-elementen*[17,19]. In deze cohesive-elementen dient een *cohesive-model* dat de cement-bot interfacerespons beschrijft geïmplementeerd te worden. Dit behelst de interfacerespons in normaal richting, tangentiële en een combinatie van de twee; de *mixed-mode respons*. Het is daarom essentieel een goed inzicht in de mixed-mode respons van de cement-bot interface te hebben. Experimenteel is het lastig de mixed-mode respons van de cement-bot interface te onderzoeken, omdat een specimen maar één maal tot falen kan worden belast. Het vervaardigen van EEM modellen van de cement-bot interface kan dat probleem oplossen. In de virtuele EEM omgeving kunnen de specimens namelijk meerdere malen in verschillende richtingen tot falen worden belast. Het doel van de Hoofstukken 5 tot en met 7 was om de micromechanische mixed-mode respons van de cement-bot interface in detail te onderzoeken. Daarnaast is onderzocht of de mixed-mode respons kon worden gerelateerd aan verschillende morfologische parameters van de cement-bot interface en vervolgens omgeschreven kon worden naar een cohesive-model.

In Hoofdstuk 5 werd de EEM gebruikt om de mixed-mode respons van lab-geprepareerde cement-bot interfaces te onderzoeken. De simulaties lieten zien dat wanneer de modellen in pure trek belasting, de interfacerespons werd gekarakteriseerd door een lineaire elastische fase, gevolgd door versteviging en plastische vervorming. Een bijzondere bevinding was de respons in pure schuif. Hier werd geen falen van de interface gevonden, ondanks aanzienlijke scheurvorming in het cement en bot. Bovendien werd er in pure schuif een aanmerkelijke compressie gegenereerd om openen van de interface tegen te gaan. De mixed-mode respons kon niet worden gerelateerd aan de penetratiediepte van het cement in het bot.

In Hoofdstuk 6 werden *in vitro* experimenten gebruikt om de mixed-mode respons van lab-geprepareerde en post-mortem cement-bot interfaces te onderzoeken. Dit was alleen mogelijk door de deformatie waaraan de specimens werden onderworpen in de elastische fase te houden en de deformatie was daarom niet destructief. De experimenten lieten zien dat de compliantie van de lab-geprepareerde en post-mortem specimens niet afhing van de belastingshoek. Dit zou betekenen dat de cement-bot interface in EEM modellen geïmplementeerd zou kunnen worden als een zachte laag met linear isotrope materiaal eigenschappen.

Net zoals in Hoofdstuk 5 werd er geen relatie gevonden tussen de compliantie van de interface en de penetratiediepte van het cement in het bot. Deze compliantie van de cement-bot interface bleek wel omgekeerd evenredig te zijn met de hoeveelheid contact tussen cement en bot. Interessant was dat voor dezelfde hoeveelheid contact tussen het bot en cement de post-mortem specimens veel compliánter waren dan de lab-geprepareerde specimens.

Gebruik makend van de gegevens van Hoofdstuk 6 werd in Hoofdstuk 7 de mixed-mode respons van post-mortem cement-bot interfaces onderzocht door middel van de EEM. Deze specimens waren aanzienlijk gedegradeerd door botresorptie. Dit resulteerde in relatief grote holtes tussen het bot en cement, ook wel *gaps* genaamd. De mixed-mode respons kwam overeen met die zoals beschreven in Hoofdstuk 5, alhoewel de sterkte en stijfheid aanzienlijk lager waren dan bij de lab-geprepareerde specimens. Dit hoofdstuk onderscheidt zich van Hoofdstuk 5, omdat de mixed-mode respons succesvol beschreven kon worden door twee cohesive-modellen; een volledig elastisch model en een model waarin ook het falen van de interface beschreven werd. Beide cohesie modellen konden worden gerelateerd aan de gapdikte tussen het bot en cement, waarin de gapdikte de interface zwakker maakt door grotere gaps.

Cementmantel falen (Hoofdstuk 8)

In EEM modellen van gecementeerde heup reconstructies is de cement-bot interface vaak gemodelleerd als enerzijds een oneindig stijve interface[7,21], een uniforme laag van zacht weefsel elementen[3,23], een contactlaag met wrijving[1,9], of met behulp van cohesive-elementen[17,19]. Het is onbekend hoe deze verschillende beschrijvingen van de cement-bot interface andere faalmechanismes in de gecementeerde heup reconstructie beïnvloeden. In Hoofdstuk 8 werd beschreven hoe het falen van de cementmantel ten gevolge van een vermoeiingsbelasting wordt beïnvloed door vier verschillende mechanische modellen van de cement-bot interface: (I) een oneindig stijve interface; (II) een compliante interface met een oneindige sterkte; (III) een mixed-mode faal response volgens experimentele bevindingen; en (IV) een mixed-mode faal response volgens EEM modellen. Om het effect van de stijfheid van de interface te bestuderen werd elk model bovendien beschouwd als stijf en compliant. Wanneer een loopbelasting op de reconstructie werd gesimuleerd, werd het grootste verschil in scheurvorming in de cementmantel gevonden bij oneindige stijve ten opzichte van een compliante interface. Hierbij ontstonden in het oneindig stijve model de minste scheuren. Hieruit blijkt dat de compliantie van de cement-bot interface een aanzienlijk effect heeft op het falen van de cementmantel ten gevolge van een vermoeiingsbelasting. Verder werd aangetoond dat bij een externe belasting die optreedt tijdens het lopen van een patiënt alle spanningen onder de sterkte van de interface bleven. Dit houdt in dat onder deze condities de cement-bot interface gemodelleerd kan worden als een elastische laag zonder faaleigenschappen. Een laatste bevinding was dat op de lange termijn het falen ten gevolge van vermoeiing resulteerde in een herverdeling van spanningen op de cement-bot interface in termen van lagere trek- en schuifspanningen en minder piekspanningen.

Micromechanica of dwarsdoorsneden van gecementeerde THV
(Hoofdstuk 9)

In voorgaande EEM studies van gecementeerde heup reconstructies waarin de cement-bot interface werd gemodelleerd door cohesive-elementen werd het cohesive-model, zoals afgeleid op een micro niveau, direct geïmplementeerd op een macro niveau[17,19]. In dat geval werd de gesimuleerde interfacerespons voor lief genomen en werd niet geverifieerd of deze respons nog wel betrouwbaar was. Het belangrijkste doel van Hoofdstuk 8 was daarom te onderzoeken of de mechanische respons van de cement-bot interface, zoals bepaald op een microniveau, ook direct op een macroniveau geïmplementeerd kan worden door middel van cohesive-elementen. EEM modellen werden gegenereerd van dwarsdoorsneden van post-mortem gecementeerde heupreconstructies, waarin de cement-bot interface werd gemodelleerd met cohesive-elementen. Aangetoond werd dat het cohesive-model zoals afgeleid in Hoofdstuk 7 niet direct toepasbaar was op macroniveau. Ten eerste moest de verdeling van gaps rondom de omtrek van de cement-bot interface geïnterpoleerd worden om mesh-afhankelijke artefacten te vermijden, ten tweede moest het cohesive-model zodanig aangepast worden dat het ook toepasbaar was voor relatief grote gaps. Na deze aanpassing kon de gemiddelde microbeweging rondom de omtrek van de cement-bot interface gereproduceerd worden. Het reproduceren van de exacte verdeling van microbewegingen was lastig. De micromechanica van de cement-bot interface bleek ook een aanzienlijk effect te hebben op de mechanische eigenschappen van de totale heupreconstructie. Dit benadrukt dat een correcte beschrijving van de cement-bot interface essentieel is in de modellering van gecementeerde heupreconstructies.

References

1. **Afsharpoya, B., Barton, D. C., Fisher, J., Purbach, B., Wroblewski, M., Stewart, T. D., (2009).** Cement mantle stress under retroversion torque at heel-strike. Med.Eng Phys. 31, 1323-1330.
2. **Arola, D., Stoffel, K. A., Yang, D. T., (2006).** Fatigue of the cement/bone interface: the surface texture of bone and loosening. J.Biomed.Mater.Res.B Appl.Biomater. 76, 287-297.
3. **Colombi, P., (2002).** Fatigue analysis of cemented hip prosthesis: model definition and damage evolution algorithms. International Journal of Fatigue 24, 895-901.
4. **Espehaug, B., Furnes, O., Engesaeter, L. B., Havelin, L. I., (2009).** 18 years of results with cemented primary hip prostheses in the Norwegian Arthroplasty Register: concerns about some newer implants. Acta Orthop 80, 402-412.
5. **Janssen, D., Mann, K. A., Verdonschot, N., (2008).** Micro-mechanical modeling of the cement-bone interface: The effect of friction, morphology and material properties on the micromechanical response. J.Biomech. 41, 3158-3163.
6. **Janssen, D., Mann, K. A., Verdonschot, N., (2009).** Finite element simulation of cement-bone interface micromechanics: a comparison to experimental results. J.Orthop.Res. 27, 1312-1318.
7. **Jeffers, J. R., Browne, M., Lennon, A. B., Prendergast, P. J., Taylor, M., (2007).** Cement mantle fatigue failure in total hip replacement: experimental and computational testing. J Biomech. 40, 1525-1533.
8. **Kim, D. G., Miller, M. A., Mann, K. A., (2004).** Creep dominates tensile fatigue damage of the cement-bone interface. J.Orthop.Res. 22, 633-640.
9. **Lewis, G., Duggineni, R., (2006).** Finite element analysis of a three-dimensional model of a proximal femur-cemented femoral THJR component construct: Influence of assigned interface conditions on strain energy density. Bio-Medical Materials and Engineering 16, 319-327.
10. **Lucksanasombool, P., Higgs, W. A., Ignat, M., Higgs, R. J., Swain, M. V., (2003).** Comparison of failure characteristics of a range of cancellous bone-bone cement composites. J.Biomed.Mater.Res.A 64, 93-104.
11. **MacDonald, W., Swarts, E., Beaver, R., (1993).** Penetration and shear strength of cement-bone interfaces in vivo. Clin.Orthop.Relat Res. 286, 283-288.
12. **Majkowski, R. S., Bannister, G. C., Miles, A. W., (1994).** The effect of bleeding on the cement-bone interface. An experimental study. Clin.Orthop.Relat Res. 299, 293-297.
13. **Mann, K. A., Ayers, D. C., Werner, F. W., Nicoletta, R. J., Fortino, M. D., (1997).** Tensile strength of the cement-bone interface depends on the amount of bone interdigitated with PMMA cement. J.Biomech. 30, 339-346.
14. **Mann, K. A., Miller, M. A., Cleary, R. J., Janssen, D., Verdonschot, N., (2008).** Experimental micromechanics of the cement-bone interface. J.Orthop.Res. 26, 872-879.
15. **Mann, K. A., Miller, M. A., Race, A., Verdonschot, N., (2009).** Shear fatigue micromechanics of the cement-bone interface: An in vitro study using digital image correlation techniques. J.Orthop.Res. 27, 340-346.

16. **Miller, M. A., Race, A., Gupta, S., Higham, P., Clarke, M. T., Mann, K. A., (2007).**
The role of cement viscosity on cement-bone apposition and strength: an in vitro model with medullary bleeding. J.Arthroplasty 22, 109-116.
17. **Moreo, P., Perez, M. A., Garcia-Amar, J. M., Doblare, M., (2006).**
Modelling the mixed-mode failure of cement-bone interfaces.
Engineering Fracture Mechanics 73, 1379-1395.
18. **Oonishi, H., Ohashi, H., Oonishi, H., Jr., Kim, S. C., (2008).**
THA with hydroxyapatite granules at cement-bone interface: 15- to 20-year results.
Clin.Orthop Relat Res 466, 373-379.
19. **Perez, M. A., Garcia-Aznar, J. M., Doblare, M., (2009).**
Does increased bone-cement interface strength have negative consequences for bulk cement integrity? A finite element study. Ann.Biomed.Eng 37, 454-466.
20. **Race, A., Miller, M. A., Ayers, D. C., Mann, K. A., (2003).**
Early cement damage around a femoral stem is concentrated at the cement/bone interface. J.Biomech. 36, 489-496.
21. **Stolk, J., Janssen, D., Huiskes, R., Verdonschot, N., (2007).**
Finite element-based preclinical testing of cemented total hip implants.
Clin.Orthop.Relat Res. 456, 138-147.
22. **Verdonschot, N., Huiskes, R., (1997).**
Acrylic cement creeps but does not allow much subsidence of femoral stems.
J.Bone Joint Surg.Br. 79, 665-669.
23. **Verdonschot, N., Huiskes, R., (1997).**
The effects of cement-stem debonding in THA on the long-term failure probability of cement. J.Biomech. 30, 795-802.
24. **Wang, J. Y., Tozzi, G., Chen, J., Contal, F., Lupton, C., Tong, J., (2010).**
Bone-cement interfacial behaviour under mixed mode loading conditions.
J Mech Behav Biomed Mater 3, 392-398.

Dankwoord

Zo… Boekje is klaar… Maar nu nog het dankwoord…

In de afgelopen vier jaar ben ik erachter gekomen dat promotieonderzoek doen veel weg heeft van wielrennen. Bij wielrennen heb je net als bij promoveren ploegleiders om je heen die voor elke koers de tactiek bepalen en je constant blijven coachen. Daarnaast zijn er de mechaniekers die ervoor zorgen dat het materiaal perfect in orde is. En er zijn soigneurs die zaken voor je regelen waar je helemaal geen benul van hebt dat die geregeld moeten worden. Verder zijn er nog de collega-renners waarmee je tijdens de koers en daarbuiten optrekt en je uit de wind houden waar dat kan. En, last but not least, is er de supportersgroep die je in tijden van glorie aanmoedigt en vooruitschreeuwt, maar ook langs de kant van de weg op je blijft wachten wanneer je met een uur achterstand en met de tong tussen de spaken voorbij komt bollen.
Graag zou ik iedereen afzonderlijk willen bedanken.

Allereerst mijn promotor: **Nico**, het moment tijdens mijn afstuderen op het ORL waarop jij mij een promotieplek aanbood zal ik niet snel vergeten. Ik vond het bijzonder eervol en wist niet hoe snel ik deze kans aan moest grijpen. In de jaren die hierop volgden heb ik echt ontzettend veel van jou geleerd. Telkens wist jij mij ook weer scherp te krijgen wanneer ik weer eens de helikopter view uit het oog dreigde te verliezen en me blind zat te staren op één stompzinnig detail.
Regelmatig sta ik echt paf van jouw drive en jouw enorme kennis van de biomechanica. Ik vind het echt bewonderenswaardig hoe jij, ondanks alle drukte, mensen weet te enthousiasmeren en te motiveren. Zo heb je mij ervan weten te overtuigen dat we, vanwege een zekere deadline, een complete studie konden doen in maar drie weken (!!!). Maar we hebben het gered! Met vragen kon ik ook altijd bij jou terecht, want de deur van jouw kantoor stond, en staat, altijd open (behalve wanneer er weer eens een gele post-it note op jouw deur geplakt was met de tekst: "I do no exist today…"). Ik ben echt ontzettend dankbaar voor het vertrouwen dat je in mij stelt. Maar natuurlijk ook voor alle kansen die je mij geboden hebt en nog steeds biedt.

Mijn copromotor en dagelijks begeleider: **Dennis**, vanaf mijn eerste dag op het ORL was jij degene die mij altijd met alles hielp met van alles en nog wat. Ik ben erg dankbaar voor al jouw inzet. Schrijftechnisch heb ik erg veel van jou geleerd. Jij was altijd de eerste die mijn nog niet gecorrigeerde schrijfwerk op zijn bureau kreeg. Vooral in het begin kreeg ik het bijna compleet rood terug met de woorden: "Ik weet wat je wilt zeggen, maar dan moet je dat ook zo opschrijven." Maar ook bij het analyseren van mijn soms haperende eindige elementen modellen wist jij altijd weer het kritische punt boven water te halen. Het is ontzettend plezierig om met jou samen te werken en jouw grappen, tijdens congressen of gewoon op het lab, zijn altijd weer grandioos!

Dear **Ken**, my other 'copromotor'. How many people from the USA drive a Saab, eat lots of fruit and love bicycle racing? Not that many I presume and therefore I sometimes wondered whether you are actually an American. I enjoyed our email and Skype conversations in which we discussed the latest cycling events and, of course, our research. Every time I was flabbergasted when you knew a trick in order to support 'poor' numerical output or a knack that tackled mechanical issues. I really appreciate the hospitality you, Marcie and Caroline showed me during my stay in Syracuse where I visited your lab. It was a great experience!

Dear **Mark**. You helped me a lot with providing me with all the necessary experimental data. Quite many times you must have thought: "Why does he want that particular experimental data, and how am I going to acquire or dig up these data?" I really appreciate it, because without your efforts it would not have been possible to validate the simulations.

Dear **Katia**. You introduced me into the world of multiscale modeling. Your enthusiasm and motivation with which you do your research is every time amazing. Thanks for all the discussions we had, your valuable input and your hospitality during my stay in Boston. Thanks!

De leden van de manuscriptcommissie, **Nico Karssemeijer, Nico Creugers en Han Huétink**; heel erg bedankt voor de kritische beoordeling van mijn manuscript.

"En? Convergeert ie al?" **Pieter**, dit waren jouw woorden toen ik mijn allereerste micro CT-dataset aan segmenteren was. Ik vind dat jij, samen met Nico, een lab runt waar niet alleen mooi onderzoek wordt gedaan, maar waar ook een geweldige sfeer hangt.

René, mede door mijn simulaties stond de server regelmatig bijna op crashen. Maar door jouw kunde bleef de hele unit steeds weer draaien. Ik sta er telkens weer van te kijken wat jij allemaal weet te programmeren en te automatiseren. Mooi werk!

"Euhh, **Ineke**? Mag ik jou wat vragen?" Ik wil niet weten hoe vaak ik jou deze vraag gesteld heb. Bedankt voor alle administratieve zaken die je voor mij geregeld hebt. Ik heb jouw oprechte vrolijkheid, gezelligheid en betrokkenheid altijd zeer gewaardeerd.

Alle andere ORL collega's: **Astrid, Eric, Esther, Gerjon, Hendi, Huub, Jorrit, Leon, Loes, Maud, Miranda, Pieter H, René A, Willem en Wojciech**. Bedankt voor de samenwerking, maar vooral voor alle gezelligheid op het lab en daarbuiten!

Jordi, door al jouw stages op het ORL, heb je bijna mijn hele promotieonderzoek live kunnen volgen. Bedankt voor de gezelligheid en jouw kennis, want die was tijdens de pubquizzen hard nodig.

Sanaz, jij bent de enige student die ik heb mogen begeleiden. Ik vond het ontzettend leuk om te doen met ook nog een mooi resultaat als gevolg (Chapter 9). Veel succes met jouw eigen promotieonderzoek op het ORL. Mamnoon!

Chantal, bedankt voor het proper houden van mijn werkplek en de gezellige vijf babbelminutjes elke dag.

De afgelopen vier jaar heb ik verschillende kamergenoten gehad met wie ik ontzettend veel lol heb beleefd. Altijd waren ze bereid hun frisse blik op mijn werk te werpen wat iedere keer weer heel verhelderend werkte.
Allereerst **Liesbeth**. Bedankt voor de drie jaar dat je rechts van mij zat. Je bent altijd een prettig luisterend oor voor me geweest. Onze reis naar Milaan en Polen met Maria zal ik nooit vergeten, net zomin als de andere tripjes waar we elkaar letterlijk en figuurlijk ondersteund hebben. Ik realiseer mij dat jouw eerste indruk van mij niet de beste was. Want wie vraagt er nou in hemelsnaam op je allereerste werkdag wat je denkt dat de kleur van een proton is? Succes met je opleiding tot orthopeed. Mocht ik ooit 'botte pech' krijgen, dan weet ik jou te vinden!
Anne, jouw bureau was altijd de meest geordende van alle kamergenoten die ik heb gehad. Daar kan ik nog veel van leren. Bedankt voor jouw enthousiasme en gezelligheid.
Erwin, tijdens de pubquizzen stond ik telkens weer te kijken van jouw scherpte en muziekkennis. Zou dat komen door al mijn 'slappe bakken' koffie?
Pawel, you are a great lad! Always calm, keen and optimistic. I always enjoyed the dinners I had with you and Gosia.

Monique, bedankt voor al jouw hulp bij het maken van dit proefschrift. Het is erg mooi geworden!

Maria, what began as a fellow student during my master assignment at the ORL, resulted in a colleague, permanent roommate, but most of all a great GREAT friend. Sometimes I am wondering how many bottles of 'Fat Bastard' we have drunk during all the dinners we have had in the five years we were in Nijmegen. Thanks a lot for all your trust and hospitality. It was really an honor to be asked to be your best man at your wedding and I really appreciate you want to be my 'paranimf'.

Igo, jij ben echt een geweldige vriend! Ik vind het altijd weer prachtig wanneer we beiden iets aanschouwen, elkaar vervolgens aankijken en dan direct in lachen uitbarsten, omdat we beiden hetzelfde denken. Bedankt voor alle spiegels die je mij de afgelopen jaren hebt voorgehouden en dat je mijn paranimf wilt zijn.

Dennis, ik zie jou niet zozeer als de 'vriend van mijn zus', maar meer als een echte vriend waar ik altijd en met alles terecht kan. Hoe zouden wij in het leven staan zonder de regels van Sly? HUH!!!

Ruud, Agnes en Maartje. Ik ben echt ontzettend blij met het ongelooflijk mooie en warme nest waar ik uit kom. Altijd zijn jullie er voor mij geweest, no matter what, en die steun heb ik erg nodig gehad. Bedankt!

Lieve **Nora**. Bedankt voor alles wat je voor me betekent. Ik ben enorm gelukkig samen met jou. Liebe dich, liefie… Kuss…

Curriculum vitae

About the author

Daan Waanders was born on September 8 1983 in Lichtenvoorde. In 2000, he received his HAVO certificate at the "Scholengemeenschap Marianum" in Groenlo. Subsequently, he studied mechanical engineering at the "Saxion Hogeschool Enschede", with a specialization in human care and technology. During this period he did internships at WE Engineering, Stork MPS and Bronkhorst High Tech. After obtaining his bachelor degree in 2004, he studied mechanical engineering at Twente University, with a specialization in biomechanical engineering. He did his master assignment in the Orthopaedic Research Laboratory (ORL) in Nijmegen under the supervision of Nico Verdonschot and Dennis Janssen. He obtained his masters degree in 2007 on his thesis titled 'Bone Ingrowth and Tissue Differentiation around Uncemented Hip Implants'. During his master assignment he was offered a PhD position at the ORL, which he gratefully accepted. His research focused on the micromechanics of the cement-bone interface in total hip arthroplasty what eventually resulted in this thesis.

List of publications

Tarala M, Janssen D, **Waanders D**, Hannink G, Biemond L, Buma P, Verdonschot N: "The Effect of Bone Ingrowth Depth on the Tensile and Shear Strength of the Implant-Bone E-Beam Produced Interface", Journal of Materials Science: Materials in Medicine **2011** 22(10):2339-46

Waanders D, Janssen D, Mann KA, Verdonschot N: "Morphology Based Cohesive Zone Modeling of the cement-bone interface from postmortem retrievals", Journal of Mechanical Behavior of Biomedical Materials **2011** 4(7):1492-503

Tarala M, Janssen D, Telka A, **Waanders D**, Verdonschot N: "Experimental versus computational analysis of micro-motions at the implant-bone interface", Proc. IMechE Vol. 224 Part H: J. Engineering in Medicine **2011** Vol 225(1) 8-15

Miller MA, Race A, **Waanders D**, Cleary R, Janssen D, Verdonschot N, Mann KA: "Multi-axial loading micromechanics of the cement-bone interface in post-mortem retrievals and lab-prepared specimens", Journal of Mechanical Behavior of Biomedical Materials **2011** 4(3):366-374

Waanders D, Janssen D, Bertoldi K, Mann KA, Verdonschot N: "Mixed-mode loading of the cement-bone interface: a finite element study", Computer Methods in Biomechanics and Biomedical Engineering **2011** Feb 14(2) 145-55

Waanders D, Janssen D, Mann KA, Verdonschot N: "The behavior of the micro-mechanical cement-bone interface affects the cement failure in total hip replacement", Journal of Biomechanics **2011** 44(2):228-234

Waanders D, Janssen D, Mann KA, Verdonschot N: "The effect of cement creep and cement fatigue damage on the micromechanics of the cement-bone interface", Journal of Biomechanics **2010** 43(15):3028-3034

Waanders D, Janssen D, Mann KA, Verdonschot N: "The mechanical effects of different levels of cement penetration at the cement-bone interface", Journal of Biomechanics **2010** 43(6):1167-75

Waanders D, Janssen D, Miller MA, Mann KA, Verdonschot N: "Fatigue creep damage at the cement-bone interface: an experimental and a micro-mechanical finite element study", Journal of Biomechanics **2019** 42(15):2513-9